116

116 B

DYNAMICS OF CONTINUOUS-MODE ICEBREAKING BY A POLAR-CLASS ICEBREAKER HULL

by

R. Ettema, F. Stern, and J. Lazaro

Sponsored by

United States Department of Transportation
Maritime Administration
Grant No. DTMA91-85-C-50115

U.S. Department of Transportation
Maritime Administration

IIHR Report No.

Iowa Institute of Hydraulic Research
The University of Iowa
Iowa City, Iowa 52242-1585

April 1987

ABSTRACT

Presented are the results of an experimentally based study aimed at determining the relationships between resistance, icebreaking pattern and hull motions for a POLAR-Class hull. The study involved two sets of experiments conducted with a 1:48-scale model hull. For one set, the hull was free to pitch, heave and undergo limited roll; free-hull condition. The other was conducted with the hull restrained from motions; fixed-hull condition. For each condition, the hull was towed at the same range of speeds through urea ice sheets of similar properties (thickness, strength, etc.). The free hull was instrumented so that its pitch, heave, and roll motions (displacements as well as accelerations) could be measured, together with ice resistance. For the fixed hull, the restraining forces and moments were measured, together with ice resistance. The temporal records were analyzed to yield values of their mean and standard deviation and spectral densities. These quantities are related to observed patterns of icebreaking in order to reveal relationships between icebreaking and ice resistance, and how they are influenced by hull motions.

It was found that the free hull experienced larger values of mean resistance than did the fixed hull. The difference is attributed to the influences of hull motions. For both hull conditions; mean resistance increased proportionately with the square of ice-sheet thickness. The relationship between mean resistance and hull speed was not linear for the free hull, as was the case for the fixed hull. Instead, the relationship was characterized by what is commonly known as a "Milano hump."

Hull motions and icebreaking pattern determined the dominant cycles of resistance experienced by the free hull. Icebreaking frequency, ω_b, the frequency of individual breaking events, was significant only when the hull transitted thin ice such that significant pitch and heave did not occur. When ω_b is less than the hull's natural frequency of coupled pitch and heave, ω_n, the dominant frequency of ice resistance and hull motions is the frequency of track opening, ω_o; this is the frequency associated with the cyclic manner by which hull trim changes as the hull breaks open a track that is sufficiently wide for the hull to pass through. When ω_b equals or exceeds ω_n, the dominant frequency of ice resistance coincides with ω_n. Under certain conditions, roll was found to be important and caused a large increase in resistance. Some limited measurements of roll angle were made. The fixed hull experienced dominant frequencies of resistance at both ω_b and ω_o.

ACNOWLEDGEMENTS

This research was sponsored by the United States Department of Transportation, Maritime Administration (MARAD) under Grant No. DTMA91-85-C-50115. The authors thank Dr. F. Seibold of MARAD for reviewing the draft of this report. The authors would also like to thank the United States Coast Guard, Icebreaker Technology Section, for the loan of a 1:48-scale model of a USCGC POLAR-Class hull. Commander Dr. D. Humphreys was particularly helpful in arranging the loan of the model. Support provided by IIHR's mechanical and electronic shops, especially by R. Hamer, and J. Cramer, was essential and very much appreciated.

TABLE OF CONTENTS

LIST OF SYMBOLS

A_{wp}	waterplane area
A_{ij}	added-mass coefficients
B_{ij}	damping coefficients
B_t	track width
C_{ij}	hydrostatic restoring coefficients
C	openwater resistance coefficient
C_{IB}	resistance coefficient associated with breaking of ice
C_{IS}	resistance coefficient associated with submergence of ice
C_V	resistance coefficient associated with to velocity
d	cantilever beam width
D_f	resolution band width of spectra
ΔE	change in voltage
E	elastic modulus for flexure of ice sheet
f_x	ice resistance
f_y	ice force in the y-direction
f_z	ice force in the z-direction (heave force)
F	Froude number, $V/\sqrt{gt}$
$F_j(\omega)$	Fourier transform of $f_j(t)$
F_n	Froude number, $V/\sqrt{gL_s}$
g	acceleration due to gravity
h	ice-sheet thickness
H_{ij}	transfer function
I_{ii}	moment of inertia with respect i-axis
I_{ij}	product of inertia with respect i- and j-axes
I_{wp}	waterplane moment of inertia
L_s	length of the ship

ℓ_b	icebreaking length
ℓ_c	characteristic length of ice sheet
M	mass of the model hull
M_{wp}	waterplane moment
m_ϕ	moment with respect to the x-axis
m_θ	moment with respect to the y-axis (pitch moment)
m_ψ	moment with respect to the z-axis (yaw moment)
N	number of segments in spectra
n	index
P	fracture load of cantilever beam
q_j	hull motions vector
$Q_j(\omega)$	Fourier transform of the hull motions vector
R_e	Reynolds number
S	wetted area of hull
$S_x(\omega)$	spectral density of a random variable x
$S_{ij}(\omega)$	spectral density matrix of a random vector x_j
s	index
t	time
T	record length of time series
T_s	length of time segments for calculation of power spectra
v	voltage
V	hull speed
V_i	ice-sheet speed
$x_s(t)$	time series
$X_s(nD\omega_s)$	Fourier transform of $x_s(t)$
x	surge displacement of hull
y	sway displacement of hull

z	heave displacement of hull
α_1, α_2	waterplane angle, flair angle
β	angle between normal to the bow waterline and centerplane
γ	specific weight of water
σ_x	standard deviation of the variable x
ϕ	roll angular displacement of hull
θ	pitch angular displacement of hull
ψ	yaw angular displacement of hull
ω	frequency
ω_i	icebreaking frequency of fixed structures
ω_{ic}	frequency of ice crushing against a rigid cylinder
ω_n	natural frequencies of coupled pitch and heave
ω_h	natural frequency of pure heave in openwater
ω_o	opening frequency
ω_p	natural frequency of pure pitch in openwater
ω_d	sampling frequency
ω_b	icebreaking frequency
ν	Poisson's ratio for ice
ν_k	kinematic viscosity of water
ρ	density of water
σ_f	flexural strength of ice sheet
δ	displacement of ice sheet
$\bar{}$	time mean
$\dot{}$	derivative with respect to time

I. INTRODUCTION

This study is concerned with the dynamics of continuous-mode icebreaking by a POLAR-Class icebreaker hull moving with steady speed through a monolithic ice sheet. In particular, the study focuses on the relationships between ice resistance and patterns of icebreaking and shows how both are influenced by (and, in turn, influence) hull motions.

A ship hull continuously breaking its way through a level sheet of ice comprises a complex three-dimensional, nonlinear dynamic system with six degrees of freedom that is as yet insufficiently understood. This is due primarily to the present lack of knowledge on the physics of icebreaking, especially for moving structures. The situation is further complicated by the stochastic nature of icebreaking. There is a current need to better understand the time-dependent relationships between ice resistance, icebreaking pattern, and hull motions. This need is prompted by concerns for higher fuel costs, improved geometric and structural design of hulls (often utilizing plastic structural-design concepts that result in lighter-weight hull structures), greater efficiency of propulsion systems, and minimizing of excessive hull motion and vibration.

In order to shed light on the dynamics of continuous-mode icebreaking, an extensive program of experiments was conducted using an ice towing tank, urea model ice, and a 1:48-scale model of a POLAR-Class icebreaker hull. The program consisted of two parts. In one, the model hull was instrumented so that its pitch, heave, and roll motions (displacements as well as accelerations) could be measured, together with ice resistance; free-hull condition. In the other, the hull was rigidly restrained from motions, and the restraining forces and moments were measured, together with ice resistance; fixed-hull condition. The latter series of experiments was conducted for the purpose of relating icebreaking and ice resistance without the influence of hull motions. Comparison of the two series of experiments would aid in determining the influences on resistance and breaking pattern of hull motions.

For each condition, the hull was towed at the same range of speeds through ice sheets of similar properties (thickness, strength, etc.). Fifty resistance experiments, each involving a tank-long ice sheet, were completed. Temporal records of ice resistance, hull motions and motion restraining forces

and moments were analyzed to yield values of their mean and standard deviation, and spectral densities. These quantities are related to observed patterns of icebreaking.

A unique feature of the present study is the extensive use of spectral analysis of the time histories of ice resistance and hull motions. Spectral analysis, although frequently used in the analysis of random-wave loads experienced by ship hulls and offshore structures, has rarely been used to relate ice resistance to icebreaking pattern and hull motions. Interpretation of the results revealed from spectral analysis is enhanced through the use of the linearized equations of motion. Through these equations, estimates can be made of the hydrodynamic coefficients associated with hull motions during icebreaking, and of the transfer functions that relate motions to external, or excitation, forces such that the natural frequencies of hull motions and excitations can be deduced.

As mentioned above, the present study involves a towed hull that could not surge and which was not fitted with propellers, although it was fitted with a rudder and had propeller cowlings. Consequently, the effects on resistance and hull motions of propeller-ice impact are not considered.

An outline of the report is as follows. In Chapter II, the processes involved in continuous-mode icebreaking are discussed. The set-up and program of model-scale experiments are described in Chapter III. The equations of motion for a ship hull transitting a level sheet of ice in continuous-mode of icebreaking, and their spectral analysis, are provided in Chapter IV.

Results forthcoming from the experiments are presented in Chapter V through VIII. Patterns of icebreaking are presented and discussed in Chapter V. Mean values of ice resistance measured for the free hull are presented in Chapter VI, and are compared with resistance measured for the fixed hull. Mean values of pitch and heave motions experienced by the free hull are presented and discussed in Chapter VII. These values are compared with mean values of pitch-restraining moment and heave-restraining force exerted against the fixed hull. Also presented in this chapter are standard deviations of roll motion and pitch and heave accelerations experienced by the free hull and standard deviation of yaw-restraining moment exerted against the fixed hull. The relationships between icebreaking and ice resistance, and the influences

of hull motions, are described through the use of spectral analysis in Chapter VIII. The descriptions integrate the results presented in Chapters V through VII.

The principal conclusions from the study are discussed in Chapter IX.

II. CONTINUOUS-MODE ICEBREAKING

A review of the literature on continuous-mode icebreaking, by a hull steadily transitting an ice sheet, reveals scant information regarding the dynamic relationships between ice resistance and patterns of icebreaking, and how they are influenced by (and, in turn, influence) hull motions. Most studies of continuous-mode icebreaking empirically relate mean resistance encountered by a particular hull form to thickness and flexural strength of the ice sheet, and to hull speed. This is primarily because most studies have been oriented toward the design, or performance testing, of specific hull forms. Comparatively few studies have been undertaken with the aim of illuminating the dynamics of continuous-mode icebreaking.

This chapter commences with a description of continuous-mode icebreaking. The ensuing discussion then outlines the dynamics of continuous-mode icebreaking, beginning with a review of factors contributing to ice resistance, and their relative importance. The discussion then focuses on the use of spectral analysis. Ice-sheet movement around fixed, rigid structures such as piers are first considered and then the discussion is extended to include the effects of structure compliance, flexibility and motion.

A. Description

The resistance encountered by a hull transitting a level sheet of ice depends primarily on the processes by which its hull, especially its bow, breaks and displaces ice. Some of these processes are indicated in Figure 1. At the contact perimeter between bow and ice sheet, ice is sheared and crushed as the bow loads and flexes the ice sheet. The load increases as forward motion of the hull is resisted by the ice sheet. The ice sheet is depressed by the bow, but, in turn, causes the hull to increase both its pitch and heave displacements. The vertical component of the load applied to the sheet by the bow increases, its magnitude being moderated by changing stem

angle at contact, until the ice sheet flexurally fails. Depending on a number of factors, including hull beam, hull speed, bow form, and ice-sheet properties (thickness, strength, etc.) and their uniformity, the ice sheet may not fail simultaneously around the bow.

If flexural failure of the ice sheet occurs simultaneously around the bow, or at least around a substantial portion of it, and a sufficiently wide portion of the sheet has been opened to allow the hull to pass through, the resistance experienced by the hull relaxes momentarily before subsequently increasing. In response, the hull's pitch and heave displacements may decrease, and the hull may surge forward, provided that it displaces sufficient broken ice from beneath its bow. Generally, the pitch and heave response slightly lead ice resistance. When momentarily released from contact with the ice sheet, the hull may oscillate at its natural frequency of pitching, or of coupled pitch-heave motion, as long as this frequency adequately exceeds the frequency of flexural icebreaking events. The motions are, however, heavily damped by the presence of broken ice beneath the hull and by the ice sheet surrounding the hull. If the frequency of flexural icebreaking exceeds the hull's natural frequency of pitching, there is insufficient time for the hull to return to its openwater trim. When the frequency of icebreaking is equal to any of the the hull's natural frequencies of motion, a resonance condition occurs.

If the failure is localized, as is the case for a hull slowly transitting a thin ice sheet, total resistance is not significantly reduced. In thicker ice sheets, ice pressure nonuniformly distributed around the bow causes the hull to yaw or roll. These motions may lead to further nonuniformity of ice pressure.

Whether or not ice fails simultaneously around the hull's bow, it breaks in fairly regular patterns comprised of cusp- and wedge-form ice pieces, as indicated in Figure 1. The sizes of the cusps and wedges depend primarily on ice-sheet properties, bow form and hull speed. Broken ice is submerged, overridden and further broken by the hull. Some broken ice eventually emerge in the track opened by the hull; the remainder having been cast laterally beneath the bordering ice sheet. Pattern of icebreaking represents, in effect, the process by which a hull's bow opens a sufficiently wide track to enable the hull to transit the ice sheet.

Continuous-mode icebreaking involves cycles, or sequences of events, in which ice is broken and displaced by a hull steadily transitting an ice sheet. One might expect, therefore, that resistance encountered by a hull would be cyclic or at least narrow-banded about a frequency associated with icebreaking. Under certain conditions it can be. However, under most conditions, individual processes may not act in unison, the hull may interact with a pattern of icebreaking rather than individual breaking events, and hull motions may affect the cyclic processes. Hull motions (pitch, heave, roll, yaw, sway and surge) may significantly alter contact geometry and loading pattern, and result in different rates of ice-sheet loading if significant accelerations occur as ice fails and is suddenly displaced from beneath the bow. Important noncyclic processes also occur. For example, although the flexural breaking, subsequent submergence of broken ice, and further flexing of an ice sheet may be described as being cyclic, at least at any bow location, an ice sheet may not fail simultaneously around the bow. Moreover, the hull is always in contact with ice; sliding against it, submerging it, crushing as well as possibly shearing it, and further fragmenting ice broken from the ice sheet.

Given the nature of the processes that it entails, continuous-mode icebreaking is appropriately treated as stochastic. Dynamically, it may be narrow-banded about a single dominant frequency (e.g., icebreaking), about multiples of one frequency (e.g., multiples of icebreaking), or about several frequencies. It may also be broad-banded due to shearing and crushing of ice, together with ongoing submergence and frictional effects of broken ice moving around the hull. Yaw and roll as well as ice-sheet irregularities also broaden spectral densities of resistance.

The dynamics of continuous-mode icebreaking are not adequately understood. This situation partially is attributable to the lack of detailed observations and data on, not to mention appropriate analyses of, icebreaking. Furthermore, variations in ice-sheet properties, as well as in hull geometry contacting an ice sheet, and hull speed, influence and likely alter the dynamics and physics of continuous-mode icebreaking so as to fuel controversy concerning the relative importance of component processes. It is important to note here that the influences of hull motions on mean values of resistance have as yet not been determined.

There is a current need for a rigorous study to determine the detailed relationships between the sequential development of an icebreaking pattern, and the resulting temporal variation of ice resistance, and how both are influenced by (and, in turn, influence) hull motions; especially pitch, heave and roll. Such a study would necessarily involve extensive experimentation conducted with an ice tank. Field experiments are difficult to perform under controlled conditions, and are exorbitantly expensive to conduct. And, because the dynamics of continuous-mode icebreaking are inadequately understood, a purely analytical approach is not yet possible.

B. Icebreaking Pattern

During continuous-mode icebreaking, regular patterns of broken ice may develop around the bow of a hull. The patterns are comprised of broken ice in the form of a mosaic of cusps and wedges, and depend on breaking length of ice, bow form, hull speed and hull motions. Figure 2 shows an icebreaking pattern reported by Voelker et al. (1985) for a full-scale POLAR-Class hull.

For a given bow form, it is customary to characterize icebreaking patterns in terms of icebreaking length or resulting cusp width, W, as indicated in Figure 2. Cusp width is commonly (e.g., Enkvist, 1972) related to the characteristic length, ℓ_c, of an ice sheet;

$$\ell_c = \left[\frac{Eh^3}{12\rho g(1-\nu^2)} \right]^{0.25} \qquad \text{(II-1)}$$

in which E = elastic modulus associated with an ice sheet of thickness h; ν = Poisson's ratio for ice sheets, usually taken as 0.3 (Mellor, 1983); ρ = density of water; and g = gravity acceleration. The length, ℓ_c, is a characteristic breaking length of an ice sheet, if it is treated as an elastic plate on an elastic foundation.

There are surprisingly little data on the effects on icebreaking pattern of ice-sheet properties, hull speed and motions, and bow form. Existing data sets often are incomplete, missing important measurements such as ice-sheet thickness and strength. Usually cusp sizes, or broken-ice dimensions were

observed in the wake of the hull where, due to further breaking after having passed beneath and around the hull, they are smaller than pieces freshly broken. Lewis and Edwards (1970), Enkvist (1972), McKindra and Lutton (1981), Voelker et al. (1985) and others report values of W measured during tests with full-scale hulls. Their data generally show that W decreases with increasing hull speed, V, and increases with increasing ice-sheet thickness, h. Except for icebreaking at creeping speeds, cusp widths were usually less than the calculated characteristic lengths of ice sheets. Similar results were obtained from model-scale studies (e.g., Mueller and Ettema, 1984; Tatinclaux, 1984a). No study has yet related measured time-histories of ice resistance to icebreaking pattern. Throughout the remainder of this report, hull speed is simply referred to as speed, V, and ice-sheeet thickness as thickness, h, other than for reasons of clarity.

Semi-empirical predictors of ice resistance have been developed which include empirical expressions for cusp width, W, or a related dimension. Milano's (1973, 1975, 1980, 1982) predictive algorithm, herein referred to as "Milano," uses the following expression based on values of W obtained from diverse data sources:

$$W = 0.8612h - 0.238V + 8.978 \qquad \text{(II-2)}$$

in which V and h are in units of ft. and fps., respectively, Equation (II-2) applies for full-scale speeds of $V \leq$ 10fps. Kotras et al. (1983) developed the following expression for W based on field measurements with a POLAR-Class hull transitting ice sheets 0.3 to 0.6m thick and 200kPa flexural strength:

$$W = R_1 \ell_c (2.4 + 6.0) \left(\frac{\sin \alpha_1}{\tan \alpha_2}\right)\left(\frac{V}{\sqrt{g\ell_c}}\right)^{-1} \qquad \text{(II-3)}$$

in which $R_1 = 50.7\eta_3^2 - 64.3\eta_3 + 21.3$; η_3 = hull-shape factor = 0.712 for a POLAR-Class hull; α_1 = waterplane angle (assumed constant at 19°); and, α_2 = flair angle (42°). Expressions such as (II-2) and (II-3) are of crucial importance to their respective ice-resistance algorithms because computed, or estimated, values of W determine icebreaking patterns which, in turn, prescribe the resistance values associated with a train of processes assumed to comprise continuous-mode icebreaking.

C. Mean Resistance

The processes contributing to ice resistance encountered by a hull during continuous-mode icebreaking can be divided into the following general categories:

(i) icebreaking;

(ii) submergence, displacement, and momentum exchange to, broken ice; and

(iii) friction associated with ice contact and movement around the hull surface.

These processes generally occur for continuous-mode icebreaking by fixed structures. However, the relatively complex hull forms of ships, and other floating structures, as well as their facility to move with as many as six degrees of freedom, further complicate continuous-mode icebreaking.

The description of continuous-mode icebreaking given in Section II.A, indicates the manifold subprocesses involved in each of items (i) through (iii), above. For example, icebreaking may entail crushing and shearing as well as flexural failure of ice sheets. For most bow forms, flexural failure contributes the significant portion of resistance to icebreaking; but not always.

Empiricism based on dimensional and regression analyses is the most common approach used to relate mean resistance to items (i) through (iii), above, for varying thickness and strength of ice sheet, and hull form and speed. Typically (e.g., Kasteljan, 1968; Lewis and Edwards, 1970; Edwards et al., 1972; Vance, 1975; Schwarz, 1977; Tatinclaux, 1984a,b; Williams, 1986), mean ice resistance, $\overline{f}_x$, is subdivided into several (usually three) parts. Edwards et al., for example, equate $\overline{f}_x$ to the sum of three terms:

$$\frac{\overline{f}_x}{\rho g B h^2} = \underset{(a)}{C_{IB}\,\frac{\sigma_f}{\rho g h}} + \underset{(b)}{C_V\,\frac{V}{\sqrt{gh}}} + \underset{(c)}{C_{IS}} \qquad \text{(II-4)}$$

in which (a) is resistance due to flexural failure of the ice sheet; (b) is resistance attributable to hull passage through broken ice (velocity-dependent, or inertia-related resistance); and (c) is resistance associated with the hull's interaction with broken ice (gravity resistance). In (II-4), σ_f = flexural strength of ice; B = hull beam; and C_{IB}, C_{IS} and C_V are coefficients, which are assumed to be independent of the variables in (II-4). From the results of extensive model-tests using a 1:48-scale model of a POLAR-Class hull, Lecourt and Deslauriers (1976) obtained

$$\frac{\overline{f}_x}{\rho g B h^2} = 3.57 + 4.68 \frac{V}{\sqrt{gh}} \qquad \text{(II-5)}$$

for a coefficient of hull-ice friction, $\mu_d = 0.20$. Other regression-based equations similar to (II-4) and (II-5) have been developed for particular hull forms (e.g., Schwarz, 1977; Tatinclaux, 1984a).

The influence on $\overline{f}_x$ of thickness, h, is fairly well established; generally, $\overline{f}_x$ increases proportionately with h^2. The influence of speed, V, and hull motions, on $\overline{f}_x$ are far less clearly understood. Typical practice (e.g., Tatinclaux, 1984a) is to relate normalized ice resistance $\overline{f}_x/(\rho g B h^2)$ with Froude number $F_n = V/\sqrt{gh}$, as in (II-4) or (II-5). Some studies (e.g., Poznyak and Ionov, 1981; Vance, 1979) propose $\overline{f}_x/(\rho g B h^2)$ as being proportional to F_n^2. Most empirical relationships (all references cited above) give $\overline{f}_x/(\rho g B h^2)$ as being directly proportional to σ_f/h.

Other than indicating the sensitivities of mean ice resistance to normalized expresions of h, σ_f and V, empiricism reveals little information on the relationships between ice resistance and icebreaking pattern and how these are influenced by hull motions. Also the effects on resistance of crushing and shearing are not explicity included, nor is the effect of friction between ice and hull. These aspects of ice resistance are usually taken into account by varying the coefficients in empirical expressions such as those in (II-4) or (II-5).

A number of studies have been performed to estimate, with greater certitude than used in regression analysis, the relative magnitudes and importances of component processes contributing to ice resistance. Enkvist (1972, 1983), for example, offers information on the proportion of resistance that is attri-

butable to icebreaking, at least to the flexural failure of ice. Using the results of model- and full-scale tests involving ice sheets and precut icebreaking patterns, Enkvist (1983) showed that icebreaking may contribute from 40 to 80% of the total resistance encountered by a hull; the proportion increasing with decreasing hull beam. Model-scale experiments conducted by Kitazawa and Ettema (1984) also suggest that icebreaking contributes about 80% of total ice resistance. Model-scale experiments performed by Poznyak and Ionov (1981), and Nyman (1986) show similar results. In a recent study, Enkvist and Mustamaki (1986) more-or-less eliminated from icebreaking the occurrence of crushing and shearing of ice at the bow-stem of a hull. They did this by comparing the resistance experienced by a hull transitting an ice sheet both with, and without, a central slot of width equivalent to the bow-stem width. They found that in full-scale tests resistance was reduced by 20 to 40%. In a series of model tests they found a similar reduction.

Several semi-empirical methods have been developed for predicting mean values of ice resistance. They are based on formulations of component processes of continuous mode icebreaking. Two leading methods are those proposed by Milano and Kotras et al. (1983); the second method is based on an algorithm developed by Naegle (1980) which was subsequently modified by Lewis et al. (1983) and Kotras et al. who computer-coded it as "SPLICE." "Milano" and "SPLICE" are fairly complex algorithms involving detailed, static analysis of forces exerted against a hull during continuous mode icebreaking.

In his original approach, Naegle related the three, coupled equations of hull motion--in surge, heave and pitch--to icebreaking and hydrodynamic forces. Using, for the most part, Enkvist's (1972) concepts for evaluating ice forces, Naegle constructed a fairly detailed algorithm in which resistance terms are determined quasi-statically. Ice resistance is related to incremental changes in pitch and heave. Kotras et al. report finding that pitch and heave have minimal effect on values of $\overline{f}_x$ predicted using Naegle's algorithm. Consequently, they simplified it such that, a hull is assumed to maintain a constant trim. We compare (in Chapter V) values of $\overline{f}_x$ predicted using "SPLICE" with values experimentally determined during the present study. Values of $\overline{f}_x$ predicted using "SPLICE" are calculated as the average value of ice forces summed over a cycle of icebreaking; continuous-mode icebreaking is assumed to be periodic at a single frequency associated with icebreaking.

Milano (all references) followed a Lagrangian approach to the dynamics of continuous-mode icebreaking. He divided the processes contributing to ice resistance, evaluated the energy associated with each, and summed the energies. His energy summation involved five terms: E_1, transit through broken ice; E_2, impact with, and breaking of ice; E_3, hull (pitch and heave) motion through ice; E_4, hull falling through ice; and E_5, ice submergence. The total energy is

$$E_T = \sum_{i=1}^{5} E_i \qquad \text{(II-6)}$$

The mean ice resistance experienced by a hull is determined as

$$\overline{f}_x = \frac{E_T \sin \delta}{W} \qquad \text{(II-7)}$$

in which δ = entrance angle of the bow.

Milano argued that with increasing pitch and heave, terms E_3 and E_4 increase and, therefore, so does $\overline{f}_x$. He takes speed, V, into account by including its effect on W, and by relating the period for a hull to undergo a pitch cycle,

$$T_2 = \frac{W}{V \sin \delta} \qquad \text{(II-8)}$$

to the period required for the hull to reduce its trim by settling downwards through broken ice,

$$T_1 = \frac{1}{\gamma} \cot \frac{\gamma}{\xi} \qquad \text{(II-9)}$$

in which γ and ξ are terms involving the virtual moment of inertia associated with pitch. Both γ and ξ are velocity dependent through the inclusion of added-mass and added-mass moment-of-inertia terms (Milano, 1980). From (II-8), it is evident that T_2, at least, diminishes with increasing speed, V. If T_2 exceeds T_1, the hull may settle back to its trim before undergoing the next breaking cycle. With increasing V, the time available for the hull to settle back decreases, consequently the amplitudes of pitch and heave decrease with increasing V. In accordance with Milano's prognostications, the relationship

between $\overline{f}_x$ and V is characterized by the occurrence of a bulge that has been dubbed the "Milano hump," as illustrated in Figure 3, which also indicates the relative magnitudes of the terms E_i for the USCGC "MACKINAW." The occurrence of a "Milano hump" is still a subject of debate. Schwarz (1977) and Tatinclaux (1984b) present data supporting its existence. Other data presented, for example, by Enkvist (1972) or Williams (1986), seem not to show it.

The possible occurrence of the so-called "Milano hump" suggests that, with increasing speed, V, pitch and heave attain maximum amplitudes, and do not simply vary monotonically with V. To the best of the authors' knowledge, this has never been documented by means of experiment.

D. Hull Motions

The influences on ice resistance of motions (notably: pitch, heave and roll), and vice-versa, have never been fully examined. It is not surprising, therefore, that there appears to be some controversy concerning the influences on ice resistance of hull motions. On the one hand, Milano's predictions suggest the occurrence of a motions-related "hump" in plots of $\overline{f}_x$ versus V. On the other, the work of Kotras et al. suggest that motions do not affect $\overline{f}_x$. Only a small amount of experimental effort has been directed toward investigating the influence of motions on $\overline{f}_x$.

Enkvist (1972) performed two model-scale experiments involving free and restrained conditions of towing, and concluded that pitch and heave motions do not significantly influence the mean resistance; or, at least, any attributable resistance to pitch and heave is within data scatter. However, our reanalysis of these experiments indicates that the fixed model experienced notably less resistance than did the free hull. Additionally, it appears the motion-restraining mechanism used by Enkvist still would have enabled the hull to roll, and thereby experience a motion-related resistance.

Two studies were performed using floating (moored) conical hull forms which were both free to pitch and heave and also could be restrained from these motions. One study, that by Frederking and Schwarz (1982), showed that a conical hull form free to pitch and heave experienced horizontal ice forces that were two-thirds the magnitude of those it experienced when it was restrained. In another study involving a similar floating structure, Matsuishi

and Ettema (1985) found that, for relatively slow speeds of ice-sheet movement, the restrained platform experienced greater ice force than it did when it was free to pitch and heave. At higher speeds, however, the free platform experienced greater resistance. Curiously, the results from these studies indicate the opposite effect on resistance of motions than that inferred by formulations such as Milano; viz., a moving hull experiences lesser values of $\overline{f}_x$ than does a fixed hull. However, an important factor in the ice loading of non-translating bodies is the facility of ice rubble to accumulate around the structure. This enables, during continuous-mode icebreaking, an ice sheet to impart greater forces against such structures. Keeled hulls moving through water do not facilitate ice rubble accumulation.

E. Spectral Analysis

It appears that only during two studies has spectral analysis been used to explain the processes causing temporal variations of ice resistance experienced by a hull during continuous-mode icebreaking. Both studies involved a POLAR-Class hull. One (Mueller and Ettema, 1984) used the same model-scale hull as was used herein, and is precursory to the present study. The other (Voelker et al., 1985) involved full-scale field tests conducted with the USCGC "POLAR STAR."

The cycles of ice forces experienced by fixed structures undergoing continuous-mode icebreaking are more readily identifiable than those experienced by ship hulls, therefore, the following discussion begins with fixed structures.

Under certain conditions, a single, dominant frequency of ice loading may be experienced by a fixed rigid structure continuously impacted by an ice sheet. These conditions generally require that the width of the structure be comparable in magnitude to the width of ice pieces broken from the ice sheet, and that the ice fail flexurally. The resulting dominant frequency of icebreaking, ω_i, is

$$\omega_i = V_i / \ell_b \qquad \text{(II-10)}$$

in which V_i is ice-sheet speed; and ℓ_b is length of ice pieces, or spacing between flexural cracks. The length ℓ_b depends on the thickness and elastic properties of the ice sheet, and on ice-sheet speed, V_i. As mentioned in Section II.B, breaking length ℓ_b is usually related to the characteristic length, ℓ_c (II-1). It is generally accepted that, in accordance with elastic theory for semi-infinite beams and plates on elastic foundations, ℓ_b should be proportional to ℓ_c, provided the ice sheet breaks before its free end becomes submerged.

If the structure is relatively wide compared to thickness, h, such that ice does not fail uniformly or simultaneously around the structure, or if ice fails in crushing, the time-histories of ice loads are stochastic (Kry, 1978). Data prescribed by Timco (1984), do, however, infer that dominant frequencies for flexural failure of ice against a sloped structure coincide with ω_i.

Interestingly, Sodhi and Morris (1986) were able to identify a dominant frequency for ice crushing against a rigid cylinder as,

$$\omega_{ic} = cV_i/h \qquad \text{(II-12)}$$

in which c typically is about 3; and h/c is the nominal width of the damage zone formed ahead of the cylinder during continuous crushing.

For a more detailed discussion on the cyclic loading of fixed rigid structures, refer to Neill (1976, 1980), Timco (1984), and Sodhi and Morris (1986).

For moving structures, the situation is more complicated because interactions between body motions and icebreaking are possible. Maattanen (1975) extensively discusses the dynamics of icebreaking by compliant structures such as slender light-houses. "SPLICE" and "Milano," assume continuous-mode icebreaking by a ship hull to be periodic and deterministic. Both are based on assumed cycles of icebreaking with frequency V/ℓ_b. Mueller and Ettema (1984) found that, as an approximation, the dynamic behavior of a hull during icebreaking can be described in terms of the ratio of the frequency V/ℓ_c (c.f., $\omega_i = V_i/\ell_b$ (II-10)) to the hull's natural frequencies of pitch and heave. For the model-scale hull the natural frequencies of pitch and heave have about the same value, ω_n. In simple terms, for a hull moving at speed V through an

ice sheet of characteristic length ℓ_c, the mean spacing between consecutive icebreaking events, or flexural cracks, is proportional to ℓ_c, consequently, the frequency V/ℓ_c should be a measure of the dominant frequency of ice forces.

By using the frequency ratio $V/(\omega_n \ell_c)$, Mueller and Ettema attempt to assess and explain the relative importance of forces resulting from hull motions. They suggest that, at relatively low speeds, $V/(\omega_n \ell_c) << 1$, buoyancy forces related to change in hull displacement are responsible for icebreaking; inertia forces being negligible. If $V/(\omega_n \ell_c) = 1$, the hull is in state of resonance. As buoyancy-related forces are 180-degrees out of phase with inertia-related forces, they counteract one another. When this occurs, one might expect the hull to experience additional resistance because it is not operating as effectively as it could. At relatively high speeds, $V/(\omega_n \ell_c) >> 1$, the inertia forces of the hull become of important magnitude and are responsible for icebreaking.

Voelker et al. (1985) report results of full-scale performance tests with the USCGC POLAR-Class ship "POLAR STAR." The tests were aimed at determining the magnitude and distribution of level-ice resistance and motions as a function of speed and thickness. The tests were also conducted to measure icebreaking pattern and cusp size. Spectral analyses of resistance and motions show them to be essentially stochastic. Voelker et al. report that, under certain conditions, a significant energy peak occurred at $V/(\omega_n \ell_c) = 0.6$, for resistance and for all motions. They attribute this value to the fact that observed breaking lengths averaged about $0.6\ell_c$. However, they appear to have erroneously multiplied $V/(\omega_n \ell_c)$ by 0.6 instead of dividing by 0.6. The corrected frequency ratio is about 1.67. If $V/(\omega_n \ell_c)$ is rewritten as $V/(\omega_n \ell_b)$ then the peak reported by Voelker et al. occur at $V/(\omega_n \ell_c)$ approximately equal to 1.0, so a resonance condition was developed.

The results of the full-scale tests performed by Voelker et al. are discussed further and compared in Chapter VIII with the results forthcoming from the present study. The field data obtained by Voelker et al. require further analysis.

III. EXPERIMENTS

Two series of experiments were conducted using an ice towing tank and a model hull instrumented for measurement of ice resistance, ice-induced forces and hull motions (displacements as well as accelerations). For one series, the hull was free to heave and pitch, as well as to undergo limited roll and yaw. For the other series, the hull was restrained, or fixed, from heaving and pitching.

An additional set of experiments was performed in order to determine the hydrodynamic coefficients associated with motions of the hull as it moved through ice-covered water.

A. The Model Icebreaker Hull and Ice Towing Tank

A 1:48-scale, 2.53m long model of a USCGC POLAR-Class hull (WAGB10), on loan from the U.S. Coast Guard, was used for the experiments. The abbreviated lines of a POLAR-Class hull are given in Figure 4, together with a photograph of the model hull. The principal dimensions of the model hull are listed in Table 1.

The hull was ballasted with a mass of 102.6kg so that its center of gravity was located, to within a tolerance of 0.014m, at its longitudinal center of buoyancy. The area of the waterplane (the plan area of the hull at its waterline), A_{wp}, the waterplane moment, M_{wp}, and the waterplane moment of inertia, I_{wp}, were determined from the hull offsets by integration. The moment of inertia of the model was calculated after suspending the hull as a pendulum and applying the equation of the radial frequency of oscillation with all the other parameters known.

The hull was coated with epoxy paint so as to have a comparatively smooth finish. The coefficient of dynamic friction, μ_d, between the ice and the model was determined experimentally to be 0.10 (c.f., (II-5), in which $\mu_d = 0.20$), for the range of ice pressures exerted against it. In order to obtain μ_d, a block of urea ice was placed on the underside of the hull, which had previously been levelled. The block was loaded with a normal force, P_N, of 14.8N, and then pulled, by means of a force gauge, along the hull at a speed of about 0.01m/s. The pulling force, T, was recorded and μ_d was calculated as

$$\mu_d = T/P_N \qquad \text{(III-1)}$$

The hull was towed through a 20m long, 5m wide and 1.3m deep ice towing tank. The tank is housed in a refrigerated laboratory, as can be seen from the schematic layout of it, shown in Figure 5. A 5m wide by 2.4m long motorized carriage was used to tow the model. The tank has a central trench that is fitted with an underwater video camera for viewing icebreaking and ice passage beneath a towed hull. The camera can be towed beneath the hull. The voltages from intrumentation attached to the model and the towing carriage were scanned and digitized using a digital voltmeter, then transmitted to a HP-A1000 minicomputer for storage on computer disk for later analysis.

B. Instrumentation

Two sets of intrumentation were used for the experiments: one set for measuring the resistance and motions experienced by the hull when it was free to pitch and heave; and, another set to measure resistance and restraining forces and moments when it was restrained from motions.

1. Free Hull. The hull configured so that it could pitch, heave and undergo limited roll and yaw is herein referred to as the free hull. In this configuration, as depicted in Figure 6a, the model was connected by means of a 25mm diameter shaft to a dynamometer supported from the towing carriage. The shaft was connected to a vertical plate of the dynamometer by way of two ball-bushings which enabled it, and thereby the hull, to move without vertical restraint. The shaft was hinged to the base of the hull by way of a universal ball-joint so that the hull could pitch, roll and yaw without restraint.

A 200N Statham UL4-50 load cell coupled to a Statham UC-3 force transducer was used to measure resistance force, f_x.

Yawing and rolling of the hull were restricted by the use of a vertical guide rod, 10mm in diameter, located at its stern. The guide rod was constrained to a slot formed by two horizontal circular rods separated 80mm apart. In the course of conducting the experiments it was determined that roll significantly affects icebreaking resistance. Therefore, during several experiments, roll, ϕ, was measured using a helipotentiometer and a cable

attached to one side of the hull's midsection. The helipotentiometer's full stroke of 227mm corresponded to 1.05volts.

Pitch rotation and heave displacements, θ and z, were measured by means of linear-voltage-displacement-potentiometers (LVDT's) located on plates placed 2m apart on the hull. The full, 0.15m stroke of each LVDT corresponded to 12volts. The output of the LVDT's were transmitted to the digitizing voltmeter by means of two voltage followers.

Pitch and heave accelerations, $\ddot{\theta}$ and $\ddot{z}$, were determined using accelerometers mounted on the bow and stern. The first 12 tests involved the use of accelerometers comprised of a 22N UL4-5 Statham load cell loaded with a mass of 0.740kg in order to sensitize it to vertical accelerations. In the remaining experiments, which include all the higher speeds, two 2-g ($19.6m/s^2$) KYOWA ASQ-2BL accelerometers were used.

Each channel, connected to the corresponding instrument of measure, was digitized at a rate of 10Hz (10 readings per second) for speeds ranging from 0.05 to 0.25m/s, and at a rate of 20Hz for speeds of 0.5 and 0.9m/s.

2. Fixed Hull. A parallel series of tests was conducted with the hull connected directly to, and restrained by, a four-component load cell, as depicted in Figure 6b. The hull configured so that it could not move (i.e., pitch, heave, roll, etc.) is hereafter referred to as the fixed hull. The horizontal and vertical restraining forces, f_x and f_z, and the pitch and yaw restraining moments, m_θ and m_ψ, experienced by the fixed hull were measured using a 196N and 98Nm NISHO DENKI LMC-4107-20 load cell.

Voltages from each load-cell channel were digitized at a rate of 10Hz for all the experiments conducted with the fixed hull.

3. Calibration of Transducers. Before each experiment, the sensitivity and zero level of each transducer were determined.

The sensitivity of the dynamometer, used for towing the free hull, was measured by exerting known horizontal loads against the hull. The calibration value for each of the experiments are provided in Table 2. The sensitivities of the accelerometers used in the first twelve tests were determined by measuring the change in output voltage, Δv, due to an applied load increment, ΔF; the corresponding sensitivity was equal to $\Delta F/(Ma\Delta v)$, in which Ma was the

mass suspended in the accelerometer. The sensitivities of the KYOWA ASQ-2BL accelerometers were electronically set at either 0.06g/volts or 0.6g/volts as indicated in Table 2. The sensitivity of the LVDT's, reckoned to be 13.0 mm/volt, were measured as the ratio of a change in length to a change in output voltage.

The sensitivity and zero level of each channel of the four-component load cell were determined prior to each experiment with the fixed hull. The sensitivities of all channels were measured by means of loads applied at different locations of the hull in order to obtain the respective force or moment output voltage ratio. Values of transducer sensitivities for each experiment are summarized in Table 3.

Table 4 is a list of the experimental errors corresponding to each measured parameter. It is also important to mention that measurement of heave and pitch displacements, by means of 2 LVDT's only, involved error due to roll and yaw motions of the hull.

C. Model Ice Sheets

Ice sheets were grown from a 0.7-percent, by weight, urea solution in accordance with the following procedure. The solution was cooled to a temperature of -0.1C while the room was simultaneously cooled to about -15C. A system of water jets provided the necessary mixing and agitation of the solution to prevent the growth of unwanted ice. Before being wet-seeded, the surface of the urea solution was screened to remove any floating ice. Then, the water jets and the refrigeration units were stopped and the refrigerated laboratory was fogged with a spray of fine ice crystals. Wet-seeding prevented the formation of relatively large ice crystals, enabling a multitude of small crystals to grow simultaneously over the surface of the urea solution.

Each ice sheet was grown to about 80% of its required thickness, h. The air temperature 0.10m above the ice sheet was then raised to about 2°C so that the ice sheet warmed and weakened. During this phase, the ice-sheet growth decelerated and the sheet attained the requisite thickness. The flexural strength, σ_f, and the flexural elastic modulus, E, were monitored until flexural strength reached the value prescribed for the experiment. For most experiments σ_f = 20 to 25kPa. A few additional experiments were conducted with σ_f = 29 and 40kPa.

The force, f, to flexurally fail a cantilever beam of length ℓ, width d and thickness h, was used to estimate the flexural strength, σ_f, of each ice sheet as (e.g., Schwarz, 1983);

$$\sigma_f = \frac{6f\ell}{dh^2} \qquad \text{(III-2)}$$

The monitored ice sheet was not always perfectly uniform, slight variations in thickness and flexural strength occurred along its length. Uniformity errors were always within ± 5% of specified mean values for an entire sheet.

Three to four cantiliver beams were failed in order to determine, at regular periods, the flexural strength. The flexural elastic modulus, E, was determined by measuring the increment, δ, of the vertical deflection of the ice sheet due to small increments of a point load, P, at the center of the ice sheet:

$$E = 0.1875 \frac{(1-\nu^2)}{\rho g h^3} \frac{P^2}{\delta^2} \qquad \text{(III-3)}$$

Note that, here, ρ is the density of the urea solution. The characteristic length, ℓ_c, of each ice sheet was then calculated using (III-3) and (II-1).

D. Experimental Program

A series of openwater tests were performed to determine the mean values of the hull's openwater resistance, $\overline{f}_{xo}$, as a function of speed. The resistance force $\overline{f}_{xo}$ and the resistance coefficient C are listed in Table 5 together with Froude number, $V/\sqrt{gL_s}$, and Reynolds number, VL_s/ν_k, for each test run. The coefficient C is identified as

$$C = \frac{\overline{f}_{xo}}{0.5\rho V^2 S} \qquad \text{(III-5)}$$

where S = the wetted area of the hull; ν_k = kinematic viscosity of urea solution at 0°C; and L_s = hull length. As shown subsequently, values of $\overline{f}_{xo}$ are quite small compared with mean values of ice resistance, $\overline{f}_x$.

Oscillation tests were conducted in order to determine natural frequencies of heave, pitch and roll motions of the hull in openwater. Tests were also conducted with the hull in the middle of the track that it had just broken in order to determine natural frequencies as well as added-mass and damping coefficients associated with hull motions in ice-covered water. The results of these tests are discussed further in Sections IV.B and IV.C.

Fifty experiments were conducted with full-length (21m long) sheets of urea ice. Of these experiments, 33 were performed with the free hull and the remaining 17 were performed with the fixed hull. Details of the experiments are summarized in Tables 6 and 7 for the free- and fixed-hull conditions, respectively. The ranges of thickness, speed and flexural strength tested are: 8.5 to 43mm, 0.05 to 0.9m/s, and 18 to 40kPa, respectively.

In order to assess the relative magnitude of ice resistance that is attributable to shearing and crushing of ice at the bow stem of a POLAR-Class hull, an additional experiment was performed with half an ice sheet precut with a central slot cut along the transit path to be followed by the hull. The slot was 40mm wide (about 10% of the model-hull beam) and it extended half the length of a 31mm thick ice sheet. The remaining half of the ice sheet was left uncut so that the resistance could be compared. Speed for this experiment was 0.25m/s.

E. Experimental Procedure

Prior to each experiment, the hull was launched and held for transducer calibration while the ice sheet was warmed and weakened to a prescribed flexural strength, which for most experiments was 20 to 25kPa. When the ice sheet attained the prescribed strength, the hull was towed at steady speed for 16m (about 6.5 hull lengths) of the ice sheet, or 80% of the tank's length. The remaining 20% of the tank's length was used for accelerating and decelerating the hull.

The transit of the hull was recorded on video tape using video cameras located both underwater and above ice. The cameras moved with the towing carriage. On completing a transit, photographs were used to record icebreaking patterns, and the dimensions of ice cusps comprising the icebreaking patterns in the channel were measured using calipers.

IV. EQUATIONS OF MOTION

Consider an icebreaker hull transitting an ice sheet in continuous-mode icebreaking. Hull speed as well as the ice-sheet properties (thickness, strength, etc.) are assumed constant. Ice loads exerted against the hull as well as hull motions are stochastic. Under certain conditions motions are of sufficient amplitude that nonlinear effects are important. However, as a first approximation and to provide a framework for discussion, hull motions are assumed to be linear such that the linear superposition principle is applicable. That is, the response at a given frequency depends only on the excitation at that frequency.

In Section IV.A of this chapter, the linear equations of motion for a single frequency are presented and discussed. In Section IV.B, attention is focused on heave and pitch, and through the use of experimentally obtained added-mass and damping coefficients their natural frequencies are obtained. Next, in Section IV.C, the influence on resistance of roll is briefly discussed. Lastly, in Section IV.D, the superposition principle and spectral analysis are used to obtain general relationships between hull motions and external (ice) forces, or excitations.

A. General Equations of Motion

Let (X,Y,Z) be a right-handed coordinate system fixed with respect to the mean position of the ship with Z vertically upward, X in the direction of forward motion, and the origin at the hull's center of gravity. Under the assumptions that the responses are linear and harmonic, six linear coupled differential equations of motion can be written, using subscript notation, in the following form

$$(M_{ij} + A_{ij})\,\ddot{q}_j + B_{ij}\dot{q}_j + C_{ij}q_j = f_j \qquad \text{(IV-1)}$$

where $q_j = (x(t), y(t), z(t), \phi(t), \theta(t), \psi(t))$ are the responses corresponding to surge, sway, heave, roll, pitch and yaw, respectively; M_{ij} is the generalized-mass matrix; A_{ij} and B_{ij} are the added-mass and damping coefficients, respectively; C_{ij} are the hydrostatic-restoring coefficients; and f_j =

(f_x, f_y, f_z, m_ϕ, m_θ, m_ψ) are the excitation forces and moments. The coordinate system and translatory and angular displacements are shown in Figure 8.

If it is assumed that the ship has lateral symmetry, then the generalized-mass matrix is given by

$$M_{ij} = \begin{bmatrix} M & 0 & 0 & 0 & 0 & 0 \\ 0 & M & 0 & 0 & 0 & 0 \\ 0 & 0 & M & 0 & 0 & 0 \\ 0 & 0 & 0 & I_{xx} & 0 & -I_{xz} \\ 0 & 0 & 0 & 0^{xx} & I_{yy} & 0^{xz} \\ 0 & 0 & 0 & -I_{xz} & 0^{yy} & I_{zz} \end{bmatrix} \qquad \text{(IV-2)}$$

where M is the mass of the ship, I_{ii} is the moment of inertia in the ith mode, and I_{ij} is the product of inertia. The inertia terms are with respect to the coordinate system shown in Figure 8. The only product of inertia that appears is I_{xz}, the roll-yaw product which is zero if the hull is symmetrical with respect to midships and is otherwise small.

If in addition to geometric lateral symmetry, it is also assumed that the loading is laterally symmetric, then the added-mass (or damping) coefficients are

$$A_{ij} \text{ (or } B_{ij}) = \begin{bmatrix} A_{11} & 0 & A_{13} & 0 & A_{15} & 0 \\ 0^{11} & A_{22} & 0^{13} & A_{24} & 0^{15} & A_{26} \\ A_{31} & 0^{22} & A_{33} & 0^{24} & A_{35} & 0^{26} \\ 0^{31} & A_{42} & 0^{33} & A_{44} & 0^{35} & A_{46} \\ A_{51} & 0^{42} & A_{53} & 0^{44} & A_{55} & 0^{46} \\ 0^{51} & A_{62} & 0^{53} & A_{64} & 0^{55} & A_{66} \end{bmatrix} \qquad \text{(IV-3)}$$

As is shown subsequently, the assumption of lateral symmetry leads to the uncoupling of the equations of motion for surge, heave and pitch from those of sway, roll and yaw. For a hull in openwater, the hydrodynamic loading is, in fact, laterally symmetric. For a hull moving through an ice sheet, the distributions of ice loads at any instant are not necessarily symmetric with respect to the hull's centerplane. This means that A_{ij} and B_{ij} are full matrices resulting in complete coupling between all six modes of motion. However, as an approximation, it is assumed that (IV-3) are also valid for a hull moving through an ice sheet.

Lastly, the only nonzero hydrostatic restoring coefficients are:

$$\begin{aligned} C_{33} &= \rho g A_{wp} \\ C_{55} &= \rho g I_{wp} \\ C_{35} &= C_{53} = -\rho g M_{wp} \end{aligned} \qquad \text{(IV-4)}$$

in which A_{wp}, M_{wp}, and I_{wp} are the area, moment, and moment of inertia of the waterplane, respectively. The values of these coefficients were determined for the hull to be 7950N/m, 2450Nm and -7.18N, respectively.

If the generalized-mass matrix, (IV-2), the added-mass and damping coefficients, (IV-3), and hydrostatic restoring coefficients, (IV-4), are substituted in the equations of motion, (IV-1), it is seen that the six coupled equations of motion, (IV-1), reduce to two sets of equations: one set of three coupled equations for surge, heave and pitch and another set for sway, roll, and yaw. Herein, we are primary concerned with the former. However, during the present study roll was found under certain conditions to be significant and played an important role in the dynamics of icebreaking. Roll is discussed in Section IV.C.

B. Pitch and Heave Motions

The experiments involved a hull that was towed at constant speed such that $\ddot{x} = x = 0$; reference frame is attached to the hull, as per Figure 8. Consequently, the pitch and heave equations of motion have the form:

$$\begin{bmatrix} M+A_{33} & A_{35} \\ A_{53} & I+A_{55} \end{bmatrix} \begin{Vmatrix} \ddot{z} \\ \ddot{\theta} \end{Vmatrix} + \begin{bmatrix} B_{33} & B_{35} \\ B_{53} & B_{55} \end{bmatrix} \begin{Vmatrix} z \\ \theta \end{Vmatrix} + \begin{bmatrix} C_{33} & C_{35} \\ C_{53} & C_{55} \end{bmatrix} \begin{Vmatrix} z \\ \theta \end{Vmatrix} = \begin{bmatrix} f_z(t) \\ m_y(t) \end{bmatrix} \qquad \text{(IV-5)}$$

The solution to (IV-5) for harmonic motions and excitations, i.e.

$$\begin{aligned} q_j &= \tilde{q}_j(\omega)\, e^{i\omega t} \\ f_j &= \tilde{f}_j(\omega)\, e^{i\omega t} \end{aligned} \qquad \text{(IV-6)}$$

is well known (e.g., Meirovitch, 1975), and is generally written as

$$\tilde{q}_j(\omega) = H_{ij}(\omega)\tilde{f}_j(\omega) \qquad \text{(IV-7)}$$

where $\tilde{q}_j$ and $\tilde{f}_j$ are the complex motion and excitation amplitudes, respectively, and H_{ij} is the transfer function defined as

$$H_{ij} = \begin{bmatrix} -\omega^2(M+A_{33}) + B_{33}\omega i + C_{33} & -\omega^2 A_{35} + B_{35}\omega i + C_{35} \\ -\omega^2 A_{53} + B_{53}\omega i + C_{53} & -\omega^2(I+A_{55}) + B_{55}\omega i + C_{55} \end{bmatrix}^{-1} \qquad \text{(IV-8)}$$

When the hull was free to pitch and heave, $\tilde{q}_j(\omega)$ is known because the hull's heave and pitch were measured. In order to determine the external forces causing the motions, it is necessary to determine the excitations. This is accomplished by inverting (IV-7), i.e.

$$\tilde{f}_j(\omega) = H_{ij}^{-1}(\omega)\,\tilde{q}_j(\omega) \qquad \text{(IV-9)}$$

which can be solved if the transfer function H_{ij}, (IV-8), is known. The terms in H_{ij} depend on ω, A_{ij}, B_{ij} and C_{ij}. Generally, the former and the latter are known, however, the added mass, A_{ij}, and damping, B_{ij}, must be determined.

For a hull in openwater, potential flow methods are available for predicting A_{ij} and B_{ij}. Little is known, and no theory is available, for predicting the influences of ice-sheet presence on A_{ij} and B_{ij}. The influences are likely large because the surrounding ice sheet and distribution of ice pieces near the hull strongly influence the flow field, including the wave pattern produced by the hull. Therefore, in the present study, as is discussed next, the added-mass and damping coefficients were determined experimentally.

1. Experimental Values of Added-Mass and Damping Coefficients. A series of experiments was conducted in order to determine the added-mass and damping coefficients associated with hull motions during icebreaking. Generally, the Froude number, $F_n(= V/\sqrt{gL_s})$, for an icebreaker hull is quite small, typically less than about 0.19, and for the openwater condition, zero-speed added-mass and damping coefficients are a good approximation. Herein, the zero-speed added-mass and damping coefficients are used, however, it should be recognized that the influence of forward speed, even for small F_n, for the ice-covered condition may be significant. Ice-sheet thickness is another factor influencing the added-mass and damping coefficients.

Three experiments were performed: (1) the hull was restrained from heaving and the bow was displaced downwards such that the hull oscillated in pitch only; (2) the hull was restrained from pitching and displaced downwards such that the hull oscillated in heave only; and, (3) the hull was unrestrained and displaced such that it both heaved and pitched. The tests were conducted for two thicknesses, h = 30 and 38mm, and were performed when the hull was amidst, and overrode, broken ice, in a track opened after a resistance experiment.

For each experiment, the pertinent hull motion was measured and expressed as

$$q_j(t) = \tilde{q}_j e^{s_j t} \qquad \text{(IV-10)}$$

in which $\tilde{q}_j$ is the amplitude and

$$s_j = \xi + i\omega$$

with ξ = damping rate, and ω = frequency of oscillation. The values of ξ and ω determined from these experiments are summarized in Table 8. Combining (IV-10) and (IV-5) for each of the three test conditions enables evaluation of the coefficients A_{55}, B_{55}, A_{33}, B_{33}, A_{35} ($=A_{53}$), and B_{35} ($=B_{53}$). The values determined for these coefficients are summarized in Table 9. Also shown for comparison in Table 9 are the openwater values predicted using Lewis forms for A_{33}, A_{35}, A_{55} and obtained from "SPLICE." As might be expected, it can be seen from Table 9 that the presence of an ice sheet significantly increases both the added-mass and damping coefficients associated with pitch and heave. Consequently, as discussed next, the hull's natural frequencies of pitch and heave decreased.

2. Natural Frequencies. With known added-mass and damping coefficients, the natural frequencies for coupled heave and pitch can be determined through the solution of the characteristic equation associated with (IV-5); i.e.

$$\begin{vmatrix} (M+A_{33})s^2 + B_{33}s + C_{33} & A_{35}s^2 + B_{35}s + C_{35} \\ A_{35}s^2 + B_{35}s + C_{35} & (I+A_{55})s^2 + B_{55}s + C_{55} \end{vmatrix} = 0 \qquad \text{(IV-11)}$$

The solutions to (IV-11) are complex; the real part is associated with the damping rate, and the imaginary part with the natural frequencies of hull motions. Table 10 is a summary of the natural frequencies computed for coupled pitch and heave motions. Also, included in Table 10 for comparison are the natural frequencies for the undamped system (i.e., $B_{35} = B_{33} = B_{55} = 0$) and also those both calculated and measured for the openwater condition. The calculated openwater values were obtained using the Lewis form added-mass coefficients, and do not include the effects of damping. The measured openwater values were obtained from openwater experiments performed for conditions (1) and (2) described in Section IV.B.1. It is evident from Tables 8 and 10 that the natural frequencies for hull motions during continuous-mode icebreaking are substantially lower than those for openwater. For the present study the natural frequencies of pitch and heave, during continuous-mode icebreaking, are estimated to be 0.83 and 0.68, respectively. Herein, these frequencies are lumped together as $\omega_n \simeq 0.7$ to 0.9.

C. Roll Motion

During continuous-mode icebreaking, ice loads are not always symmetrical with respect to the hull centerplane because icebreaking may not always occur simultaneously around the bow. This induces nonsymmetric responses; i.e., roll, sway and yaw. The equations governing these coupled motions can be readily derived using (IV-1), in a similar manner as for coupled pitch, heave and surge. The hull used in the experiments was instrumented such that sway was restrained completely and yaw was confined within small margins, but not measured, and only roll was measured in several test to determine its influence on the icebreaking mechanisms. Initially, measurements of roll were not planned. However, during the course of the experiments, under certain conditions, large amplitude roll motions were observed. As roll no doubt plays an important roll in resistance, it was decided that some limited measurements of it should be made.

As an aid in identifying frequencies related to roll, the zero speed openwater natural frequency of roll was experimentaly obtained to be 0.45Hz. The hull was placed in position and rotated such that the hull oscillated in roll only. The influences on roll frequency of ice and limited yaw moment were not determined.

D. Spectral Analysis

During continuous-mode icebreaking, the forces and moments experienced by the model hull and resulting hull motions are stochastic. A similar situation occurs for ship motions in a seaway with random waves for which a well-developed theory exits (Price and Bishop, 1974). Stochastic records, and, therefore, records of ice resistance and hull motions, are appropiately analyzed through the use of statistical theory and are most conveniently described in terms of their frequency content. In the following, the necessary developments for such spectral analyses are described.

1. General Theory. From the outset it is assumed that the temporal records of ice-related forces and moments, as well as resulting motions, are both stationary and ergodic processes. The former implies that the statistics of the signal are not time-dependent, and the latter that a single measured realization is representative of all other possible realizations. The assumption of ergodicity permits the interchange of a function's expected value with its temporal average. Thus, with x(t) representing either a force, moment, or motion signal, the mean value of x(t) is

$$\overline{x} = \underset{T \to \infty}{\text{Limit}} \left\{ \frac{1}{T} \int_{-T/2}^{T/2} x(t)dt \right\} \qquad \text{(IV-12)}$$

The standard deviation, which characterizes the spread of the values of x(t) about the mean $\overline{x}$, is defined as

$$\sigma_x = \left[\underset{T \to \infty}{\text{Limit}} \left\{ \frac{1}{T} \int_{-T/2}^{T/2} (x(t)-\overline{x})^2 dt \right\} \right]^{0.5} \qquad \text{(IV-13)}$$

In order to deduce further detailed information concerning the manner in which x(t) varies with time it is necessary to compute the frequency content of x(t). For this purpose, x(t) is adjusted to have zero mean and its definition is extended for all time as

$$x(t) = \begin{cases} x(t) - \overline{x} & \text{for } 0<t<T \\ 0 & \text{otherwise} \end{cases} \qquad \text{(IV-14)}$$

The latter permits the definition of the Fourier transform pair

$$x(t) = \int_{-\infty}^{\infty} X(\omega)\, e^{i2\pi\omega t} d\omega \qquad \text{(IV-15)}$$

$$X(\omega) = \int_{-\infty}^{\infty} x(t)\, e^{-i2\pi\omega t} dt \qquad \text{(IV-16)}$$

It is possible to express the variance of the original record x(t) in terms of $X(\omega)$ as

$$\sigma_x^2 = \int_0^{\infty} \underset{T \to \infty}{\text{Limit}} \left\{\frac{2}{T} |X(\omega)|^2\right\} d\omega \qquad \text{(IV-17)}$$

which formally defines the spectral density

$$S_x(\omega) = \underset{T \to \infty}{\text{Limit}} \left\{\frac{2}{T}|X(\omega)|^2\right\} \qquad \text{(IV-18)}$$

With reference to (IV-17) and (IV-18), it is seen that $S_x(\omega)d\omega$ represents the contribution to the variance (or "energy") of the record x(t) due to its content within the frequency range ω to $\omega+d\omega$. The spectral density, $S_x(\omega)$, essentially enables a signal to be represented in the frequency domain rather than the time domain. Stochastic signals are characterized by their spectral density distributions as either broad or narrow banded, as depicted in Figure 8.

In order to relate spectral densities of hull motions and corresponding forces, or excitations, it is necessary to introduce in the equations of motion, (IV-5), the Fourier transforms of the hull's motions and the excitations (ice forces) exerted against it. The transforms are

$$\begin{aligned} q_j(t) &= \int_{-\infty}^{\infty} Q_j(\omega)\, e^{i2\pi\omega t} d\omega \\ f_j(t) &= \int_{-\infty}^{\infty} F_j(\omega)\, e^{i2\pi\omega t} d\omega \end{aligned} \qquad \text{(IV-19)}$$

in which $Q_j(\omega)$ and $F_j(\omega)$ are vectors representing the Fourier transforms of motions and excitations, respectively. Therefore, (IV-9) can be rewritten as

$$F_j(\omega) = H_{ij}^{-1}(\omega) Q_j(\omega) \qquad \text{(IV-20)}$$

where $H_{ij}^{-1}(\omega)$ is the transfer function (IV-8). The spectral density matrix, $S_{ij}(\omega)$, of a random vector $x_j(t)$ can be defined as

$$S_{ij}(\omega) = \underset{T \to \infty}{\text{Limit}} \left\{\frac{2}{T} X_i^*(\omega)\, X_j(\omega)\right\} \qquad \text{(IV-21)}$$

in which $X_i^*(\omega)$ is the conjugate of $X_i(\omega)$.

Equation (IV-21) can be applied to the motion and excitation vectors of (IV-19) such that

$$S_{ij}^F(\omega) = \underset{T \to \infty}{\text{Limit}} \left\{\frac{2}{T} F_i^*(\omega)\, F_j(\omega)\right\} \qquad \text{(IV-22)}$$

$$S_{ij}^Q(\omega) = \underset{T \to \infty}{\text{Limit}} \left\{\frac{2}{T} Q_i^*(\omega)\, Q_j(\omega)\right\} \qquad \text{(IV-23)}$$

where $S_{ij}^F(\omega)$ and $S_{ij}^Q(\omega)$ are the spectral density matrices of the hull excitation and motion vectors, respectively. Inserting (IV-20) into (IV-22) and using (IV-23), leads to

$$S_{ij}^F(\omega) = H_{ij}^{-1^*}(\omega)\, S_{ij}^Q(\omega) H_{ij}^{-1^T}(\omega) \qquad \text{(IV-24)}$$

in which the superscript T denotes the transpose of $H_{ij}^{-1}(\omega)$. For pitch and heave motions, (IV-24) can be written as

$$\begin{bmatrix} H'_{11} & H'_{12} \\ H'_{21} & H'_{22} \end{bmatrix}^* \begin{bmatrix} S_{zz} & S_{z\theta} \\ S_{\theta z} & S_{\theta\theta} \end{bmatrix} \begin{bmatrix} H'_{11} & H'_{12} \\ H'_{21} & H'_{22} \end{bmatrix}^T = \begin{bmatrix} S_{F_zF_z} & S_{F_zM_\theta} \\ S_{M_\theta F_z} & S_{M_\theta M_\theta} \end{bmatrix} \qquad \text{(IV-25)}$$

in which $H'_{ij} = H_{ij}^{-1}$ and the superscript on S has been dropped. If the transfer function and the spectral density matrix for pitch and heave are known, then the spectral density matrix of the pitch and heave excitations can be computed by means of (IV-25).

2. Numerical Analysis. In order to perform the statistical and spectral analyses of the time-histories of experimental data, the following numerical scheme was used to obtain the required values of mean, standard deviation and spectral density functions of the measured motions, forces and moments.

Values of the mean, $\bar{x}$, and standard deviation, σ_x, of each time series x(t) of record T and sample rate ω_s were calculated as

$$\bar{x} = \frac{1}{T\omega_s} \sum_{n=1}^{T\omega_s} x(n/\omega_s) \qquad \text{(IV-26)}$$

and

$$\sigma_x = \left\{ \frac{1}{T\omega_s} \sum_{n=1}^{T\omega_s} (x(n/\omega_s)-\bar{x})^2 \right\}^{0.5} \qquad \text{(IV-27)}$$

Calculation of spectral densities involved the ensuing steps. The time series were divided into N segments each with M samples or segment period $T_s = M/\omega_s$. For each segment, a Fourier series was calculated with a resolution bandwith $D\omega_s = 1/T_s$. Frequency leakage was reduced by subtracting the time mean from the records.

Each tapered segment $x_s(t)$ of the signal was then estimated as

$$x_s(t) = \sum_{n=-M/2}^{n=M/2} \frac{1}{T_s} X_s\,(nD\omega_s)\, \exp\,(i2\pi nD\omega_s t) \qquad \text{(IV-28)}$$

in which $X_s\,(nD\omega_s)$ is the Fourier transform at $(nD\omega_s)$ and

$$X_s(nD\omega_s) = \int_0^{T_s} x_s(t)\, \exp(-i2\pi nD\omega_s t)dt \qquad \text{(IV-29)}$$

The discrete Fourier transforms were computed using the Fast Fourier Transform algorithm developed by Stanley (1975). The summation over the range [-M/2, +M/2] is sufficient as $x_s(t)$ was filtered at $\omega_s/2$ prior to the analog to digital conversion of the data. The complex number $(1/T_s)\, X_s(nD\omega_s)$ describes the amplitude and the phase of the oscillator at the frequency $(nD\omega_s)$.

The two-sided spectral density $S_{ij}(nD\omega_s)$ is estimated as

$$S_{ij}(nD\omega_s) = \frac{1}{NT_s} \sum_{s=1}^{N} (X^*_{ij})_s(nD\omega_s)\, (X_{ij})_s(nD\omega_s) \qquad \text{(IV-30)}$$

and $S_{ij}(nD\omega_s)$ is the density of the power in the frequency space; it infers the contribution of the frequency interval $[n-1/2)D\omega_s,\ (n+1/2)D\omega_s]$ to the mean square value

$$\overline{(x(t) - \bar{x})^2} = 2 \sum_{n=1}^{M/2} S_{ij}(nD\omega_s)D\omega_s$$

V. ICEBREAKING PATTERNS

A. Observations

For the free hull, continuous-mode icebreaking began with the bow depressing and nosing onto the ice sheet, which increased the hull's pitch and heave displacements. Simultaneously, the hull encountered increased resistance, as ice crushed and sheared at its bow stem, and, sequentially, ice was flexurally broken around either side of its bow. After each flexural icebreaking event, resistance, as well as pitch and heave momentarily decreased. Only when a pattern of broken ice was sufficiently wide so as to create a track into which the hull could settle, did resistance as well as pitch and heave displacements decrease significantly. This description of icebreaking encapsulates the interdependence, and the intrinsically cyclic nature of ice resistance, hull motions and icebreaking pattern. Moreover, it indicates the potential for two important frequencies in resistance and hull motions; namely, icebreaking frequency and track-opening, or opening, frequency. The fixed hull, being restrained from motions, thrust through the ice sheet, deflecting and breaking it.

If the free hull, or the fixed hull, was moving with creeping speed, V = 0.05m/s (Figure 9a), the depressed ice sheet would be flooded prior to flexural failure. With increasing speed, the time available for flooding would diminish such that, for moderate and higher speeds, say V = 0.5m/s (Figure 9b), there was insufficient time for the depressed ice sheet to flood. For these speeds, the hull depressed both the sheet and the water level around the bow.

A pattern of icebreaking was initiated when a circumferential crack developed more-or-less parallel to the waterline along one side of the hull's bow. The crack then propagated by arcing circumferentially toward the bow's stem and shoulder. A major circumferential crack would develop either side of the bow, but not always simultaneously. Generally, the length of the arced,

or cuspate, circumferential crack was approximately equal to the waterline distance from the bow's stem to its shoulder, for the condition of hull trim when the crack is formed. The length of the circumferential crack varied slightly with ice-sheet thickness and strength, and with speed. If a cusp was narrower than the hull's half beam, the hull broke additional wedges from the ice sheet such that, eventually a full track width was broken through the sheet. Track width was usually 1.1 to 1.2 times the hull beam, B.

Generally, icebreaking patterns were comprised of cusps, that arced from the model's bow stem to its shoulder. The icebreaking pattern was of herring-bone form. On being overridden by the bow, the cusps were further broken to form a pattern of smaller cusps and wedges. Figure 10 illustrates the ice-breaking pattern under the bow for a 30mm thick, 25kPa, ice sheet. The pattern as observed via the underwater television camera is shown in Figure 11. Figures 10 and 11 appear to present a different pattern of icebreaking than that which is depicted in Figure 2 for a full-scale POLAR-Class hull (see Section II.B).

Two causes may explain the difference observed for the model- and full-scale icebreaking patterns. One is that deck-level observers cannot adequately see icebreaking beneath the bow during full-scale icebreaking. If the icebreaking pattern were viewed by an observer standing at deck-level, it would look as depicted in Figure 12. Instead of appearing as herring-bone cusps, icebreaking pattern around the waterline would seem to comprise a mosaic of several smaller cusps. Figure 12 is similar to the pattern shown in Figure 2. We believe this to be the more likely cause.

A second cause is attributable to urea model ice, which, at 20 to 25kPa flexural strength, is less brittle than ice at a comparable full-scale strength. Mis-scaling of brittleness may translate to mis-scaling of the speed at which a flexural crack propagates relative to hull speed; reduced brittleness resulting in slower crack propagation and, thereby larger ice cusps. The relative speed of crack propagation and hull transit influences the form of the major cusp formed at each side of the hull's bow because loading geometry changes as a cusp forms. At times, the major cusp may develop a lobe near the bow stem as shown in Figure 13.

Increasing amplitude and frequency of hull motions led to decreasing regularity and uniformity of icebreaking pattern. Figure 14a-d displays photographs of breaking pattern resulting from the free- and fixed-hull conditions for 30mm thick ice sheets and speeds of 0.05 to 0.9m/s, respectively. Although values of cusp width, W, were approximately the same (discussed further in Section V.B), the facility of the free hull to move resulted in a greater standard deviation of ice rubble sizes in the track than was the case for the fixed hull. It is interesting to observe, however, that at the highest speed, V = 0.9m/s, almost identical tracks resulted from the free- and fixed-hull conditions. At this speed, the free hull maintained a steady trim and essentially "planed" through the ice sheet.

Roll and yaw caused further irregularity of icebreaking pattern, as lateral motions quite radically altered the contact geometry between hull and ice. Figure 15 illustrates the distortion to icebreaking pattern resulting from roll and yaw. During these motions, the hull's forward projected area and bluffness increased, causing the hull to break a wider and sinuous track.

Broken cusps were pushed downward beneath the bow, and overriden by the hull. The ice cusps passed along the underside of the hull in a regular pattern which was affected by thickness and speed. The distance between cusps increased with distance from the bow (Figure 11). After sliding beneath the hull, some of the broken ice reappeared in the track behind the hull. For the thicker ice sheets ($h \geq 20$mm), increasing speed resulted in less ice remaining in the track, while the reverse appeared to hold for thinner ice sheets. This trend is due to the influences of hull motions and the confining action of the bordering ice sheet. The additional breaking of ice beneath the hull somewhat masked the variation of initial cusp size with speed for the same thickness of ice sheet, the influence of speed on the average size of broken ice was considerably less clear than that for the width of the initial cusps.

B. Icebreaking Length

Measured values of cusp width, W, for the free hull are plotted versus thickness h in Figure 16 which shows that W increased with increasing h and decreased with increasing speed, V. Values of W are average widths measured (as indicated in Figure 11) for several cusps beneath the bow, not in the

wake. The ratio W/h ranged from about 3 to 5, for speeds of 0.5m/s and above, to about 7 for creeping speeds of 0.05m/s. The variation of W/h with V can be attributed, in part, to the hydrodynamics of water displacement during ice sheet deflection, and, in part, to altered geometry of loading associated with the simultaneous shearing and flexing of the ice sheet.

Three experiments were performed with stronger, more brittle, ice: two experiments with $\sigma_f \simeq 40$kPa and one with $\sigma_f = 29$kPa. For these flexural strengths, ice broke to form smaller cusps, as indicated in Figure 16, for the 20kPa ice sheet. The stronger ice was more brittle such that cracks propagated more rapidly toward the stem and shoulder of the bow, reaching there before the contact geometry between bow and ice sheet was significantly altered by shearing and crushing of ice at the bow's stem.

Cusp widths produced by the fixed hull did not vary significantly from those produced by the free hull. However, for the fixed hull, the track contained a more uniform pattern of broken ice. This result is attributed to the steady trim maintained by the fixed hull. Icebreaking occurred in a more regular pattern at the bow of the fixed hull. However, some irregularity was inevitable due to slight nonuniformities in ice-sheet properties (thickness, strength, etc.) along the length of the tank. Measured values of cusp width, W, resulting from the fixed hull, are shown in Figure 16 together with values resulting from experiments with the free hull (not distinguished by symbol).

Cusp widths, W, interpolated from the model-scale data in Figure 16 are compared in Figure 17 with field measurements (Voelker et al., 1985) reduced to 1:48-scale. The two sets of data show fairly good agreement, thereby indicating the reasonable veracity of the model ice to simulate sea ice. The model-scale W are about 20% larger than the full-scale values.

Values of cusp width, W, predicted using (II-3) ("SPLICE"), and (II-2) ("Milano"), are plotted versus thickness, h, in Figure 18. "SPLICE" predictions agree with the measured values (Figure 16). Although, for speeds of 0.05 and 0.1m/s and thicknesses greater than 30mm, the measured values of W exceed those predicted. Even though the predicted values show the experimental trend of W increasing with decreasing speed, the measured values increased more markedly. Both measured and predicted values of W increased significantly with increasing h. Values of W predicted using (II-2) ("Mi-

lano") do not agree well with values measured during the present study; compare Figures 16 and 18. Also, (II-2) gives values of W that are much less affected by speed than are either the measured values or values obtained using (II-3).

The main difference between the measured icebreaking pattern and those assumed for (II-2) and (II-3) is the number of cusps forming around the hull's waterline. Generally, in line with Figure 2, a greater number of cusps and wedges are assumed for (II-2) and (II-3) than were observed during the experiments (Figure 10).

C. Comparison with Characteristic Length

Measured values of W are compared in Figures 19a,b with calculated values of characteristic length, ℓ_c, for the free- and fixed-hull conditions, respectively. Generally, values of W/ℓ_c are less than unity, ranging from about 0.8 to 0.4; decreasing with increasing speed, V. Values of W/ℓ_c did not vary with hull condition.

The effects on W and, thereby, on icebreaking pattern, of h and V are explainable in terms of the flexure of a semi-infinite plate or, more simply, a semi-infinite beam on an elastic foundation (water). Hetenyi (1966), Nevel (1965, 1970), Enkvist (1972), Yean et al. (1981) and others have discussed the loading of semi-infinite plates; the latter two references are particularly useful for explaining the variations of W with h, V and σ_f. Through consideration of the location of the locus of the maximum stress in an edge-loaded plate (e.g., loaded by icebreaker bow), it can be shown that W increases with increasing h. The relationship between W and h is more complicated if submergence of the sheet's loaded end is accounted for (Yean et al.). According to Enkvist's argument, W diminishes with increasing speed because increased impact speed results in increased foundation modulus as the hydrodynamic forces associated with displacing water and ice increase. Correspondingly, characteristic length should be modified to account for increasing foundation modulus. Values of ℓ_c as given by (II-1), apply for slow loading rates, or at least do not account for loading rate; nor does (II-1) take into account flooding of the deflected ice sheet.

It is generally accepted (e.g., Enkvist, 1972; Tatinclaux, 1986) that in accordance with elastic theory for semi-infinite plates on elastic foundations, cusp width, W, should be proportional to ℓ_c, provided the cusp breaks before its free end becomes submerged, and $E/\sigma_f > C_1\sigma_f/(\gamma h)$; in which C_1 approximately equals 400 (Keinonen, 1983). Yean et al. (1981), (also, Tatinclaux, 1986) suggest that for

$$\frac{E}{\sigma_f} < C_2 \frac{\sigma_f}{\gamma h} \qquad \text{(V-3)}$$

cusp width, or breaking length, likely is proportional to $(\sigma_f h/\gamma)^{0.5}$ and not to ℓ_c; $C_2 = 40$. For the present study, $E/\sigma_f > 400 > C_1\sigma_f/(\gamma h) > C_2\sigma_f/(\gamma h)$; and values of W are proportional to ℓ_c, and do not increase with increasing σ_f.

VI. ICE RESISTANCE

In this Chapter, attention is focused on the variations of mean ice resistance, $\overline{f}_x$, with thickness, h, and speed, V. First, in Section VI.A, the results for the free- and fixed-hull conditions are compared. Then, in Section VI.B, the free hull results are compared with full-scale measurements. Lastly, in Section VI.C, the experimental results are compared with values of $\overline{f}_x$ predicted using "SPLICE" and "Milano."

In the discussions to follow, reference is also made to the mean plus two standard deviations of resistance: $\overline{f}_x + 2\sigma$. For clarity of presentation (note that σ_f refers to flexural strength of the ice sheet and that σ refers to the standard deviation), the subscript on σ has been dropped (see (IV-13)). In cases where confusion might arise, the subscript is retained. Values of $\overline{f}_x + 2\sigma$ are used to indicate peak values of resistance. Values of f_x higher than $\overline{f}_x + 2\sigma$ may result from ice-sheet irregularities (e.g., hard, poorly seeded spots) and, therefore, may be unrepresentative.

The measured time-histories of ice resistance from which values of $\overline{f}_x$ and σ were determined, are provided in Appendices A and B for the free- and fixed-hull conditions, respectively.

A. Free Hull and Fixed Hull

Mean value of ice resistance, $\overline{f}_x$, experienced by the free hull increased with both increasing thickness, h, and speed, V, as is shown in Figure 20. It is evident from Figure 20 that

$$\overline{f}_x \alpha\ ah^b \qquad \text{(VI-1)}$$

If $\overline{f}_x$ versus h, is plotted in log-log format (Appendix D), the indice b is found to be 2.0 ± 0.1. The coefficient a increases with V. Note that for the lowest (V = 0.05,0.1m/s) and highest (V = 0.5, 0.9m/s) speeds the resistance curves are in close proximity compared to those for the mid-range speeds (V = 0.1, 0.25, 0.5m/s). Significantly increased values of $\overline{f}_x$ occurred as speed increased from 0.1 to 0.25 and 0.5m/s.

Values of $\overline{f}_x$ experienced by the fixed hull also increased with increasing h and V, as shown in Figure 21. However, it is apparent by way of comparison with Figure 20, that the free hull experienced larger values of $\overline{f}_x$ than did the fixed hull, at least for increasing values of h and V. For the fixed hull, the indice b, in (VI-1), is also 2.0 ± 0.1 (Appendix D). However, for each speed the coefficient a is smaller for the fixed hull than for the free hull. Identical values of b, but lower values of a, for the fixed hull suggests that hull motions increase resistance.

Values of $\overline{f}_x + 2\sigma$ experienced by the free hull and fixed hull are compared in Figures 22 through 26 for the same values of V, h and for σ_f = 20 to 25 kPa. For both conditions, σ increased with increasing h. For thicker ice ($h \geq 30$mm), σ increases with increasing speed up to V = 0.5m/s, and then decreases for the highest speed (V = 0.9m/s). This trend is more pronounced for the free hull.

The influences on $\overline{f}_x$ and $\overline{f}_x + 2\sigma$ of speed, V, for both the free- and fixed-hull conditions are shown in Figures 27 and 28 for h = 30 and 20mm, respectively. Values of $\overline{f}_x$, and $\overline{f}_x + 2\sigma$, are linearly proportional to V for the fixed hull. However, for the free hull, $\overline{f}_x$ and $\overline{f}_x + 2\sigma$ have a more complex dependency on V.

It is evident that, for the two slower speeds (V = 0.05, 0.1m/s), there is little difference in the values of $\overline{f}_x$ and $\overline{f}_x + 2\sigma$ for the free- and fixed-

hull conditions. However, with increasing speed (V = 0.25, 0.5m/s), the free hull experienced signficantly larger values of $\overline{f}_x$ and $\overline{f}_x + 2\sigma$ than did the fixed hull. The free hull encountered, 60 to 70% (when V = 0.5m/s) more resistance than did the fixed hull. At the greatest speed tested (V = 0.9m/s), the curves of $\overline{f}_x$ and $\overline{f}_x + 2\sigma$ converge for the free and fixed hull. This infers that, because hull motions are greatly reduced for the free hull, it and the fixed hull break ice in essentially the same manner, but with different trims. For speeds in excess of 0.5m/s, the influence of V on $\overline{f}_x$ diminishes for the free hull. The relationship between $\overline{f}_x$ and V for the free hull bulges in a manner that is suggestive of a "Milano hump." In other words, Figures 27 and 28 show that, for the free hull, $\overline{f}_x$ is not linearly porportional to V, as (II-4) and (II-5) propose. Simple regression analysis cannot be used to relate $\overline{f}_x$ and V.

The trends outlined in this section are attributable to several factors. Among them:

1. The free hull experienced, on average, longer cycles in resistance than did the fixed hull for the same speed and ice-sheet properties. This result is further elaborated in Chapter VIII.
2. The difference $(\overline{f}_x)_{free} - (\overline{f}_x)_{fixed}$ attained a maximum value that is related to the maximum amplitude (see Section VII.B) of pitch and heave motions. The energy consumed by motions translates, as per (II-7), for example, to an increase in resistance.
3. With increasing speed, V = 0.05 to 0.5m/s, roll became important. It affected the symmetry of ice-breaking around the model, resulting in a broadened pattern of icebreaking and, thereby, led to increases in resistance encountered by the free hull.
4. With increasing speed and thickness, the average trim of the free hull increased such that the stem angle of the bow contacting the ice sheet also increased. Increased stem angle at ice contact led to increased values of $\overline{f}_x$.
5. The restraint used to fix the hull from moving provided the requisite vertical force necessary to break ice. For the free hull, energy had to be expended in pitch and heave in order that the hull could exert the vertical force needed to break ice.

Item 4, above, is somewhat specific to the conventional modified-White bow form of the POLAR-Class hull. Different relationships between ice resistance and trim may exist for other bow forms. For example, the stem angle of a spoon-bow decreases with increasing hull trim, thereby resistance may, possibly, decrease with increased hull trim. The functional variation of resistance with stem angle has been discussed by Enkvist and Mustamaki (1986), also see WIMB (1972).

Values of $\overline{f}_x$ increased with increasing flexural strength, σ_f, as is shown in Figure 29, for experiments with V = 0.25m/s. Ice resistance, for h = 30 and 40mm, increased about 30% when the flexural strength was almost doubled: σ_f increased from 22 to 40kPa. However, for h = 20mm, $\overline{f}_x$ barely increased when σ_f increased approximately 20%; from 20 to 29kPa.

The contribution to $\overline{f}_x$ of shearing and crushing of ice at the bow stem of a POLAR-Class hull can be assessed from Figure 29, in which values of $\overline{f}_x$ determined for hull transit of the preslotted ice sheet, depicted in Figure 30, are compared with values obtained for the nonslotted half of the ice sheet. Preslotting of the ice sheet reduced $\overline{f}_x$ by 28%. If preslotting is taken to be equivalent to eliminating shearing and crushing of ice, and is assumed not to influence significantly the flexural breaking of ice, then the result of this experiment infers that shearing and crushing of ice at the bow stem may contribute about 28% of $\overline{f}_x$. By way of comparison, Enkvist and Mustamaki (1986) present model and full-scale data indicating that shearing and crushing may contribute 20 to 40% of $\overline{f}_x$.

B. Comparison with Full-Scale Resistance

The experimental values of $\overline{f}_x$, agree with values determined from field tests with a full-scale POLAR-Class hull (Voelker et al., 1985). Values of $\overline{f}_x$ are compared in Figure 31. For low speeds, model- and full-scale values are reasonably close. However, for high speeds, although only a few full-scale data were obtained, the values were lower than the model-scale values. This is likely because the flexural strength of the model-scale ice was proportionally greater than that of the full-scale ice.

The full-scale values of ice resistance were obtained during January 1985 from tests conducted with the USCGC "POLAR STAR." These data are reduced to 1:48-scale in Figure 31, following normal procedures for ice modeling (e.g., Schwarz, 1983; Tatinclaux, 1984a,b). The values of flexural strength of ice sheets companion to the full-scale data are approximate, as they were not measured but were computed using measured values of the temperature and salinity of ice cores.

C. Comparison with "SPLICE" and "Milano"

"SPLICE" was designed for prediction of the mean ice resistance, $\overline{f}_x$, encountered by full-scale icebreaker hulls. Recent modifications to "SPLICE" (Kotras et al., 1983) have tuned it for predictions for the POLAR-Class hull. For the present study, "SPLICE" was modified to perform model-scale predictions, which involved use of the same values of E and σ_f as were determined for the experiments.

Experimental values of $\overline{f}_x$ are compared in Figures 22 through 26 with values of $\overline{f}_x$ predicted using "SPLICE." The predicted values are reasonably close to the experimental values, but deviate for thicker ice and lower speeds, when the predicted number of cusps comprising the pattern of icebreaking was only one. For one cusp, the cycle of icebreaking is taken to be complete when this cusp extends to the hull's middlebody, and, within this cycle, "SPLICE" does not take into account any sliding forces. Therefore, this component is set to zero, decreasing the total resistance.

It is important to observe that the predicted and experimental values of $\overline{f}_x$ diverge for speeds in excess of about 0.25m/s, and for moderately thick ice sheets. The divergence coincides with the observed increase of hull motions when the breaking frequency is close to natural frequencies of hull motions.

Predicted values of $\overline{f}_x$ generally fall between the experimental values of $\overline{f}_x$ obtained for the free- and fixed-hull conditions. For low speeds and thick ice, however, the predicted values of $\overline{f}_x$ are less than the experimental values for both the free- and fixed-hull conditions. "SPLICE" does not provide information on $\overline{f}_x + \sigma$, or peak ice resistance. Values of $\overline{f}_x + 2\sigma$ exceeded notably the values of $\overline{f}_x$.

The curve of $\overline{f}_x$ versus V, for h = 30mm (Figure 27), is plotted in Figure 32 and compared with values of $\overline{f}_x$ predicted using both "SPLICE" and "Milano." Values of $\overline{f}_x$ predicted using "Milano" were obtained from Figure 19 of Milano (1980). Reduced to the scale of the present model, they show remarkably close agreement with the experimental values. "Milano" is conceptually correct in relating resistance cycle to cycles of pitching/heaving and icebreaking. However, as is discussed in Chapter VIII, for a POLAR-class hull the major cycles of resistance occur at a frequency either associated either with track opening or with hull motion at its natural frequency of pitching/heaving admidst ice. Major cycles of resistance generally did not occur at the frequency of single icebreaking events. Values of $\overline{f}_x$ obtained using "SPLICE" are somewhat smaller than the experimental ones, and vary linearly with V.

VII. HULL MOTIONS, AND RESTRAINING FORCES AND MOMENTS

The mean values and standard deviations of motions experienced by the free hull, and restraining forces and moments experienced by the fixed hull are presented and discussed in Sections VII.A and VII.B, respectively, of this chapter along with other quantities of interest.

The measured time-histories of hull motions and hull-restraining forces and moments are provided in Appendices A, B and C.

A. Free Hull

Mean values of pitch and heave displacements, $\overline{\theta}$ and $\overline{z}$, respectively, experienced by the free hull are plotted versus thickness, h, in Figures 33 and 34 for varying speeds, V. The mean values of $\overline{\theta}$ and $\overline{z}$ increased with increasing h, as did $\overline{f}_x$.

For the lowest speed, V = 0.05m/s, mean values of $\overline{\theta}$ and $\overline{z}$ were relatively small because, the hull settled back to its initial trim for fairly long periods between icebreaking. Using "Milano" terminology (see Section II.C) $T_1 > T_2$. For increased speeds (V = 0.1, 0.25m/s), $\overline{\theta}$ and $\overline{z}$ increased with increasing h, but $\overline{z}$ appears to be less dependent on V for this speed range. As the speed increased further to 0.5m/s, $\overline{\theta}$ and $\overline{z}$ continue to increase. However, for the highest speed (V = 0.9m/s), $\overline{\theta}$ and $\overline{z}$ show a substantial decrease. The dependency of $\overline{\theta}$ and $\overline{z}$ on speed for constant h is

completely consistent with the previous discussion regarding $\overline{f}_x$; i.e., $\overline{\theta}$ and $\overline{z}$ increase with increasing speed up to V = 0.5m/s, and then decrease for the highest speed (V = 0.9m/s).

In order to elucidate the influence of V, $\overline{\theta}$ and $\overline{z}$ are plotted in Figure 35 versus V, for experiments with h = 30mm. It is evident in Figure 35 that $\overline{\theta}$ and $\overline{z}$ attained a maximum value for a speed around 0.5m/s. Plots (not included in this report) of $\overline{\theta} + 2\sigma$ and $\overline{z} + 2\sigma$ versus h, with V as additional parameter, show the same trends as shown in Figures 33 through 35.

Standard deviations of pitch and heave accelerations, $\sigma_{\ddot{\theta}}$ and $\sigma_{\ddot{z}}$, respectively, increased with increasing values of h and V, as shown in Figures 36 and 37. Values of $\sigma_{\ddot{\theta}}$ and $\sigma_{\ddot{z}}$ are associated with the inertia terms in the equations of motion, (IV-5). Therefore, they indicate the relative importance of the inertia forces in the icebreaking process. For the two lowest speeds studied, 0.05 and 0.1m/s, $\sigma_{\ddot{\theta}}$ and $\sigma_{\ddot{z}}$ are small in value, and so are the inertia forces associated with them compared to buoyancy forces. Also for these two speeds, inertia terms did not vary significantly with thickness, h. For speeds of 0.25 and 0.5m/s, $\sigma_{\ddot{\theta}}$ and $\sigma_{\ddot{z}}$ increased markedly in magnitude as thickness increased, which is the expected result. An increase in speed from 0.5 to 0.9m/s did not result in quite the marked increase in $\sigma_{\ddot{\theta}}$ and $\sigma_{\ddot{z}}$ as occurred from 0.25 to 0.5m/s. As mentioned above, pitch and heave were diminished for the former speed range compared to the latter.

It is clear from Figures 38 through 41 that $\overline{\theta}$ and $\overline{z}$, together with $\sigma_{\ddot{\theta}}$ and $\sigma_{\ddot{z}}$, increased with increasing flexural strength, σ_f. Note that there is some scatter in the data for $\overline{z}$ which underscores some of the difficulties encounted in ice-towing-tank experiments.

Roll, ϕ, increased dramatically for speeds up to 0.5m/s, and diminished thereafter. Figure 42 shows values of standard deviation of roll, σ_ϕ, plotted versus speed for h ≈ 30mm. Measured values of σ_ϕ extend to V = 0.5m/s. For V = 0.9m/s, the hull was observed to experience considerably less roll than at V = 0.5m/s.

B. Fixed Hull

Mean values of pitch restraining moment, $\overline{m}_\theta$, heave restraining force, $\overline{f}_z$, and standard deviation of yaw restraining moment, $\sigma_{m\psi}$, exerted against the fixed hull are presented in Figures 43 through 45, respectively.

Values of $\overline{m}_\theta$ (Figure 43) increased with increasing thickness, as did θ, and its dependency on V is similar to that described previously for θ. However, the decrease at the highest speed is not as large. The effect of thickness on $\overline{m}_\theta$ seems to become more pronounced with increasing speed. This occurs because, with increasing speed, the hull flexurally depressed and broke the ice sheet before it could become flooded around the bow. At slow speeds flexural depression of ice led to flooding of the sheet around the hull's bow such that its buoyancy force was partially compensated for (Mueller and Ettema, 1982).

Figure 44 suggests that $\overline{f}_z$ is independent of speed, V, at least for speeds ranging from 0.05 to 0.5m/s. A possible explanation for this result is as follows. Increasing speed leads to an increase in the initial lifting force of the hull in accordance with the hull's first contact with the unbroken ice sheet. However, a slower moving hull is in closer contact with ice submerged beneath it, such that it experiences an increase in heave, or lifting, force. The net result of these counter-acting effects is that $\overline{f}_z$ is invariant with speed within the mentioned range.

The two data points for $\overline{f}_z$ obtained when V = 0.9m/s show (Figure 34) a curious trend; $\overline{f}_z$ for h = 30mm is smaller than $\overline{f}_z$ when h = 22mm. By way of comparison, $\overline{m}_\theta$ increased with h when V = 0.9m/s (Figure 43). Also, when h = 22mm, $\overline{f}_z$ for V = 0.9m/s exceeds values of $\overline{f}_z$ for lesser speeds. However, the reverse trend holds when h = 30mm; for V = 0.9m/s, $\overline{f}_z$ was smaller than for all the other speeds. These results are explainable when viewed in terms of $\overline{f}_z$ and $\overline{m}_\theta$, and of $\overline{\theta}$ and $\overline{z}$ versus V, as shown in Figure 35. It is evident in this figure that $\overline{\theta}$ and $\overline{m}_\theta$ have similar trends with V, as do $\overline{z}$ and $\overline{f}_z$. In particular, Figure 35 shows that $\overline{f}_z$ diminishes with increasing V; c.f., $\overline{z}$ attains a peak value at V = 0.5m/s and diminishes thereafter. At V = 0.9m/s and h = 30mm, the hull planed through the ice sheet with considerably more crushing and shearing of ice at the bow stem than at lesser speeds. Although crushing and shearing of ice may have led to increased pitch moment they did not result in increased heave force.

The standard deviation of yaw restraining moment, $\sigma_{m\psi}$, is a measure of the amplitude of lateral forces/moments acting to deflect the hull from its transit direction. In effect, $\sigma_{m\psi}$ is an indicator of the nonsymmetric and

nonsimultaneity of icebreaking around the hull. Figure 45 shows that $\sigma_{m\psi}$ is largely independent of speed, for speeds ranging from 0.05 to 0.25m/s. However, for a speed of 0.5m/s, yaw moment, m_{ψ}, increased rather dramatically, reflecting, for that speed, increased nonsymmetric motions and nonsimultaneity of icebreaking around the hull. Figure 46 shows the variation of $\sigma_{m\psi}$ with speed for a 30mm thick ice sheet. For the highest speed (V = 0.9m/s), $\sigma_{m\psi}$ decreases, as is indicated in Figure 42 for σ_{ϕ}.

VIII. SPECTRAL ANALYSIS

In this chapter, the relationships between resistance, icebreaking patterns and hull motions are further described through the use of spectral analyses of recorded time-histories of resistance, hull motions and motion-restraining forces/moments, all related to observed icebreaking patterns. Before proceeding with a detailed discussion for a selection of experiments, it is helpful briefly to summarize the key frequencies that influence, or characterize, cycles of ice resistance. Short segments of time-histories of resistance and motions are used to illustrate these frequencies.

The simplest frequency of ice resistance to envision is that associated with cycles of single icebreaking events, as discussed in Section II.D. It is possible to define a more-or-less single frequency of icebreaking, ω_b, as the ratio of speed to the distance travelled between two icebreaking events. This distance is the geometric component of ice cusp width in the direction of hull transit. Thereby,

$$\omega_b = V\cos\beta/W \qquad \text{(VIII-1)}$$

in which β = the angle between the average normal to the waterline in contact with the ice sheet and the hull's centerplane.

When icebreaking did not occur simultaneously along both sides of the hull, a frequency higher than ω_b --notably $2\omega_b$ -- may occur in ice resistance, as icebreaking events are staggered either side of the bow.

As described in Section V.A, another important resistance frequency is opening frequency ω_o. It is speed, V, divided by the travelled distance needed by the hull to break and open a sufficiently wide track to pass

through. This distance can be defined as the next highest integer, n, resultant from the relative size ratio $B_t/(2W/\sin\beta)$ multiplied by the distance travelled in a single icebreaking event, $W/\cos\beta$; B_t is the width of the track opened to enable the hull to pass through an ice sheet (Figure 47). Opening frequency is defined, therefore, as

$$\omega_o = V\cos\beta/(nW) \qquad \text{(VIII-2)}$$

Perhaps the simpliest way to envision opening frequency is to picture the bow of a POLAR-Class hull sliding and simultaneously rotating up against an ice sheet, all the while breaking ice cusps, increasing its trim and broadening its contact perimeter with the ice sheet then settling into the track once it was sufficiently opened (ice cusps broken and displaced beneath the bow). This cyclic motion proceeds as the hull continuously moves forward with steady speed. Figures 47 and 48 schematically illustrate icebreaking pattern and resistance cycles, respectively.

Other important frequencies are the natural frequencies of coupled pitch and heave motions, which are of similar values, 0.7 to 0.85, and are herein designated as ω_n. Values of ω_n are discussed in Section IV.B.2 and presented in Tables 8 and 9. These frequencies are very important when hull motions are sufficiently excited at frequencies close to, and exceeding, ω_n. Also, as discussed below (Section VIII.A), frequencies associated with antisymmetric motions, in particular roll and yaw are important under certain conditions.

Icebreaking pattern, its sequential formation, together with the influences of hull motion, determine cycles of ice resistance. For most of the experiments, identifiable cycles in resistance and hull motions occurred at one, or combinations, of the frequencies ω_o, ω_b and ω_n. For the free hull, the major cycle of resistance and hull motions (pitch and heave) occurs at ω_o, with a minor cycle at ω_b. When ω_b equalled or exceeded ω_n, the major cycle occurred at ω_n. In all cases, the free hull typically experienced cycles of resistance and motion at one major frequency; either ω_o or ω_n. However, for the fixed hull, major cycles occurred at both ω_b and ω_o. Consequently, power spectra of resistance experienced by the fixed hull are concentrated at ω_b and ω_o. Overlap of frequency bands at ω_b and ω_o cause the power spectra of fixed-hull resistance to appear more broadly banded than for the free hull.

The geometry of icebreaking pattern, in particular the widths and lengths of the cusps comprising it, depend on thickness, speed and hull (notably bow) form. Consequently, because cycles of ice resistance varied with icebreaking pattern, they also varied with thickness and flexural strength (also elastic modulus and possibly fracture toughness) of the ice sheet, and speed.

Only for free hull transit of very thin ice sheets ($h \leq 10$mm), did icebreaking pattern associated with ω_o, not govern cycles of ice resistance. This is because thin ice sheets could not support the hull further than a single breaking (ω_b), and ice cusps could be readily displaced by the hull.

Time-histories of resistance, f_x, viewed through short-duration (20 to 30 seconds) windows provide insight into the cycles of resistance experienced by the hull. Figure 49 shows that the cycles of peak resistance experienced by the free hull coincide with ω_o when $V = 0.1$m/s and $h = 30$mm. For the same values of V and h, Figure 50 reveals that cycles of peak resistance experienced by the fixed hull occurred at frequencies comparable to ω_b. When the free hull transitted thin ice at high speed, $h = 9$mm and $V = 0.5$m/s, the major resistance cycles occurred at the hull's natural frequency of pitch/heave, ω_n, with lesser cycles of resistance occurring at ω_b.

The ensuing discussion on the interdependence of icebreaking, ice resistance and hull motions, is divided in three parts. In Sections VIII.A and VIII.B, icebreaking is considered by the free hull and the fixed hull, respectively. In Section VIII.C, a comparison is made with full-scale measurements. Table 11 is a summary of the of frequencies ω_b and ω_o corresponding to the experimental conditions.

The influence of speed and, thereby, motions, is investigated through the results for both the free- and fixed-hull conditions, involving ice sheets of approximately constant, 30mm thickness, are discussed. Also considered for the free hull are the influences of ice-sheet thickness and strength. For each experiment, the power spectra of ice resistance, hull motions together with excitations (free hull), or restraining forces/moments (fixed hull), are presented.

A. Free Hull

Figures 52 through 56 show the power spectra of ice resistance, hull motions (pitch and heave) and excitations (moments and forces) for h = 30mm and V = 0.05, 0.1, 0.25, 0.5 and 0.9m/s, respectively. Subsequently, Figures 57 through 60 show the power spectra corresponding to V = 0.1 and 0.25m/s and different thicknesses, h. Lastly, for this Section, Figure 55 show the power spectra for h = 31mm, V = 0.25m/s and an increased srength of σ_f = 40kPa.

For the lowest speed, V = 0.05m/s (Figure 52), the dominant frequency of ice resistance, hull motions and excitations is 0.08Hz, which is associated with ω_o. A peak of much lesser magnitude is evident at ω_b (0.16Hz). At least two cusps, either side of the hull's centerplane, had to be broken in order for the track to be sufficiently wide such that track width exceeded the hull's beam. Frequencies near the hull's natural frequency for pitching/heaving amidst ice (0.7 to 0.85Hz) were heavily damped during the submergence and displacement of broken ice, as well as by crushing and shearing of ice at the bow's stemline.

For V = 0.1m/s (Figure 53), the dominant frequency of ice resistance is about 0.2Hz, coinciding with ω_o. Frequency peaks corresponding to ω_b are also evident in the frequency band at 0.4 to 0.5Hz for ice resistance. Frequency peaks occurring for values larger than ω_b are attributed to nonsimultaneous icebreaking around the hull, as explained earlier. The power spectra of pitch and heave and their excitations show peaks at both ω_o and ω_b. Also, note that in the power spectra of pitch and heave, relatively small peaks also occur at ω_n. For V = 0.1m/s, the hull was able to oscillate after each icebreaking impulse.

Distinct peaks centered around 0.8 to 1.0Hz are evident in the power spectra of ice resistance and pitch and heave for V = 0.25m/s (Figure 54). This frequency band coincides with ω_o and ω_n, such that a resonant condition developed. For this experiment, icebreaking frequency, ω_b, was 1.37Hz. The peaks in the spectra for the excitations coincide with ω_b. The inertia forces/moments associated with pitching and heaving of the hull were 180 degrees out of phase with buoyancy force/moment resulting from pitch and heave. Consequently, the inertia forces/moments acted against, and compensated for, buoyancy force/moment. The upshot of this condition was that the

hull encountered significantly increased resistance over that it experienced when moving at a speed of 0.1m/s, and a marked increase in ice resistance occured compared to that experienced by the fixed hull. Figure 27, in which $\overline{f}_x$ is plotted versus speed, shows this effect. The curves of $\overline{f}_x$ versus V for the free hull and fixed hull are significantly separated for V = 0.25m/s.

For V = 0.5m/s (Figure 55), the dominant frequencies did not increase as one might expect from the expressions for ω_b, (VIII-1), and ω_o, (VIII-2), by virtue of increased speed. Instead, the dominant frequency in the power spectra of ice resistance, pitch, and to lesser extent heave, is about 0.45Hz. This frequency is associated (and as was observed during the experiment) with roll and yaw. The natural frequency of roll in openwater is 0.45Hz. Whenever the hull rolled or yawed, it had a bluffer profile in contact with the ice sheet. Because a bluffer profile was less efficient for icebreaking, ice resistance increased, as Figure 19 shows, with respect to that experienced by the fixed hull. Another distinct frequency peak occurs in the range 0.8 to 1.0Hz for ice resistance, pitch and especially heave. The frequency band 0.8 to 1.0Hz corresponds to ω_o. It took approximately 3 icebreaking events (or cusps) to break a track sufficiently wide such that the hull could pass through the ice sheet. This frequency also corresponds to the hull's natural frequency of pitch and heave. The value of ω_b determined for this experiment is 3.5Hz. It is only in the power spectra of the motion excitations that a peak around ω_b is apparent.

For V = 0.9m/s (Figure 56), icebreaking occurred simultaneously around the bow such that roll or yaw were not significant. Interestingly, the dominant frequency band of ice resistance and hull motions is about 0.8 to 1.0Hz, which approximately coincides with the hull's natural frequency of pitching and heaving. For this experiment, the hull did not undergo large amplitude heave or pitch. Instead, it kept a fairly steady trim but experienced relatively large values of pitch acceleration, for small pitch displacements. A small peak accurs at ω_o = 2.83Hz. No significant resistance peak appears at ω_b = 8.5Hz, but a comparative small peak occurs at a high frequency of 5.5Hz. Peak frequencies occur at ω_n and ω_o in the spectral densities of pitch and heave.

The influence of thickness, h, on the dominant frequencies of ice resistance and hull motions is now explored through the power spectra for experiments in which V = 0.1 and 0.25m/s.

For V = 0.1m/s, results from experiments with h = 16 and 43mm (Figures 57 and 58, respectively,) are considered together with the results already discussed for h = 30mm (Figure 53). For h = 16mm and V = 0.1m/s, the dominant frequency of ice resistance, as well as hull motions, coincide with icebreaking frequency, ω_b = 0.59Hz, although small peaks are also evident at values around half and one-third ω_b. The ice sheet was thin such that it could not maintain hull displacements for cycles longer than that associated with a single icebreaking event. The hull tended to break a single ice cusp all along its side. As explained above, the dominant frequency for ice resistance, and hull motions for h = 30mm occurred at about 0.2Hz which coincides with opening frequency ω_o. For h = 43mm, dominant resistance peaks are evident in the frequency band of 0.2 to 0.3Hz. These peaks correspond to both the icebreaking frequency, ω_b (0.24Hz), and to the opening frequency ω_o (0.24Hz). A single cusp broken each side of the bow created a track that was wide enough for the hull to pass through. The same peaks are evident in the power spectra of pitch and heave. A relatively small band of peaks, around 0.7 to 0.9Hz, are evident in the power spectra of hull motions. These peaks coincide with the hull's natural frequency of coupled pitching and heaving amidst ice (0.7 to 0.85Hz).

For V = 0.25m/s, experiments were conducted with the following values of h and σ_f: σ_f = 20kPa and h = 30 (Figure 52) and 39mm (Figure 59); σ_f = 29kPa and h = 22mm (Figure 60); and, σ_f = 37kPa and h = 31mm (Figure 61). In each case, the dominant frequencies of ice resistance and hull motions occur in the frequency band containing the natural frequencies of coupled pitch and heave amidst ice (0.7 to 0.85Hz). Hull motions appear to have become tuned to, and dictated, icebreaking. For most of these cases ω_o was sufficiently close to ω_n, and ω_b greater than ω_n, for this to occur. As mentioned above, the consequence of this was a large increase in the mean value of ice resistance, for all thicknesses. Such an abrupt or relatively large increase in resistance did not occur for the fixed hull moving, with the same speed, through the same thicknesses of ice sheets.

The effects of ice-sheet strength on the dominant frequencies of ice resistance and hull motions is now considered through the power spectrum for the experiment in which V and h were 0.25m/s and 31mm, respectively, and flexural strength was 37kPa (Figure 61). Because the icebreaking frequency ω_b was sufficiently close to the hull's natural frequency of coupled pitch and heave, a resonant condition occurred, as was the case of the 20kPa ice sheet. Generally, stronger urea ice, having higher ratios of E/σ_f, tends to break with somewhat smaller cusps than weaker ice. Therefore, it is likely that different frequency peaks should be expected when a resonance condition does not prevail. Further tests need to be done in order to confirm this.

B. Fixed Hull

Figures 62 through 66 show the power spectra of ice resistance, heave-restraining force and pitch-restraining moment for h = 30mm and V = 0.05 to 0.9m/s. Generally, the dominant frequency responses of the fixed hull include or span both icebreaking frequency ω_b, and opening frequency, ω_o. Therefore, the spectra of f_x, f_z and m_θ experienced by the fixed hull are more broad-banded than those of the free hull, for which dominant frequencies under corresponding conditions, were usually at either ω_o or ω_n. Also, icebreaking occurred more synchronously around the hull then occurred for the free hull.

For V = 0.05 and 0.1m/s (Figures 62 and 63, respectively), the dominant frequencies of f_x, and m_θ coincide with both ω_b and ω_o. Frequency ω_b is especially pronounced when V = 0.1m/s (Figure 63). By way of comparison (Figure 53), for the free hull under similar conditions the dominant resistance frequency corresponded to opening frequency, ω_o.

For V = 0.25m/s (Figure 64), the hull experienced dominant frequencies of ice resistance and restraining forces and moments in overlapping frequency bands at ω_b and ω_o; 1.3 and 0.7Hz, respectively.

For V = 0.5m/s (Figure 65), the dominant frequencies of resistance appear to be concentrated in a frequency band closer to ω_o (1.4Hz) than to the frequency ω_b (2.9Hz); a pronounced peak does not occur at ω_b. Pitch-restraint moment was more susceptible to single icebreaking, and therefore shows energy concentrated at both ω_b and ω_o. Heave-restraint force was less dependent on

single icebreaking events, as was ice resistance, and experienced peaks in a frequency band around ω_o. A distinct but comparatively small peak, at 4Hz, occurred also in the power spectrum of ice resistance. This frequency is associated with rotational (θ) vibration of the load cell platen, used to restrain the fixed hull.

For V = 0.9m/s (Figure 66), several important frequencies appear to be dominant of ice resistance, the first one is a high frequency, greater than 5Hz, that may correspond to ω_b (6.5Hz), and another is experienced in a band of frequencies around 1Hz, lower than the frequency ω_o (2.1Hz). Concentration of energy around frequencies at about 1Hz, and lower, may be an artifact of the experiment in that, when accelerating the hull to speed, unsteady conditions prevailed (see time histories in Appendix B) for about 25% of the data record. A small peak around the frequency ω_o (2.14Hz) is also evident in this power spectra. Additionally, a peak around a frequency of 4Hz, as it appeared for the 0.5m/s speed, may be related to the natural vibration of the load cell when it is excited in pitch mode. The heave-restraint force experienced a dominant peak at ω_o, but the pitch-restraint moment, although a small peak is evident at ω_o, shows a dominant peak at a very low frequency.

C. Comparison with Full-Scale Dynamics

Figure 67 presents the power spectra (given by Voelker et al., 1985) of pitch experienced by a full-scale POLAR-Class hull transitting a 1.46m-thick ice sheet at a steady speed of 1.29m/s. The dominant frequency of pitch occurs at a frequency of 0.16Hz which corresponds to opening frequency ω_o. During this test, ω_b was 0.29Hz. The dominant frequency of ice resistance and motions experienced by the full-scale hull nearly always coincided with ω_o, not ω_b; most of the full-scale tests were conducted at relatively slow speeds, 2 to 4knots (about 1 to 2m/s).

Values of ω_o and ω_b, estimated from the data presented by Voelker et al. are listed in Table 12, where they are compared with dominant frequencies of pitch and roll. Several factors contribute to error in the estimations of ω_o and ω_b. To begin with, the values are based on average measured values of cusp width, W. The measurements were not made in the track where the resistance and hull motions were recorded, but were measured elsewhere. Further,

the hull was not moving at the same speed for the duration of the data record that was spectral analyzed.

IX. CONCLUDING REMARKS

The major contribution of this study is the description of the dynamics of continuous-mode icebreaking by a POLAR-Class hull. In particular, relationships between ice resistance, icebreaking patterns, and hull motions have been identified. During continuous-mode icebreaking, a POLAR-Class hull comprises a dynamic system of sufficient complexity that ice resistance and motions experienced by the hull are stochastic. Exact values of ice resistance and hull motions, at any point in time, cannot be predicted with anywhere the certainty that can openwater resistance.

Mean values of ice resistance, icebreaking pattern and hull motions separately can be related, both intuitively and empirically, to ice-sheet thickness and strength, and to hull speed, as discussed in Chapters V through VII. However, adequate understanding of continuous-mode icebreaking requires knowledge of the relationships between ice resistance, icebreaking pattern and hull motions. Some considerable insight into these relationships is provided by comparison of the trends in mean values of ice resistance ($\overline{f}_x$), icebreaking pattern (cusp width, W, and the relative sizes of cusps and hull beam) and hull motions ($\overline{\theta}$, $\overline{z}$, $\ddot{\theta}$, $\ddot{z}$) as presented in Chapter V through VII. The full, dynamic nature of the relationships has to be illuminated through use of spectral analysis of time-histories of ice resistance, hull motions and motion-excitations (ice forces). In this regard, Chapter VIII draws together information presented in Chapters V through VII so as to reveal these relationships.

Hull motions and icebreaking pattern determined the dominant cycles of resistance experienced by the free hull. Icebreaking frequency, ω_b, the frequency of individual breaking events, was significant only when the hull transitted thin ice such that significant pitch and heave did not occur. When ω_b is less than the hull's natural frequency of coupled pitch and heave, ω_n, the dominant frequency of ice resistance and hull motions is the frequency of track opening, ω_o; this is the frequency associated with the cyclic manner by which hull trim changes as the hull breaks open a track that is

sufficiently wide for the hull to pass through. When ω_b equals or exceeds ω_n, the dominant frequency of ice resistance coincides with ω_n. Under certain conditions, roll was found to be important and caused a large increase in resistance. Some limited measurements of roll angle were made. The fixed hull experienced dominant frequencies of resistance at both ω_b and ω_o.

The model-scale data and observations resulting from the present study are in good agreement with data and observations from full-scale tests with POLAR-Class hulls. Values of mean resistance are comparable (Figure 31), as are cusp widths (Figure 17). Importantly, dominant frequencies of resistance and hull motions that were identified in the experiments, are also evident in time-histories, and spectral analyses, of resistance and hull motions of a full-scale self-propelled POLAR-Class hull.

It is useful to consider briefly the implications of the present study on the dynamics of continuous-mode icebreaking by hulls with bow forms quite different to that of a POLAR-Class hull. Insofar that bow form affects icebreaking pattern, it also likely affects what we have dubbed as opening frequency, ω_o. A bow with a wide entrance angle (an extreme case is a landing-craft bow) may break open a track with a single breaking event. Consequently, for such bows, ω_o and ω_b may be identical, or at least be closer than is the case for a POLAR-Class hull.

The following principal conclusions can be drawn from the present study:

1. When undergoing significant pitch, heave and roll, the free hull experienced greater mean and peak values of resistance than it did when it was restrained from these motions. When it did not experience significant pitch, heave and roll, as was the case for high-speed transits or transits through thin ice, the resistance of the free hull was comparable to that of the fixed hull.

2. A POLAR-Class hull moving with steady speed and undergoing pitch and heave experiences dominant cycles of resistance and motions at either the opening frequency, ω_o, or the hull's natural frequency of coupled pitch and heave amidst ice, ω_n. Minor cycles at icebreaking frequency ω_b, also occur. Opening frequency, ω_o, is associated with the oscil-

latory motion experienced by a POLAR-Class hull opening a track of width in excess of hull beam:

$$\omega_o = V\cos\beta/(nW) \qquad \text{(VIII-2)}$$

in which V = hull speed; β = the waterline angle as defined in Figure 37; n = the highest integer of the relation $B_t/W\sin\beta$; B_t = track width; and, W = cusp width. When transitting thin ice, however, the dominant frequency coincided with the breaking of individual cusps, ω_b, because the hull could readily displace broken ice, and therefore, did not experience significant motions.

3. When ω_b was less than ω_n, dominant cycles of resistance and motions occurred at ω_o. However, when the speed of the free hull was such that ω_b equalled or exceeded the hull's natural frequency of pitch and heave ω_n, the dominant frequency of ice resistance and hull motions was ω_n. If $\omega_b = \omega_n$, a resonant condition was developed, in which inertia and buoyancy forces counteracted one another. Consequently, under a resonance condition, the greatest difference occurred between resistance experienced by the free and fixed hull.

4. For moderately high speeds, and $\omega_o > \omega_n$, asymmetric motions, roll and yaw, significantly increased the resistance experienced by the hull. Yaw restraining moment of the fixed hull also increased notably for this speed range.

5. The fixed hull, restrained from motions, experienced cycles of resistance at both the frequencies ω_o and ω_b. Overlap of frequency bands at ω_o and ω_b broadened the power spectra of resistance experienced by the fixed hull.

6. Icebreaking pattern characterized by cusp width, was found to depend on ice-sheet thickness and strength as well as hull speed. The fixed hull by maintaining a constant contact geometry produced a more uniform icebreaking pattern than did the free hull. However, hull restraint,

or hull motions, did not significantly affect the size of cusps comprising an icebreaking pattern.

7. Mean value of ice resistance increased proportionately with ice-sheet thickness squared. Mean ice resistance was not linearly proportional to hull speed. Instead the relationship between resistance and speed is curved indicating a "Milano hump."

8. Mean pitch and heave of the free hull increased with increasing ice-sheet thickness. They attained maximum values for a model-scale hull speed around 0.5m/s. The pitch-restraining moment of the fixed hull showed a similar trend, but the heave-restraining force seemed to be less dependent on hull speed than the above parameters.

9. Pitch and heave accelerations of the free hull increased with increasing ice-sheet thickness and became of important magnitude as hull speed increased.

10. The added-mass and damping coefficients for a hull during continuous-mode icebreaking are different from those prevailing during openwater conditions. The presence of an ice sheet significantly increased both added-mass and damping coefficients associated with pitch and heave. Therefore, the hull's natural frequencies of coupled pitch and heave were reduced from 0.91 and 1.09Hz during openwater transit to 0.68 and 0.83Hz during continuous mode icebreaking.

REFERENCES

Edwards, R.Y., Lewis, J.W., Wheaton, J.W., and Coburn, T., 1972, Full-Scale and Model Tests of a Great Lakes Icebreaker. Transactions of Society of Naval Architects and Marine Engineers, Vol. 80.

Enkvist, E., 1972, On the Ice Resistance Encountered by Ships Operating in the Continuous Mode of Icebreaking. Report No. 24. The Swedish Academy of Engineering Science in Finland, Helsinki, Finland.

Enkvist, E., 1983, A Survey of Experimental Indicators of the Relation Between Submersion and Breaking Components of Level Ice Resistance to Ship. Proceedins of 7th International Conf. of Port and Ocean Engineering under Artic Conditions, Helsinki, Finland.

Enkvist, E. and Mustamaki, E., 1986, Model and Full-Scale Tests With an Innovative Icebreaker Bow. Transactions of Society of Naval Architects and Marine Engineers, New York.

Evan-Iwanowski, R.M., 1976, Resonance Oscillations in Mechanical Systems, Elsevier Scientific Publishing Company, Amsterdam, The Netherlands.

Frederking, R. and Schwarz, J., 1982, Model Tests of Ice Forces on Fixed and Oscillating Cones, Cold Regions Science and Technology, Vol. 6, Elsevier, Amsterdam, The Netherlands.

Kasteljan, V.I., Poznjak, I.I. and Ryvlin, A., 1968, Ice Resistance to Motion of a Ship, Subostroyeniye, Leningrad, USSR. Translated by Marine Computer Application Corporation.

Keinonen, A., 1983, Major Problems with Ice Model Testing of Ships. Proceedings of 20th American Towing Tank Conference, Vol. II.

Kitazawa, T. and Ettema, R., 1986, Level Ice Resistance of an Icebreaking Ship with a Long, Parallel Middlebody. IIHR Report No. 120, Institute of Hydraulic Research, The University of Iowa, Iowa City, IA.

Kotras, T.V., Baird, A.V. and Naegle, J.N., 1982, Predicting Ship Performance in Level Ice Resistance. Transactions Society of Naval Architects and Marine Engineers, Vol. 91, Paper No. 11, New York.

Kry, P.R., 1978, A statistical Prediction of Effective Ice Crushing Stresses on Wide Structures. Proceedings of IAHR Ice Symposium, Lulea, Sweden.

Lecourt, E.Y., Deslauriers, P.C., 1976, Icebreaking Model Tests for the USGC Polar Star. Report 278 C-2, Arctec Inc., Maryland

Lewis, J.W. and Edwards, R.Y., 1970, Methods for Predicting Icebreaking and Ice Resistance Characteristics of Icebreakers. Transactions of Society of Naval Architects and Marine Engineers, Vol. 78, New York.

Lewis, J.W., Bulat, V., Glen, J.F. and Kotras, T.V., 1983, A Semi-Empirical Ice Resistance Model. Report by Arctec Canada and Arctec Inc. for U.S. Maritime Administration, Washington, D.C..

Maattanen, M., 1975, Experience of Ice Forces against a Steel Lighthouse Mounted on the Seabed. Proceedings POAC 75, Fairbanks, Alaska.

Matsuishi, M. and Ettema, R., 1985, The Dynamic Behavior of a Floating, Cable-Moored Platform Continuously Impacted by Ice Floes. IIHR Report No. 294, Institute of Hydraulic Research, The University of Iowa, Iowa City, IA.

McKindra, C.D. and Lutton, T.C., 1981, Mechanical Behavior of Sea Ice. Monograph 83-1, U.S. Army Cold Regions Research and Engineering Laboratory, Hanover, NH.

Meirovitch, L., 1975, Elements of Vibration Analysis. McGraw-Hill, New York.

Mellor, M., 1983, Mechanical Behavior of Sea Ice. Monograph 83-1, U.S. Army Cold Regions Research and Engineering Laboratory, Hanover, N.H.

Michel, B., 1978, Ice Mechanics Les Presses de l'Universite Laval, Quebec, Canada.

Milano, V.R., 1973, Ship Resistance to Continuous Motion on Ice. Transactions of the Society of Naval Architects and Marine Engineers, Vol. 81.

Milano, V.R., 1975, Variation of Ship.Ice Parameters on Ship Resistance to Continuous Motion in Ice. Proceedings of Ice Tech 75, Paper no. B1, Montreal, Canada, SNAME-Eastern Canadian Sec.

Milano, V.R., 1980, A Reanalysis of Ship Resistance When in Continuous Motion Through Solid Ice. Proceedings of INTER MARITEC 80, Hamburg.

Milano, V.R., 1982, Correlation of Analytical Prediction of Ship Resistance in Ice with Model and Full-Scale Test Results. Proceedings of INTER MARITEC 82, Hamburg.

Mueller, A. and Ettema, R., 1984, Dynamic Response of an Icebreaker Hull to Icebreaking. IIHR Report No. 273, Institute of Hydraulic Research, The University of Iowa, Iowa City, IA.

Naegle, J.R., 1980, Ice Resistance Predictions and Motion Simulation for Ships Operating in Continuous Mode of Icebreaking. Ph.D. Dissertation, The University of Michigan, Ann Arbor, MI.

Newland, D.E., 1984, An Introduction to Random Vibrations and Spectral Analysis. Longman, NY.

Neill, C.R., 1976, Dynamic Ice Forces on Piers and Piles. An Assessment of Design Guidelines in the Light of Recent Research. Canadian Journal of Civil Engineering, Vol. 3, No. 2.

Nyman, T., 1986, On the Ice-Breaking Component in the Level Ice Resistance. Proceedings of IAHR Ice Symposium 1986, Iowa City, IA.

Poznyak, I.I. and Ionov, B.P., 1981, The Division of Ice Breaker Resistance into Components. Proceedings of Sixth Ship Technology and Research (STAR) Symposium June 1981, SNAME, New York, NY.

Price, W.G. and Bishop, R.E.D., 1974, Probabilitic Theory of Ship Dynamics. Chapman and Hall, London.

Salvesen, N., Tuck, E.O., and Faltinsen, O., 1970, Ship Motion and Sea Loads. Society of Naval Architects and Marine Engineers.

Schwarz, J., 1977, New Developments in Modelling Ice Problems. Proceedings of POAC 77, Vol. 1, St. John's, Newfoundland.

Schwarz, J., 1983, Modeling Techniques in Various Ice Model Basins. Lecture notes, Western European Graduate Education in Marine Technology, WEGEMT.

Shodi, D.S. and Morris, C.E., 1986, Characteristic Frequency of Force Variations in Continuous Crushing of Ice Sheet Against Rigid Cylindrical Structure. Cold Regions Science and Technology, Elsevier, Amsterdam.

Stanley, W.D., 1975, Digital Signal Processing. Reston Publishing Co., Virginia.

Tatinclaux, J.C., 1984a, Model Tests in Ice of a Canadian Coast Guard R-Class Icebreaker. Special Report 84-6, U.S. Army Cold Regions Research and Engineering Laboratory, Hanover, NH.

Tatinclaux, J.C., 1984b, Model-Tests on Two Models of WTGB 140-foot Icebreaker. Report 86-3, U.S. Army Cold Regions Research and Engineering Laboratory, Hanover, NH.

Tatinclaux, J.C., 1986, Ice Floe Distribution in the Wake of a Simple Wedge. Proceedings 5th International Symposium on Offshore Mechanics and Arctic Engineering (OMAE), Tokyo, Japan.

Timco, G.W., 1984, Model Tests of Ice Forces on a Wide Inclined Structure. Proceedings, IAHR Ice Symposium, Hamburg, Germany.

Vance, G.P., 1975, A Scaling System for Vessels Modeled in Ice. Proceedings, Paper No. H1, in Ice Tech 75, SNAME-Eastern Canadian Section, Montreal, Canada.

Voelker, R.P., Geisel, F.A., Kotras, T.V. and Edgecombe, M., 1985, Ship Icebreaking Dynamics and Level Ice Resistance Testing Aboard USCGC Polar Star in Antarctica. Report No. 1060C-2, Arctec Inc., Maryland.

Williams, M., 1986, Model Tests R-Class Icebreaker. Proceedings, Ice Tech Conference, M.I.T., Cambridge, MA.

Wartsila Ice Model Basin (WIMB), 1972, Great Lakes Ore Carrier Series Ice Resistance Model Test Program for MARAD, WIMB Test Report No. 18.

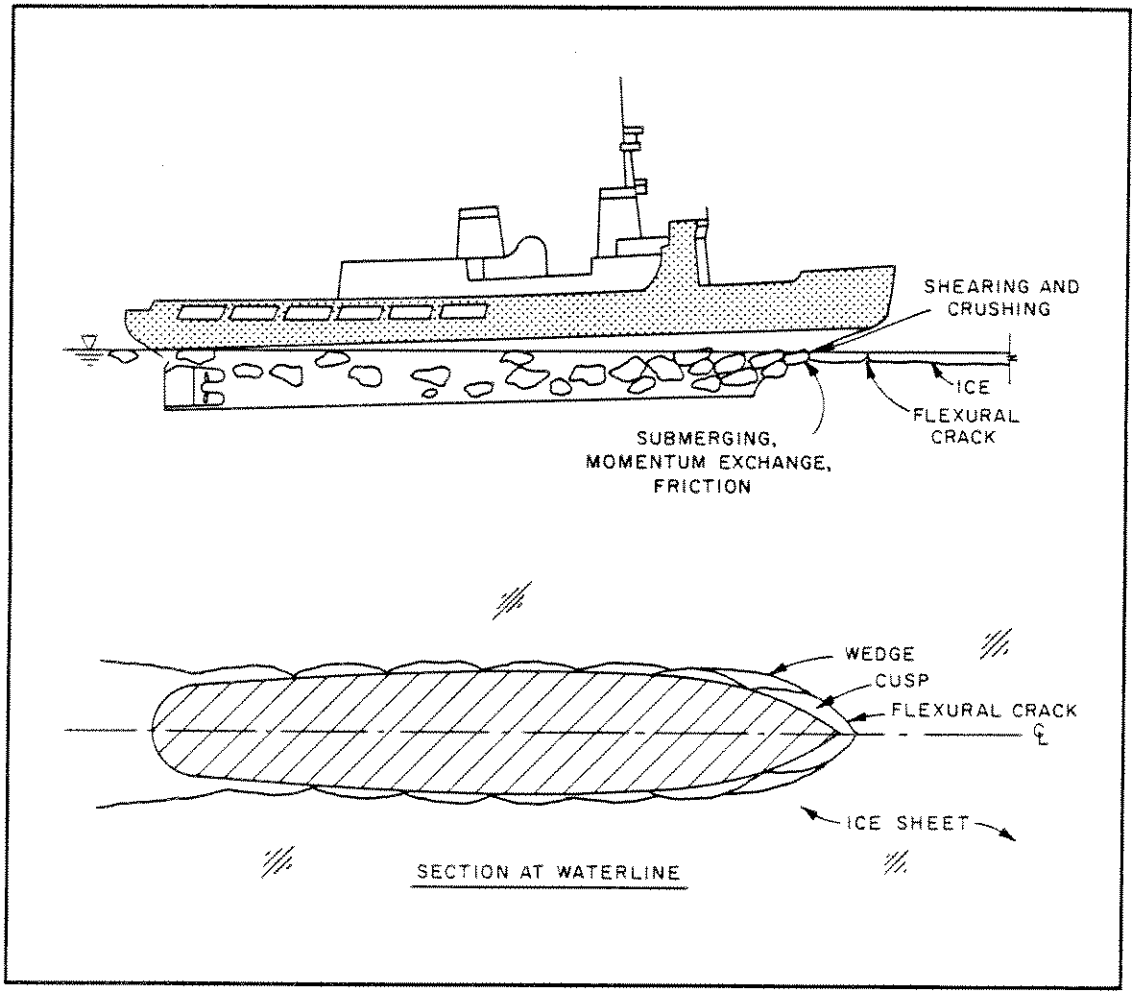

Figure 1. Continuous-mode icebreaking.

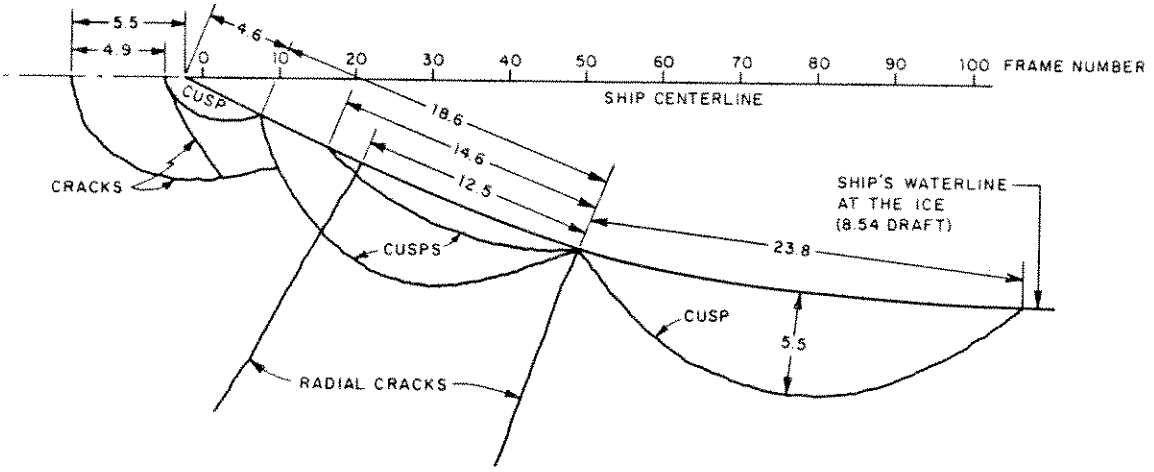

Figure 2. Icebreaking pattern observed from the deck of the USCGC "POLAR SEA" in 0.76m thick level ice (Voelker et al., 1985).

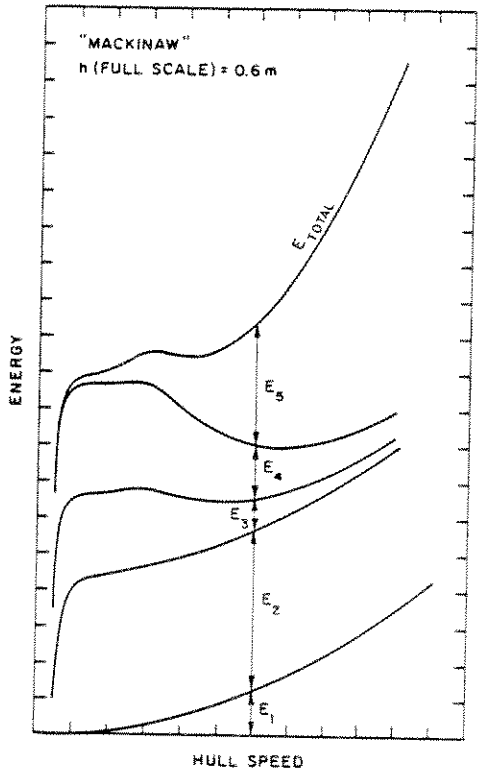

Figure 3. Energy loss versus hull speed for USCGC "MACKINAW" in 0.6m thick level ice (Milano, 1975).

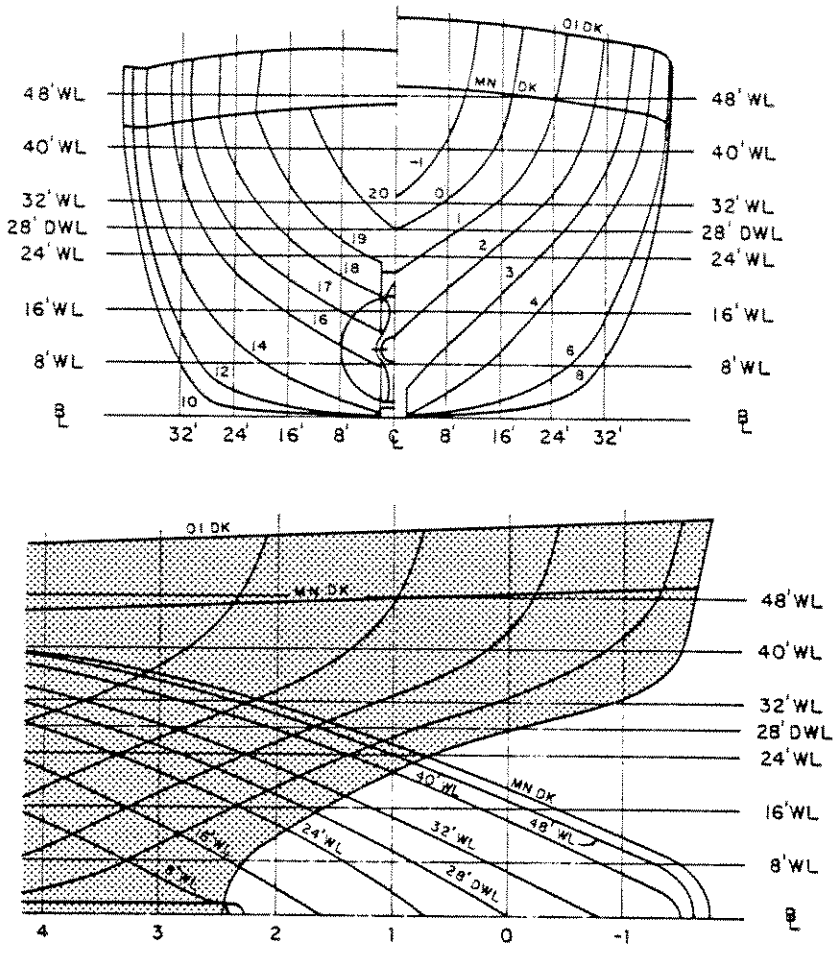

(a)

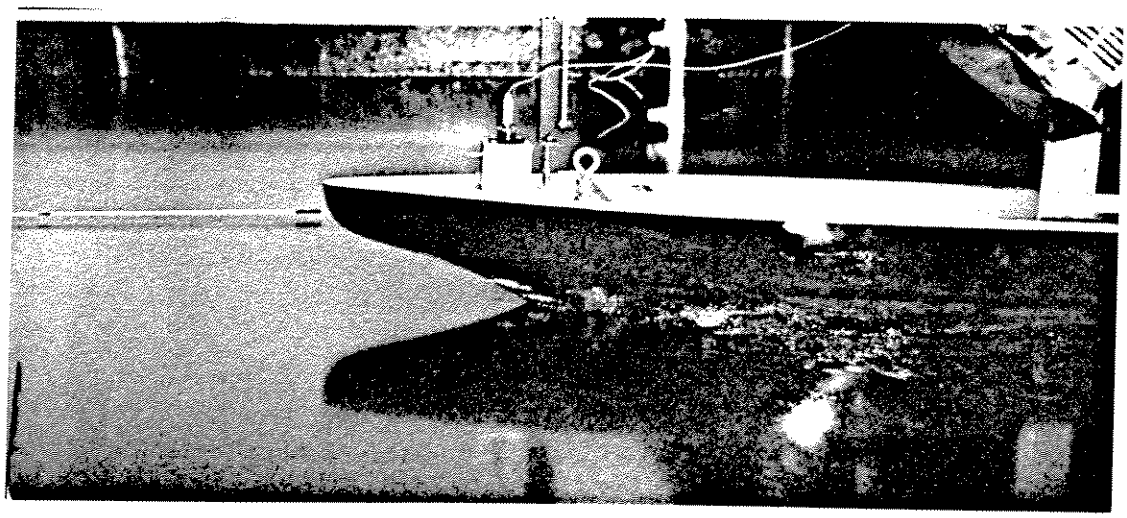

(b)

Figure 4. Abbreviated lines of the USCGC POLAR-Class hull (a); and view of model hull transitting model ice sheet (b).

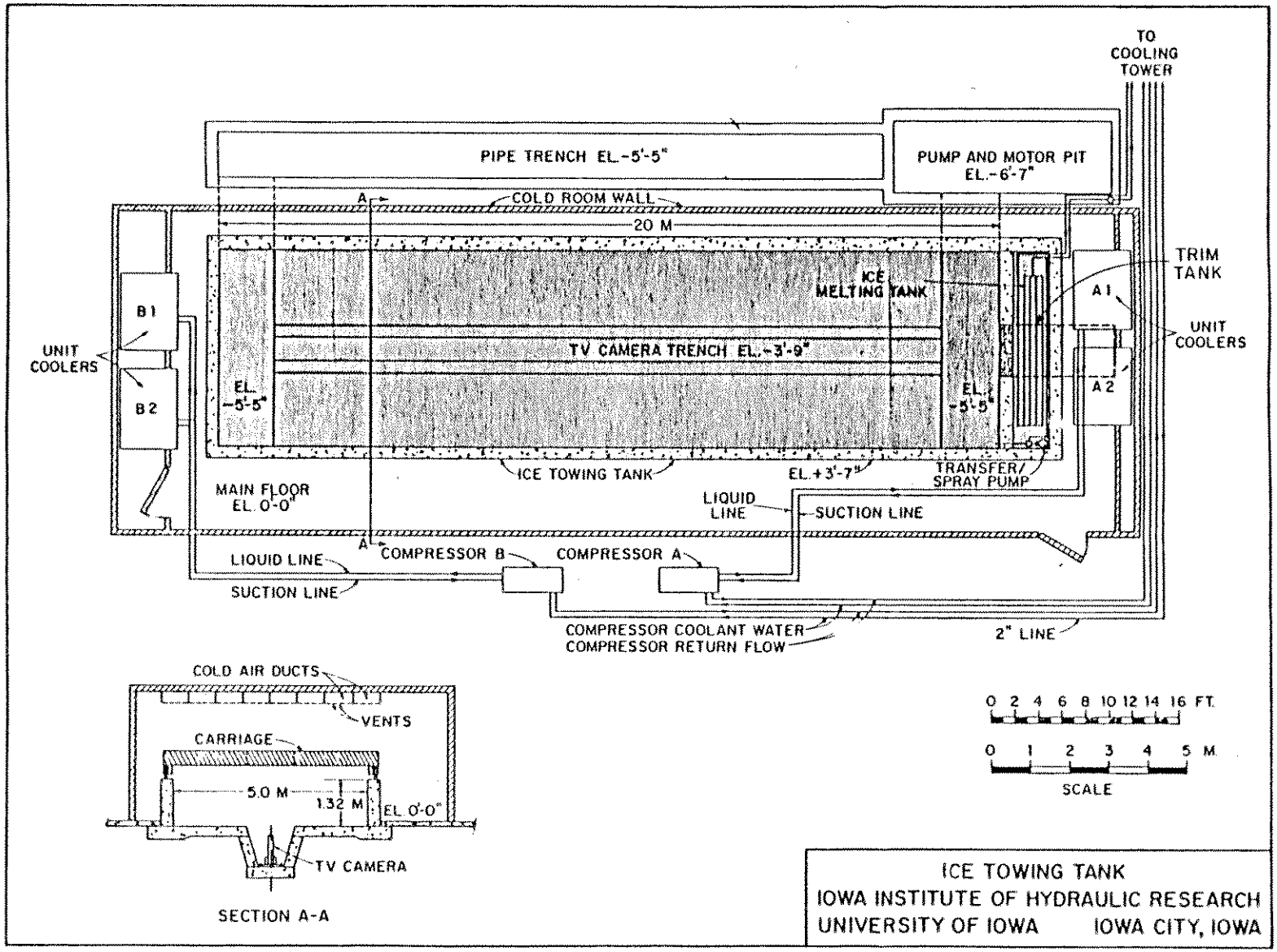

Figure 5. The IIHR Ice Towing Tank

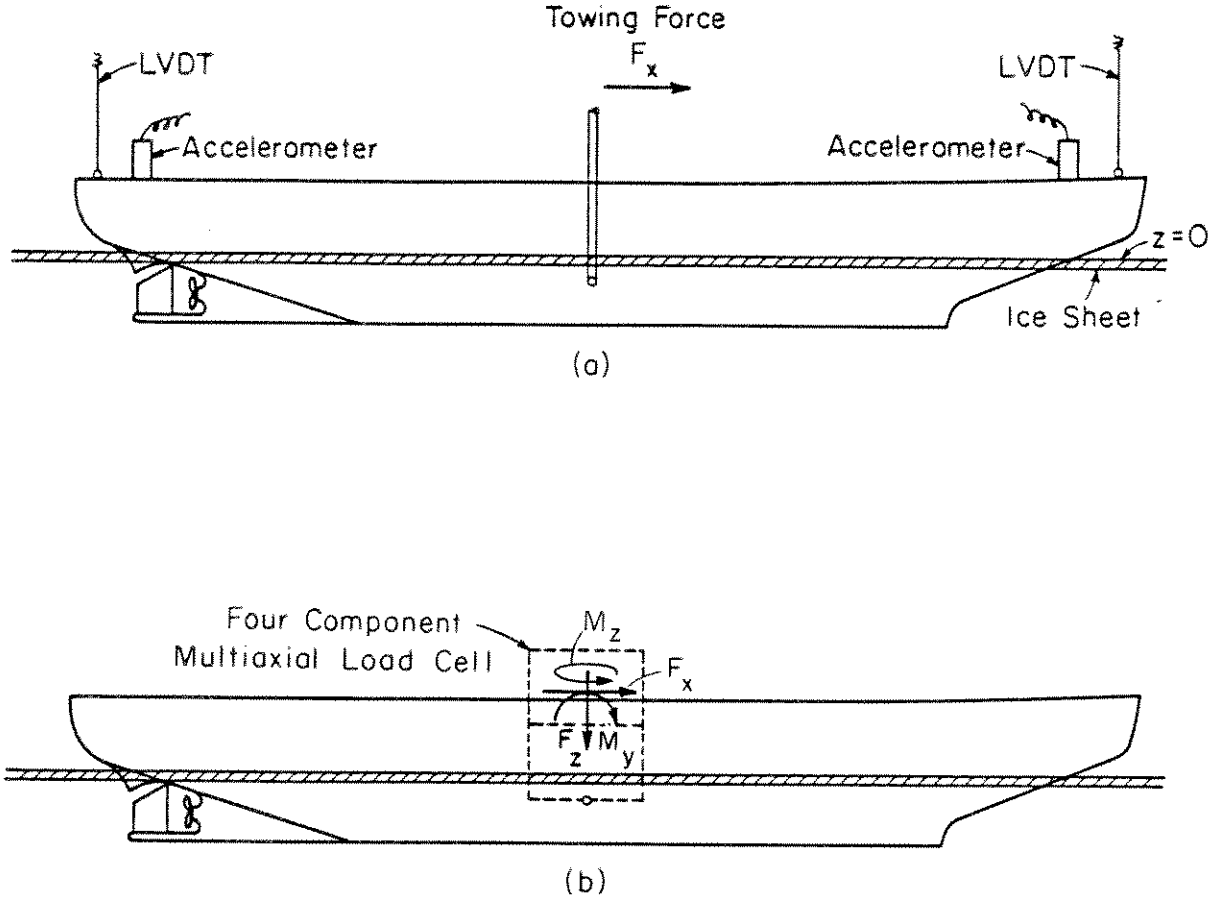

Figure 6. Instrumentation: free hull (a); and fixed hull (b).

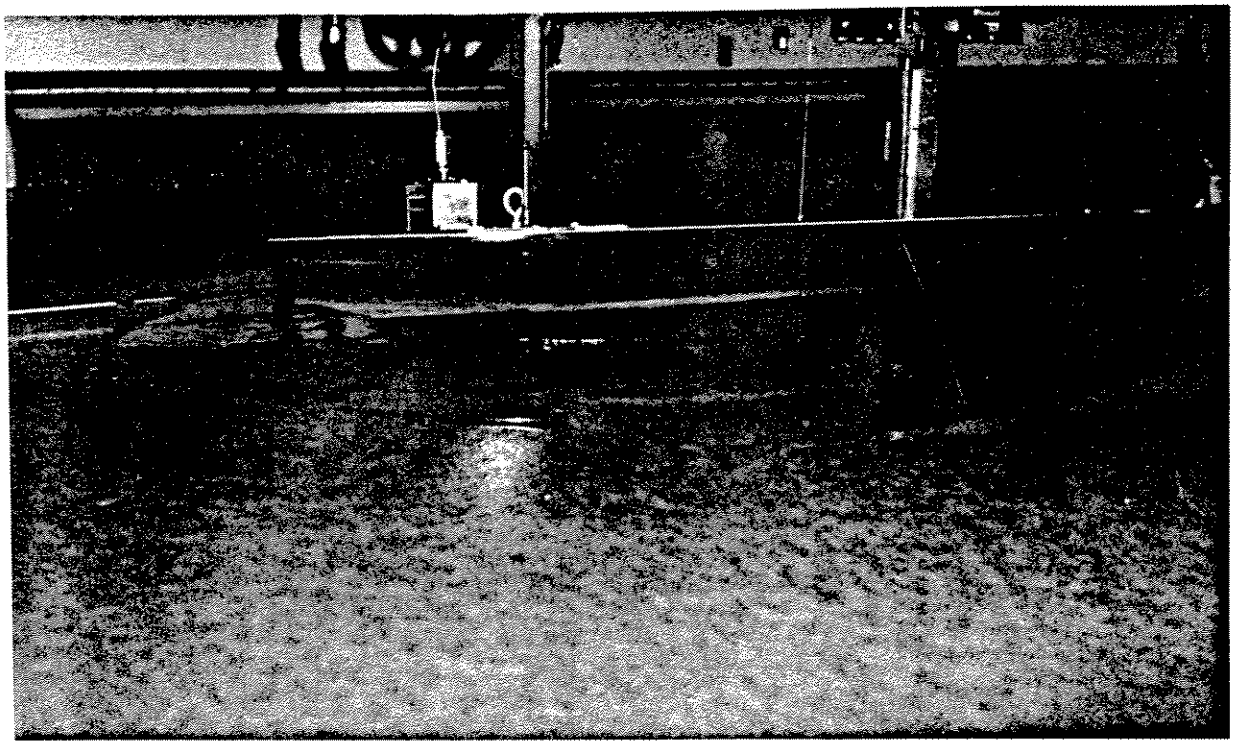

(a)

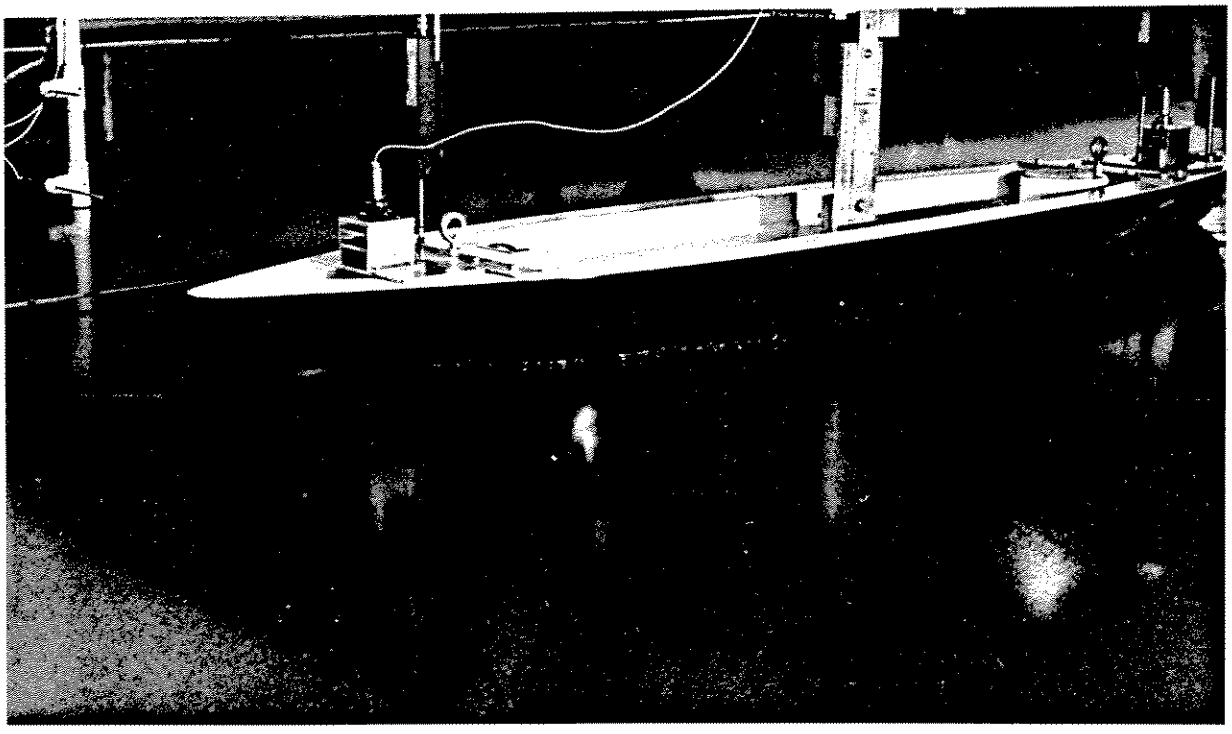

(b)

Figure 9. Hull moving through 41mm thick ice sheet at 0.05 m/s (a); and through 17mm thick ice sheet at 0.5 m/s (b).

(a)

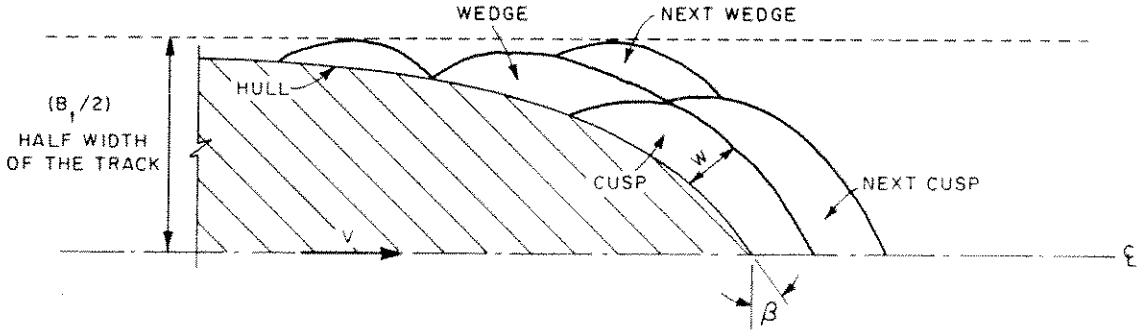

(b)

Figure 10. Observed icebreaking pattern: photograph (a); and generalized pattern (b).

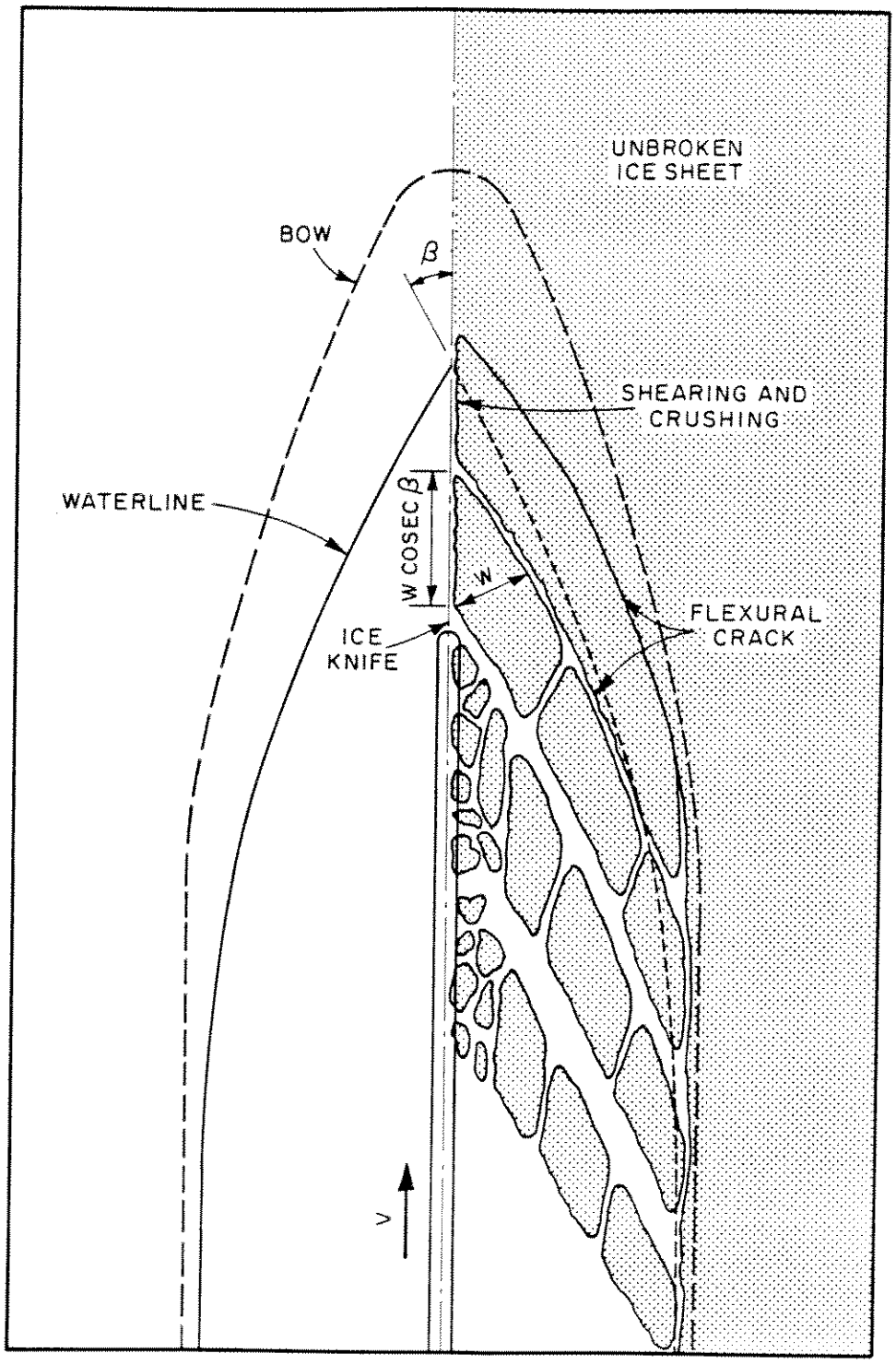

Figure 11. Icebreaking pattern observed beneath the bow of the hull.

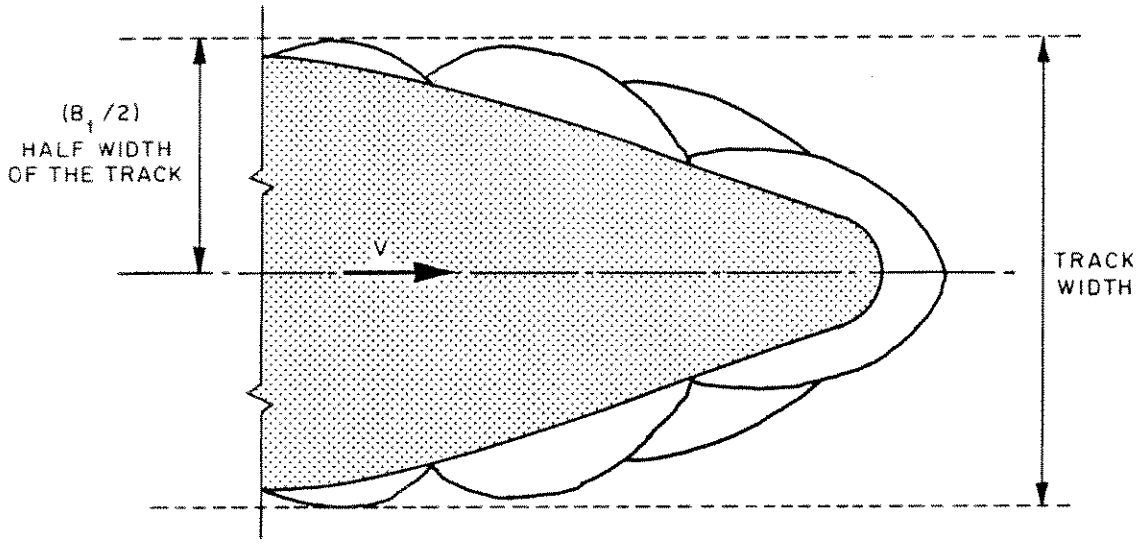

Figure 12. Icebreaking pattern in Figure 10, from a deck level perspective.

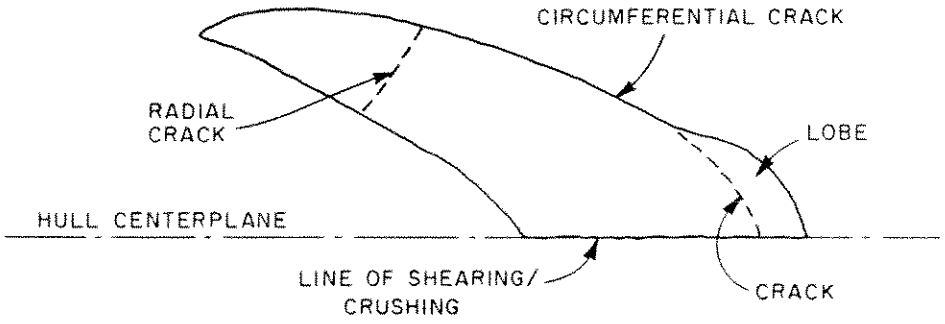

Figure 13. Cusp form with a lobe.

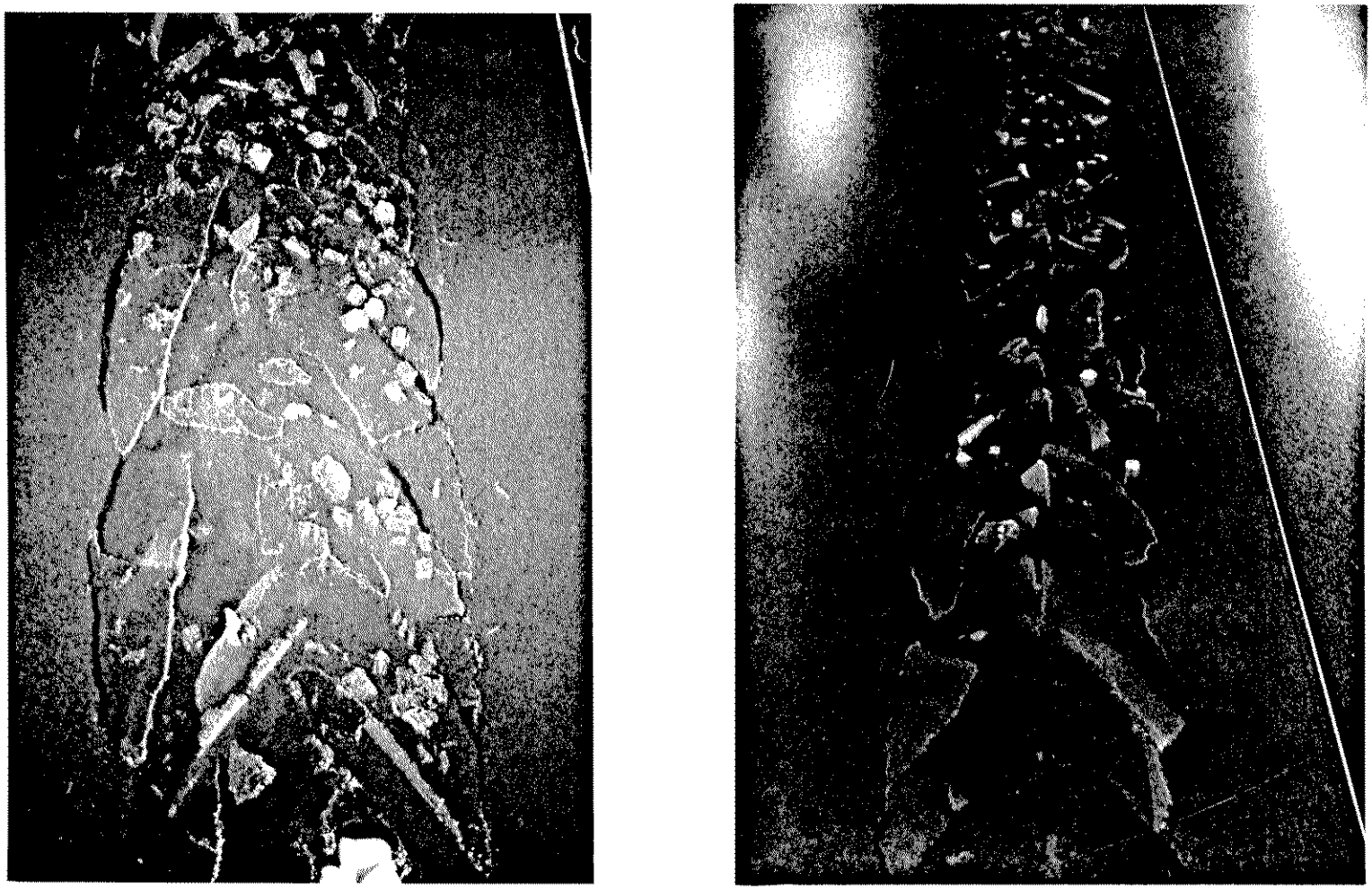

Free Fixed

(a) V = 0.5 m/s

Figure 14. Comparison of icebreaking patterns for the free-hull and the fixed-hull conditions.

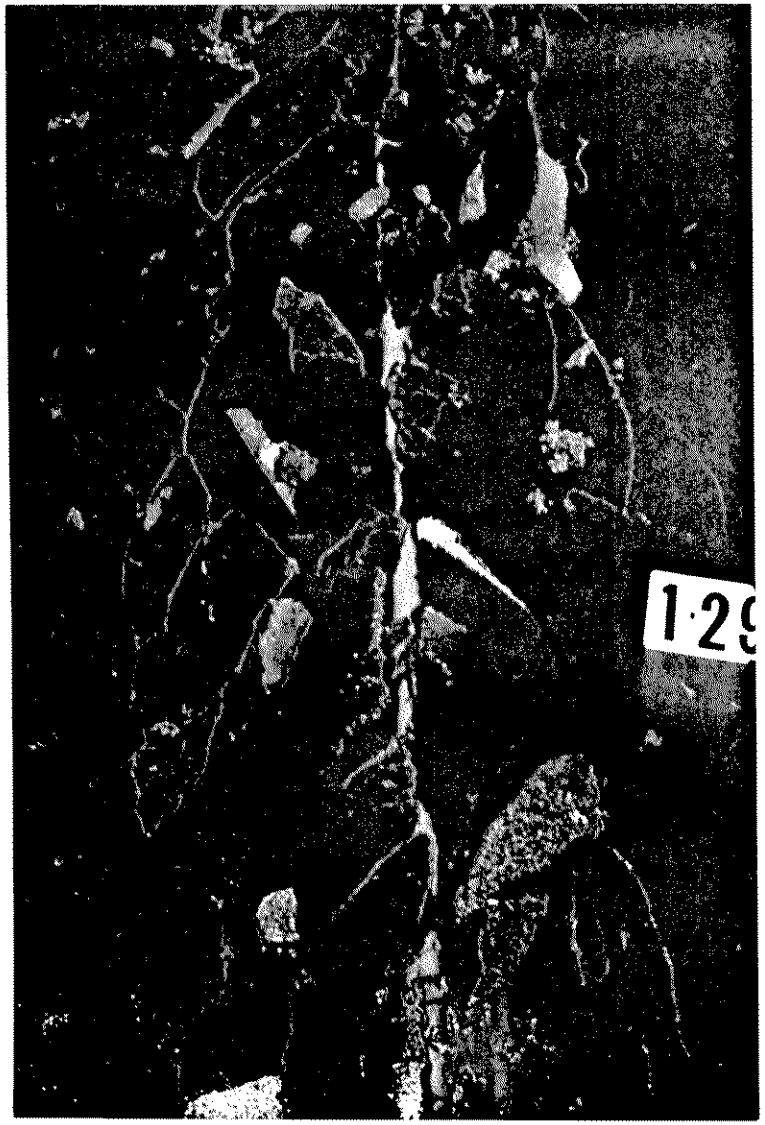

Free

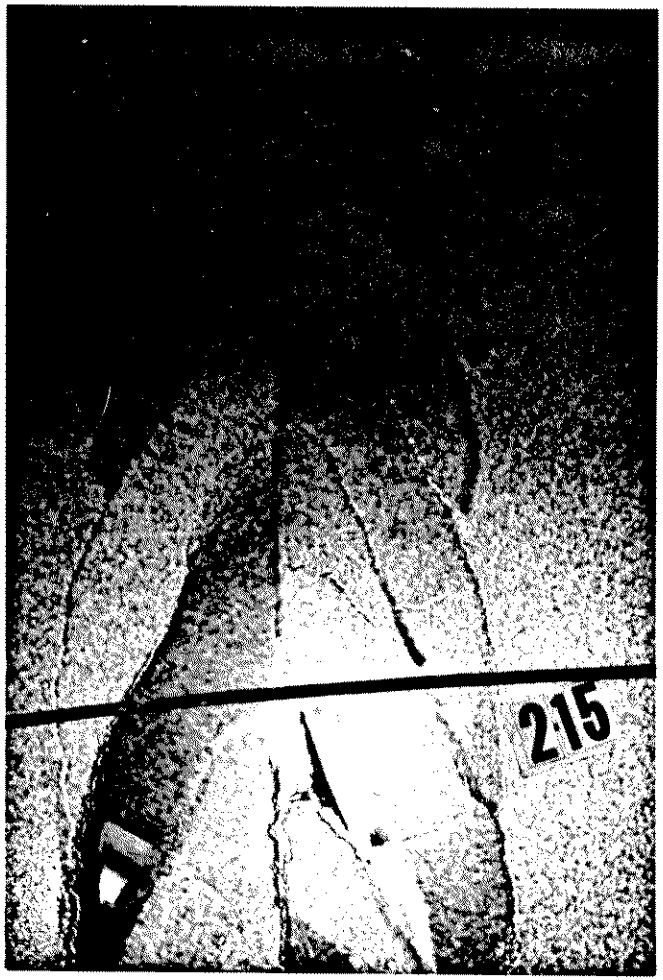

Fixed

(b) V = 0.1 m/s

Figure 14. (Continued).

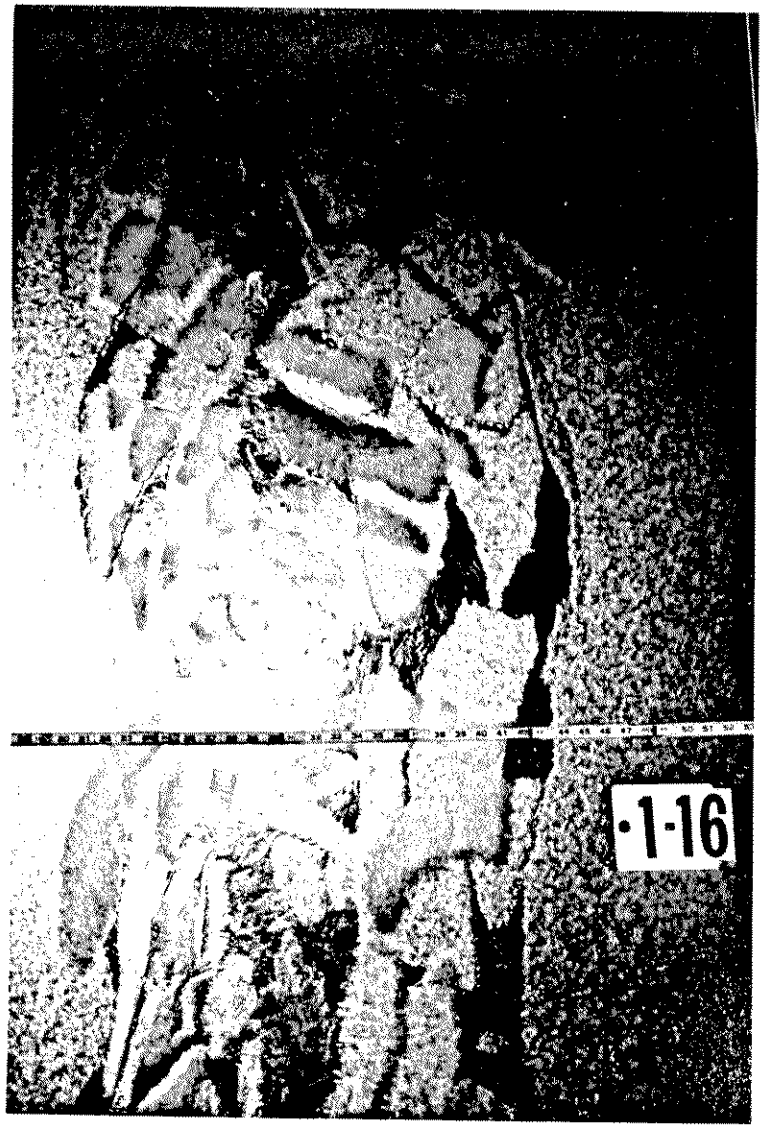

Free

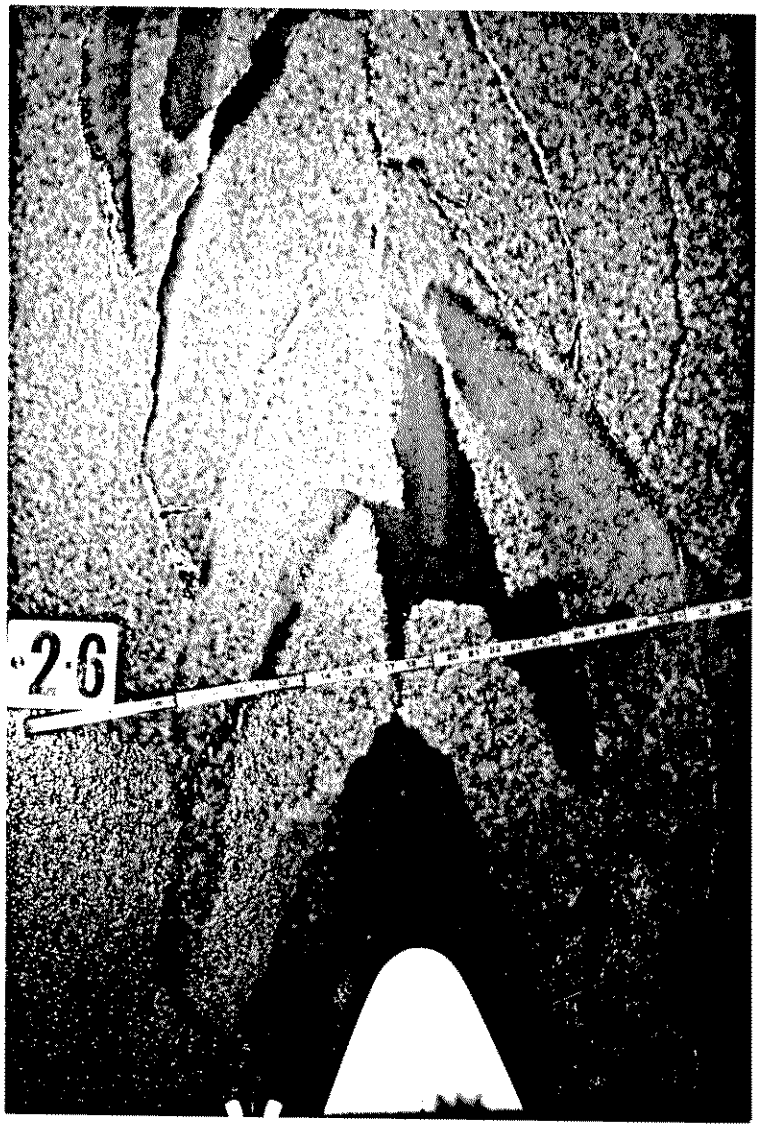

Fixed

(c) V = 0.5 m/s

Figure 14. (Continued).

Free

Fixed

(d) V = 0.9 m/s

Figure 14. (Continued).

Figure 15. Irregularities in icebreaking pattern resulting from hull roll.

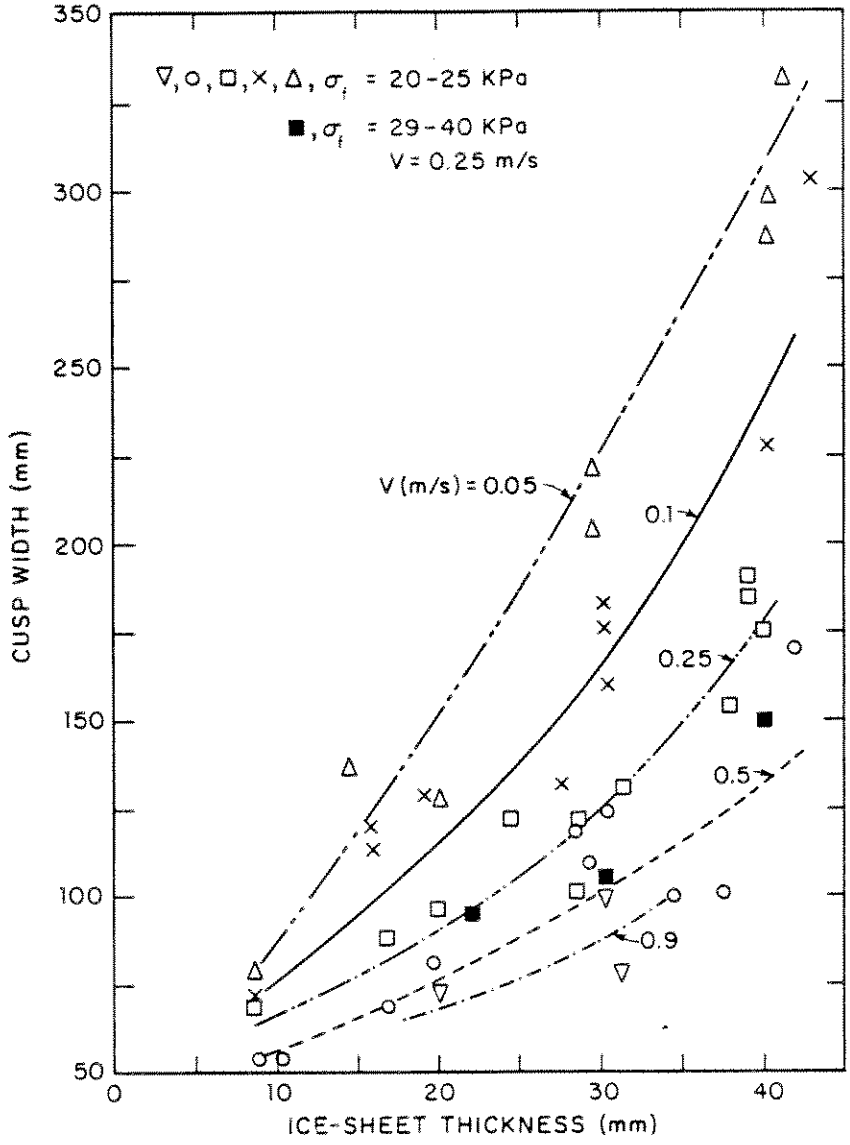

Figure 16. Variation of cusp width, W, with ice-sheet thickness and hull speed.

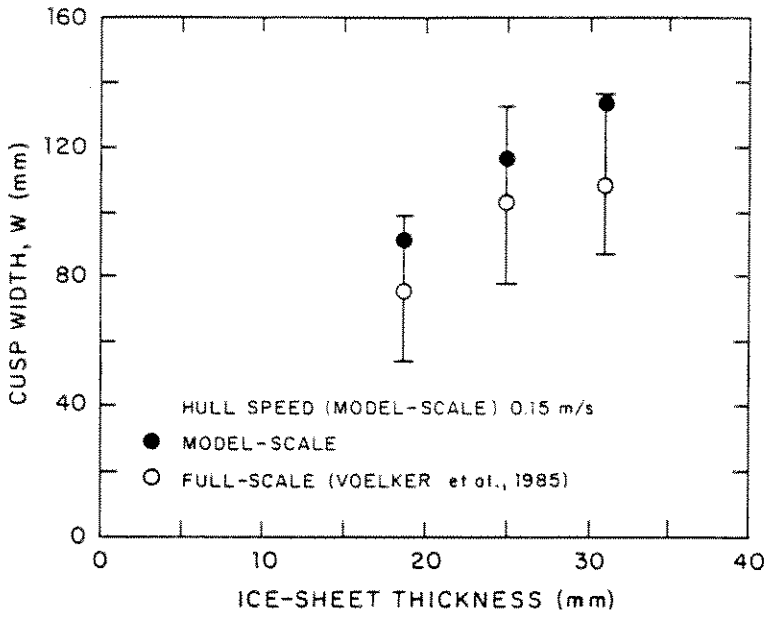

Figure 17. Comparison of experimental and full-scale (Voelker et al., 1985) values of W.

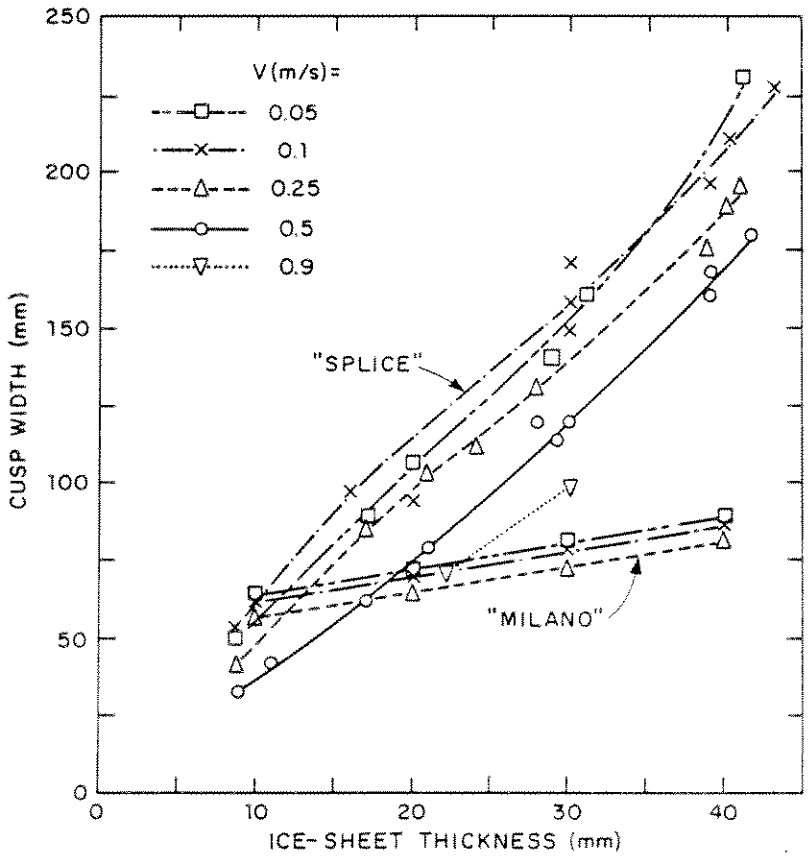

Figure 18. Variation of predicted ("SPLICE" and "Milano") cusp width, W, with ice-sheet thickness and hull speed.

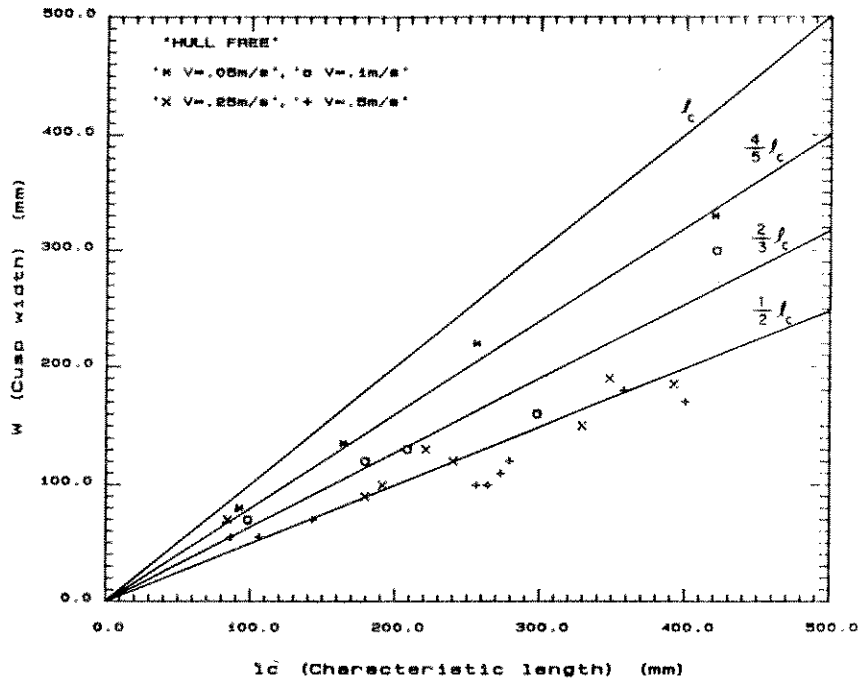

(a)

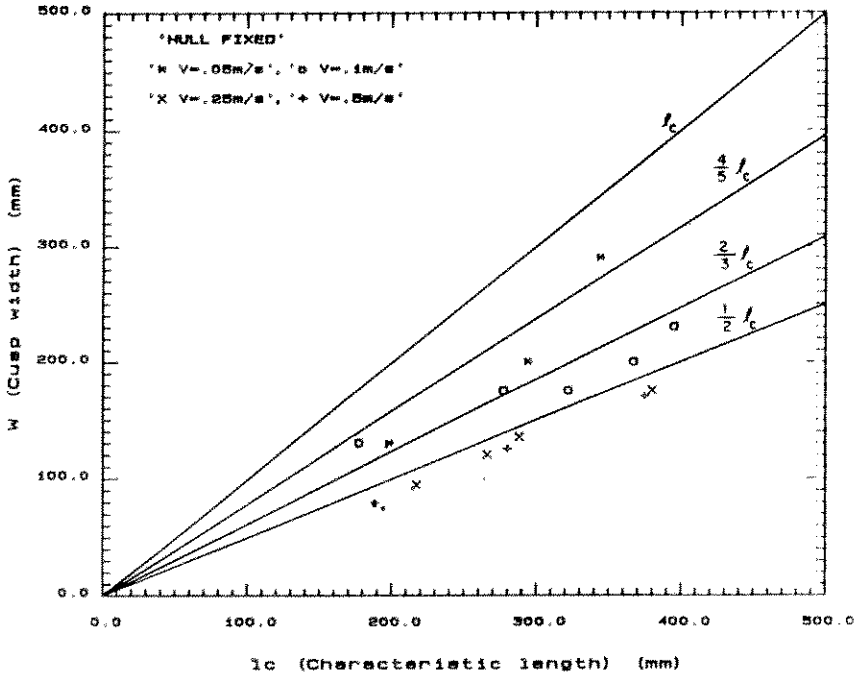

(b)

Figure 19. Correlation of cusp width, W, with characteristic length, ℓ_c: free hull (a); and fixed hull (b).

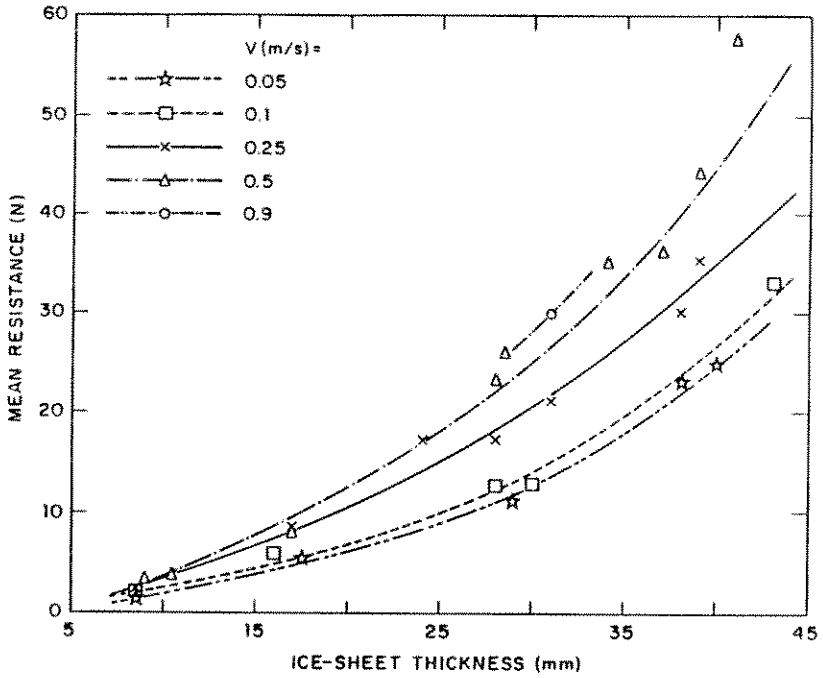

Figure 20. Variation of mean resistance, $\bar{f}_x$, with ice-sheet thickness and hull speed: free hull.

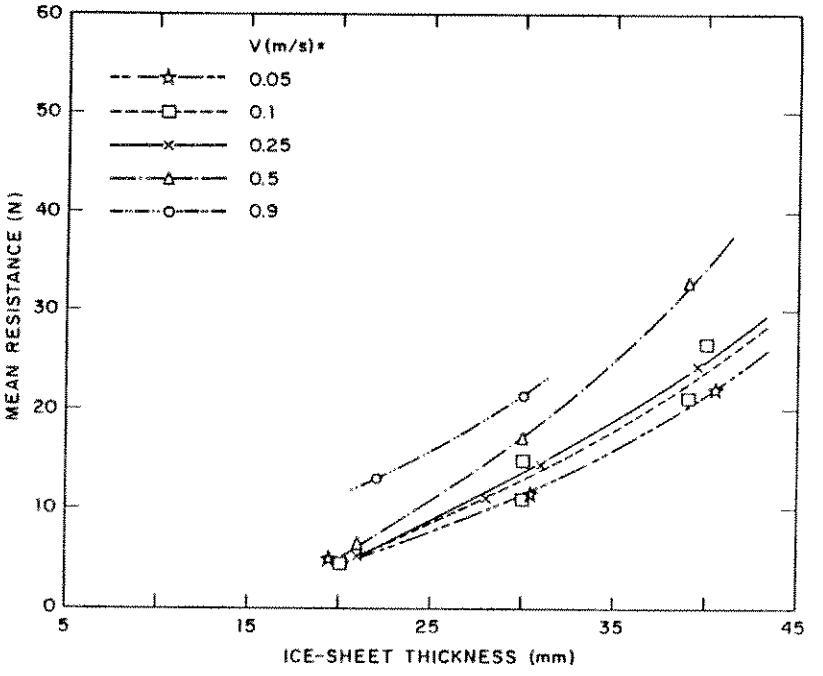

Figure 21. Variation of mean resistance, $\bar{f}_x$, with ice-sheet thickness and hull speed: fixed hull.

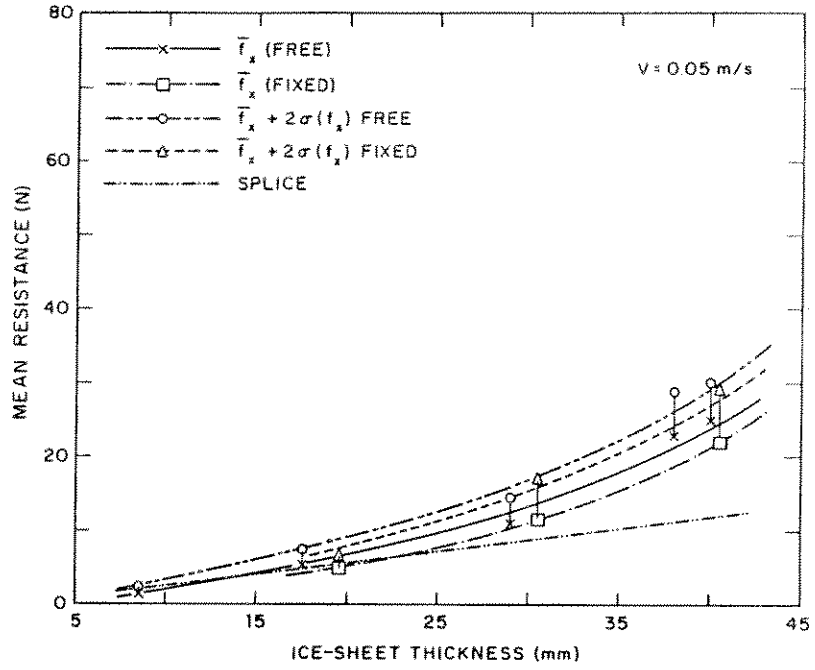

Figure 22. Comparison of $\overline{f}_x$ and $\overline{f}_x + 2\sigma$ between the free and fixed hull: V = 0.05 m/s.

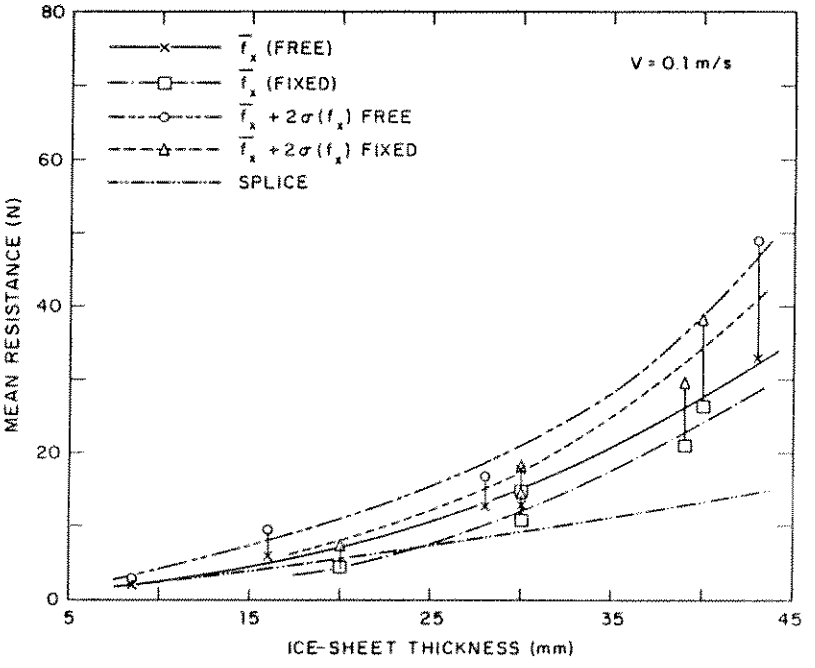

Figure 23. Comparison of $\overline{f}_x$ and $\overline{f}_x + 2\sigma$ between the free and fixed hull: V = 0.1 m/s.

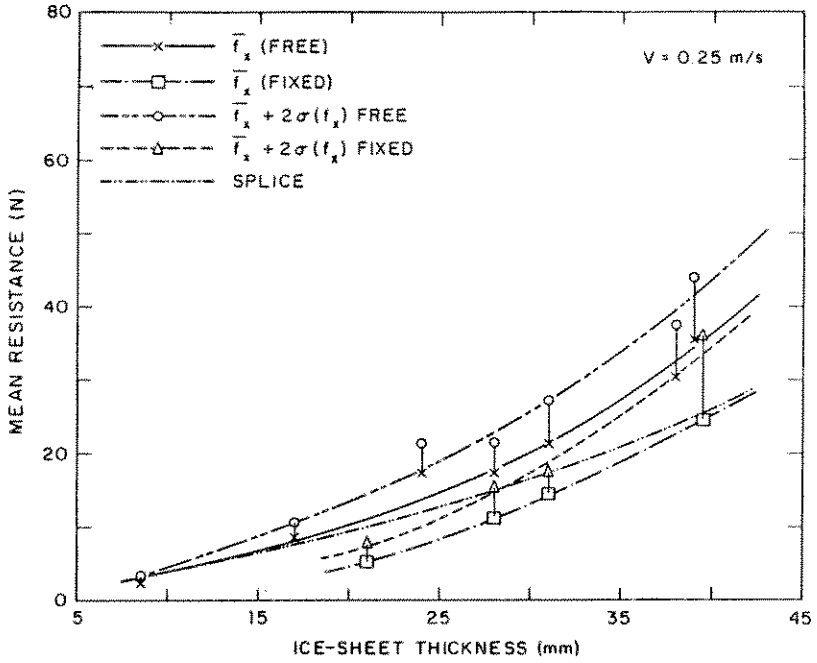

Figure 24. Comparison of $\bar{f}_x$ and $\bar{f}_x + 2\sigma$ between the free and fixed hull: V = 0.25 m/s.

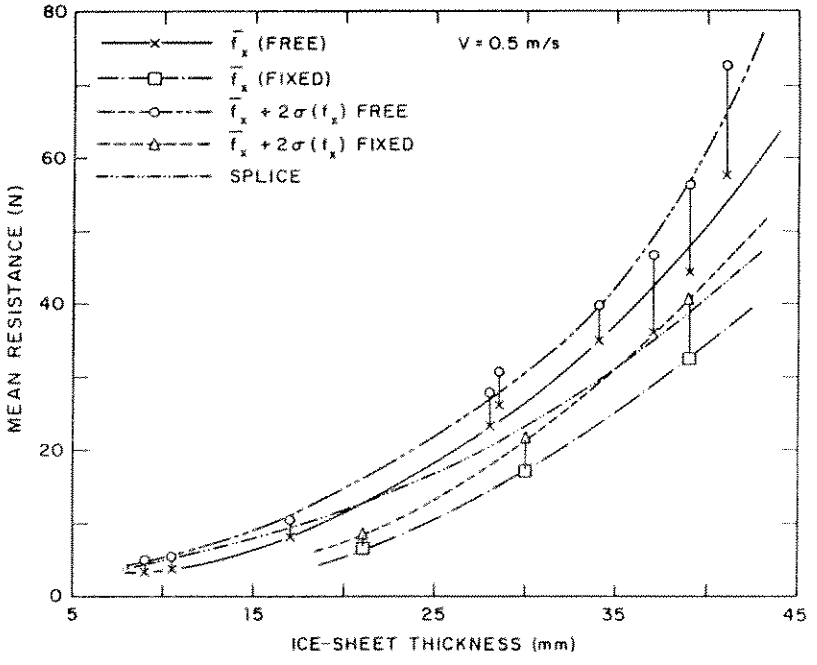

Figure 25. Comparison of $\bar{f}_x$ and $\bar{f}_x + 2\sigma$ between the free and fixed hull: V = 0.5 m/s.

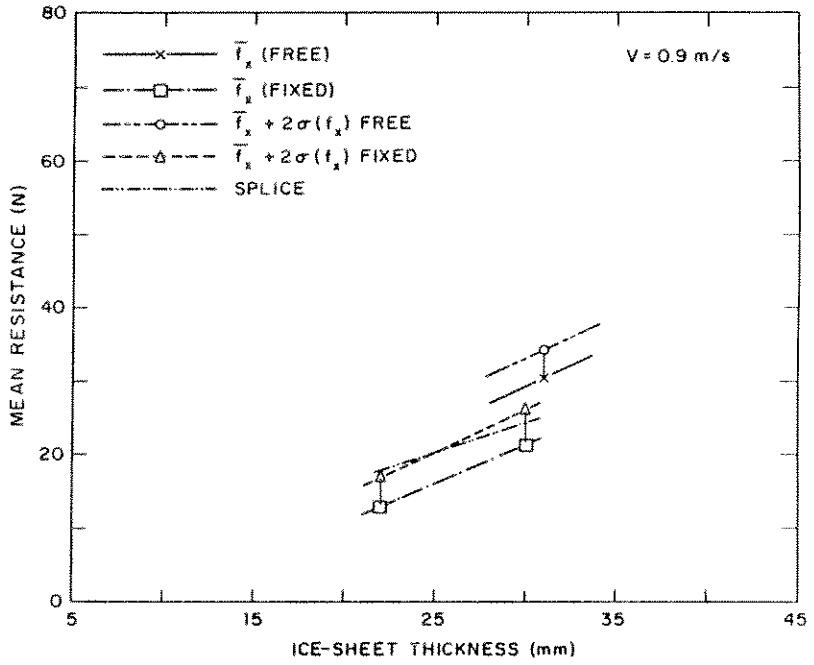

Figure 26. Comparison of $\bar{f}_x$ and $\bar{f}_x + 2\sigma$ between the free and fixed hull: V = 0.9 m/s.

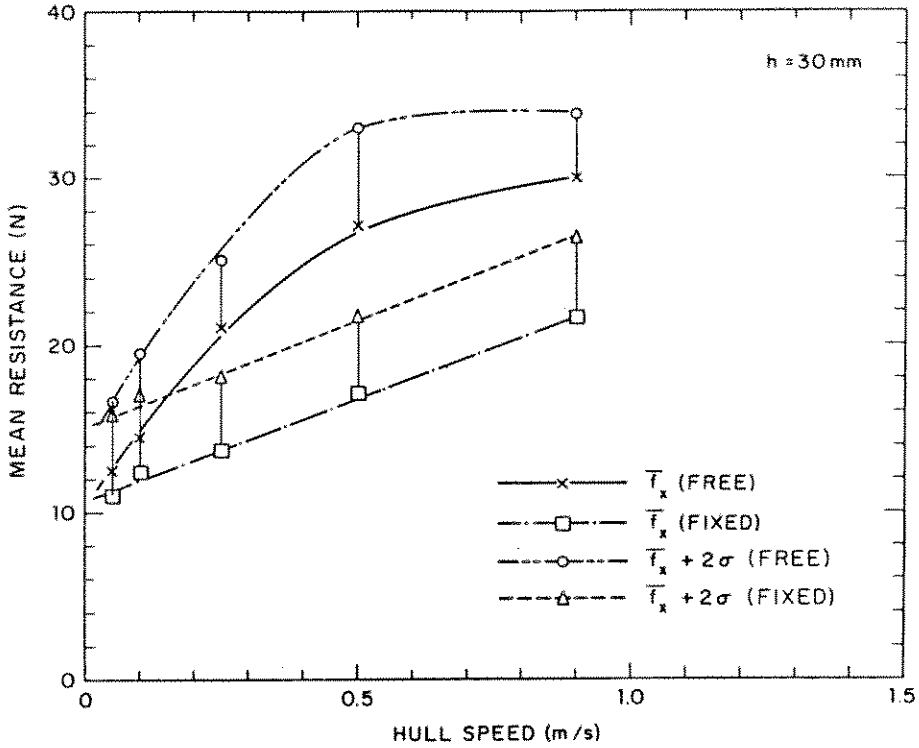

Figure 27. Comparison of $\overline{f}_x$ and $\overline{f}_x + 2\sigma$ between the free- and fixed-hull conditions: h = 30mm.

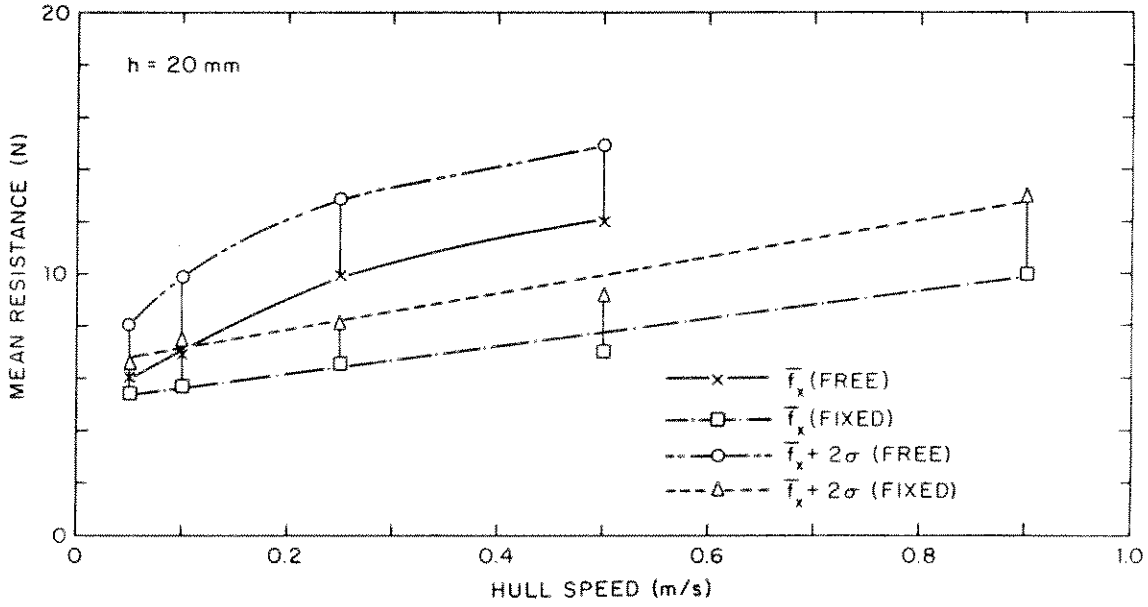

Figure 28. Comparison of $\overline{f}_x$ and $\overline{f}_x + 2\sigma$ for the free-and fixed-hull conditions: h = 20mm.

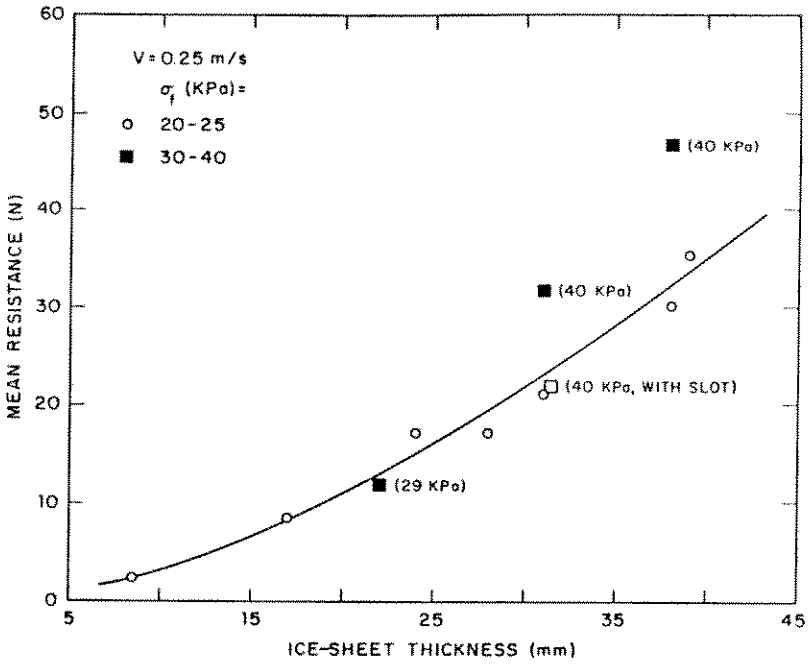

Figure 29. Variation of $\overline{f}_x$ with h and σ_f.

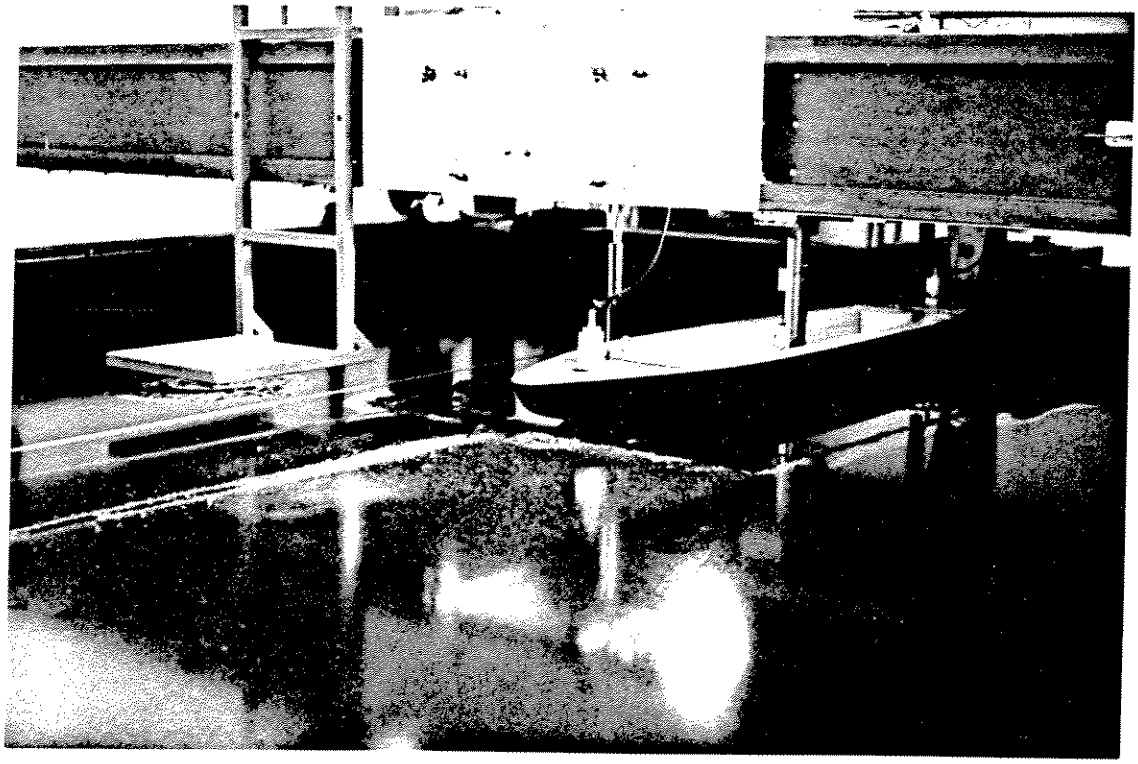

Figure 30. View of preslotted track.

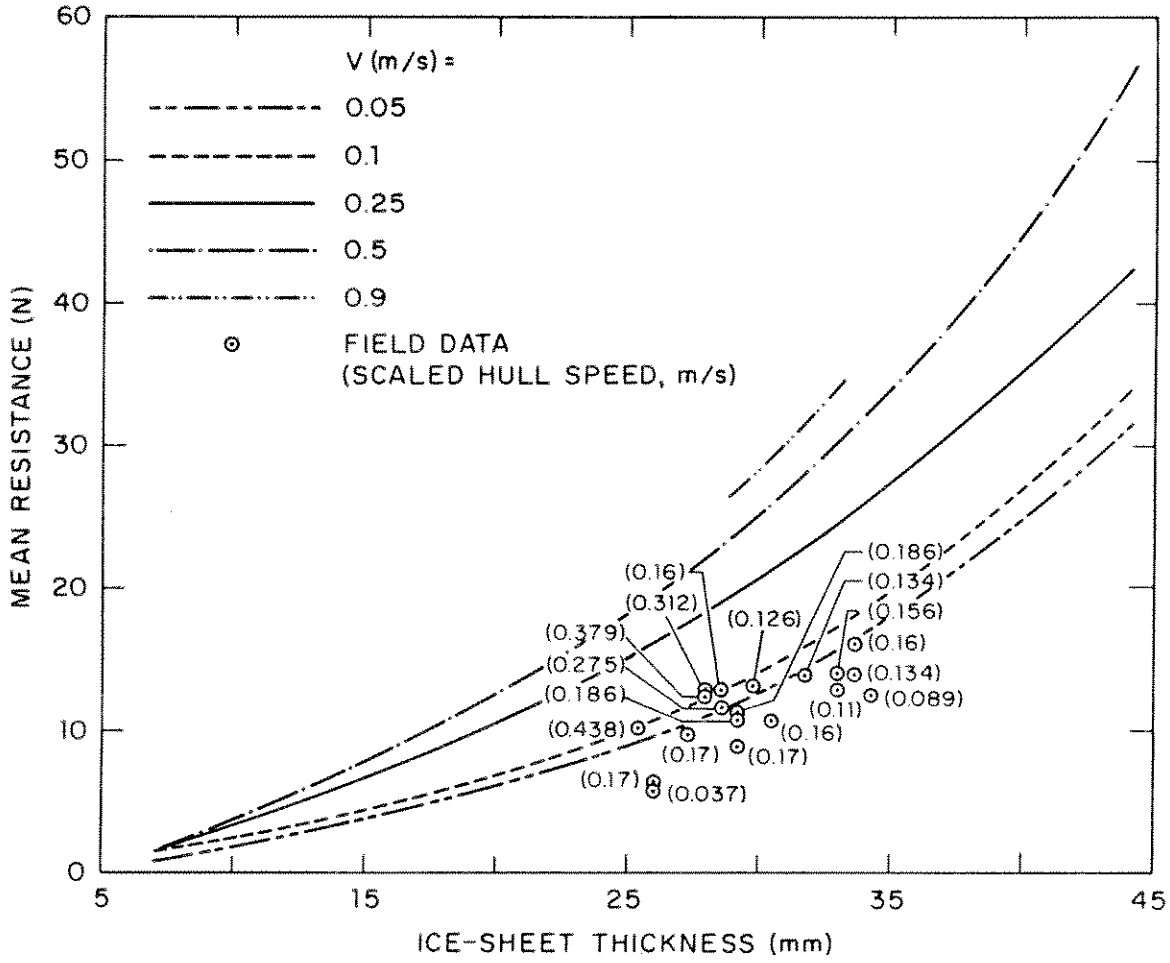

Figure 31. Comparison of experimental and full-scale (Voelker et al., 1985) values of $\bar{f}_x$.

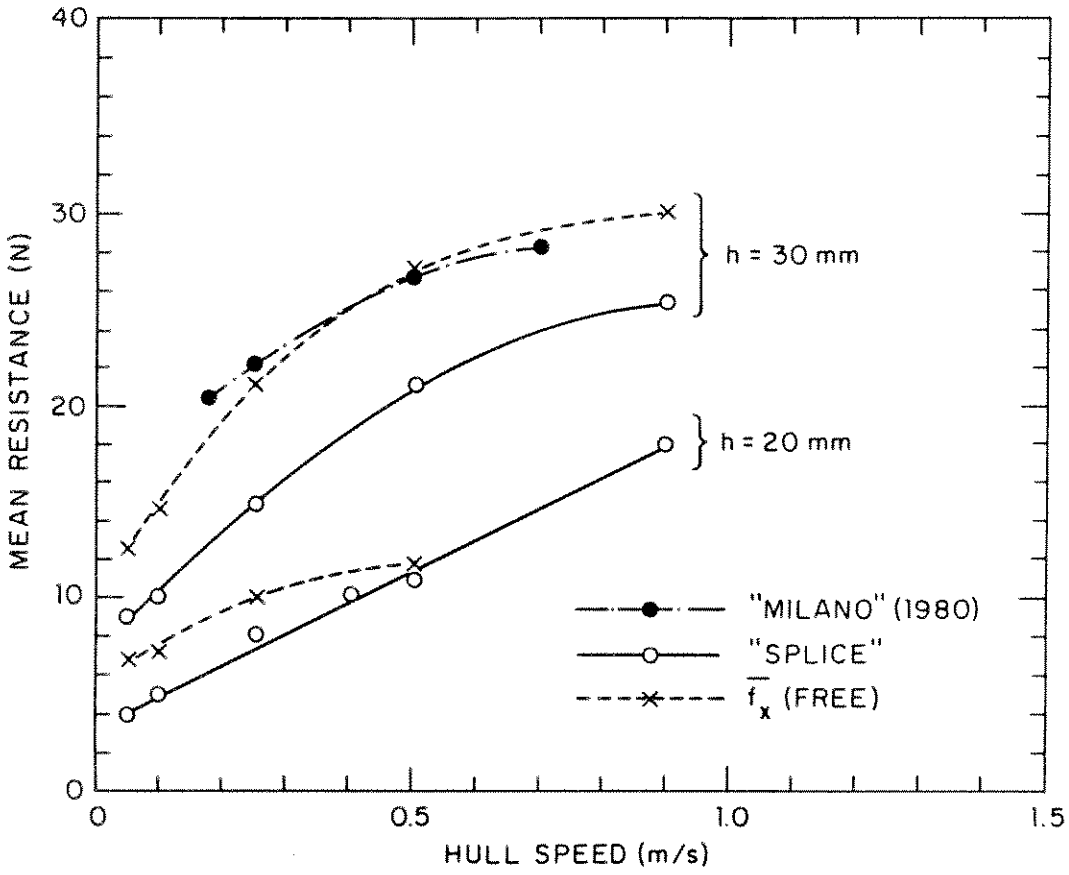

Figure 32. Comparison of experimental values of mean resistance, $\bar{f}_x$, and values predicted using "SPLICE" and "MILANO": h = 30mm.

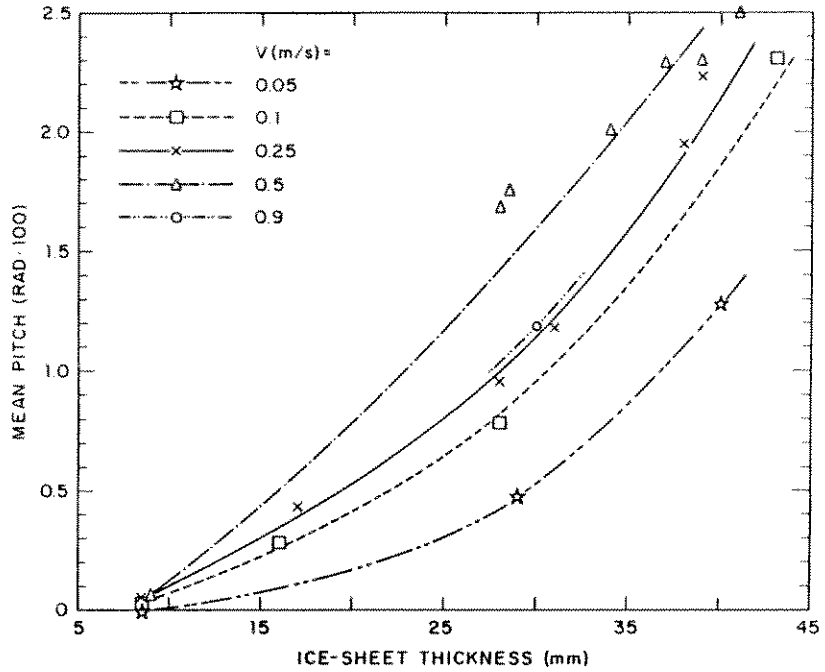

Figure 33. Variation of mean pitch rotation, $\bar{\theta}$, with ice-sheet thickness and hull speed.

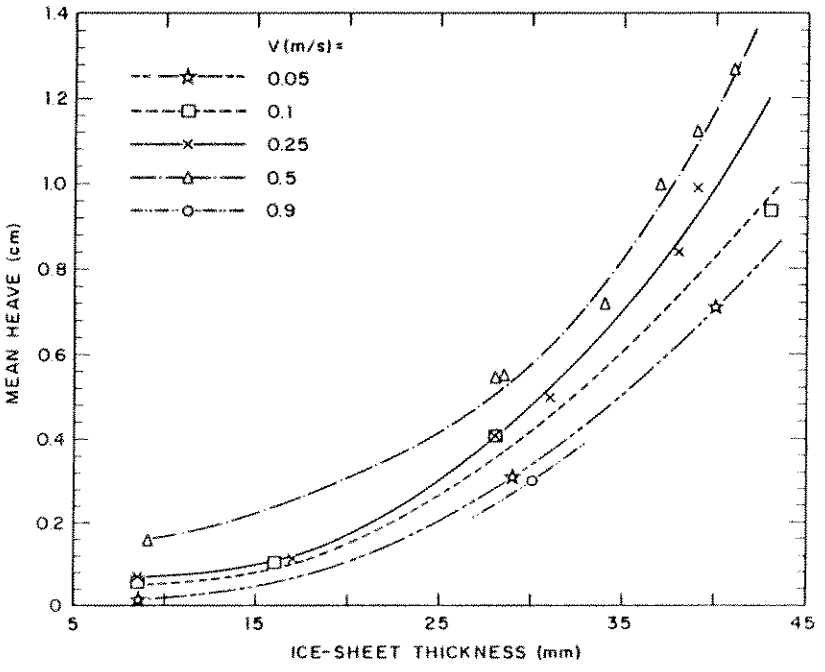

Figure 34. Variation of mean heave displacement, $\bar{z}$, with ice-sheet thickness and hull speed.

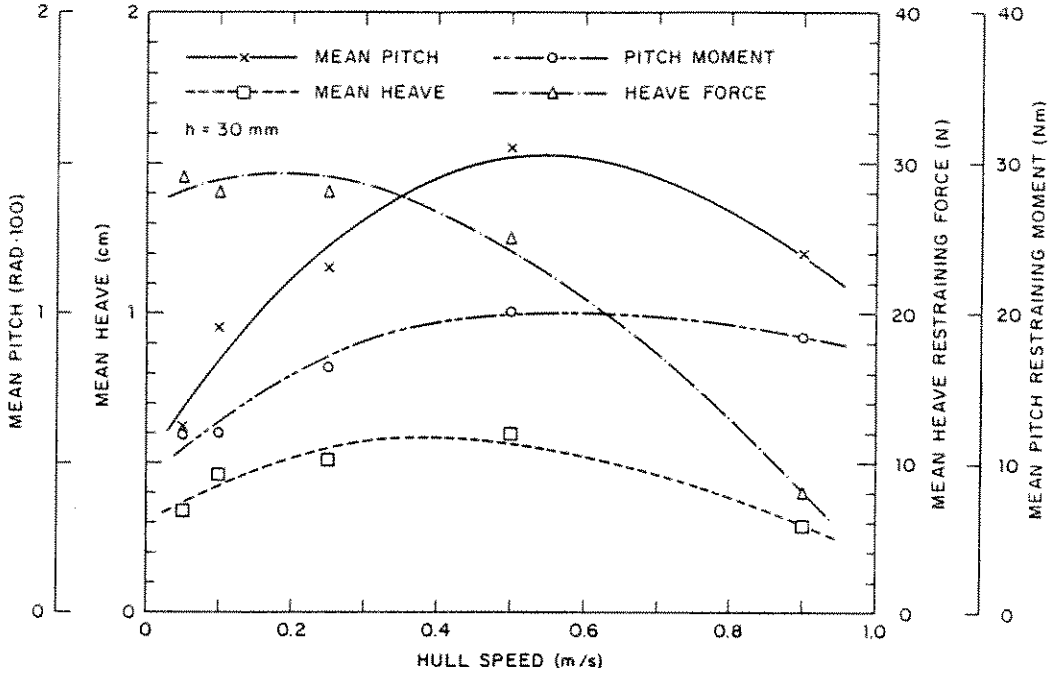

Figure 35. Variation of mean pitch, $\overline{\theta}$, and heave, $\overline{z}$, and pitch- and heave-restraining moment/force, $\overline{m}_{\theta}$ and $\overline{f}_{x}$, with hull speed: h = 30mm.

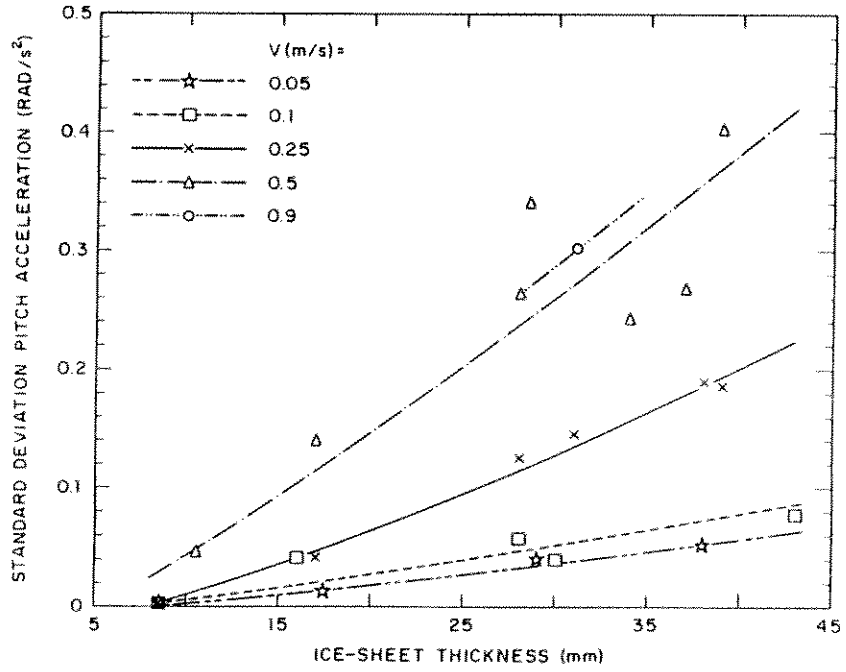

Figure 36. Variation of standard deviation of pitch acceleration, $\sigma_{\ddot{\theta}}$, with ice-sheet thickness and hull speed.

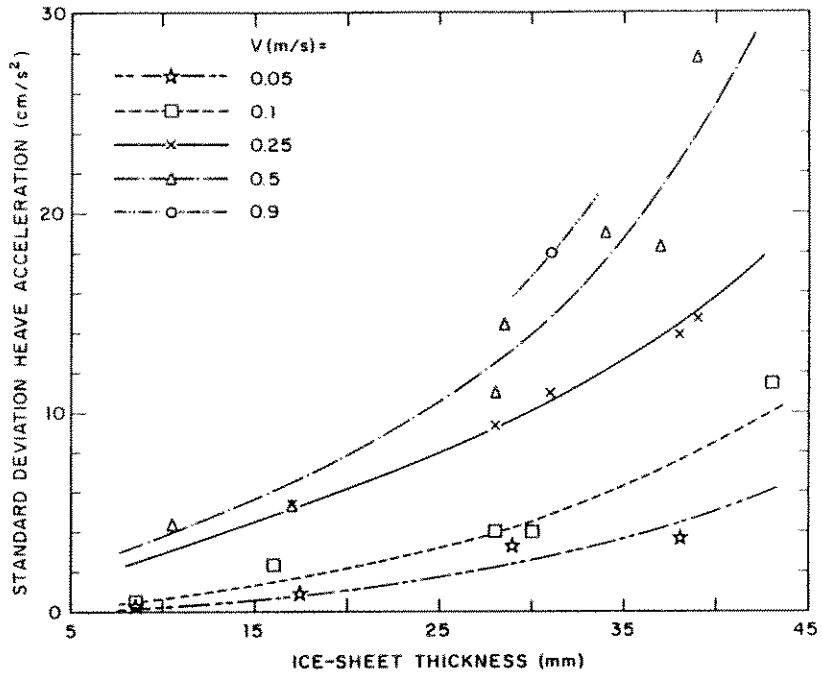

Figure 37. Variation of standard deviation of heave acceleration, σ_z'', with ice-sheet thickness and hull speed.

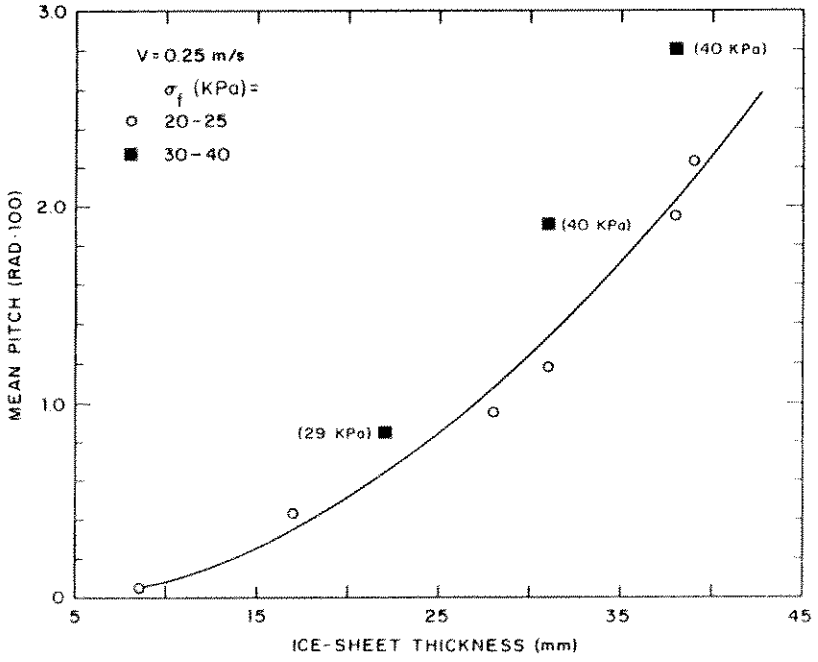

Figure 38. Variation of mean pitch rotation with ice-sheet thickness and flexural strength, σ_f: V = 0.25 m/s.

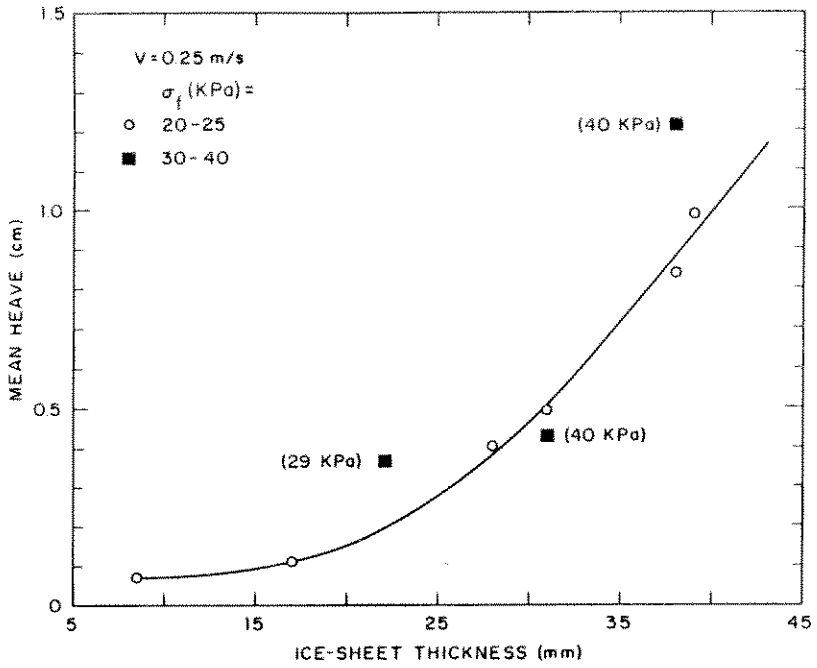

Figure 39. Variation of mean heave displacement, $\bar{z}$, with ice-sheet thickness and flexural strength: V = 0.25 m/s.

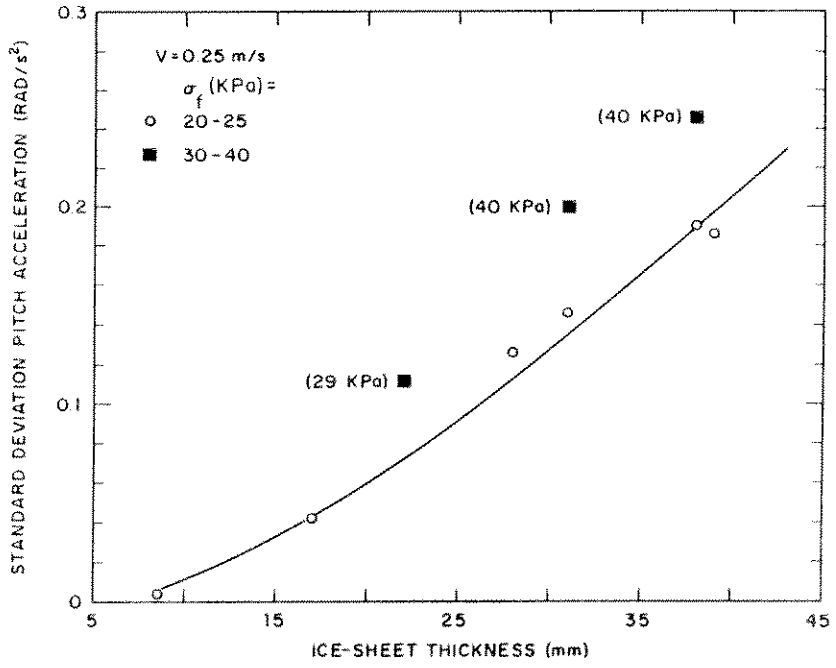

Figure 40. Variation of standard deviation of pitch acceleration, $\sigma_{\ddot{\theta}}$ with ice-sheet thickness and flexural strength, σ_f: V = 0.25 m/s.

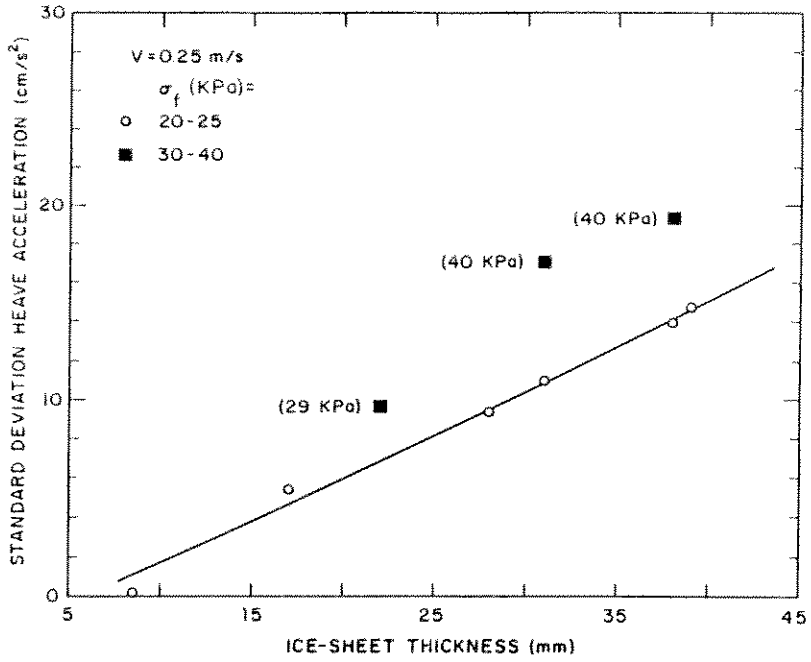

Figure 41. Variation of standard deviation of heave acceleration $\sigma^{\cdot\cdot}_z$, with ice-sheet thickness and flexural strength: V = 0.25 m/s.

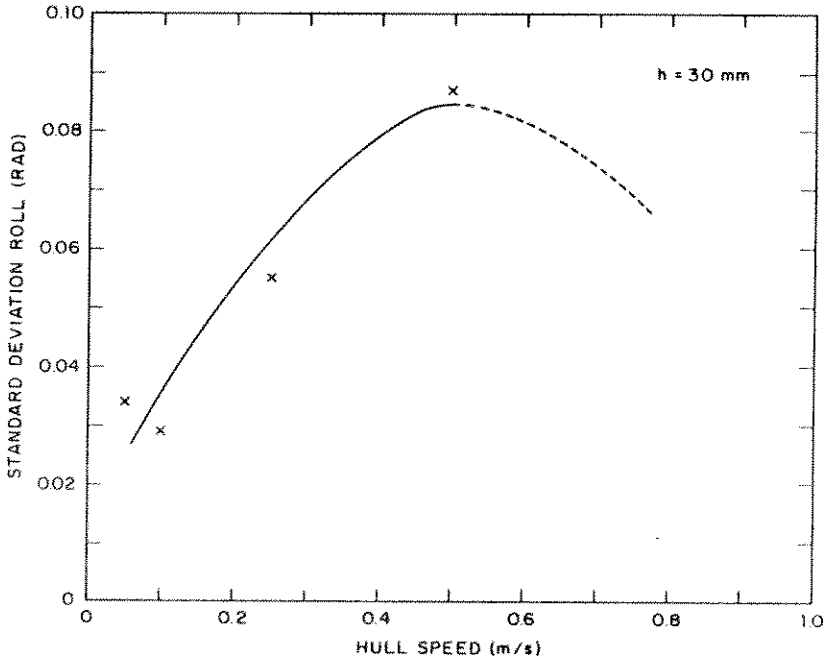

Figure 42. Variation of standard deviation of roll, σ_ϕ, with hull speed: h = 30mm.

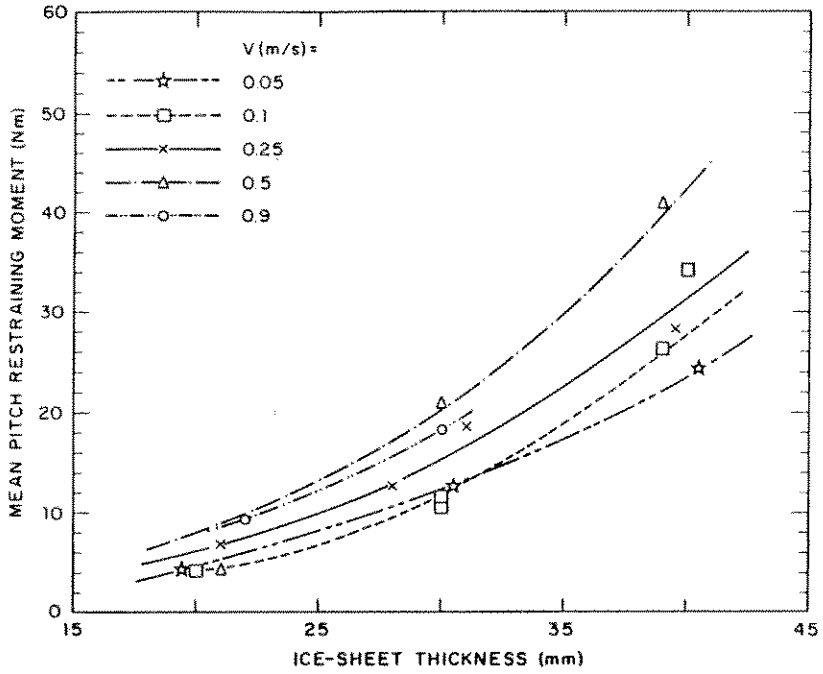

Figure 43. Variation of mean pitch-resistance moment, $\overline{m}_{\theta}$, with ice-sheet thickness and hull speed.

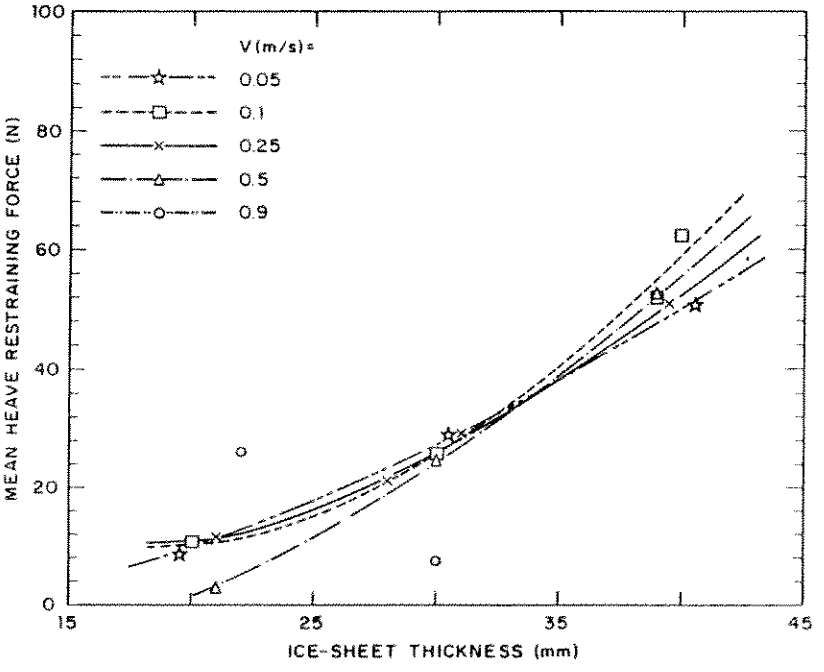

Figure 44. Variation of mean heave-restraining force, $\overline{f}_{z}$, with ice-sheet thickness and hull speed.

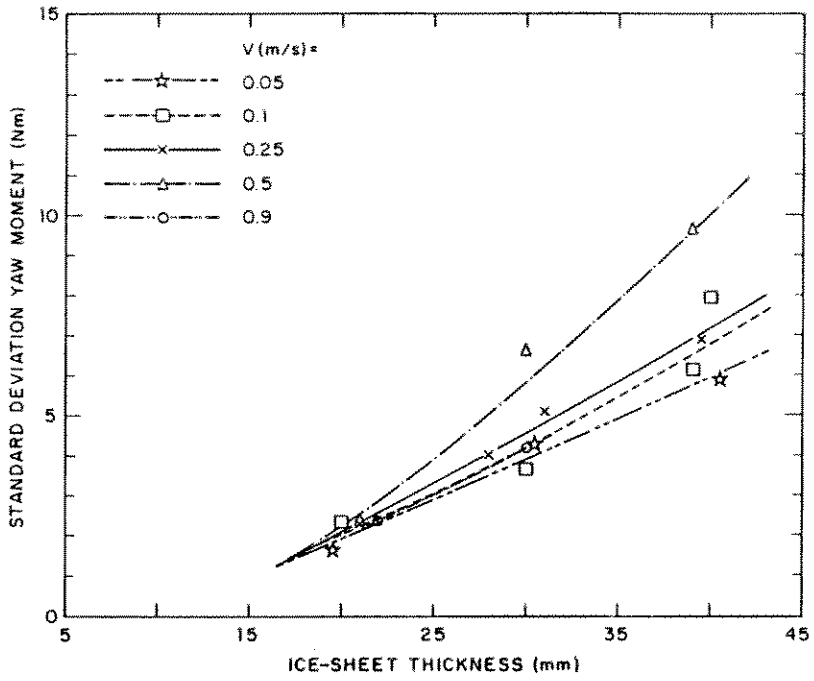

Figure 45. Variation of standard deviation of yaw-restraining moment, m_{ψ}, with ice-sheet thickness and hull speed.

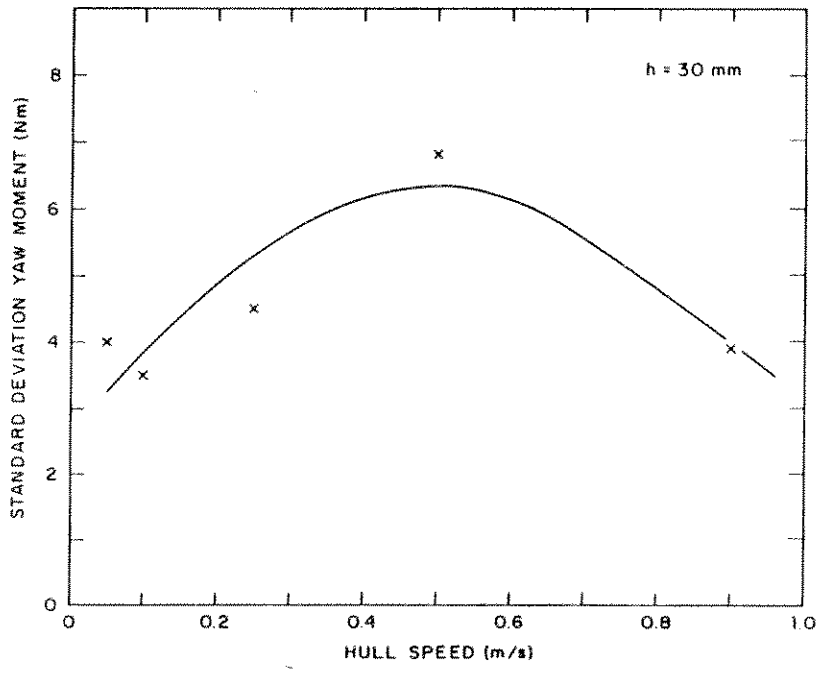

Figure 46. Variation of standard deviation of yaw-restraining moment, $\sigma_{m\psi}$, with hull speed: h = 30mm.

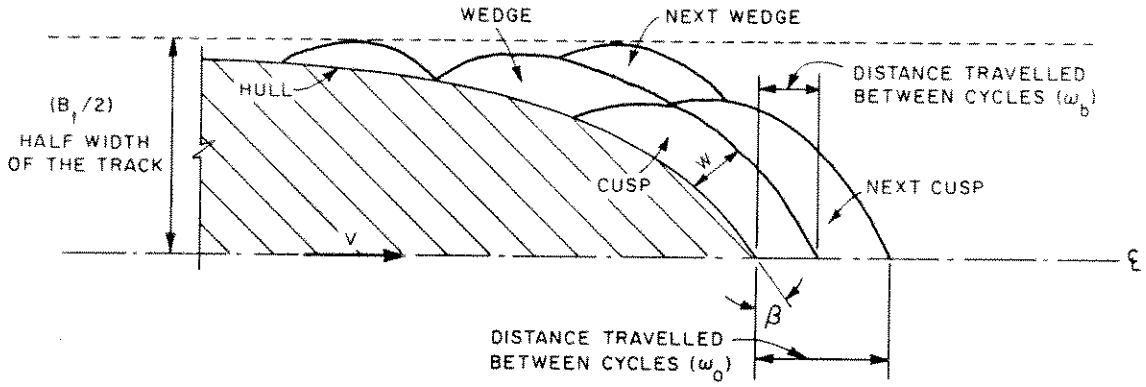

Figure 47. Icebreaking during ω_o cycles.

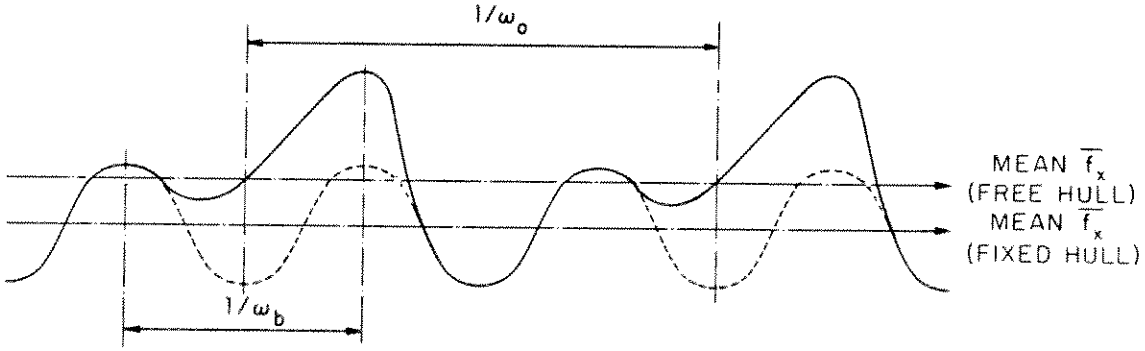

Figure 48. ω_b and ω_o cycles of resistance.

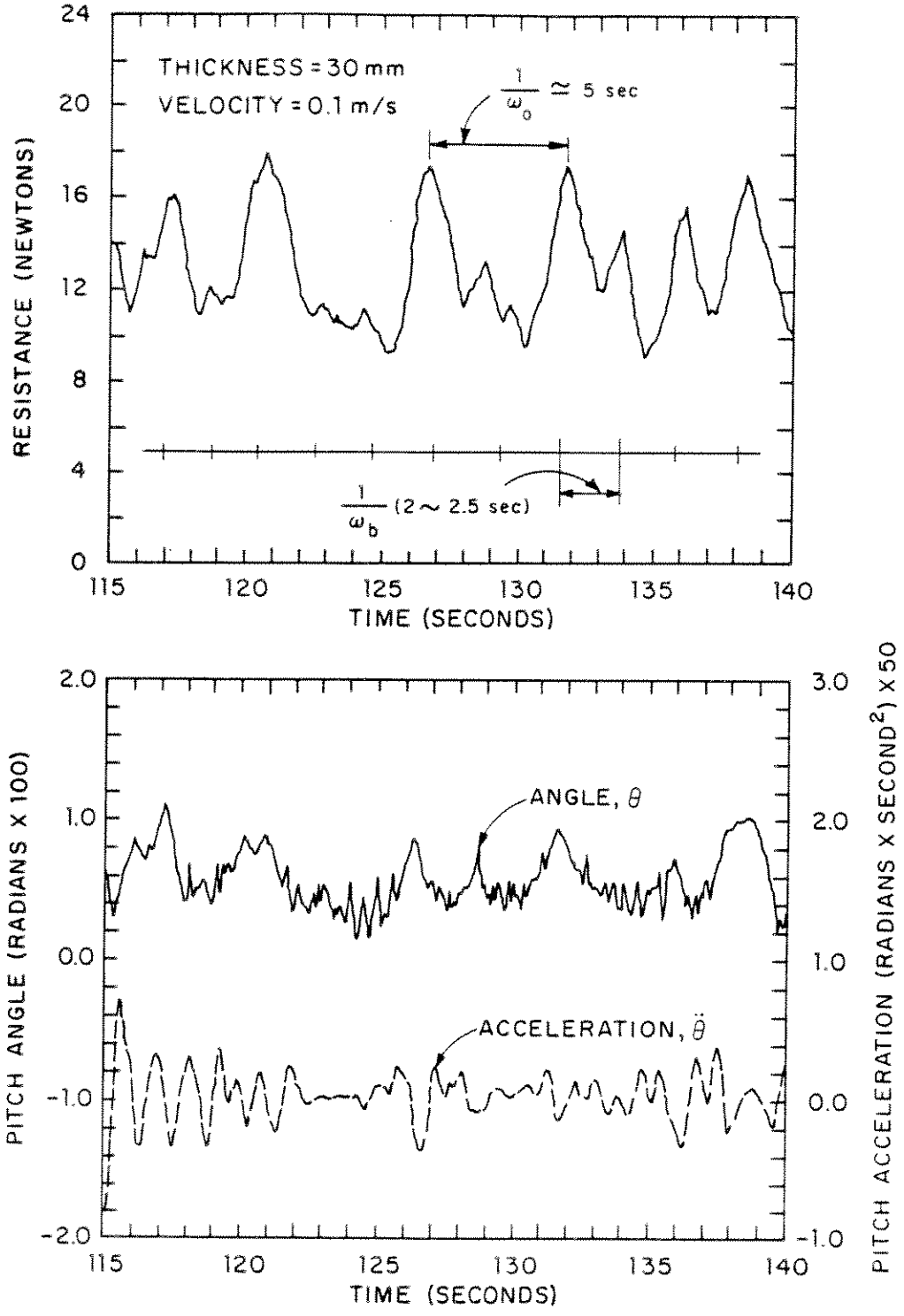

Figure 49. Window of time-histories of f_x, θ and $\ddot{\theta}$ experienced by the free hull.

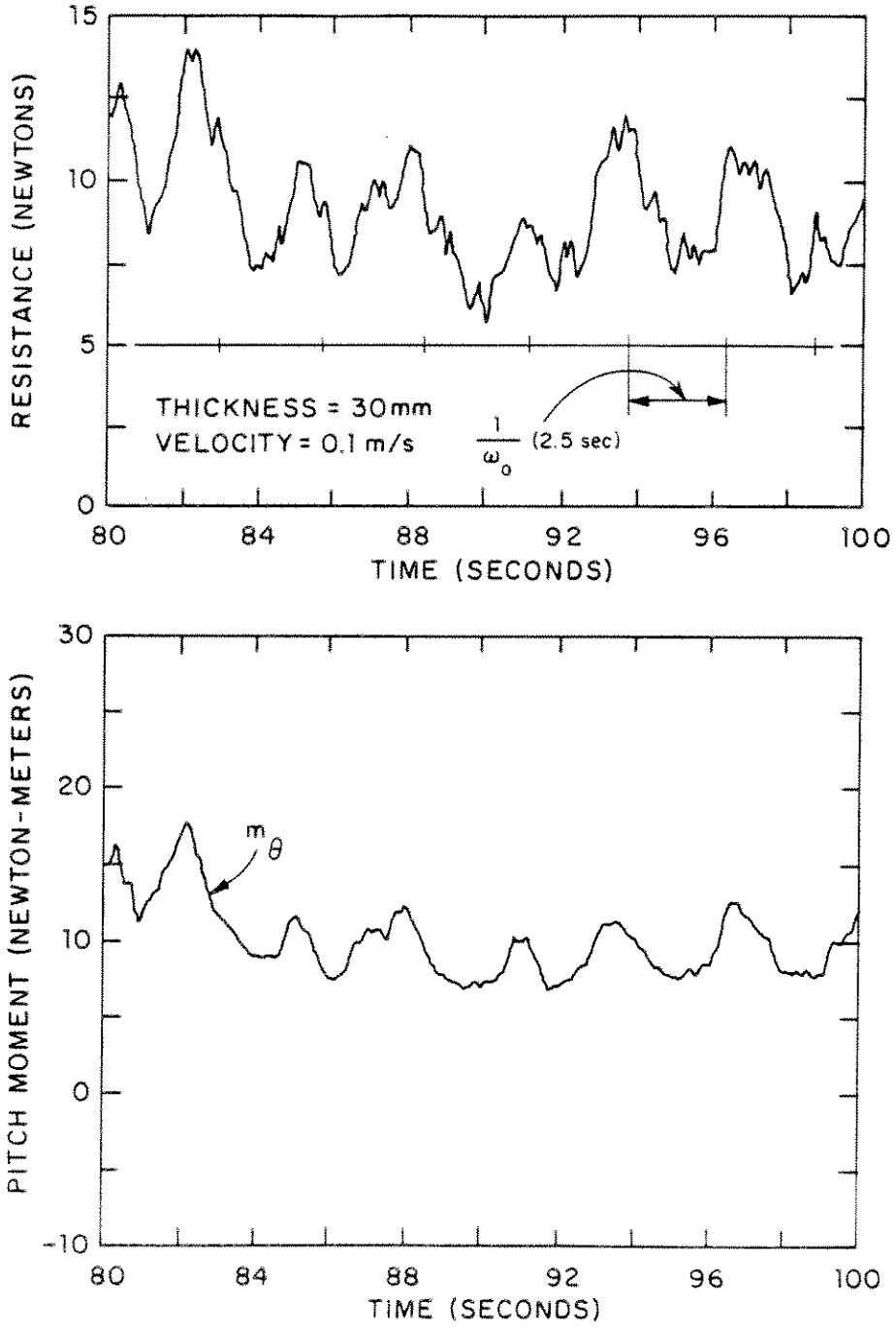

Figure 50. Window of time-histories of f_x and m_θ experienced by fixed hull.

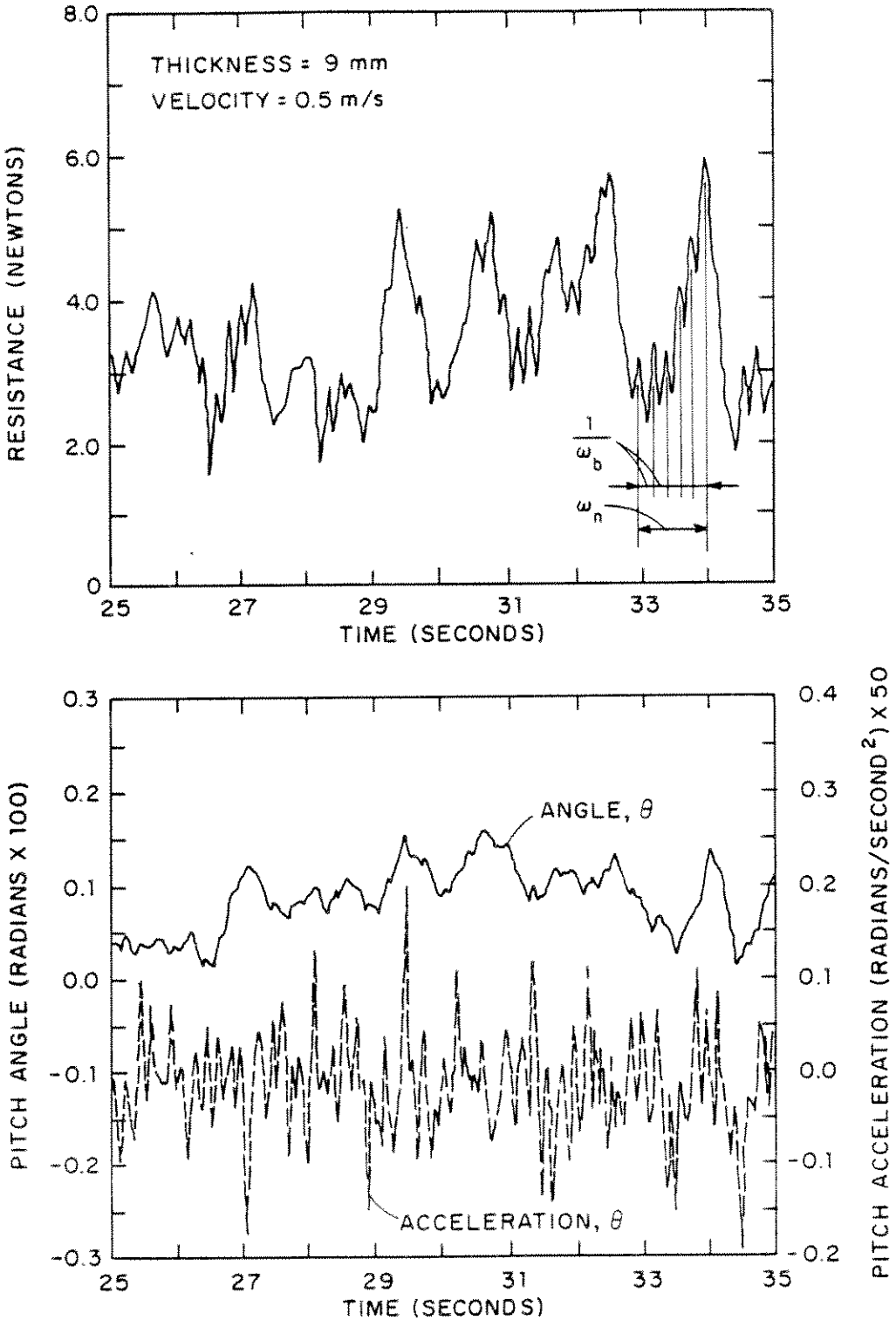

Figure 51. Window of time-histories of f_x, θ and $\ddot{\theta}$ experienced by the free hull in thin ice.

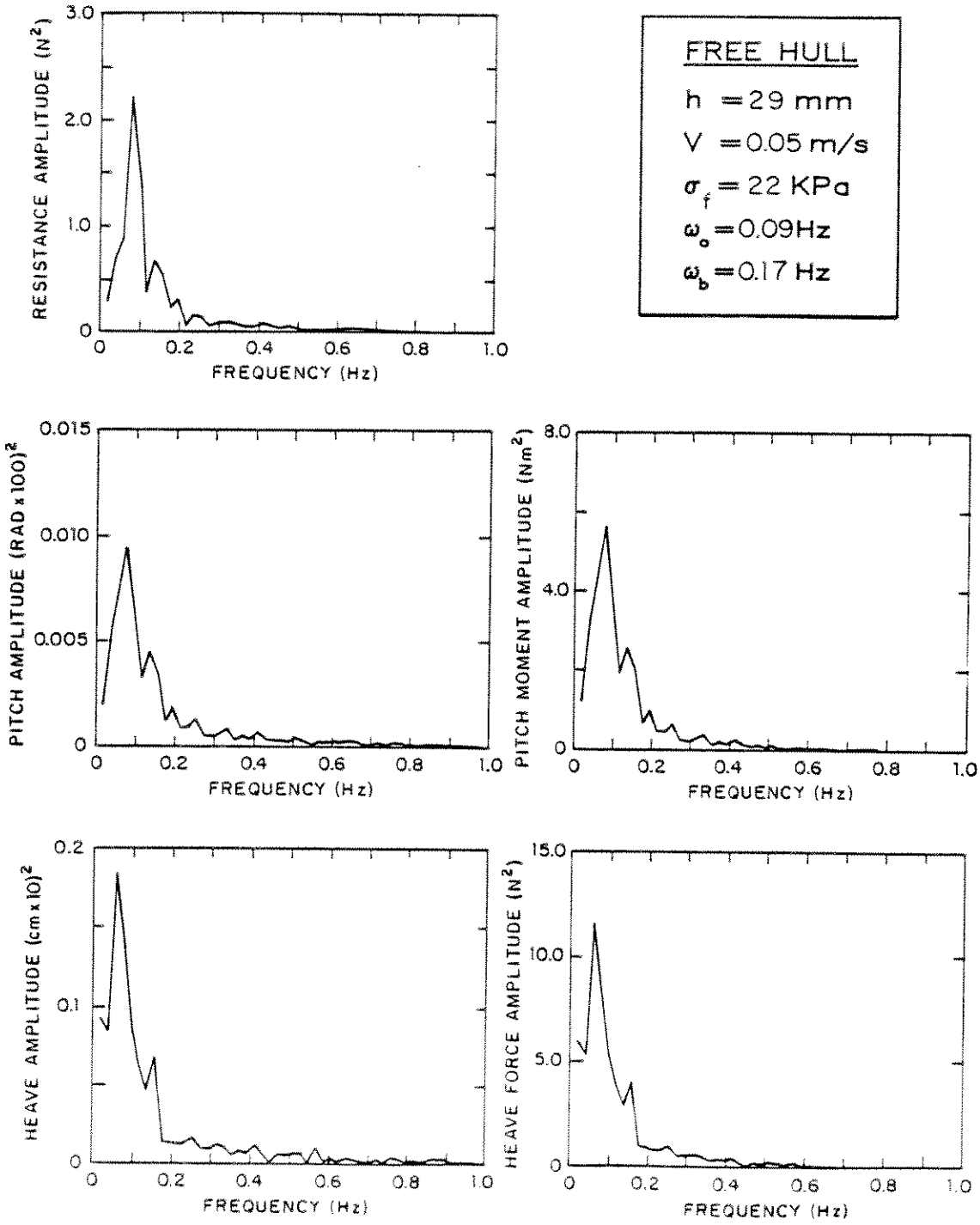

Figure 52. Power spectra, experiment 1-25.

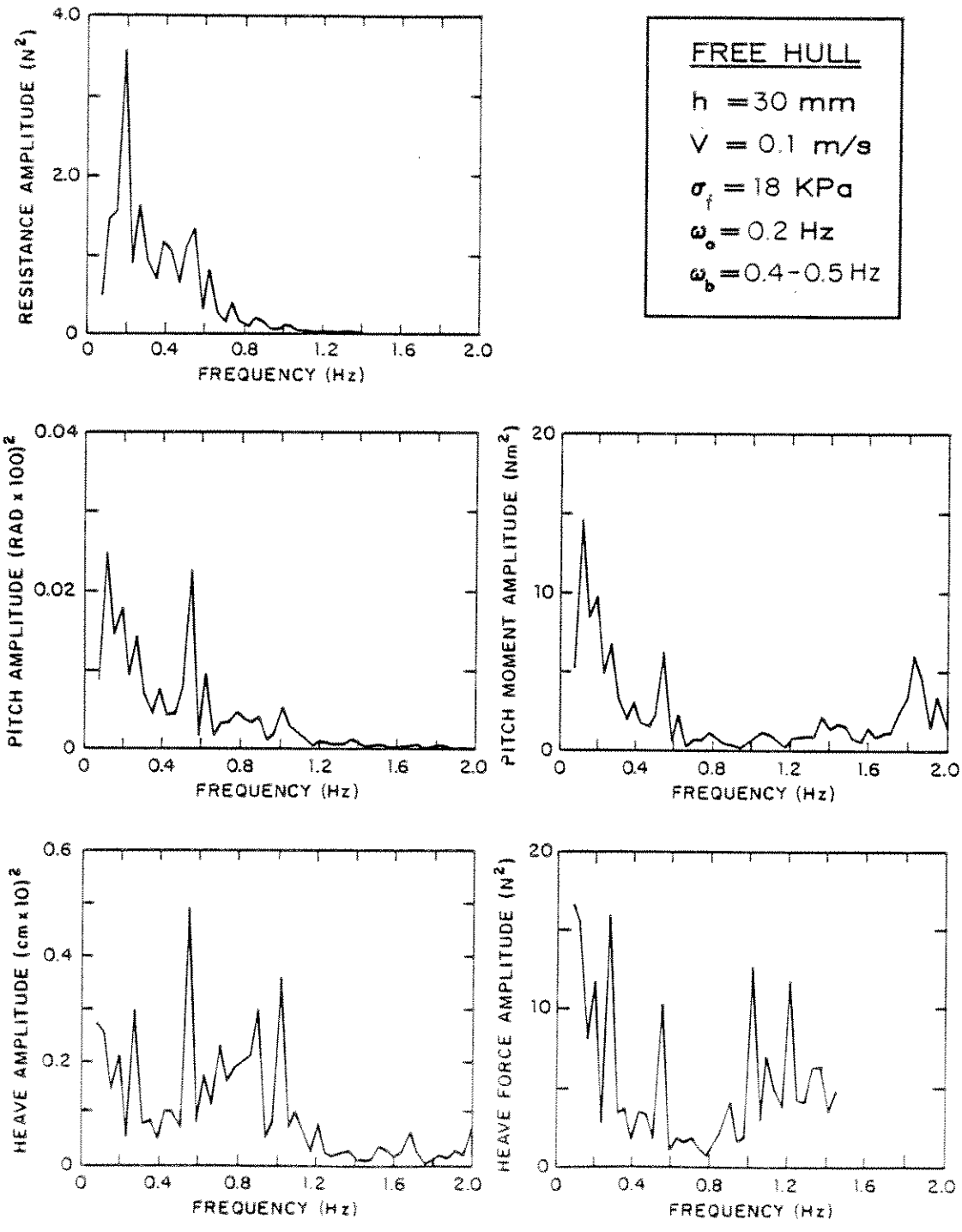

Figure 53. Power spectra, experiment 1-05.

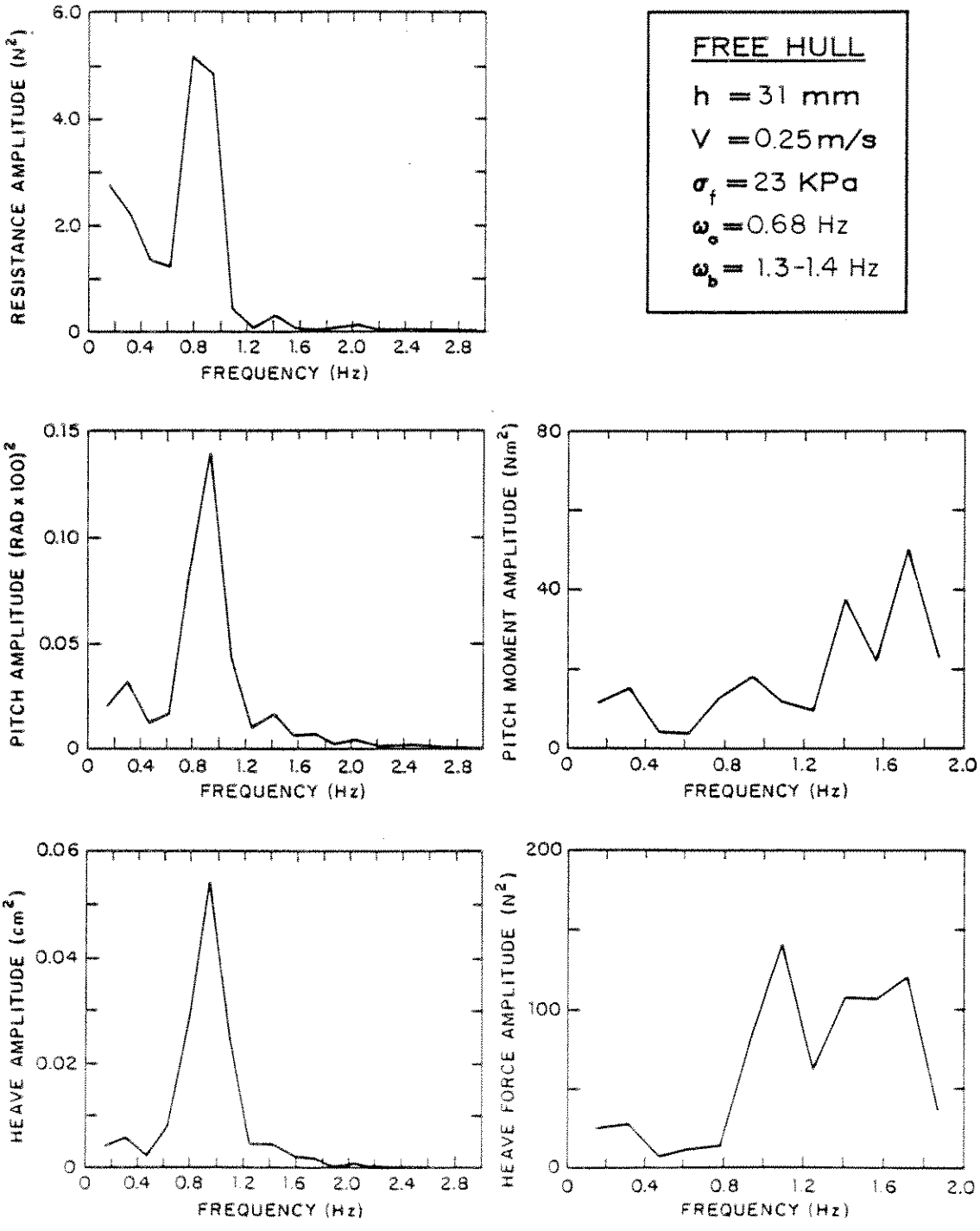

Figure 54. Power spectra, experiment 1-05.

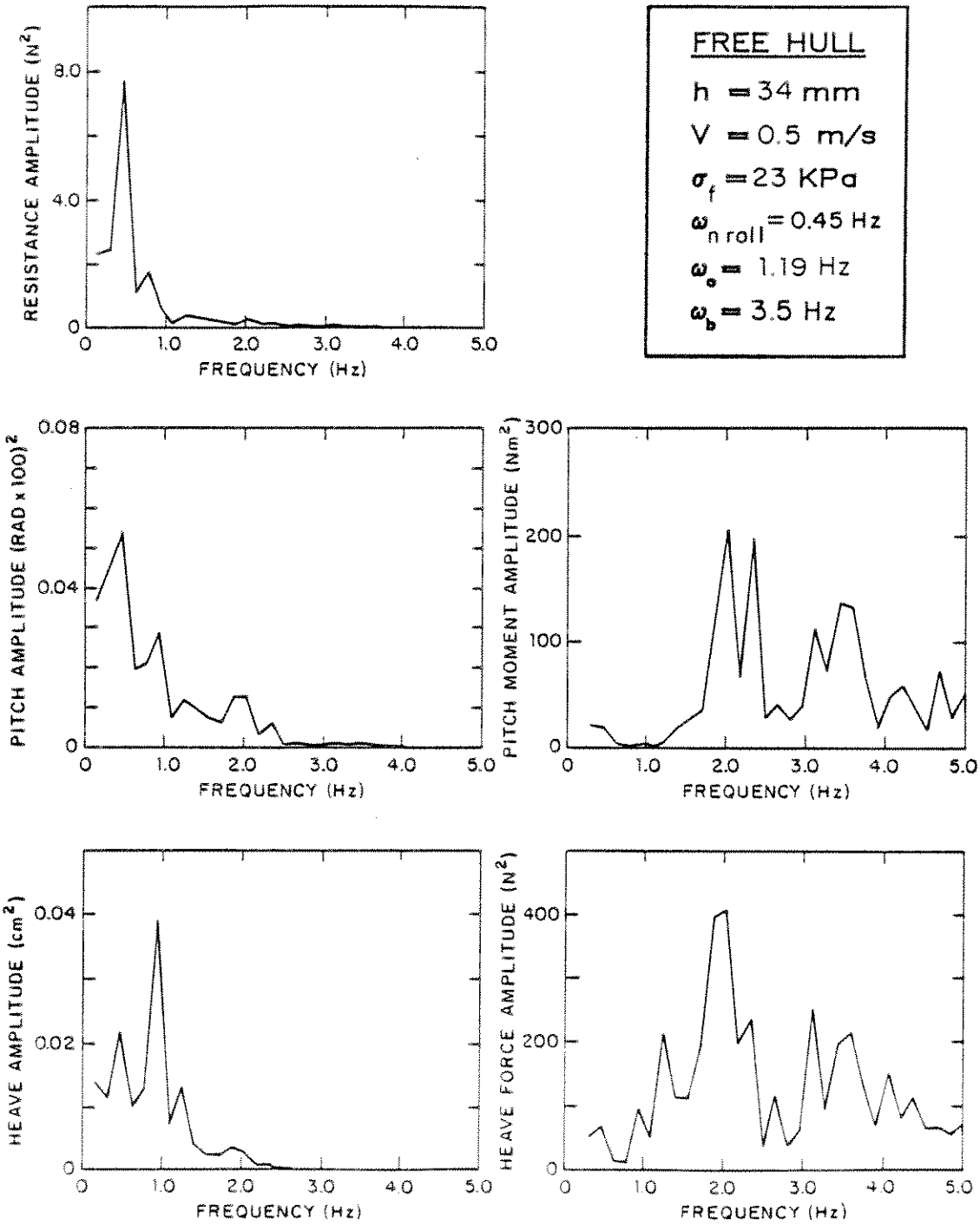

Figure 55. Power spectra, experiment 1-27.

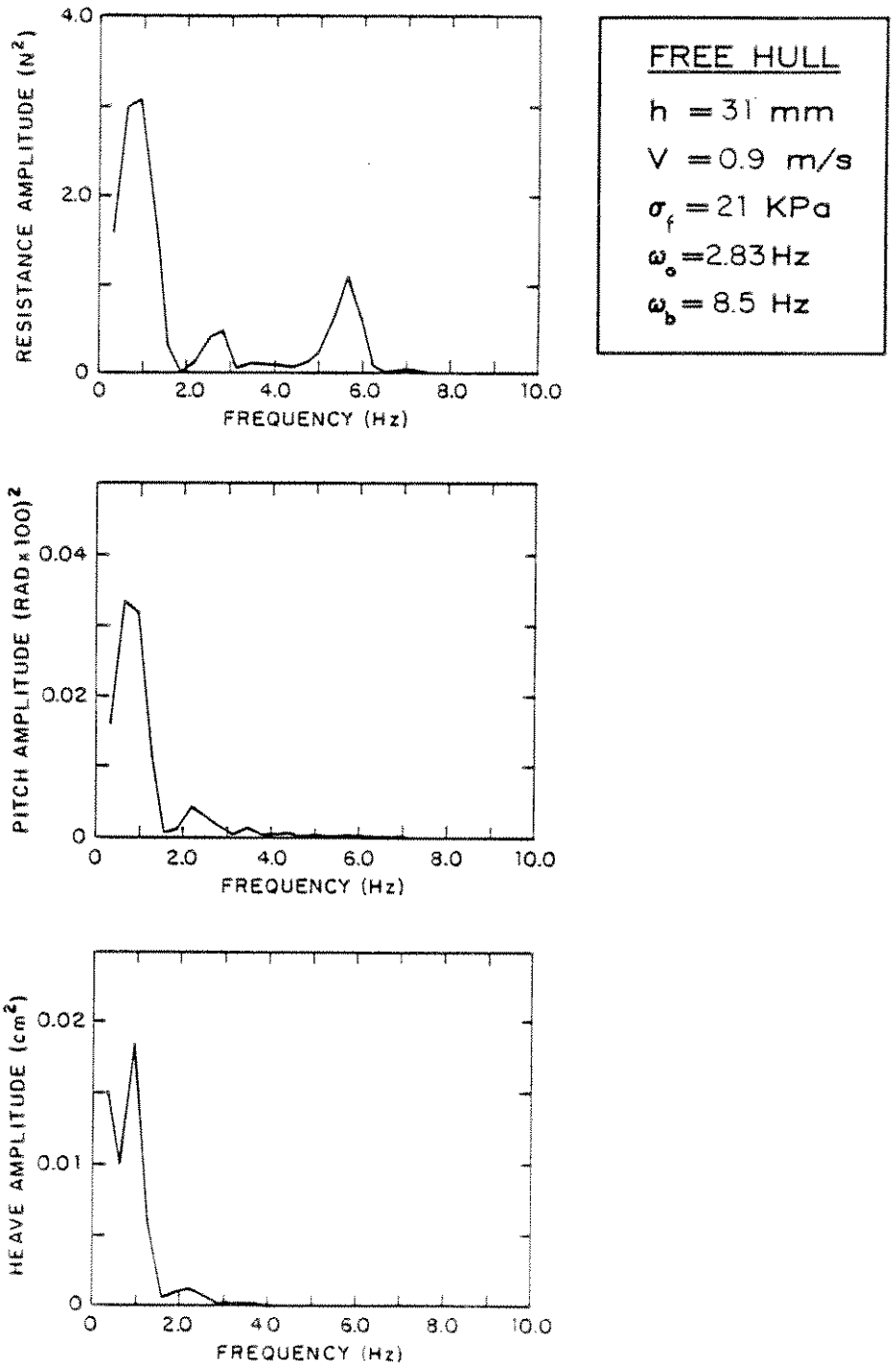

Figure 56. Power spectra, experiment No. 1-32.

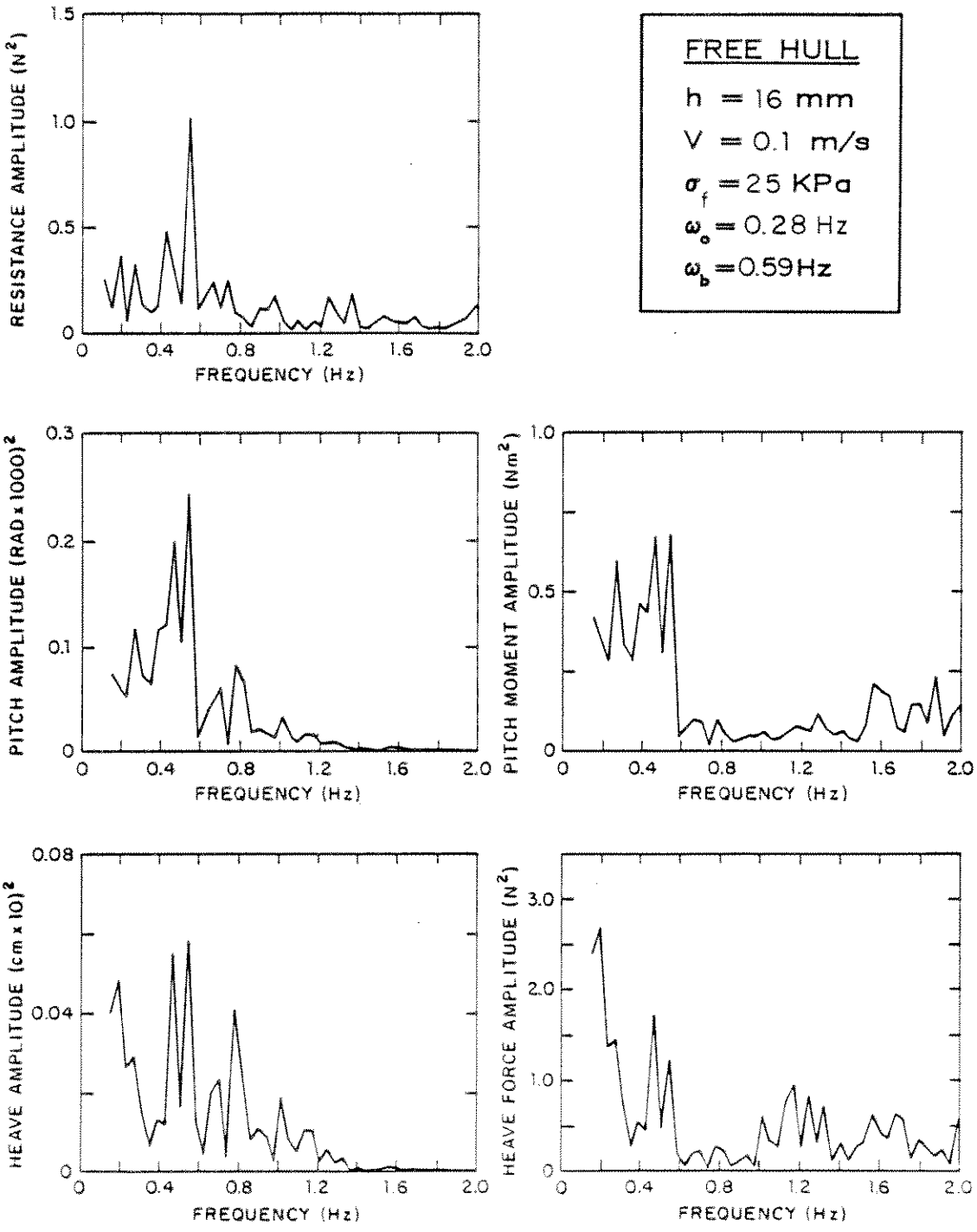

Figure 57. Power spectra, experiment 1-04.

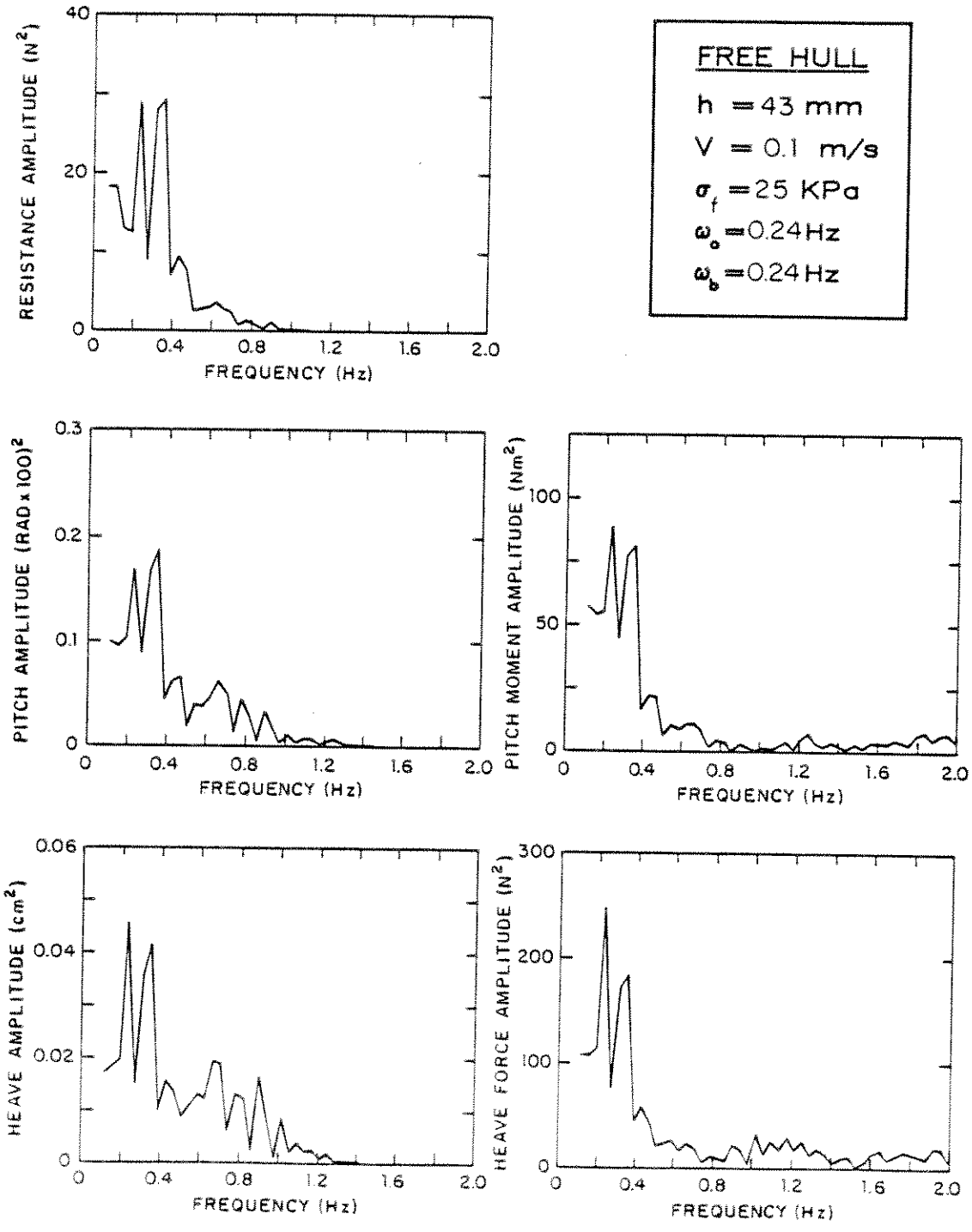

Figure 58. Power spectra, experiment 1-07.

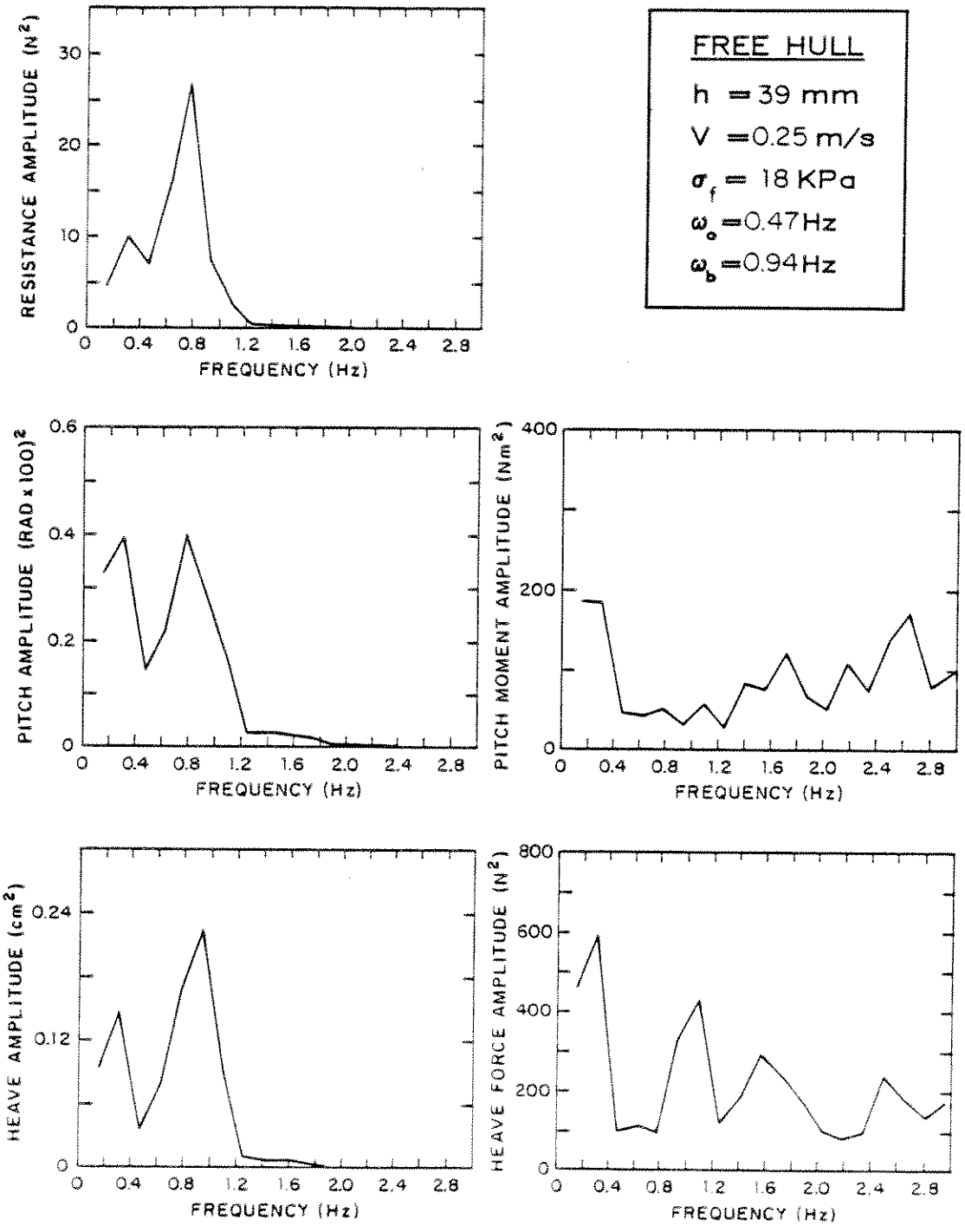

Figure 59. Power spectra, experiment 1-18.

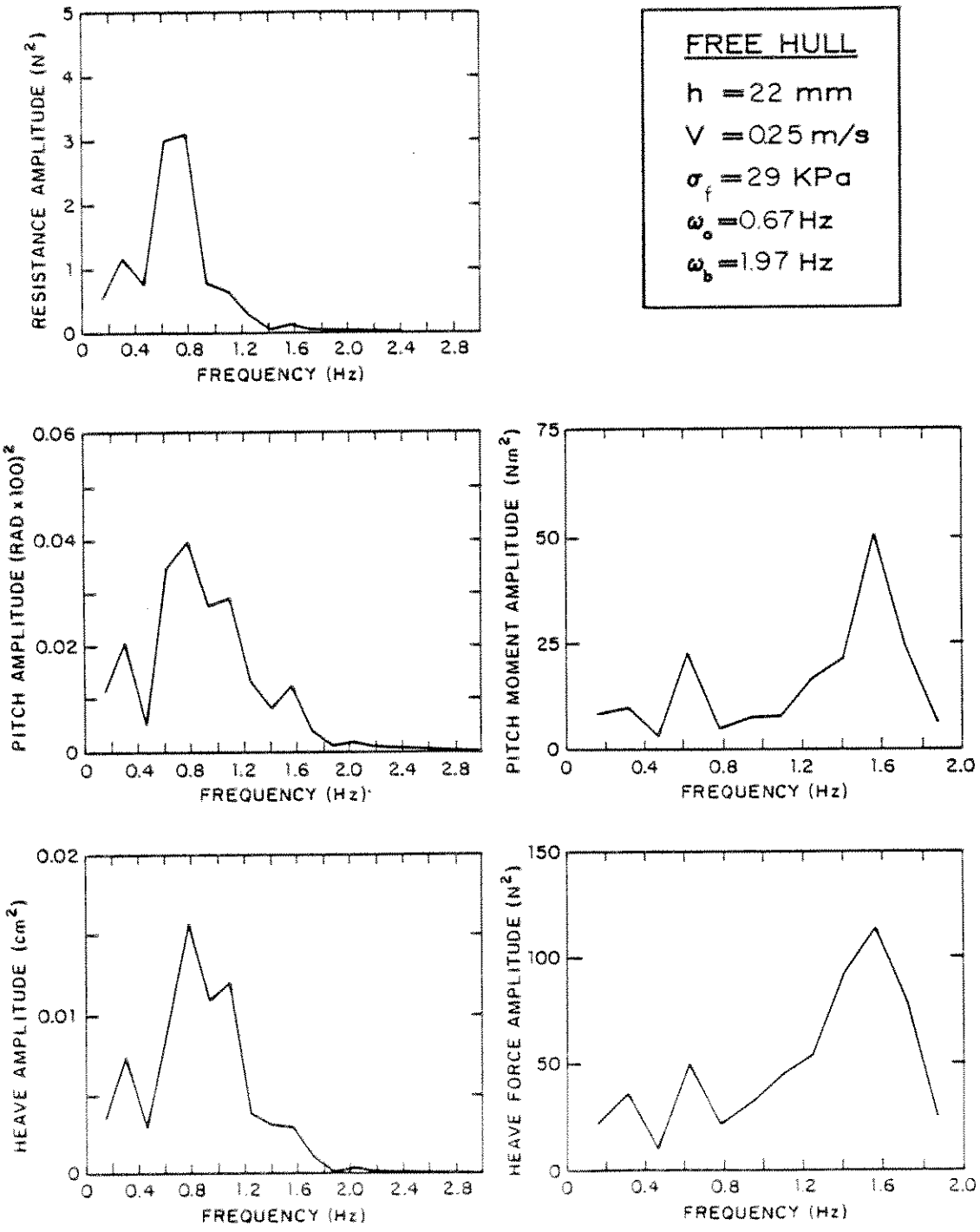

Figure 60. Power spectra, experiment 3-01.

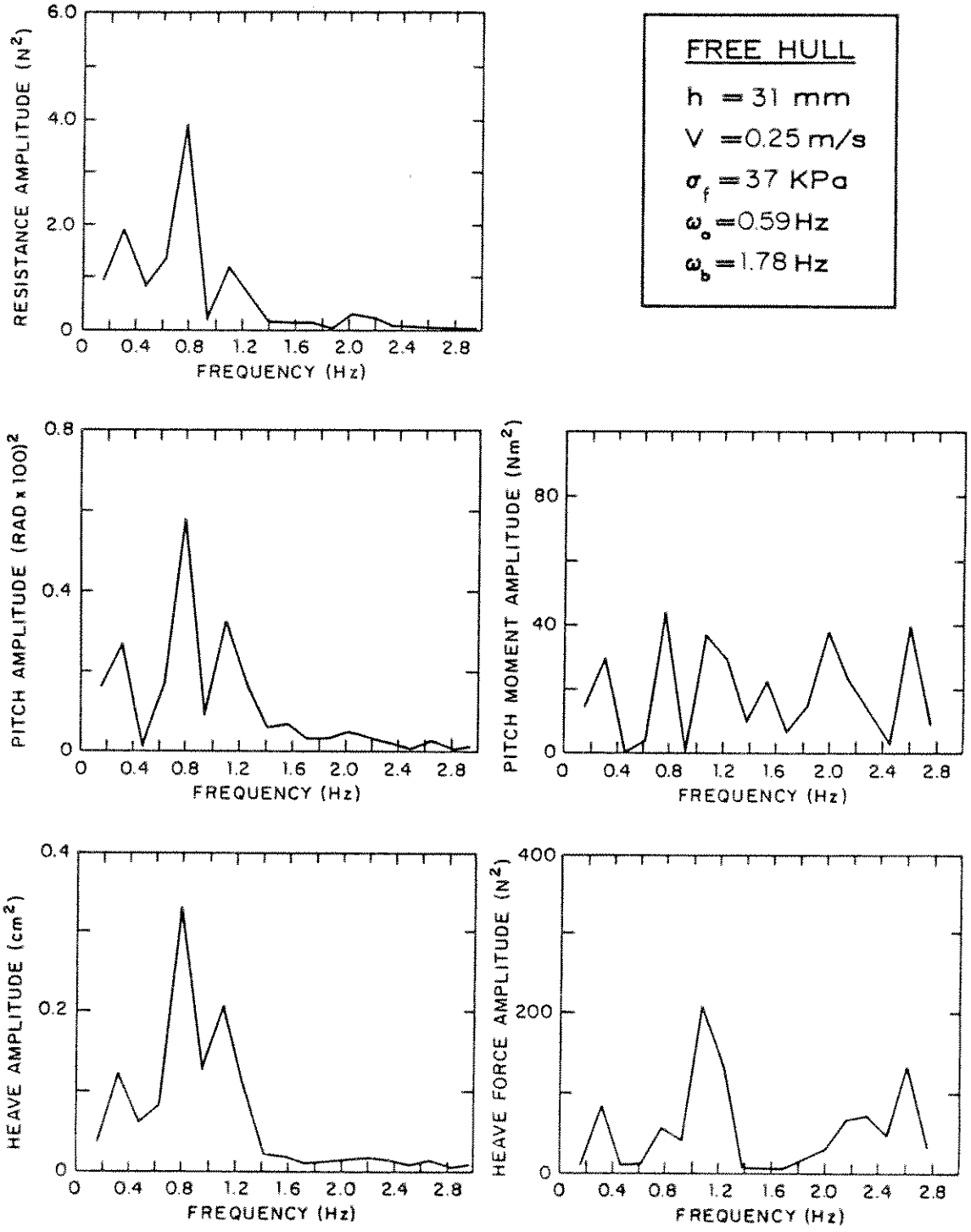

Figure 61. Power spectra, experiment 4-01.

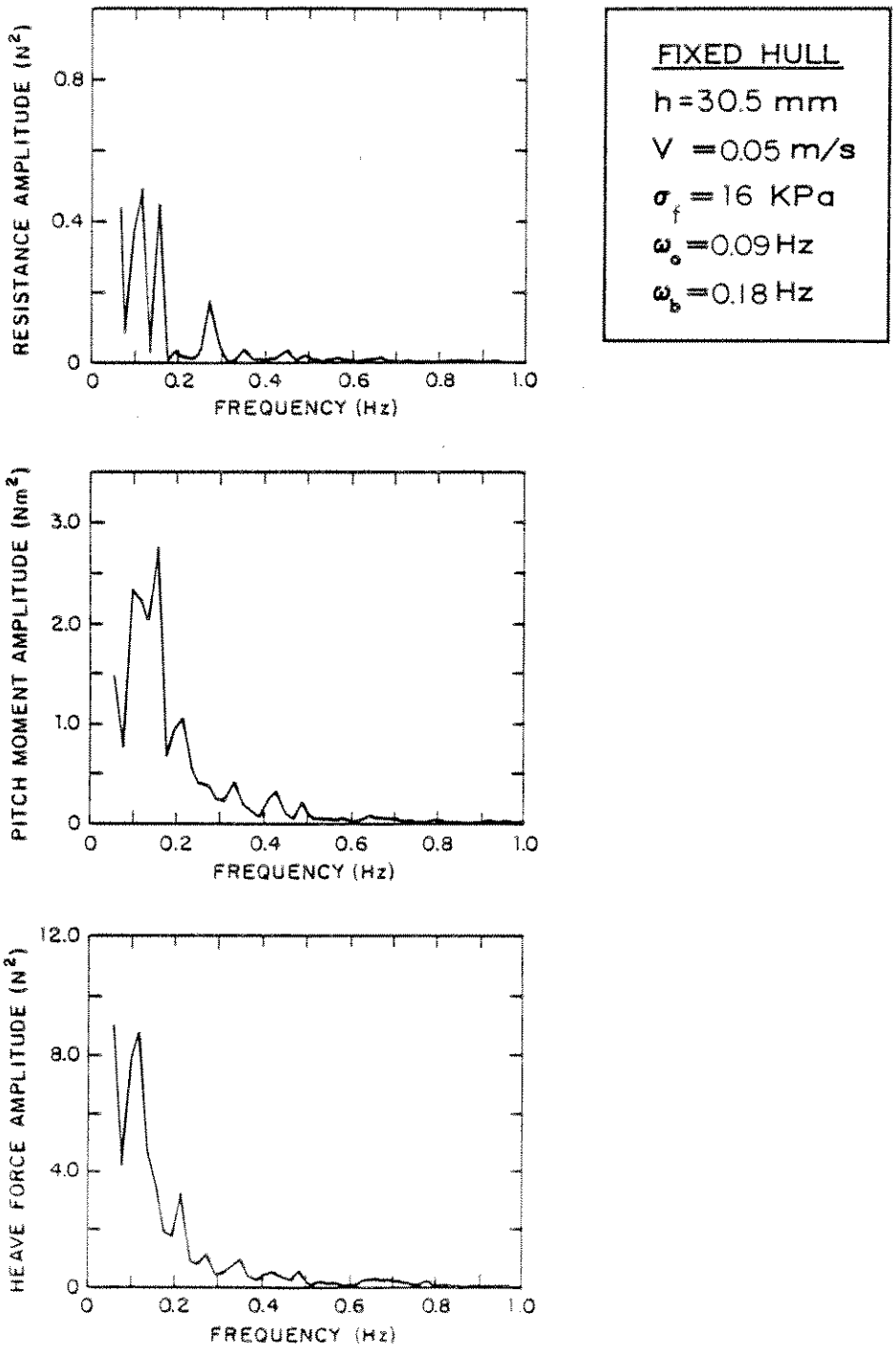

Figure 62. Power spectra, experiment 2-05.

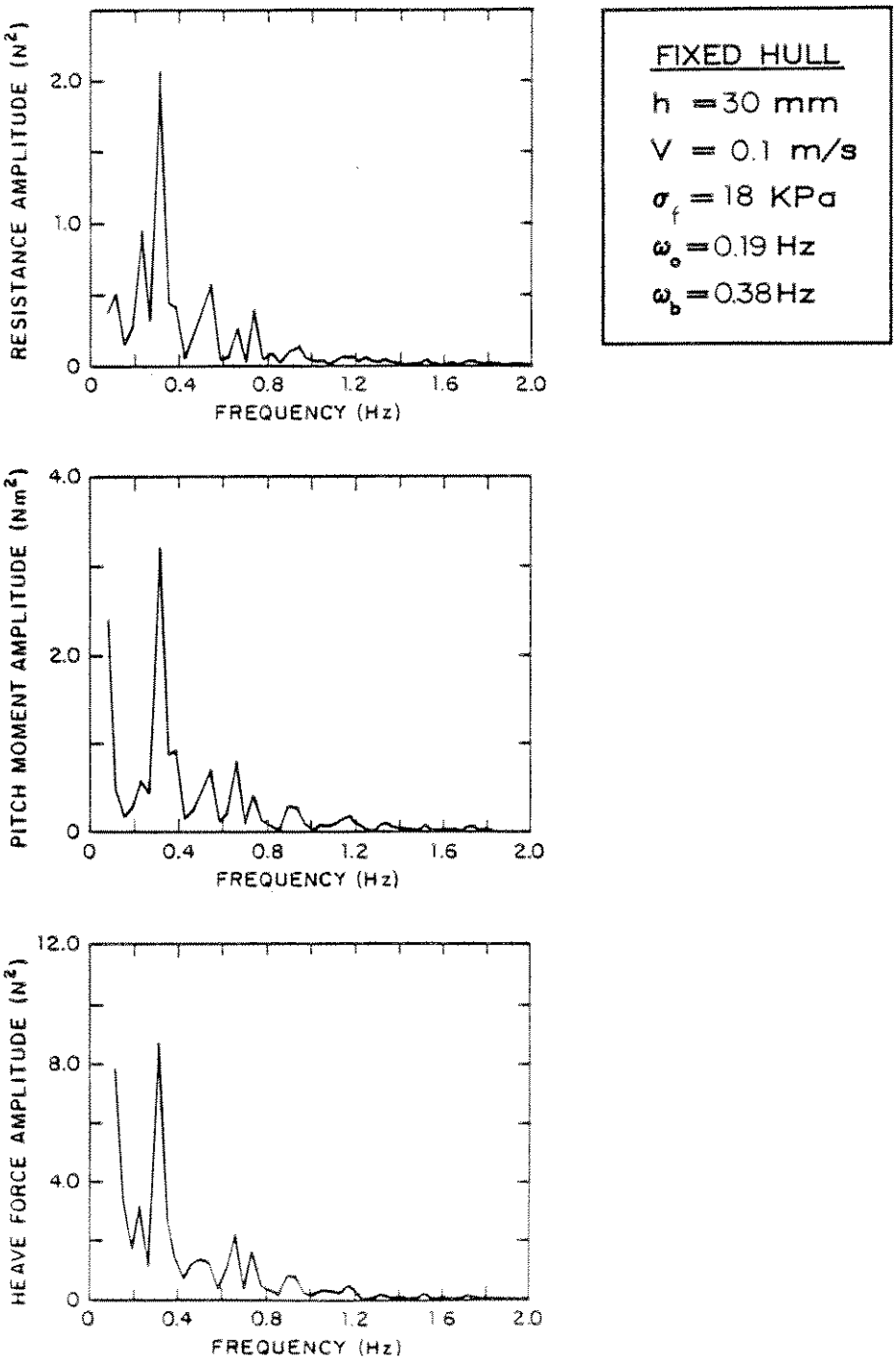

Figure 63. Power spectra, experiment 2-15.

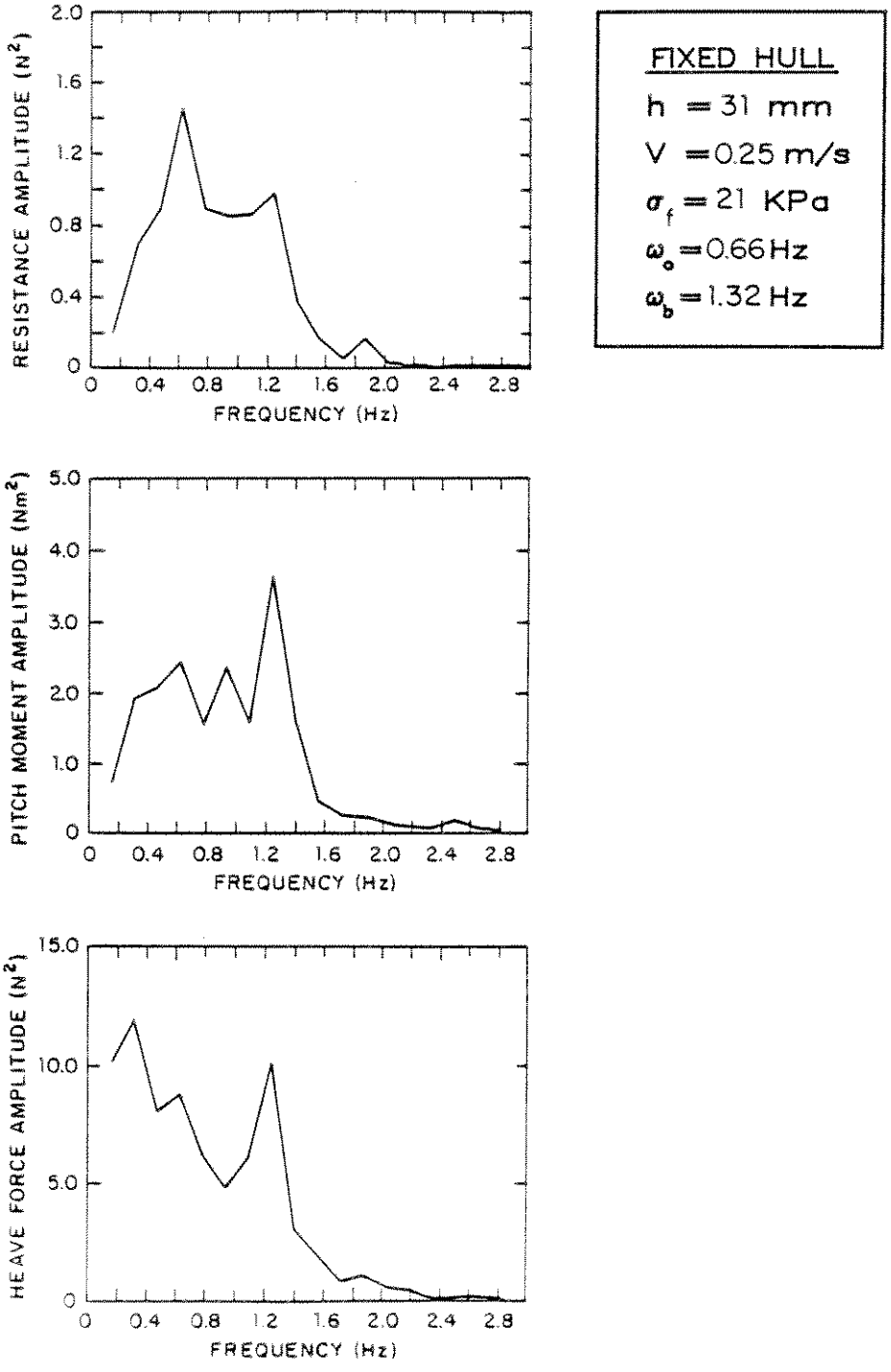

Figure 64. Power spectra, experiment 2-17.

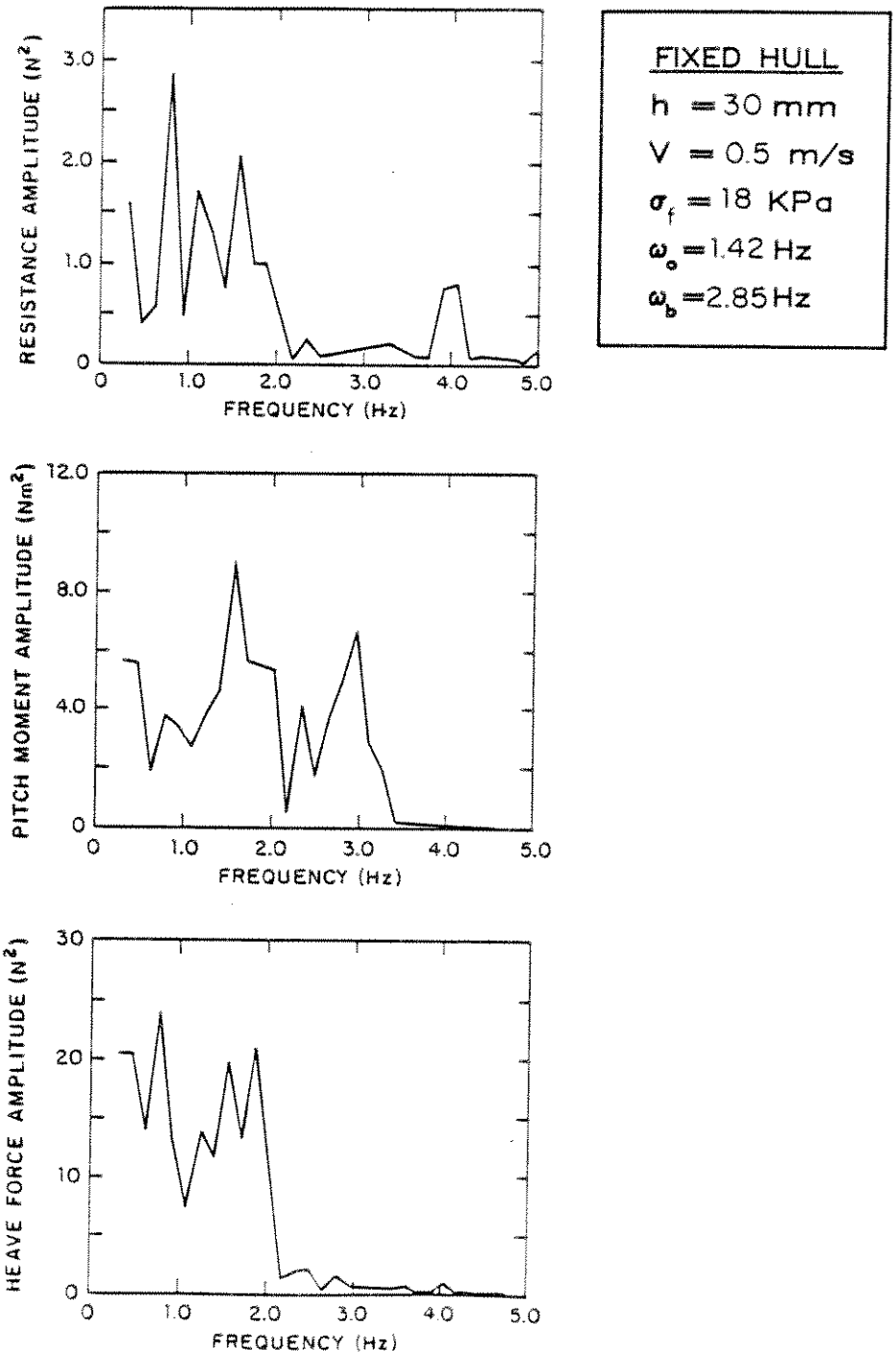

Figure 65. Power spectra, experiment 2-07.

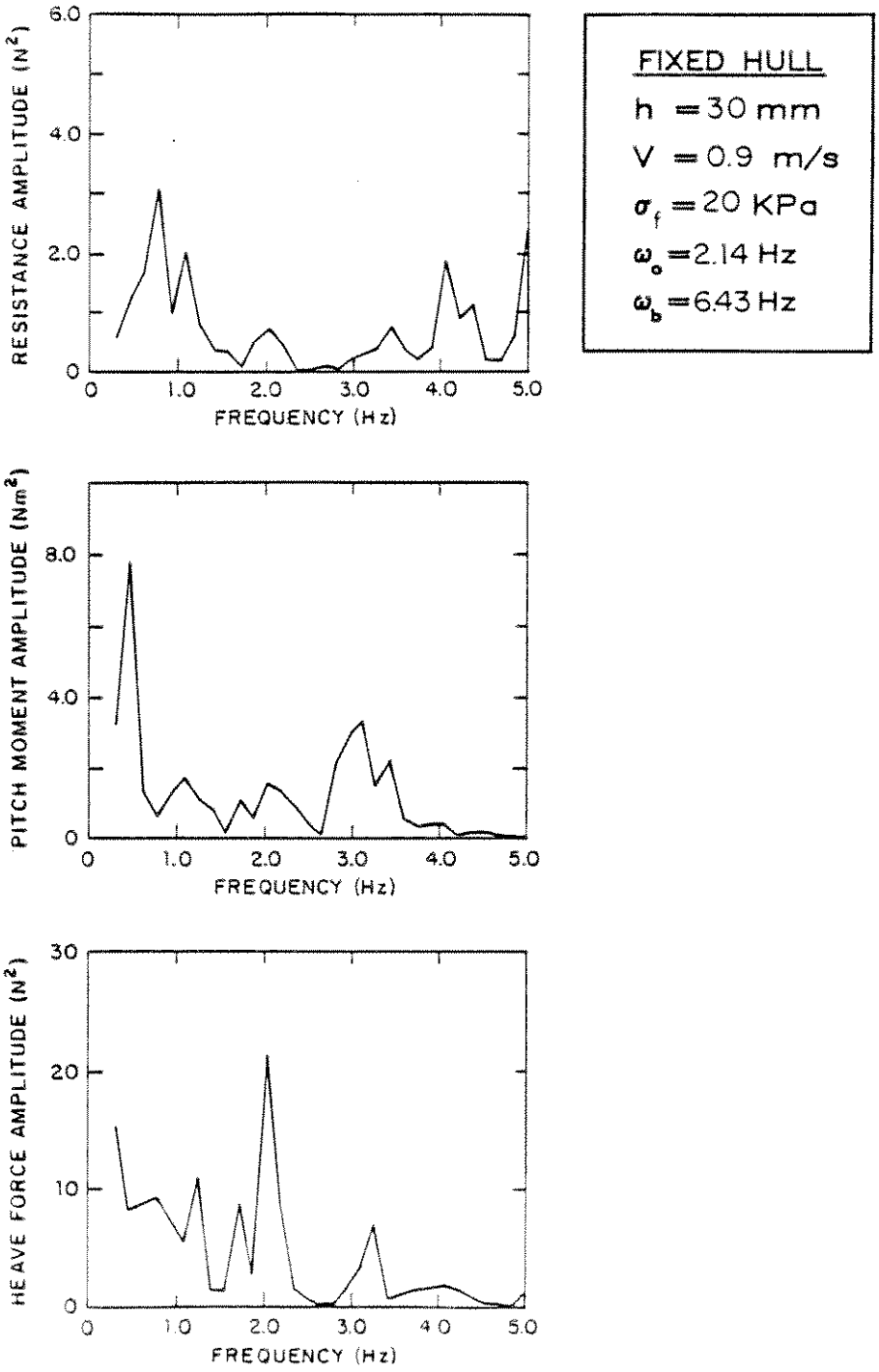

Figure 66. Power spectra, experiment 2-12.

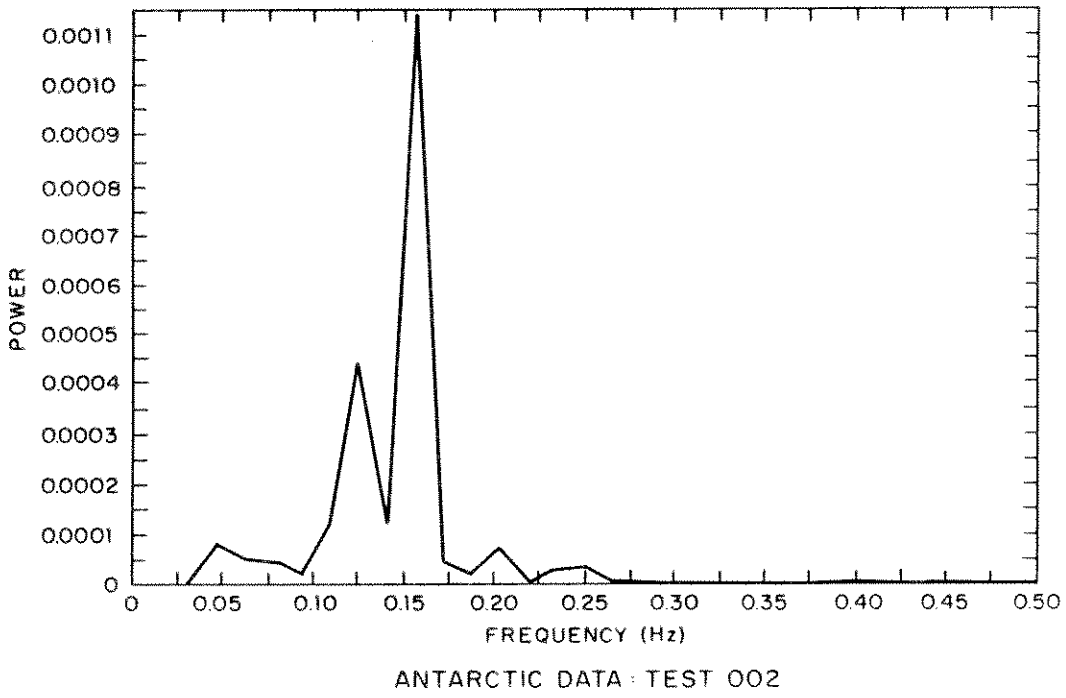

Figure 67. Power spectrum of pitch motion of a full-scale POLAR-Class hull (Voelker et al., 1985).

Table 1
Principal dimensions of the model hull

Overall length of the hull	2.534m
Length between perpendiculars	2.235m
Beam (maximum width)	0.530m
Beam (design at waterline)	0.495m
Draft (design)	0.178m
Displacement	102.6kg
Mass moment of inertia	$33.3 kgm^2$
Area of the waterplane	$0.81 m^2$
Area moment of inertia	$0.25 m^4$
Wetted area of hull	$1.32 m^2$

Table 2
Sensitivities of dynamometer
and accelerometers

Run No	Dynamometer (N/volts)	Stern Accel. (g/volts)	Bow Accel (g/volts)
1-01	28.24	0.500	0.500
1-02	28.15	0.170	0.185
1-03	33.76	0.176	0.170
1-04	28.67	0.173	0.165
1-05	28.93	0.176	0.168
1-06	29.11	0.176	0.168
1-07	29.12	0.176	0.170
1-08	29.46	0.176	0.170
1-09	29.14	0.178	0.170
1-10	29.51	0.178	0.170
1-11	29.65	0.178	0.170
1-13	29.60	0.06	0.06
1-14	2.99	0.06	0.06
1-15	28.98	0.06	0.06
1-16	31.11	0.06	0.06
1-17	29.46	0.06	0.06
1-18	28.98	0.06	0.06
1-19	29.60	0.06	0.06
1-20	29.65	0.06	0.06
1-23	28.03	0.06	0.06
1-24	28.99	0.60	0.60
1-25	28.93	0.60	0.60
1-26	29.08	0.60	0.60
1-27	29.10	0.60	0.60
1-28	29.08	0.60	0.60
1-29	29.00	0.60	0.60
1-30	28.99	0.60	0.60
1-31	29.00	0.60	0.60
1-32	29.17	0.60	0.60
3-01	28.90	0.60	0.60
3-02	29.06	0.60	0.60
4-01	29.36	0.60	0.60

Table 3
Sensitivities of load-cell channels

Run No	Resistance (N/volts)	Pitch (Nm/volts)	Heave (N/volts)	Yaw (Nm/volts)
2-01	44.83	67.54	-	-
2-02	45.41	63.35	49.98	79.58
2-03	44.91	61.48	47.82	78.35
2-04	45.08	63.35	48.35	79.58
2-05	44.93	62.40	49.15	79.58
2-06	44.93	65.33	48.88	79.58
2-07	44.48	65.33	49.42	77.17
2-08	45.41	63.35	48.89	84.88
2-09	44.93	63.35	48.61	82.14
2-10	44.48	63.35	48.88	84.88
2-11	44.48	63.35	49.15	83.49
2-12	45.97	63.35	49.42	87.81
2-13	45.73	63.35	48.35	87.81
2-14	44.93	63.35	48.35	89.10
2-15	45.37	62.53	49.42	79.58
2-16	46.41	63.35	48.35	87.81
2-17	44.93	63.35	48.09	83.49

Table 4
List of experimental errors

Parameter	Error	Main Source of Error
Dynamometer (f_x)	±0.6%	electrical drift
Draft (z)	< ±0.00065m	static friction of ball bushings
Pitch (θ)	±0.0004rad	electrical drift
Draft Accel. ($\ddot{z}$)	±0.02cm/sec^2	rolling of hull
Pitch Accel. ($\ddot{\theta}$)	±0.01sec^{-2}	electrical drift
Load cell (f_x)	±5%	degree of interference
Load cell (f_z)	±5%	degree of interference
Load cell (m_θ)	±5%	degree of interference
Load cell (m_ψ)	±5%	degree of interference

Table 5
Openwater resistance

V (m/s)	Froude No., F_n	Reynolds No., R_e ($x10^3$)	$\overline{f}_{xo}$ (N)	C
0.15	0.032	188	0.232	0.016
0.32	0.068	401	1.276	0.019
0.53	0.113	664	1.334	0.007
0.70	0.149	877	1.421	0.0044
0.86	0.183	1078	1.653	0.0034

Table 6
Experiments with the free hull

Run No.	h (mm)	V (m/s)	σ_f (kPa)	E (MPa)	E/σ	ℓ_c (mm)	Date
1-01	24	0.25	25	25.0	1000	240	11/85
1-02	17	0.25	20	22.0	1100	179	11/85
1-03	41	0.25	20	36.0	1800	392	11/85
1-04	16	0.10	25	26.5	1060	179	12/85
1-05	30	0.10	18	30.5	1694	298	12/85
1-06	9	0.10	25	13.4	536	98	12/85
1-07	43	0.10	25	41.4	1656	421	12/85
1-08	9	0.25	25	13.1	520	84	12/85
1-09	18	0.05	26	16.0	615	164	01/86
1-10	29	0.05	25	32.0	1391	242	01/86
1-11	9	0.05	25	11.3	452	92	02/86
1-13	11	0.50	20	10.2	512	106	02/86
1-14	17	0.50	18	9.0	500	143	02/86
1-15	28	0.50	25	29.0	1160	279	02/86
1-16	29	0.50	26	28.0	1077	273	03/86
1-17	39	0.50	18	29.0	1611	358	03/86
1-18	39	0.25	18	26.0	1444	348	03/86
1-19	41	0.50	18	39.0	2167	400	03/86
1-20	9	0.50	18	11.0	611	86	03/86
1-23	40	0.05	23	19.9	870	330	07/86
1-24	38	0.05	24	21.0	913	300	08/86
1-25	29	0.05	22	27.0	1227	201	09/86
1-26	38	0.25	23	28.0	1217	330	09/86
1-27	31	0.25	23	23.3	1013	221	09/86
1-28	38	0.50	24	26.2	1092	257	09/86
1-29	28	0.10	24	29.0	1200	209	09/86
1-30	28	0.25	23	27.3	1186	191	09/86
1-31	34	0.50	23	33.3	1448	264	09/86
1-32	31	0.90	21	28.1	1338	218	09/86
3-01	22	0.25	29	33.9	1169	193	09/86
3-02	40	0.25	41	48.2	1176	323	09/86
4-01	31	0.25	37	37.4	1011	295	10/86
4-02	31	0.25	37	37.4	1011	295	10/86

Table 7
Experiments with the fixed hull

Run No.	h (mm)	V (m/s)	σ_f (kPa)	E (MPa)	E/σ	ℓ_c (mm)	DATE
2-01	30	0.10	20	42	2100	322	05/86
2-02	40	0.10	19	40	2105	395	05/86
2-03	20	0.10	20	13	650	177	05/86
2-04	20	0.05	18	20	1111	198	05/86
2-05	31	0.05	16	29	1831	294	05/86
2-06	41	0.05	19	23	1211	344	06/86
2-07	30	0.50	18	24	1332	280	06/86
2-08	21	0.50	21	14	666	188	06/86
2-09	21	0.25	20	25	1250	217	06/86
2-10	40	0.25	18	34	1884	380	06/86
2-11	28	0.25	20	24	1200	266	06/86
2-12	30	0.90	20	19	950	264	06/86
2-13	22	0.90	22	14	636	194	06/86
2-14	39	0.50	18	35	1944	375	06/86
2-15	30	0.10	18	23	1278	277	07/86
2-16	39	0.10	17	32	1882	367	07/86
2-17	31	0.25	21	25	1191	288	07/86

Table 8
Natural frequencies of pitch and heave: measured values

Ice Sheet Thickness (mm)	Pure Pitch Frequency (ω) (Hz)	Pure Pitch Damping (ξ)	Pure Heave Frequency (ω) (Hz)	Pure Heave Damping (ξ)	Pitch/Heave Frequency (ω) (Hz)	Pitch/Heave Frequency (ω) (Hz)
* 0	1.09	0.47	0.91	0.22	1.00	1.00
30	0.83	1.3	0.66	1.21	0.76	0.74
38	0.83	1.3	0.66	1.21	0.74	0.72

* Openwater

Table 9

Added-mass and damping coefficients

	"Ship Amidst Ice" (experimental)	"Openwater" (Lewis forms)
A_{33}	250.80	80.31
A_{55}	72.23	16.75
A_{53}	38.20	2.57
B_{33}	714.07	
B_{55}	265.99	
B_{53}	128.22	

Table 10

Natural frequencies of pitch and heave

Motion	Ice Covered: With Damping (Hz)	Ice-Covered: Without Damping (Hz)	Openwater (Hz)	
			Calc.	Meas.
Pitch	0.83	0.85	1.12	1.09
Heave	0.68	0.70	1.05	0.91

Table 11

Summary of ω_b and ω_o: Section VIII

V (m/s)	h (mm)	ω_b (Hz)	ω_o (Hz)
		Free hull	
0.05	29	0.17	0.09
0.10	30	0.44	0.22
0.25	31	1.30 ~ 1.40	0.68 ~ 1.0
0.50	34	3.56	1.19
0.90	31	8.50	2.83
0.10	16	0.59	0.28
0.10	43	0.24	0.24
0.25	22	1.97	0.67
0.25	39	0.94	0.47
0.25	31	1.78	0.59
		Fixed hull	
0.05	31	0.18	0.09
0.10	30	0.38	0.19
0.25	31	1.32	0.66
0.50	30	2.85	1.42
0.90	30	6.43	2.14

Table 12

Dominant pitch and roll frequencies, and estimated values of ω_b and ω_o, in full-scale test data reported by Voelker et al. (1985)

Test No.	Pitch (Hz)	ω_b (Hz)	ω_o (Hz)	Roll (Hz)
*001	0.13	0.21	0.11	0.03 ~ 0.06
002	0.15	0.21	0.12	0.045
003	0.11	0.21	0.11	0.05 ~ 0.07
004	0.10	0.26	0.12	0.05
005	0.13~0.16	0.27	0.15	0.05 ~ 0.07
*006	0.14	0.27	0.13	0.075
*007	0.06~0.012	0.19	0.10	0.05
008	0.11~0.14	0.20	0.10	0.05
009	0.12	0.18	0.09	0.05
010	0.11	0.15	0.08	0.05
011	0.03~0.10	0.10	0.05	0.03 ~ 0.07
012(1)	0.10	0.17	0.09	0.06 ~ 0.10
012(2)	0.12	0.12	0.06	0.05
013	0.11	0.15	0.08	0.06
*014	0.13~0.16	0.47	0.23	0.10

* Slow sampling rate

APPENDIX A

TIME-SERIES: FREE HULL

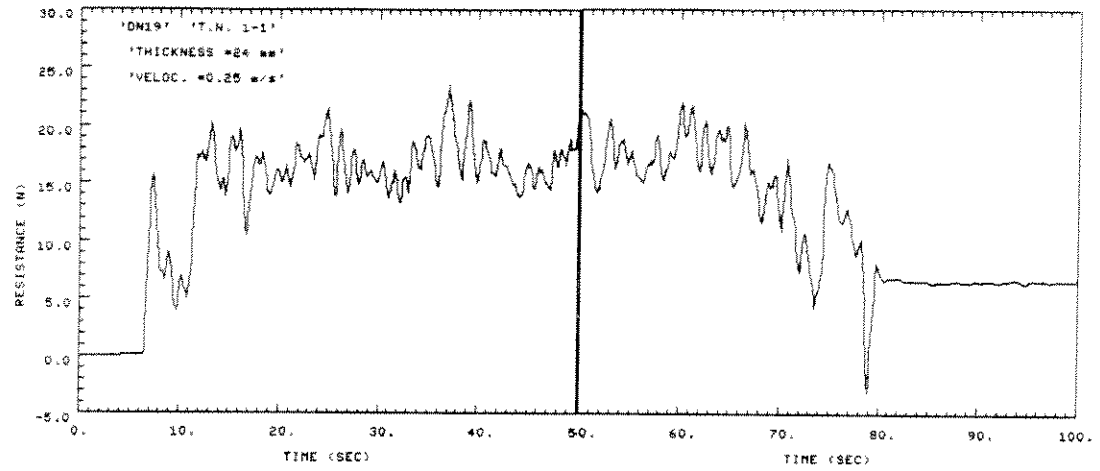
'DN19' 'T.N. 1-1'
'THICKNESS =24 mm'
'VELOC. =0.25 m/s'
RESISTANCE (N)
30.0
25.0
20.0
15.0
10.0
5.0
0.0
-5.0
0.
10.
20.
30.
40.
50.
60.
70.
80.
90.
100.
TIME (SEC)
TIME (SEC)

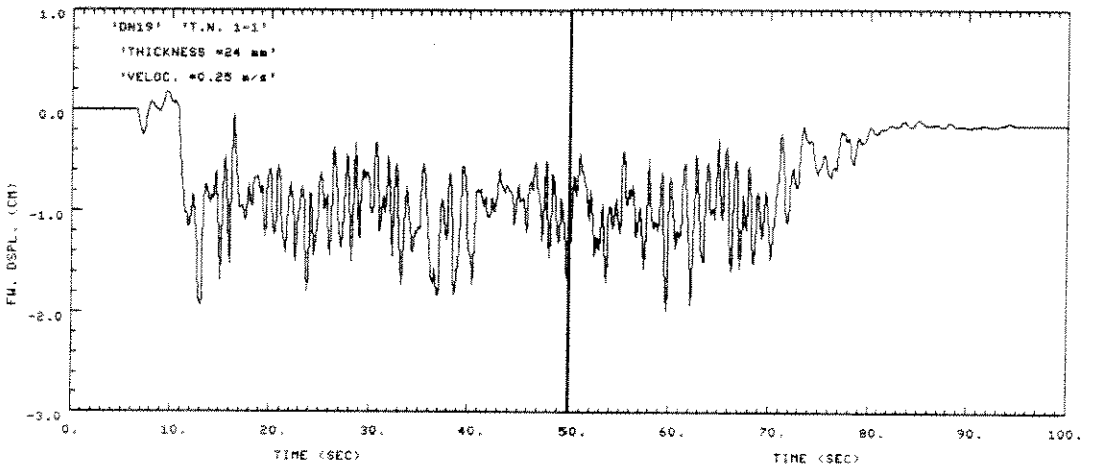
'DN19' 'T.N. 1-1'
'THICKNESS =24 mm'
'VELOC. =0.25 m/s'
FW. DSPL. (CM)
1.0
0.0
-1.0
-2.0
-3.0
0.
10.
20.
30.
40.
50.
60.
70.
80.
90.
100.
TIME (SEC)
TIME (SEC)

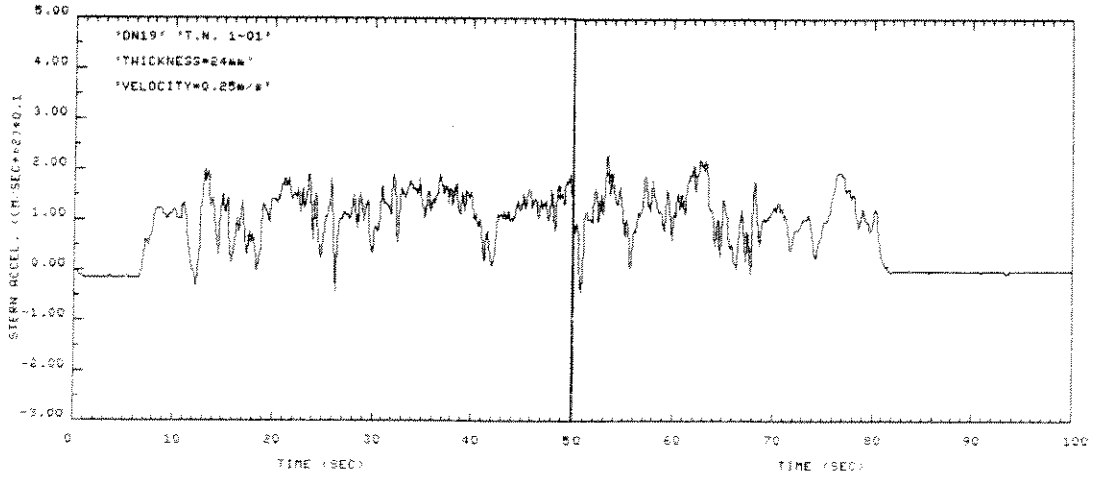
'DN19' 'T.N. 1-01'
'THICKNESS=24mm'
'VELOCITY=0.25m/s'
STERN ACCEL. ((M/SEC**2)*40.1
5.00
4.00
3.00
2.00
1.00
0.00
-1.00
-2.00
-3.00
0
10
20
30
40
50
60
70
80
90
100
TIME (SEC)
TIME (SEC)

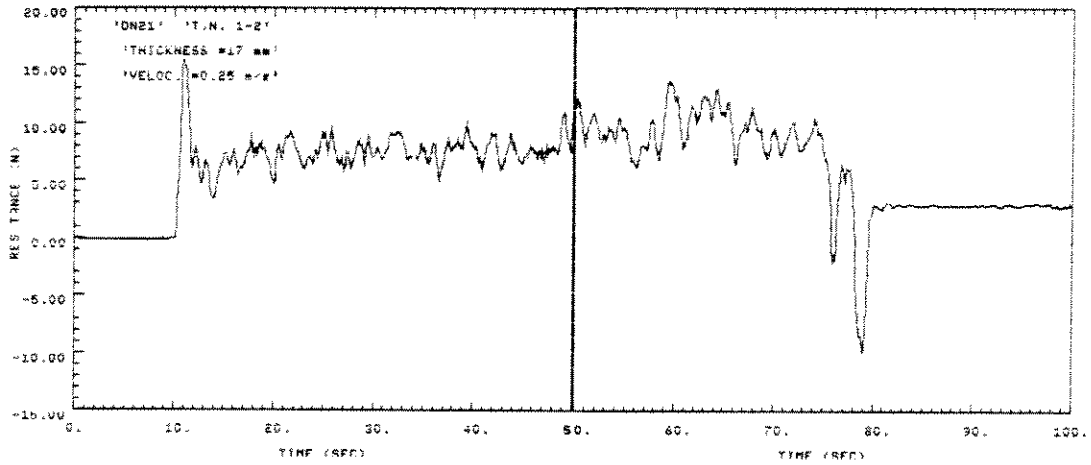
'DN21' 'T.N. 1-2'
'THICKNESS =17 mm'
'VELOC. =0.25 m/s'
RES TRACE (N)
TIME (SEC)

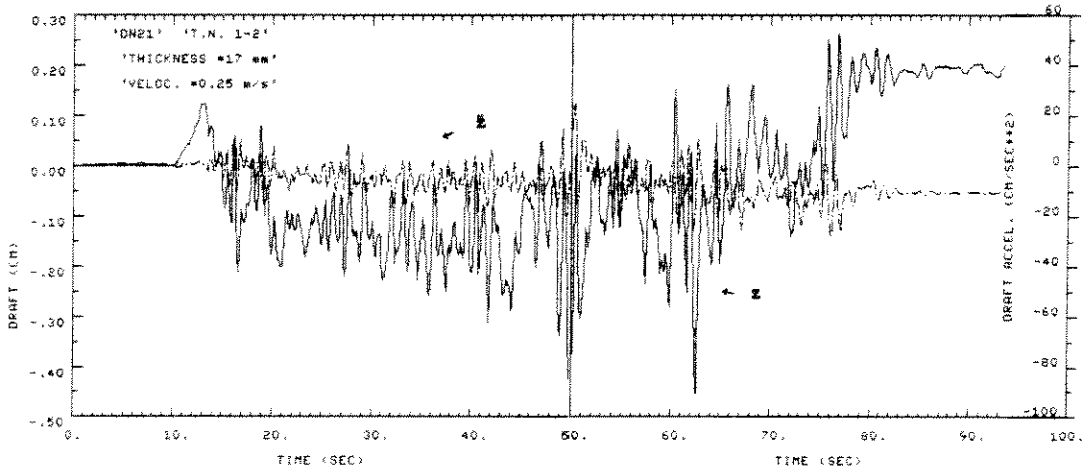
'DN21' 'T.N. 1-2'
'THICKNESS =17 mm'
'VELOC. =0.25 m/s'
DRAFT (M)
DRAFT ACCEL. (CM/SEC**2)
TIME (SEC)

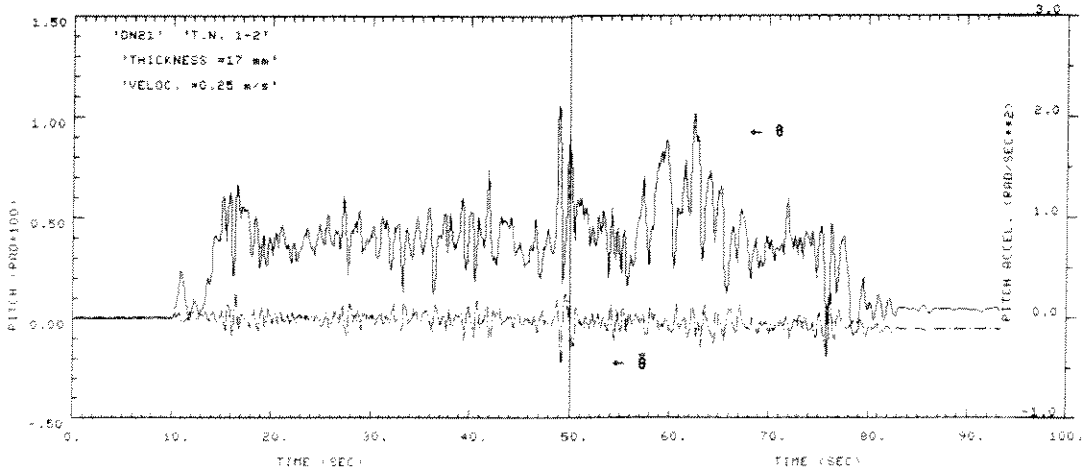
'DN21' 'T.N. 1-2'
'THICKNESS =17 mm'
'VELOC. =0.25 m/s'
PITCH (RAD*100)
PITCH ACCEL. (RAD/SEC**2)
TIME (SEC)

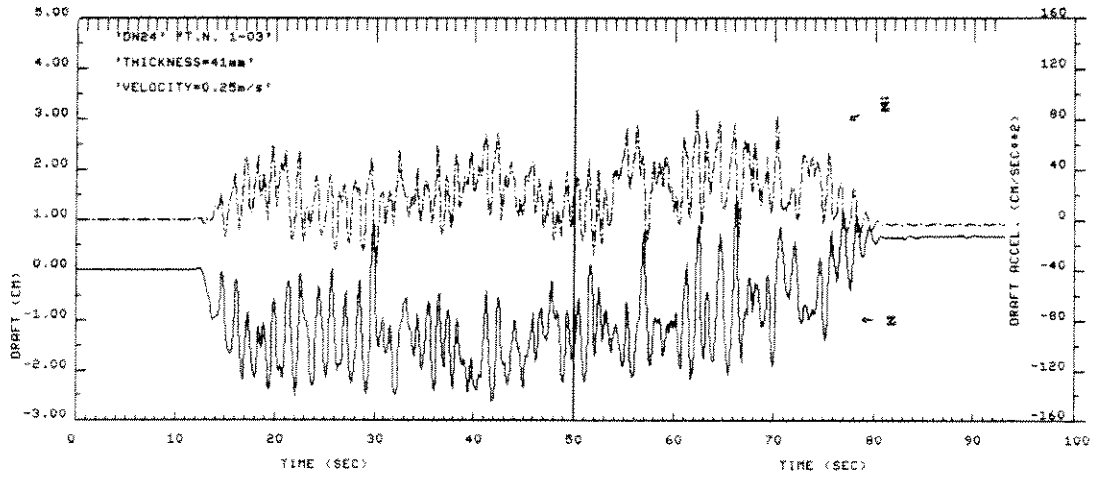
'DN24' PT.N. 1-03'
'THICKNESS=41mm'
'VELOCITY=0.25m/s'
DRAFT (CM)
DRAFT ACCEL. (CM/SEC**2)
TIME (SEC)
TIME (SEC)
η
η̈

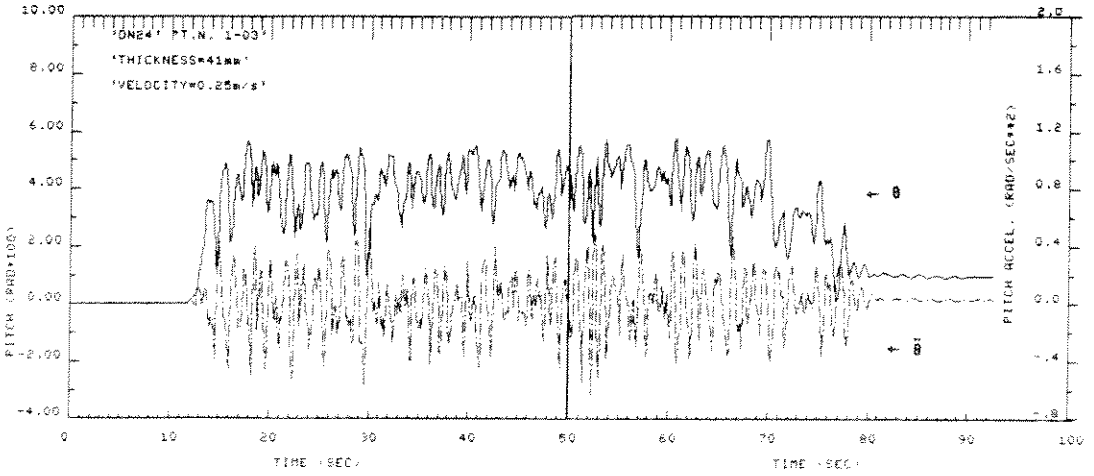
'DN24' PT.N. 1-03'
'THICKNESS=41mm'
'VELOCITY=0.25m/s'
PITCH (RAD*10E)
PITCH ACCEL. (RAD/SEC**2)
TIME (SEC)
TIME (SEC)
θ
θ̈

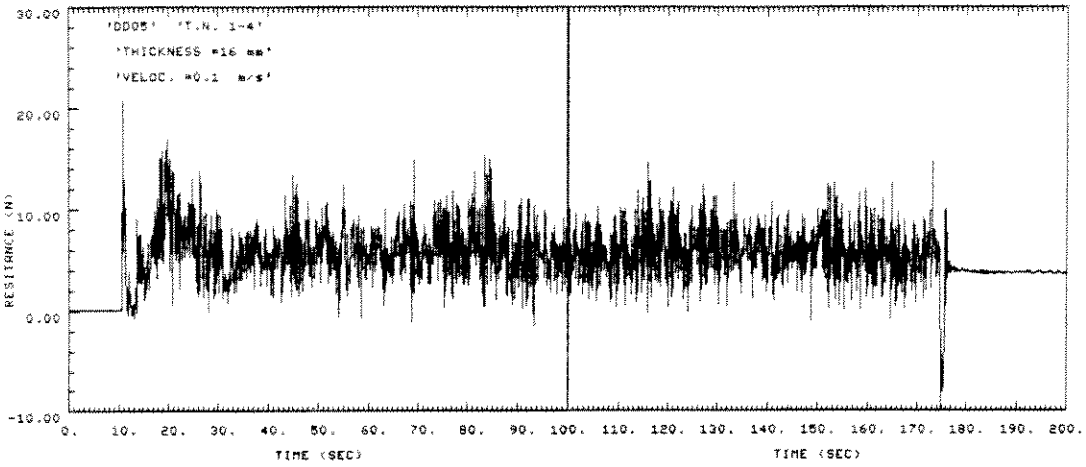
'DD05' 'T.N. 1-4'
'THICKNESS =16 mm'
'VELOC. =0.1 m/s'
RESITANCE (N)
30.00
20.00
10.00
0.00
-10.00
0. 10. 20. 30. 40. 50. 60. 70. 80. 90. 100. 110. 120. 130. 140. 150. 160. 170. 180. 190. 200.
TIME (SEC)
TIME (SEC)

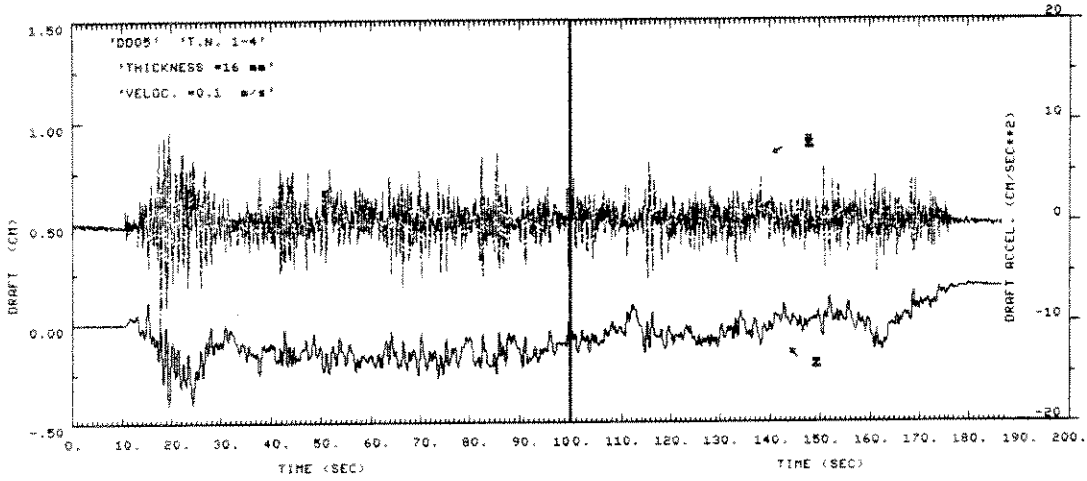
'DD05' 'T.N. 1-4'
'THICKNESS =16 mm'
'VELOC. =0.1 m/s'
DRAFT (CM)
1.50
1.00
0.50
0.00
-.50
DRAFT ACCEL. (CM/SEC**2)
20
10
0
-10
-20
Z
Z
0. 10. 20. 30. 40. 50. 60. 70. 80. 90. 100. 110. 120. 130. 140. 150. 160. 170. 180. 190. 200.
TIME (SEC)
TIME (SEC)

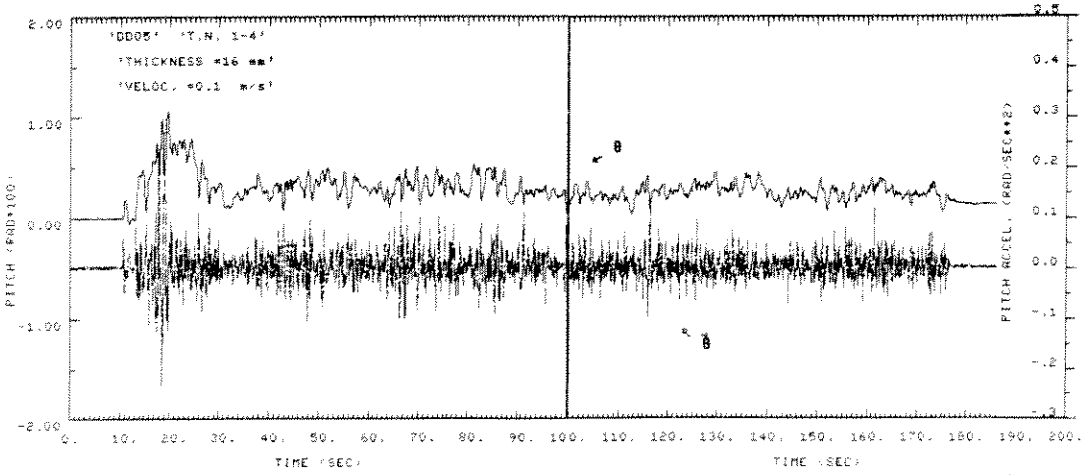
'DD05' 'T.N. 1-4'
'THICKNESS =16 mm'
'VELOC. =0.1 m/s'
PITCH (RAD*100)
2.00
1.00
0.00
-1.00
-2.00
PITCH ACCEL. (RAD/SEC**2)
0.4
0.3
0.2
0.1
0.0
-.1
-.2
θ
θ
0. 10. 20. 30. 40. 50. 60. 70. 80. 90. 100. 110. 120. 130. 140. 150. 160. 170. 180. 190. 200.
TIME (SEC)
TIME (SEC)

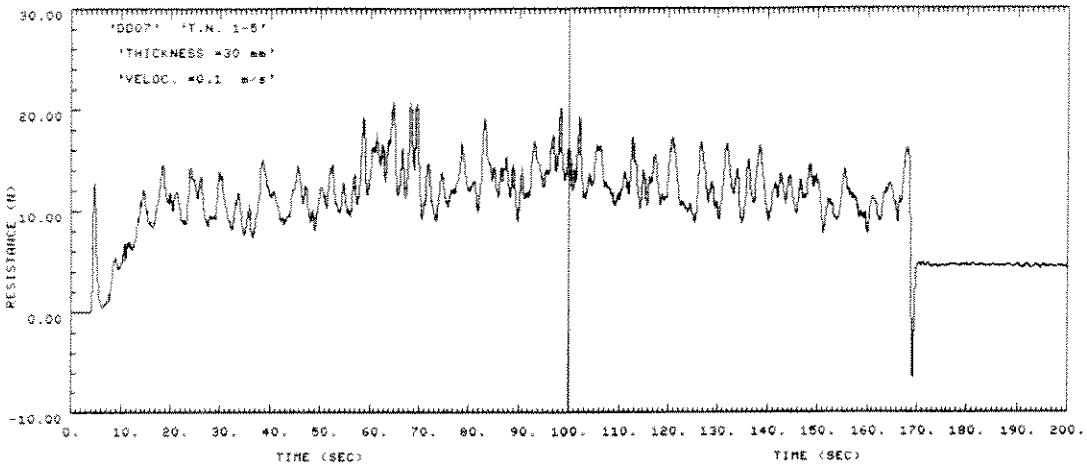
'0007' 'T.N. 1-5'
'THICKNESS =30 mm'
'VELOC. =0.1 m/s'
RESISTANCE (N)
30.00
20.00
10.00
0.00
-10.00
0. 10. 20. 30. 40. 50. 60. 70. 80. 90. 100. 110. 120. 130. 140. 150. 160. 170. 180. 190. 200.
TIME (SEC)
TIME (SEC)

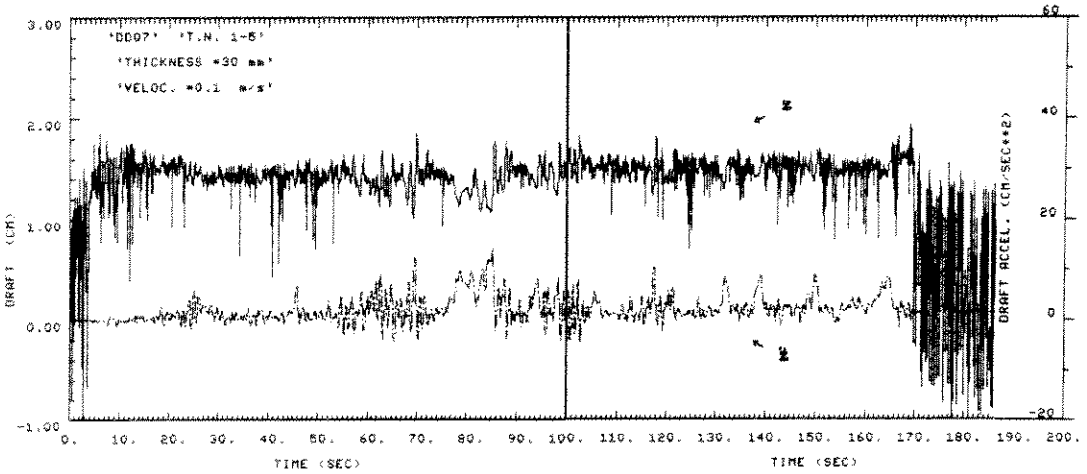
'0007' 'T.N. 1-5'
'THICKNESS =30 mm'
'VELOC. =0.1 m/s'
DRAFT (CM)
3.00
2.00
1.00
0.00
-1.00
DRAFT ACCEL. (CM/SEC**2)
60
40
20
0
-20
z
z
0. 10. 20. 30. 40. 50. 60. 70. 80. 90. 100. 110. 120. 130. 140. 150. 160. 170. 180. 190. 200.
TIME (SEC)
TIME (SEC)

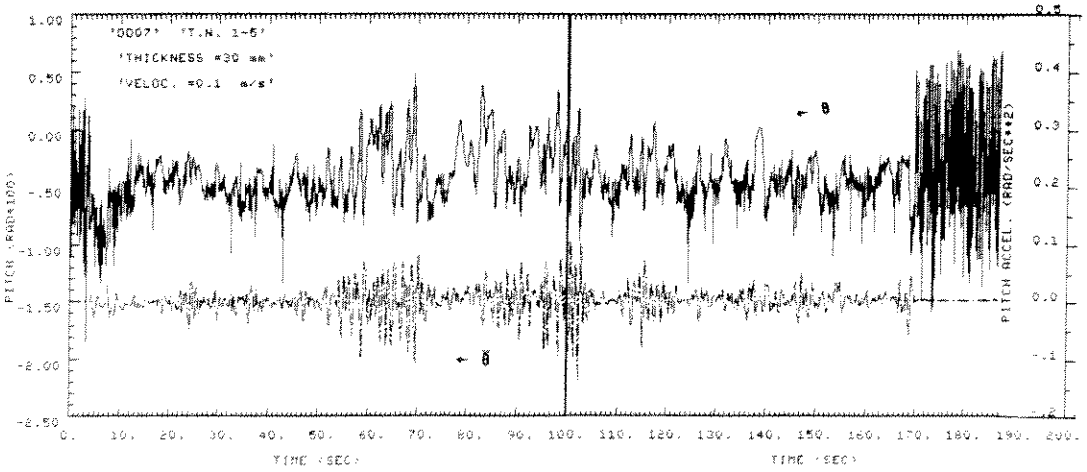
'0007' 'T.N. 1-5'
'THICKNESS =30 mm'
'VELOC. =0.1 m/s'
PITCH (RAD*100)
1.00
0.50
0.00
-.50
-1.00
-1.50
-2.00
-2.50
PITCH ACCEL. (RAD/SEC**2)
0.5
0.4
0.3
0.2
0.1
0.0
-.1
θ
θ
0. 10. 20. 30. 40. 50. 60. 70. 80. 90. 100. 110. 120. 130. 140. 150. 160. 170. 180. 190. 200.
TIME (SEC)
TIME (SEC)

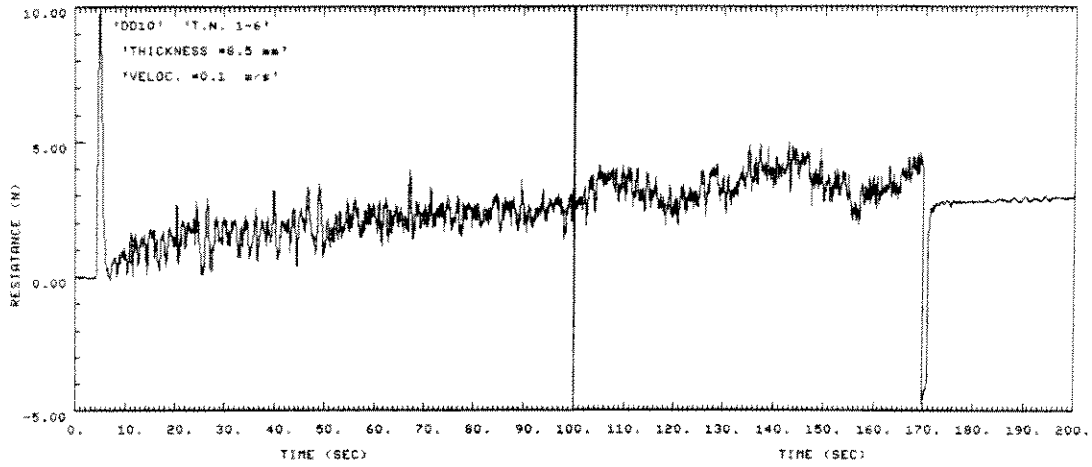
'DD10' 'T.N. 1-6'
'THICKNESS =8.5 mm'
'VELOC. =0.1 m/s'
RESISTANCE (N)
10.00
5.00
0.00
-5.00
0. 10. 20. 30. 40. 50. 60. 70. 80. 90. 100. 110. 120. 130. 140. 150. 160. 170. 180. 190. 200.
TIME (SEC)
TIME (SEC)

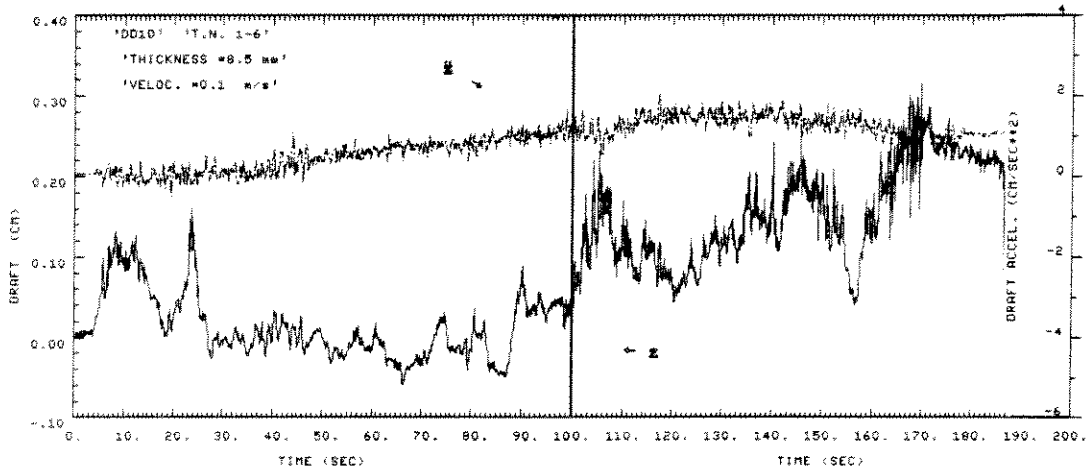
'DD10' 'T.N. 1-6'
'THICKNESS =8.5 mm'
'VELOC. =0.1 m/s'
DRAFT (CM)
0.40
0.30
0.20
0.10
0.00
-.10
DRAFT ACCEL. (CM/SEC**2)
2
0
-2
-4
-6
0. 10. 20. 30. 40. 50. 60. 70. 80. 90. 100. 110. 120. 130. 140. 150. 160. 170. 180. 190. 200.
TIME (SEC)
TIME (SEC)

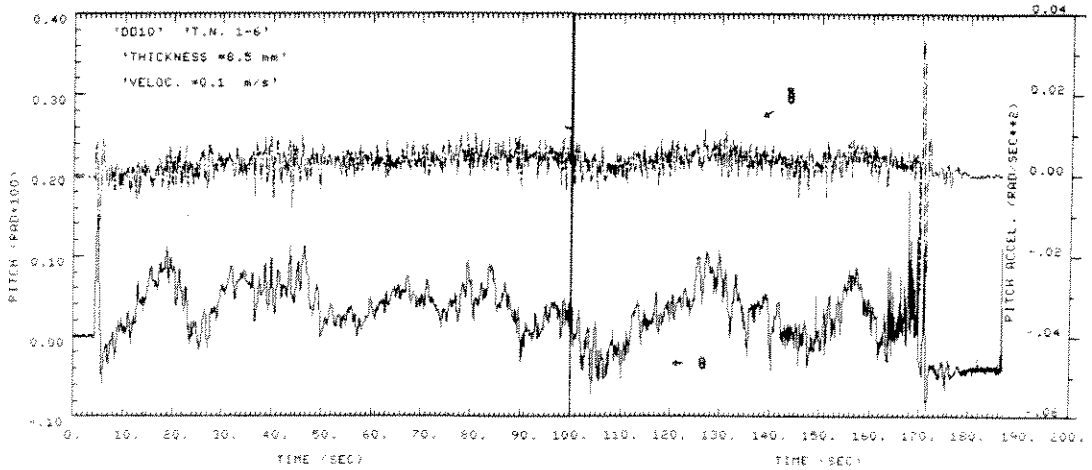
'DD10' 'T.N. 1-6'
'THICKNESS =8.5 mm'
'VELOC. =0.1 m/s'
PITCH (RAD*100)
0.40
0.30
0.20
0.10
0.00
-.10
PITCH ACCEL. (RAD/SEC**2)
0.02
0.00
-.02
-.04
0. 10. 20. 30. 40. 50. 60. 70. 80. 90. 100. 110. 120. 130. 140. 150. 160. 170. 180. 190. 200.
TIME (SEC)
TIME (SEC)

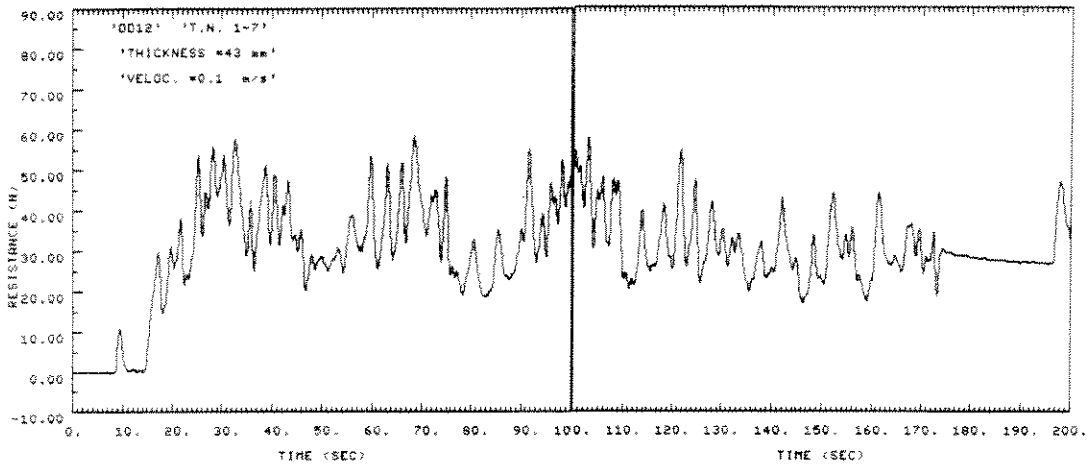
'0012' 'T.N. 1-7'
'THICKNESS =43 mm'
'VELOC. =0.1 m/s'
RESISTANCE (N)
TIME (SEC)

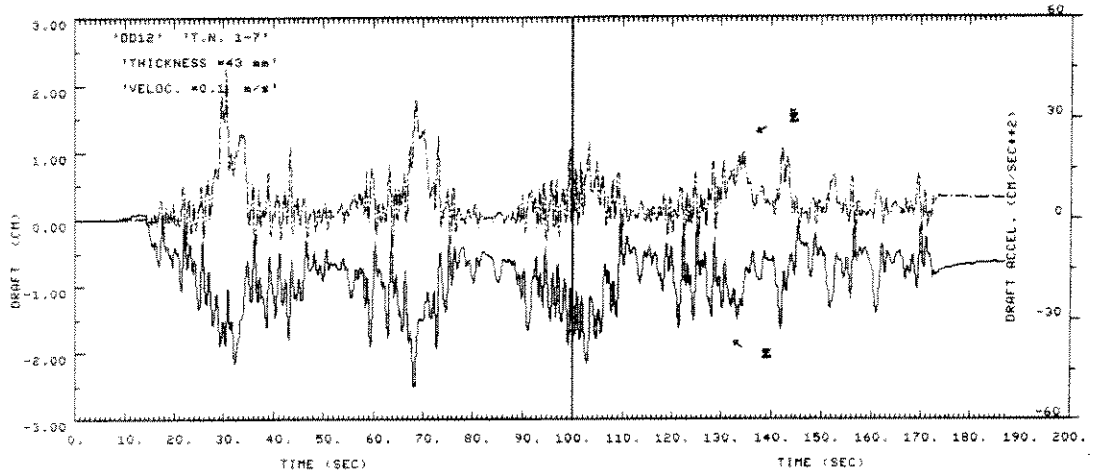
'0012' 'T.N. 1-7'
'THICKNESS =43 mm'
'VELOC. =0.1 m/s'
DRAFT (CM)
DRAFT ACCEL. (CM/SEC**2)
TIME (SEC)

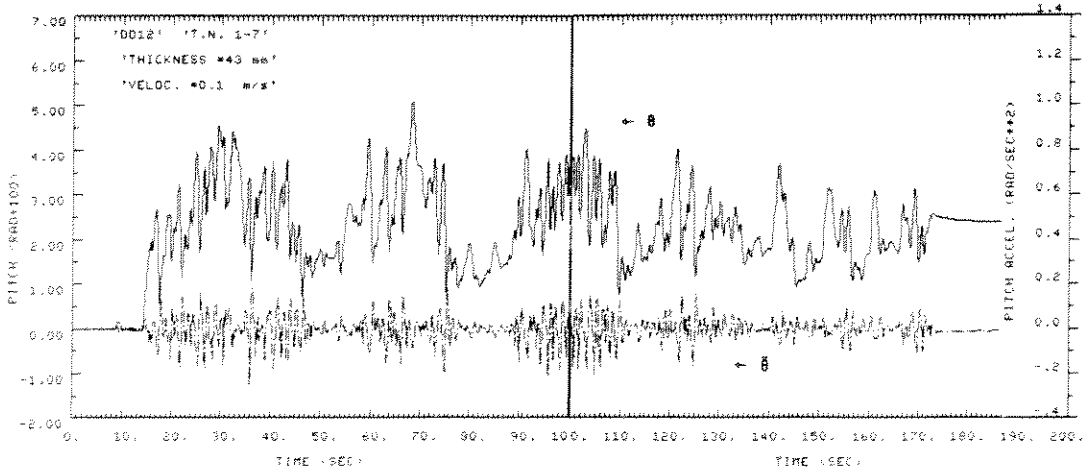
'0012' 'T.N. 1-7'
'THICKNESS =43 mm'
'VELOC. =0.1 m/s'
PITCH (RAD*100)
PITCH ACCEL. (RAD/SEC**2)
TIME (SEC)

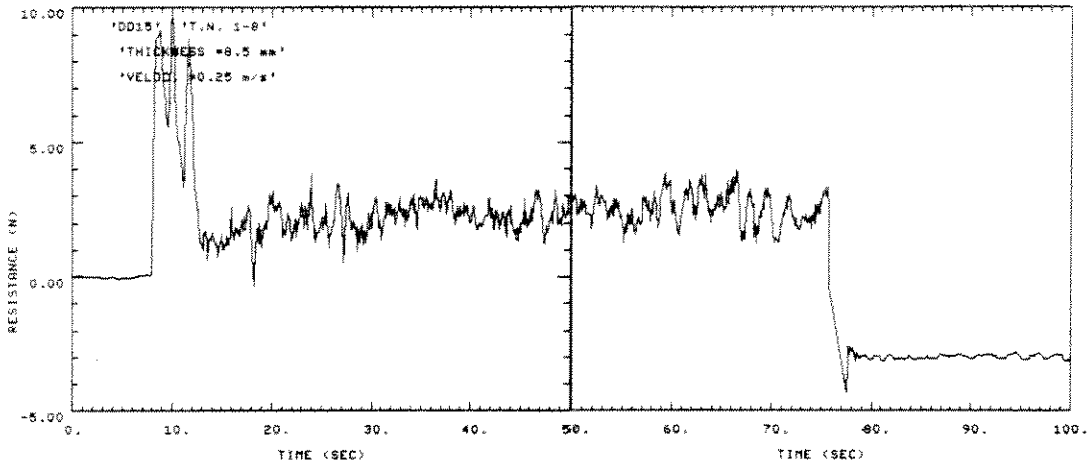
'DD15' 'T.N. 1-8'
'THICKNESS =8.5 mm'
'VELOC. =0.25 m/s'
RESISTANCE (N)
10.00
5.00
0.00
-5.00
0.
10.
20.
30.
40.
50.
60.
70.
80.
90.
100.
TIME (SEC)
TIME (SEC)

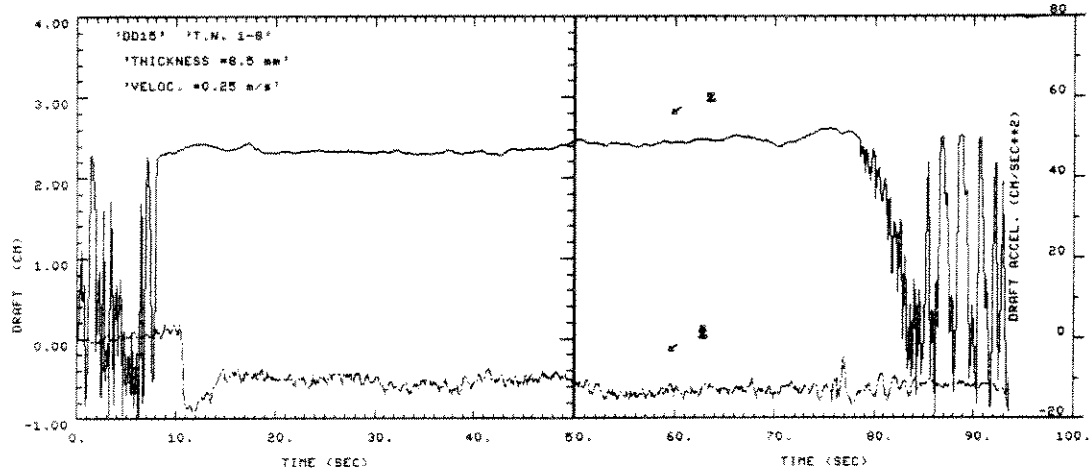
'DD15' 'T.N. 1-8'
'THICKNESS =8.5 mm'
'VELOC. =0.25 m/s'
DRAFT (CM)
4.00
3.00
2.00
1.00
0.00
-1.00
DRAFT ACCEL. (CM/SEC**2)
80
60
40
20
0
-20
0.
10.
20.
30.
40.
50.
60.
70.
80.
90.
100.
TIME (SEC)
TIME (SEC)

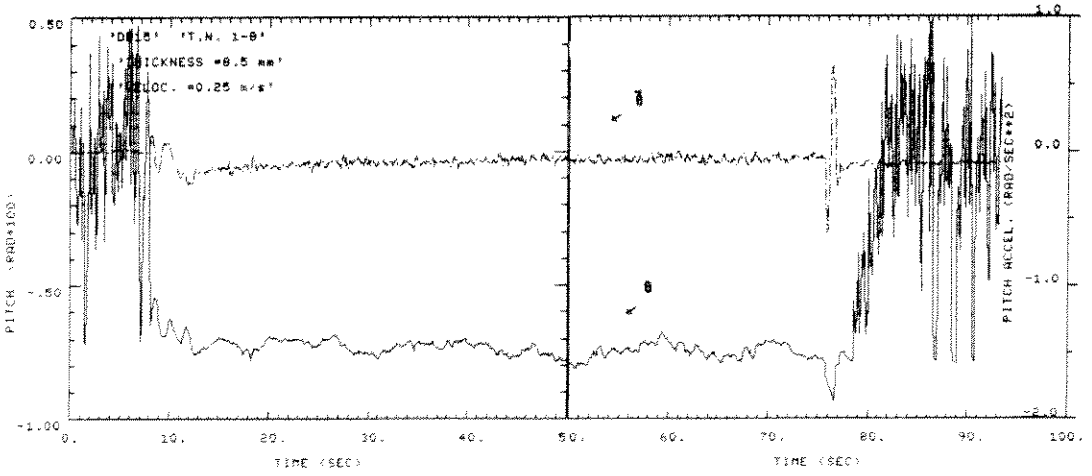
'DD15' 'T.N. 1-8'
'THICKNESS =8.5 mm'
'VELOC. =0.25 m/s'
PITCH (RAD*100)
0.50
0.00
-.50
-1.00
PITCH ACCEL. (RAD/SEC**2)
1.0
0.0
-1.0
0.
10.
20.
30.
40.
50.
60.
70.
80.
90.
100.
TIME (SEC)
TIME (SEC)

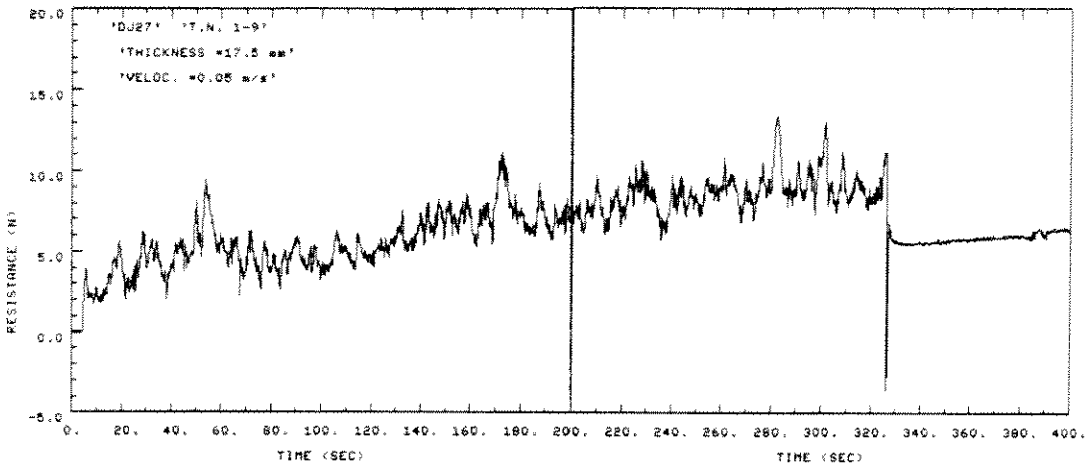
'DJ27' 'T.N. 1-9'
'THICKNESS =17.5 mm'
'VELOC. =0.05 m/s'
RESISTANCE (N)
20.0
15.0
10.0
5.0
0.0
-5.0
0. 20. 40. 60. 80. 100. 120. 140. 160. 180. 200. 220. 240. 260. 280. 300. 320. 340. 360. 380. 400.
TIME (SEC)
TIME (SEC)

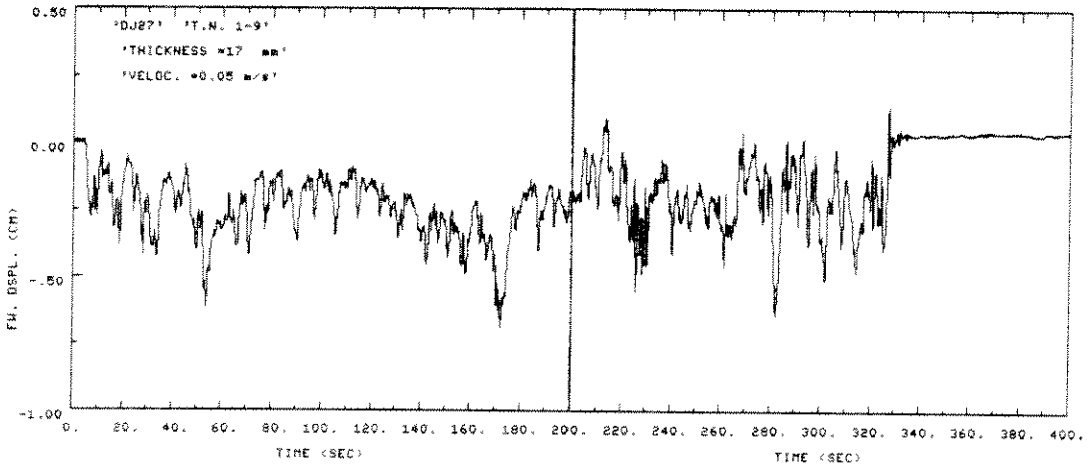
'DJ27' 'T.N. 1-9'
'THICKNESS =17 mm'
'VELOC. =0.05 m/s'
FW. DSPL. (CM)
0.50
0.00
-.50
-1.00
0. 20. 40. 60. 80. 100. 120. 140. 160. 180. 200. 220. 240. 260. 280. 300. 320. 340. 360. 380. 400.
TIME (SEC)
TIME (SEC)

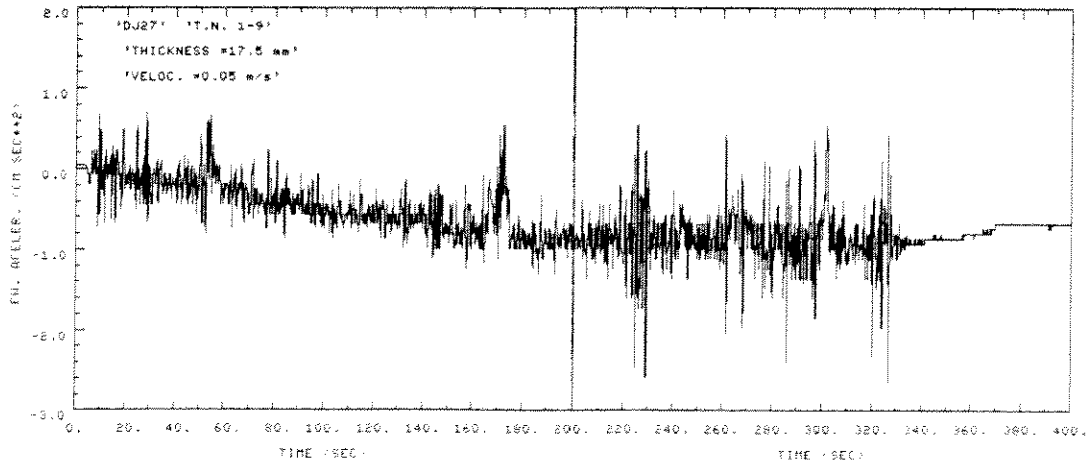
'DJ27' 'T.N. 1-9'
'THICKNESS =17.5 mm'
'VELOC. =0.05 m/s'
FW. ACCLER. (CM/SEC**2)
2.0
1.0
0.0
-1.0
-2.0
-3.0
0. 20. 40. 60. 80. 100. 120. 140. 160. 180. 200. 220. 240. 260. 280. 300. 320. 340. 360. 380. 400.
TIME (SEC)
TIME (SEC)

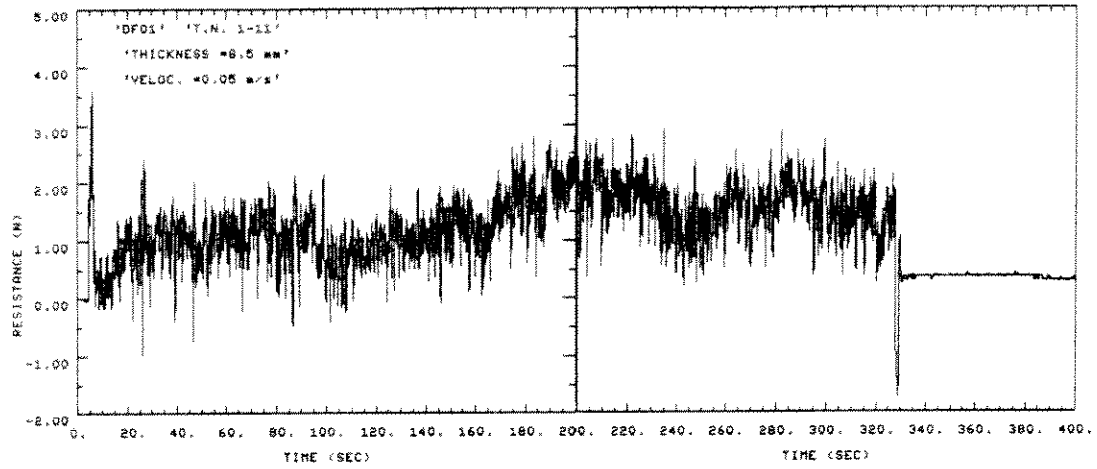
'DF01' 'T.N. 1-11'
'THICKNESS =8.5 mm'
'VELOC. =0.05 m/s'
RESISTANCE (N)
TIME (SEC)

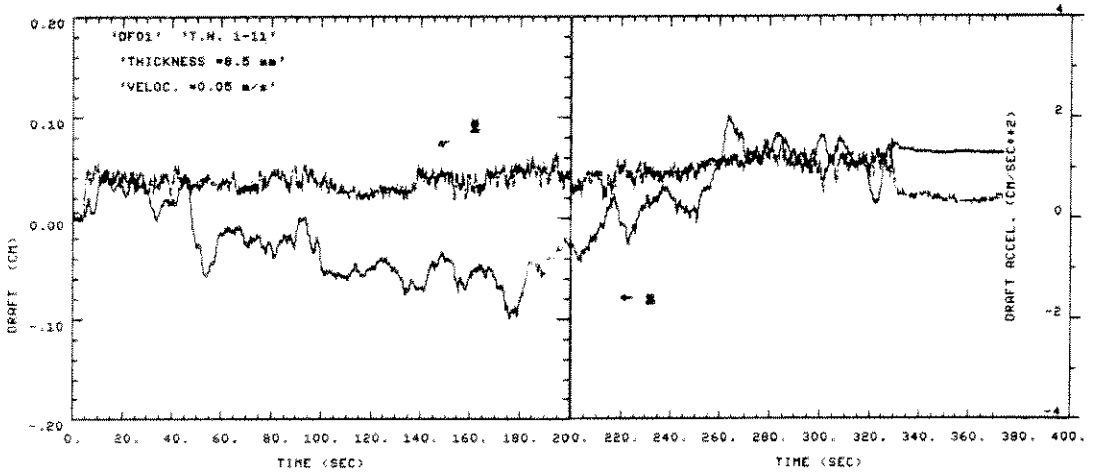
'DF01' 'T.N. 1-11'
'THICKNESS =8.5 mm'
'VELOC. =0.05 m/s'
DRAFT (CM)
DRAFT ACCEL. (CM/SEC**2)
TIME (SEC)

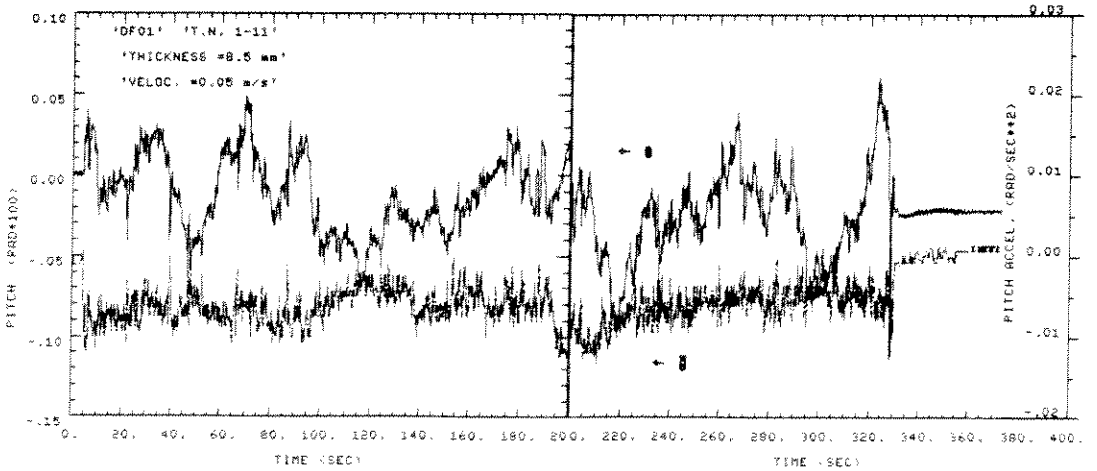
'DF01' 'T.N. 1-11'
'THICKNESS =8.5 mm'
'VELOC. =0.05 m/s'
PITCH (RAD*100)
PITCH ACCEL. (RAD/SEC**2)
TIME (SEC)

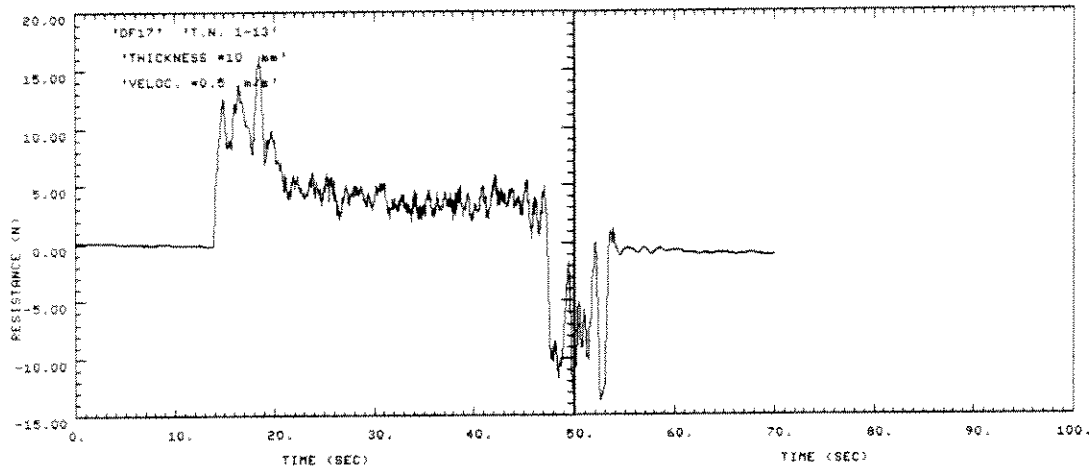
'DF17' 'T.N. 1-13'
'THICKNESS =10 mm'
'VELOC. =0.5 m/s'
RESISTANCE (N)
TIME (SEC)

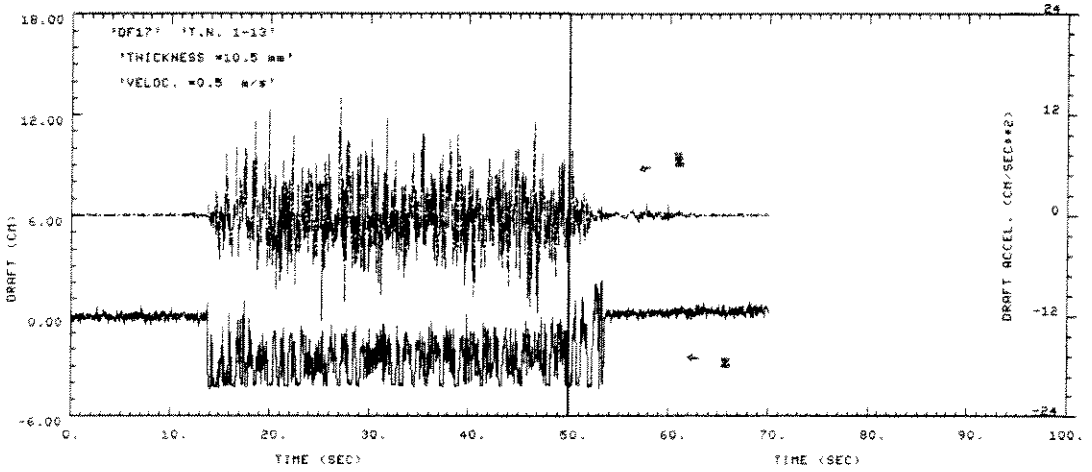
'DF17' 'T.N. 1-13'
'THICKNESS =10.5 mm'
'VELOC. =0.5 m/s'
DRAFT (CM)
DRAFT ACCEL. (CM/SEC**2)
TIME (SEC)

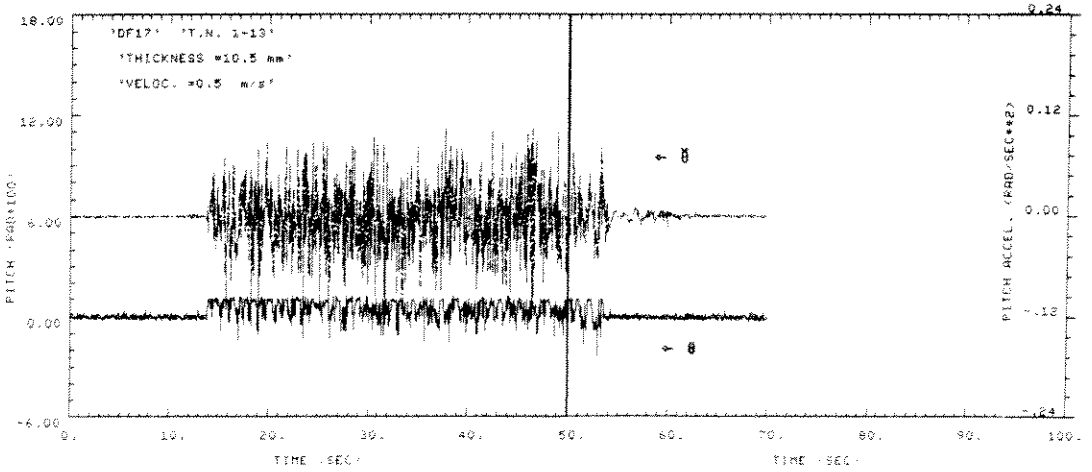
'DF17' 'T.N. 1-13'
'THICKNESS =10.5 mm'
'VELOC. =0.5 m/s'
PITCH ACCEL. (RAD/SEC**2)
TIME (SEC)

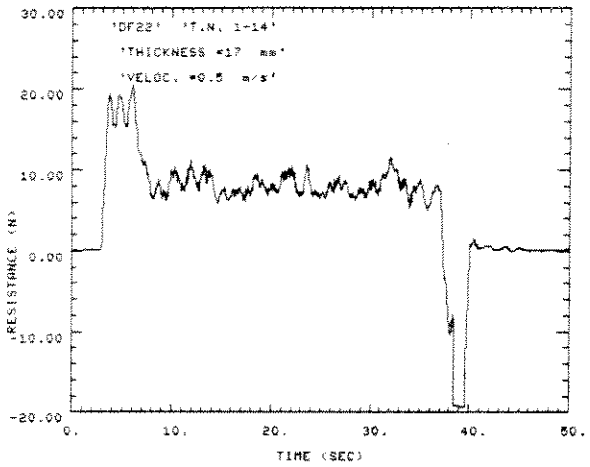
'DF22' 'T.N. 1-14'
'THICKNESS =17 mm'
'VELOC. =0.5 m/s'
RESISTANCE (N)
TIME (SEC)

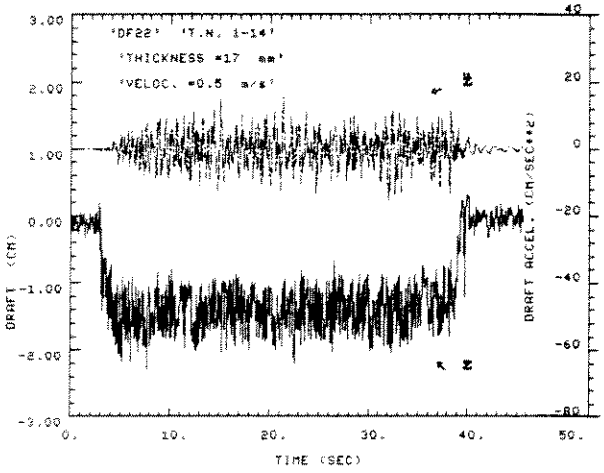
'DF22' 'T.N. 1-14'
'THICKNESS =17 mm'
'VELOC. =0.5 m/s'
DRAFT (CM)
DRAFT ACCEL. (CM/SEC**2)
TIME (SEC)

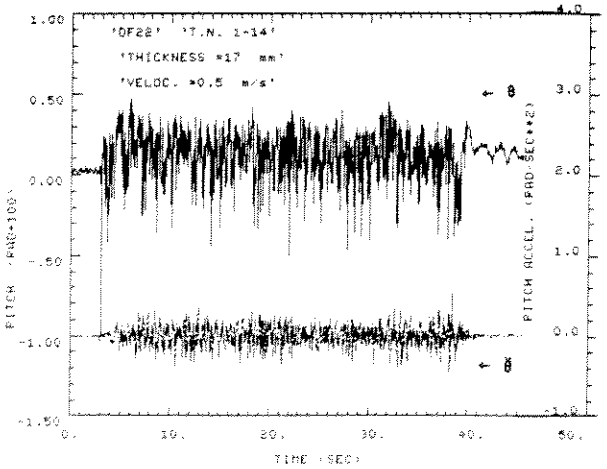
'DF22' 'T.N. 1-14'
'THICKNESS =17 mm'
'VELOC. =0.5 m/s'
PITCH (RAD*100)
PITCH ACCEL. (RAD/SEC**2)
TIME (SEC)

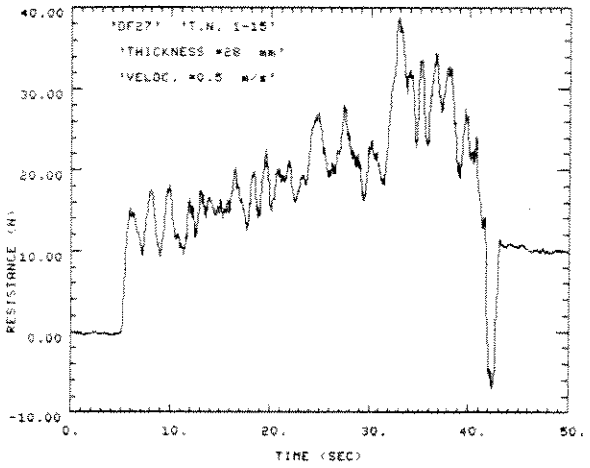
'DF27' 'T.N. 1-15'
'THICKNESS =28 mm'
'VELOC. =0.5 m/s'
RESISTANCE (N)
40.00
30.00
20.00
10.00
0.00
-10.00
0.
10.
20.
30.
40.
50.
TIME (SEC)

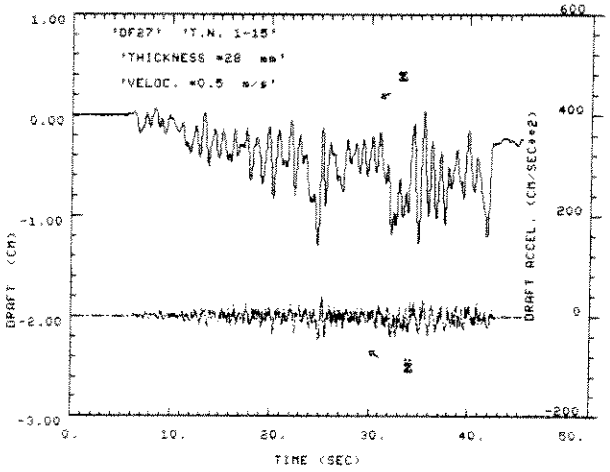
'DF27' 'T.N. 1-15'
'THICKNESS =28 mm'
'VELOC. =0.5 m/s'
DRAFT (CM)
DRAFT ACCEL. (CM/SEC**2)
1.00
0.00
-1.00
-2.00
-3.00
600
400
200
0
-200
0.
10.
20.
30.
40.
50.
TIME (SEC)

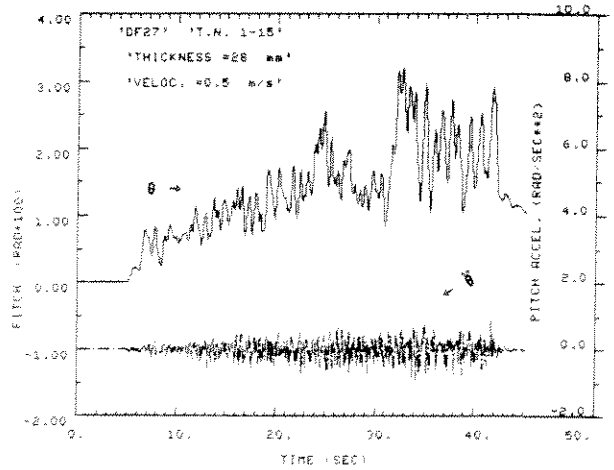
'DF27' 'T.N. 1-15'
'THICKNESS =28 mm'
'VELOC. =0.5 m/s'
PITCH (RAD*100)
PITCH ACCEL. (RAD/SEC**2)
4.00
3.00
2.00
1.00
0.00
-1.00
-2.00
10.0
8.0
6.0
4.0
2.0
0.0
-2.0
0.
10.
20.
30.
40.
50.
TIME (SEC)

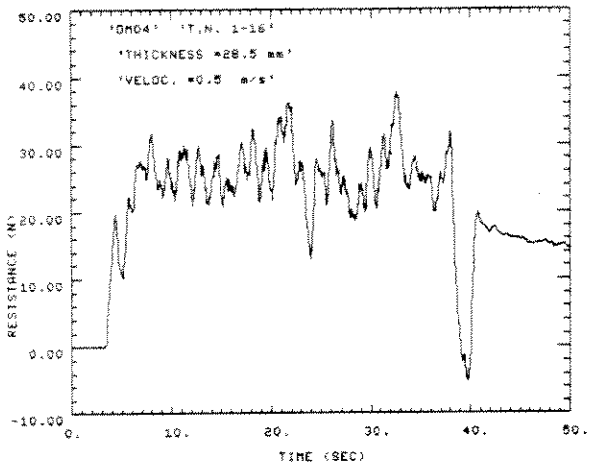
'DM04' 'T.N. 1-16'
'THICKNESS =28.5 mm'
'VELOC. =0.5 m/s'
RESISTANCE (N)
50.00
40.00
30.00
20.00
10.00
0.00
-10.00
0.
10.
20.
30.
40.
50.
TIME (SEC)

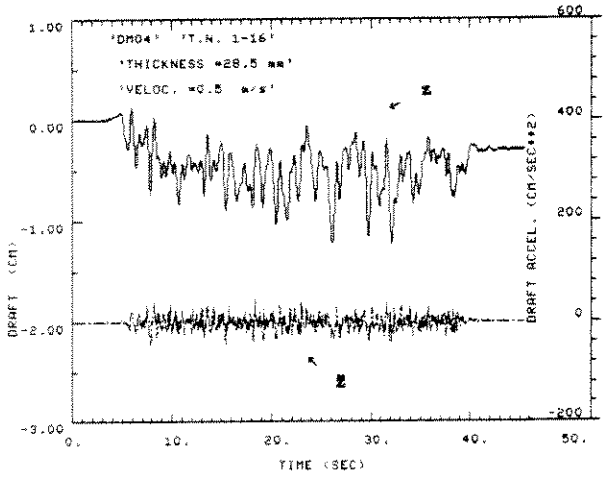
'DM04' 'T.N. 1-16'
'THICKNESS =28.5 mm'
'VELOC. =0.5 m/s'
Z
Z
DRAFT (CM)
DRAFT ACCEL. (CM/SEC**2)
1.00
0.00
-1.00
-2.00
-3.00
600
400
200
0
-200
0.
10.
20.
30.
40.
50.
TIME (SEC)

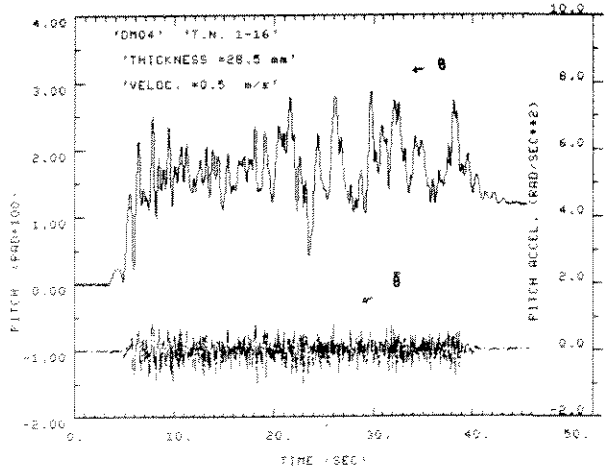
'DM04' 'T.N. 1-16'
'THICKNESS =28.5 mm'
'VELOC. =0.5 m/s'
θ
θ
PITCH (RAD*100)
PITCH ACCEL. (RAD/SEC**2)
4.00
3.00
2.00
1.00
0.00
-1.00
-2.00
8.0
6.0
4.0
2.0
0.0
0.
10.
20.
30.
40.
50.
TIME (SEC)

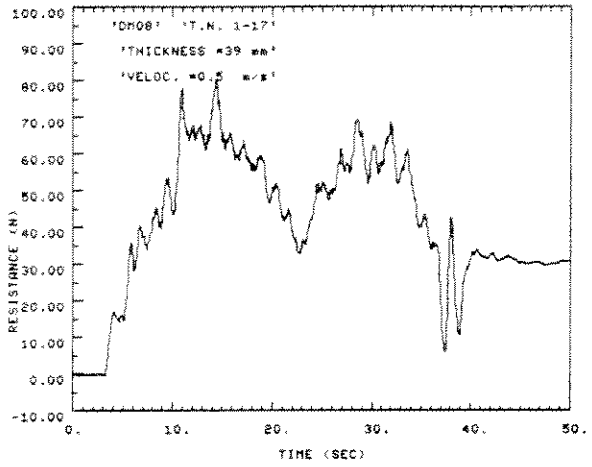
'DM08' 'T.N. 1-17'
'THICKNESS =39 mm'
'VELOC. =0.5 m/s'
RESISTANCE (N)
TIME (SEC)

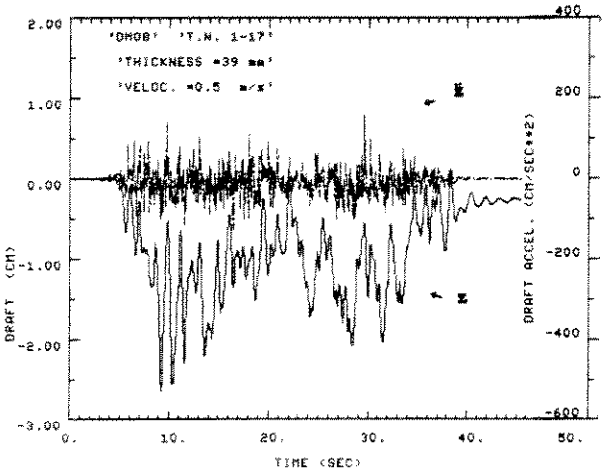
'DM08' 'T.N. 1-17'
'THICKNESS =39 mm'
'VELOC. =0.5 m/s'
DRAFT (CM)
DRAFT ACCEL. (CM/SEC**2)
TIME (SEC)

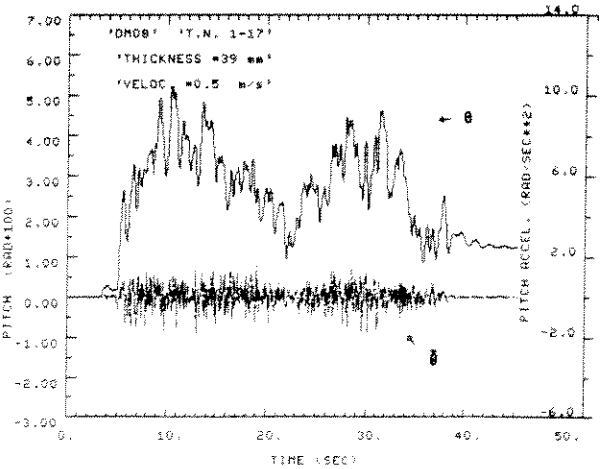
'DM08' 'T.N. 1-17'
'THICKNESS =39 mm'
'VELOC =0.5 m/s'
PITCH (RAD*100)
PITCH ACCEL. (RAD/SEC**2)
TIME (SEC)

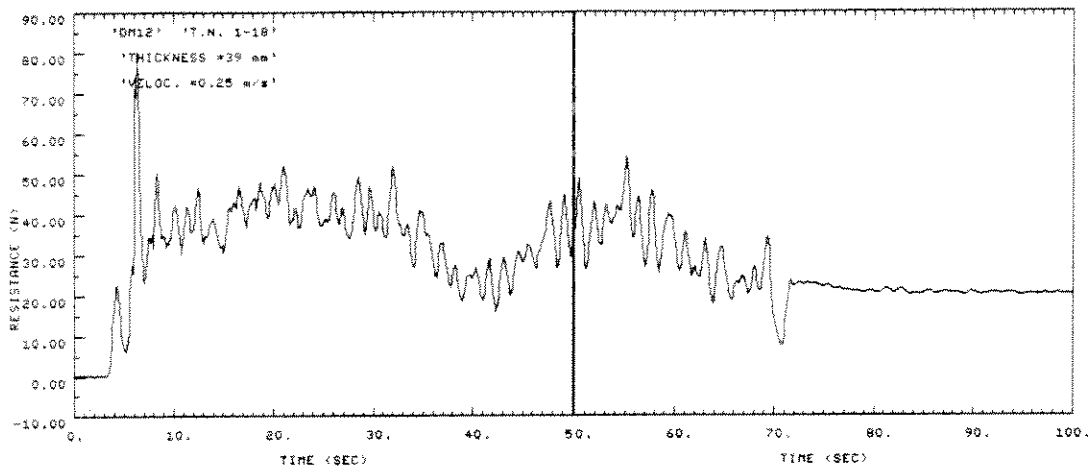
'DM12' 'T.N. 1-18'
'THICKNESS =39 mm'
'VELOC. =0.25 m/s'
RESISTANCE (N)
TIME (SEC)

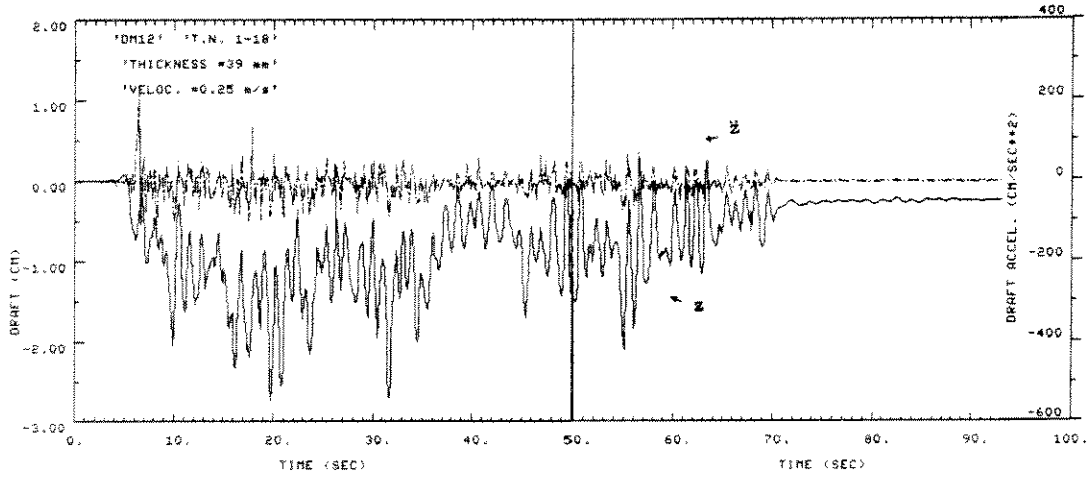
'DM12' 'T.N. 1-18'
'THICKNESS =39 mm'
'VELOC. =0.25 m/s'
DRAFT (CM)
DRAFT ACCEL. (CM/SEC**2)
TIME (SEC)

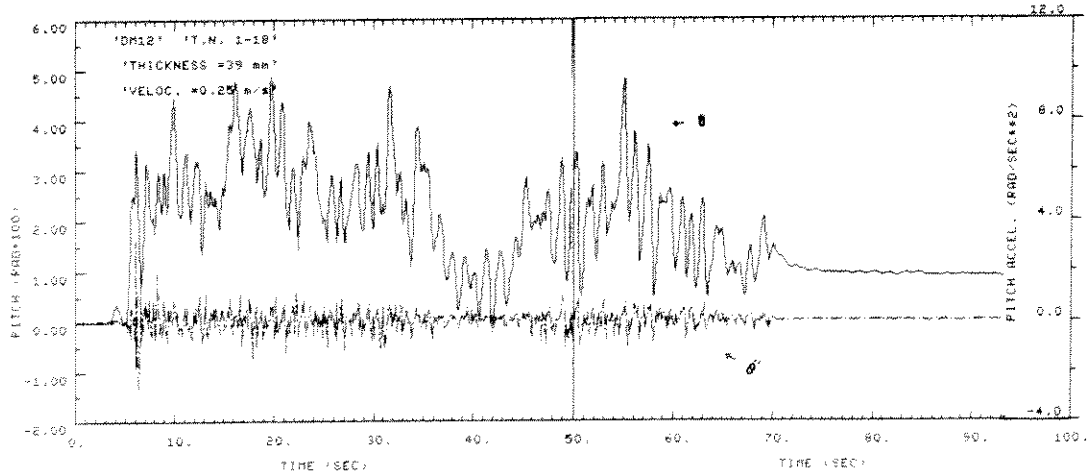
'DM12' 'T.N. 1-18'
'THICKNESS =39 mm'
'VELOC. =0.25 m/s'
PITCH ACCEL. (RAD/SEC**2)
TIME (SEC)

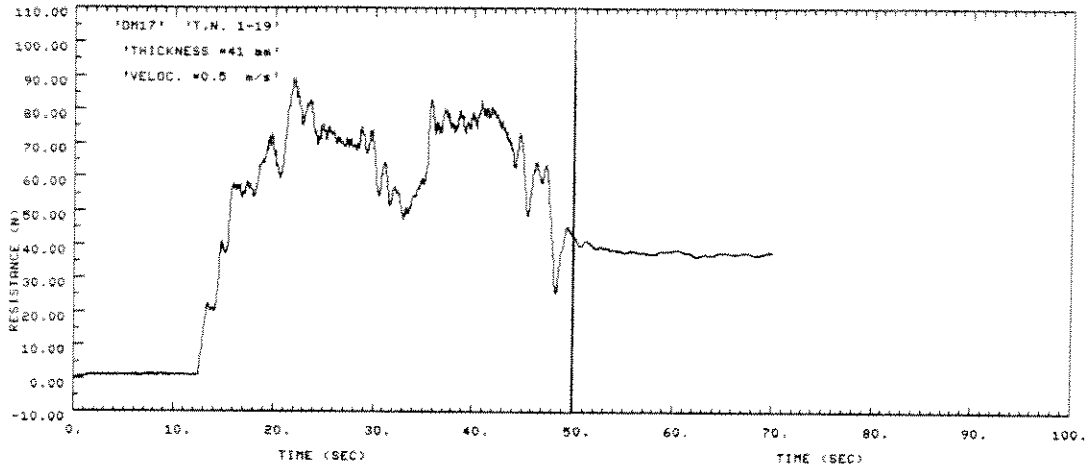
'DM17' 'T.N. 1-19'
'THICKNESS =41 mm'
'VELOC. =0.5 m/s'
RESISTANCE (N)
TIME (SEC)
TIME (SEC)

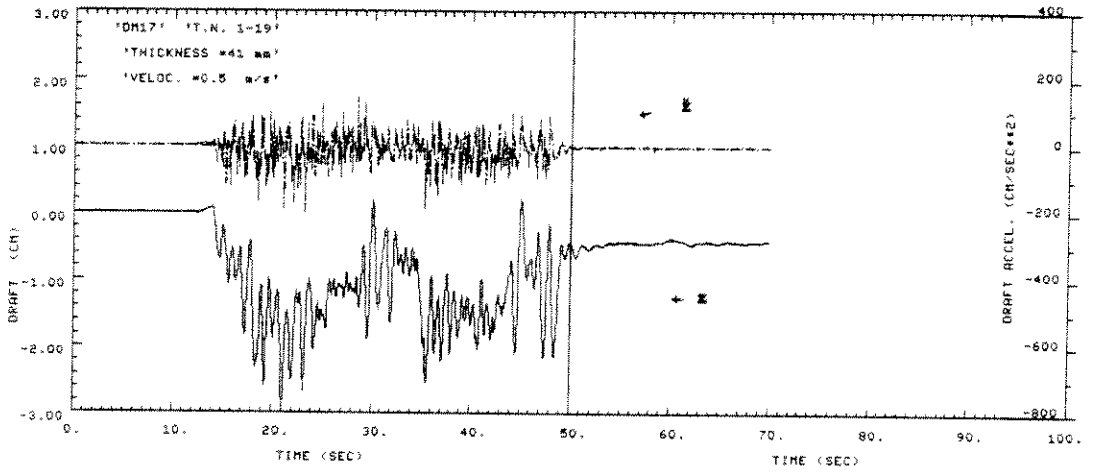
'DM17' 'T.N. 1-19'
'THICKNESS =41 mm'
'VELOC. =0.5 m/s'
DRAFT (CM)
DRAFT ACCEL. (CM/SEC**2)
TIME (SEC)
TIME (SEC)

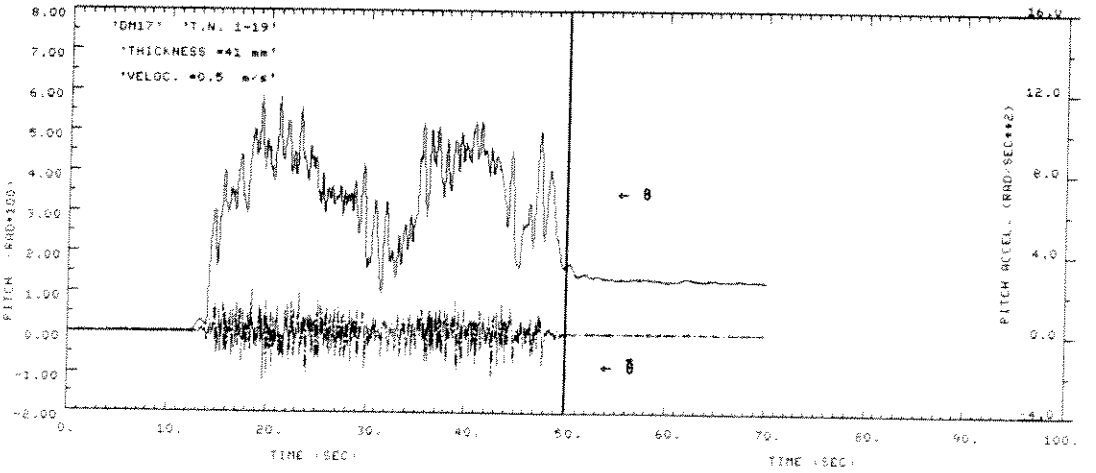
'DM17' 'T.N. 1-19'
'THICKNESS =41 mm'
'VELOC. =0.5 m/s'
PITCH (RAD*100)
PITCH ACCEL. (RAD/SEC**2)
TIME (SEC)
TIME (SEC)

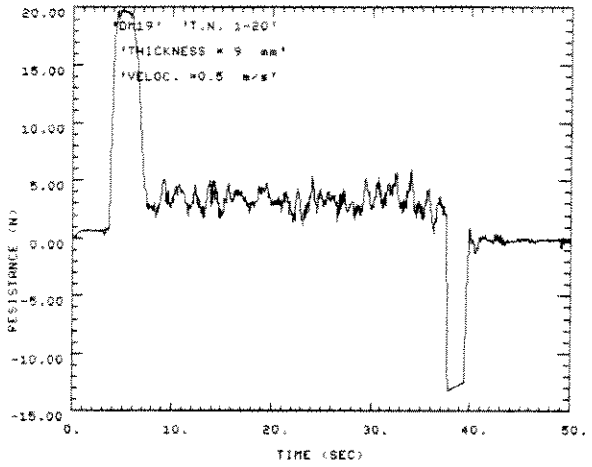
'DM19' 'T.N. 1-20'
'THICKNESS = 9 mm'
'VELOC. =0.5 m/s'
RESISTANCE (N)
TIME (SEC)

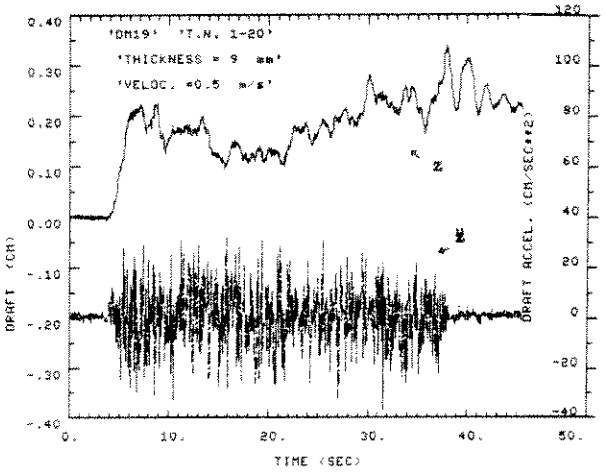
'DM19' 'T.N. 1-20'
'THICKNESS = 9 mm'
'VELOC. =0.5 m/s'
DRAFT (CM)
DRAFT ACCEL. (CM/SEC**2)
z
z̈
TIME (SEC)

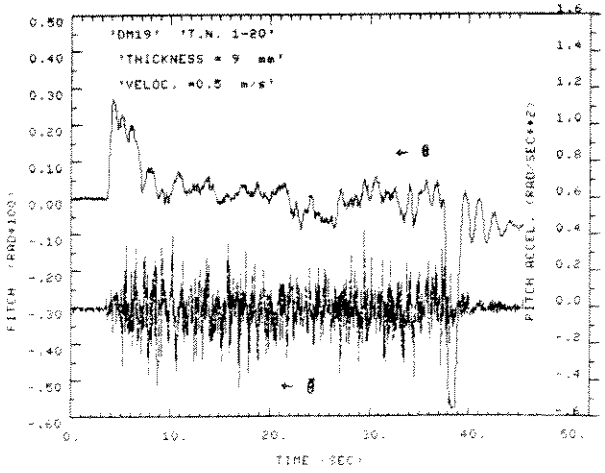
'DM19' 'T.N. 1-20'
'THICKNESS = 9 mm'
'VELOC. =0.5 m/s'
PITCH (RAD*100)
PITCH ACCEL. (RAD/SEC**2)
θ
θ̈
TIME (SEC)

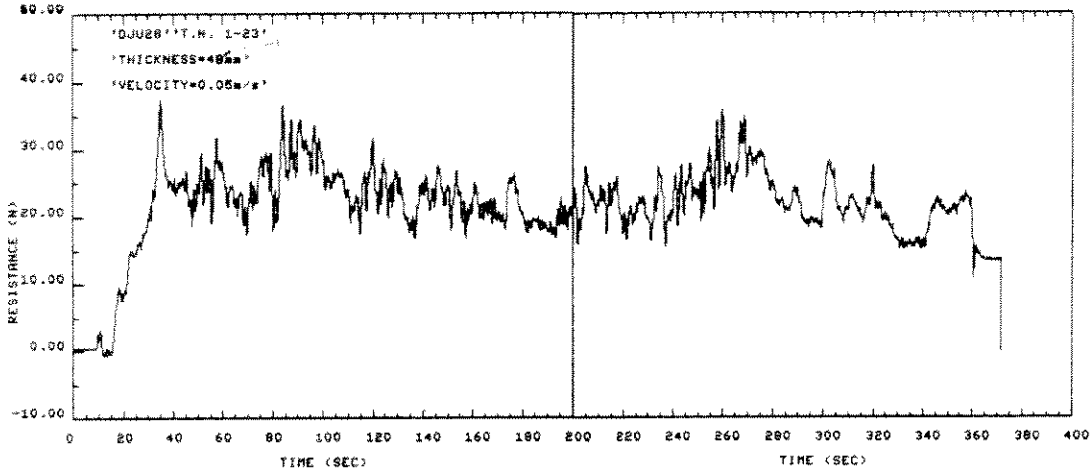
'DJU28''T.N. 1-23'
'THICKNESS=40mm'
'VELOCITY=0.05m/s'
RESISTANCE (N)
TIME (SEC)

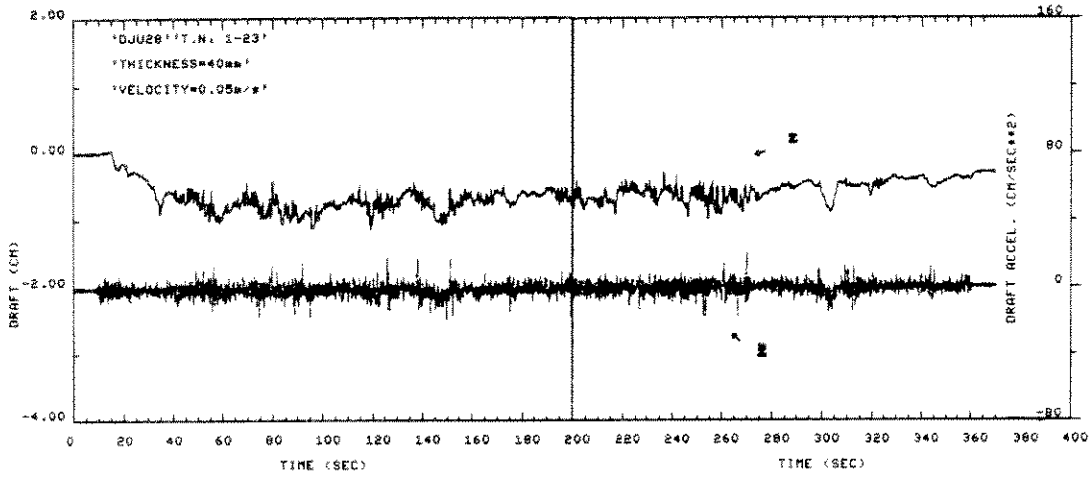
'DJU28''T.N. 1-23'
'THICKNESS=40mm'
'VELOCITY=0.05m/s'
DRAFT (CM)
DRAFT ACCEL. (CM/SEC**2)
TIME (SEC)

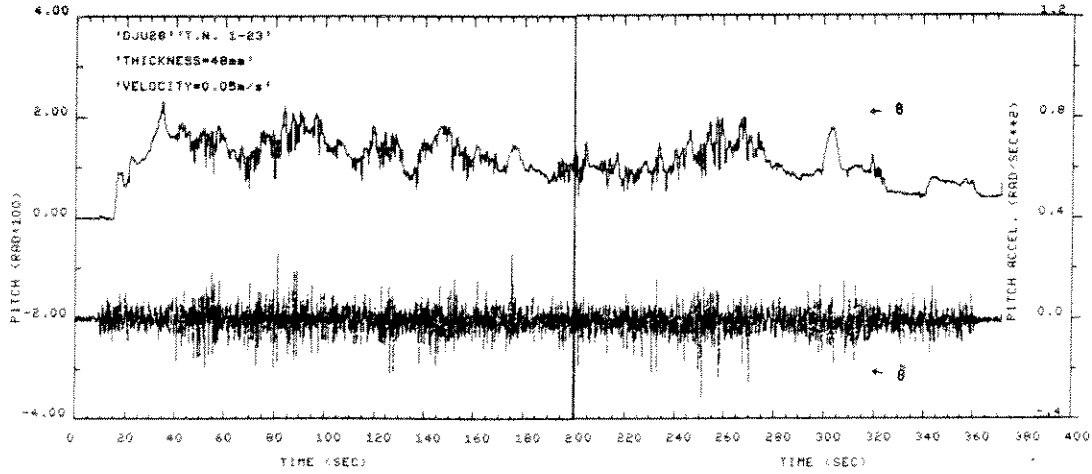
'DJU28''T.N. 1-23'
'THICKNESS=40mm'
'VELOCITY=0.05m/s'
PITCH (RAD*100)
PITCH ACCEL. (RAD/SEC**2)
TIME (SEC)

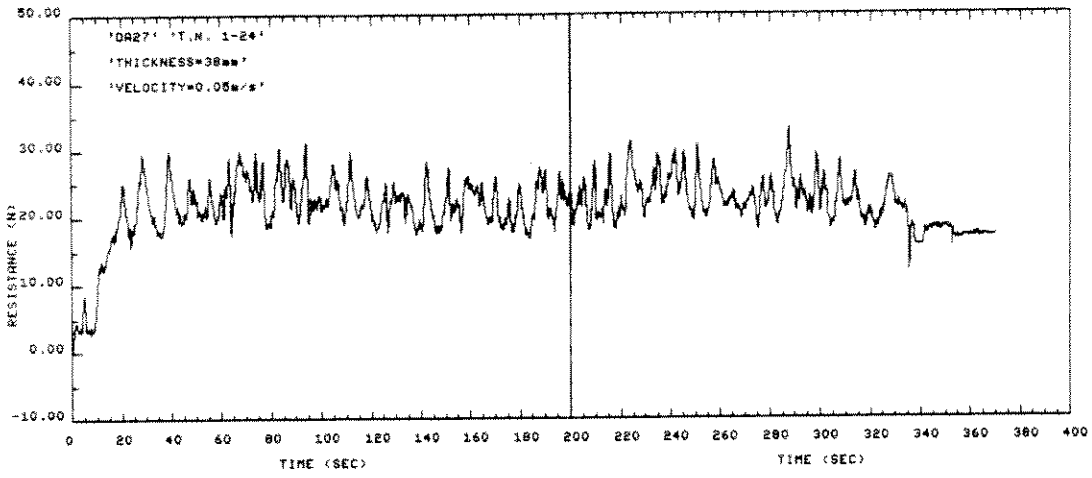
'DR27' 'T.N. 1-24'
'THICKNESS=38mm'
'VELOCITY=0.05m/s'
RESISTANCE (N)
50.00
40.00
30.00
20.00
10.00
0.00
-10.00
0 20 40 60 80 100 120 140 160 180 200 220 240 260 280 300 320 340 360 380 400
TIME (SEC)
TIME (SEC)

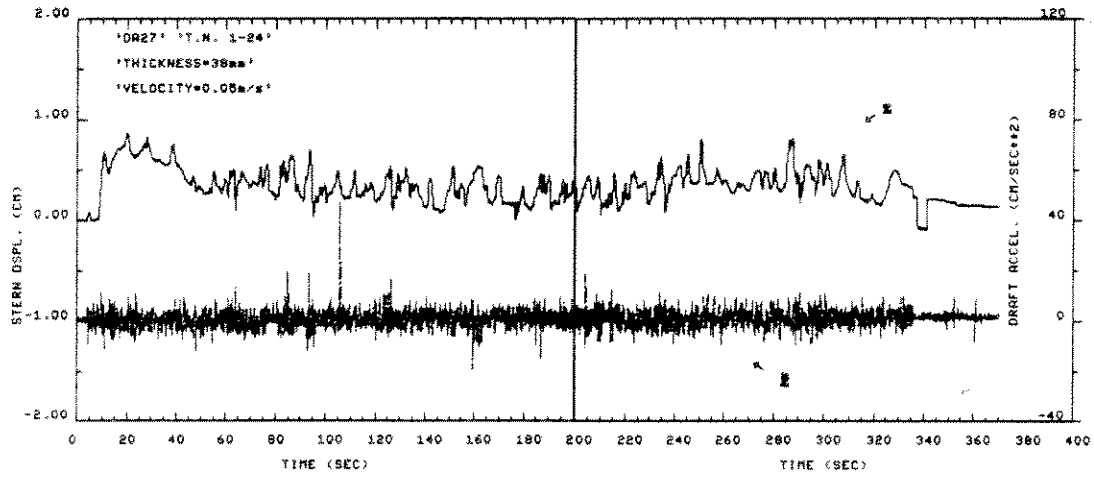
'DR27' 'T.N. 1-24'
'THICKNESS=38mm'
'VELOCITY=0.05m/s'
STERN DSPL. (CM)
2.00
1.00
0.00
-1.00
-2.00
DRAFT ACCEL. (CM/SEC**2)
120
80
40
0
-40
0 20 40 60 80 100 120 140 160 180 200 220 240 260 280 300 320 340 360 380 400
TIME (SEC)
TIME (SEC)

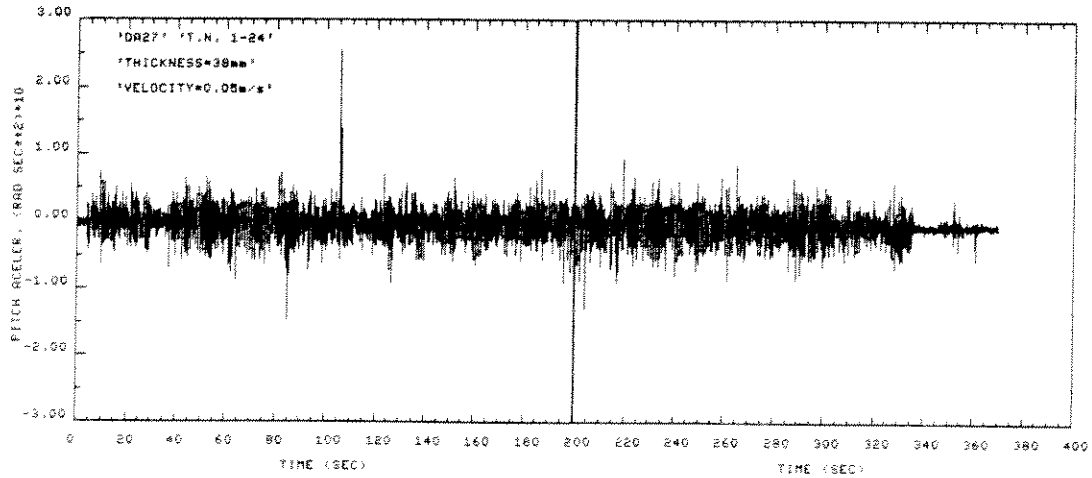
'DR27' 'T.N. 1-24'
'THICKNESS=38mm'
'VELOCITY=0.05m/s'
PITCH ACCLRN. (RAD SEC**2)*10
3.00
2.00
1.00
0.00
-1.00
-2.00
-3.00
0 20 40 60 80 100 120 140 160 180 200 220 240 260 280 300 320 340 360 380 400
TIME (SEC)
TIME (SEC)

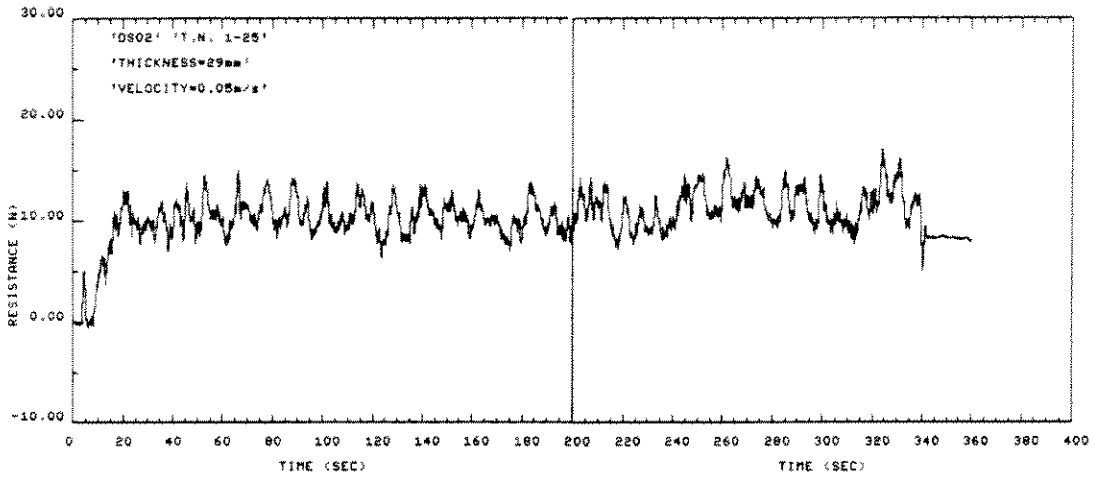
'DS02' 'T.N. 1-25'
'THICKNESS=29mm'
'VELOCITY=0.05m/s'
RESISTANCE (N)
30.00
20.00
10.00
0.00
-10.00
0 20 40 60 80 100 120 140 160 180 200 220 240 260 280 300 320 340 360 380 400
TIME (SEC)
TIME (SEC)

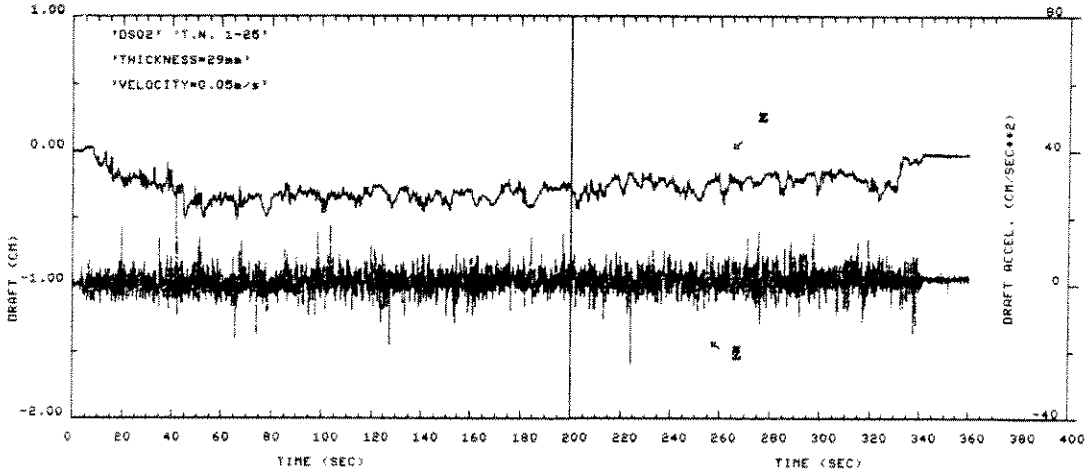
'DS02' 'T.N. 1-25'
'THICKNESS=29mm'
'VELOCITY=0.05m/s'
DRAFT (CM)
1.00
0.00
-1.00
-2.00
DRAFT ACCEL. (CM/SEC**2)
80
40
0
-40
z
z
0 20 40 60 80 100 120 140 160 180 200 220 240 260 280 300 320 340 360 380 400
TIME (SEC)
TIME (SEC)

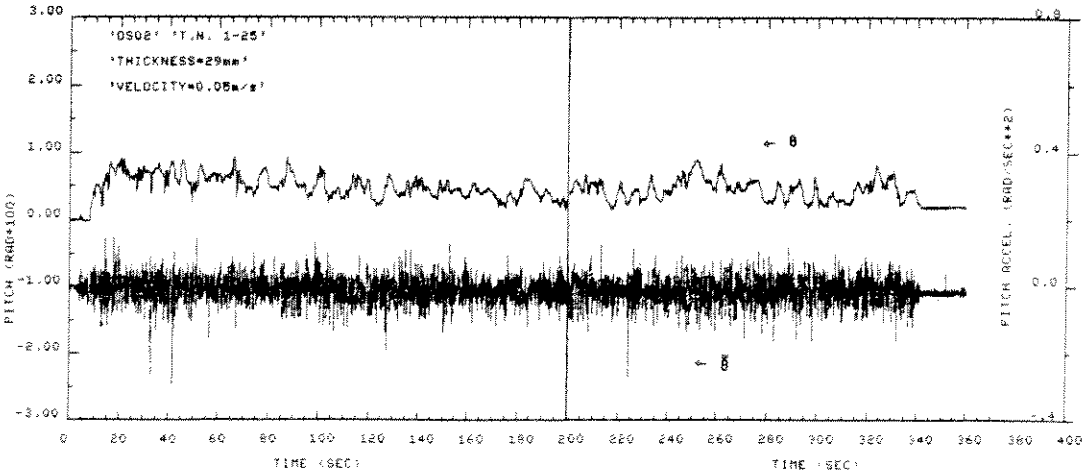
'DS02' 'T.N. 1-25'
'THICKNESS=29mm'
'VELOCITY=0.05m/s'
PITCH (RAD*100)
3.00
2.00
1.00
0.00
-1.00
-2.00
-3.00
PITCH ACCEL. (RAD/SEC**2)
0.8
0.4
0.0
θ
θ
0 20 40 60 80 100 120 140 160 180 200 220 240 260 280 300 320 340 360 380 400
TIME (SEC)
TIME (SEC)

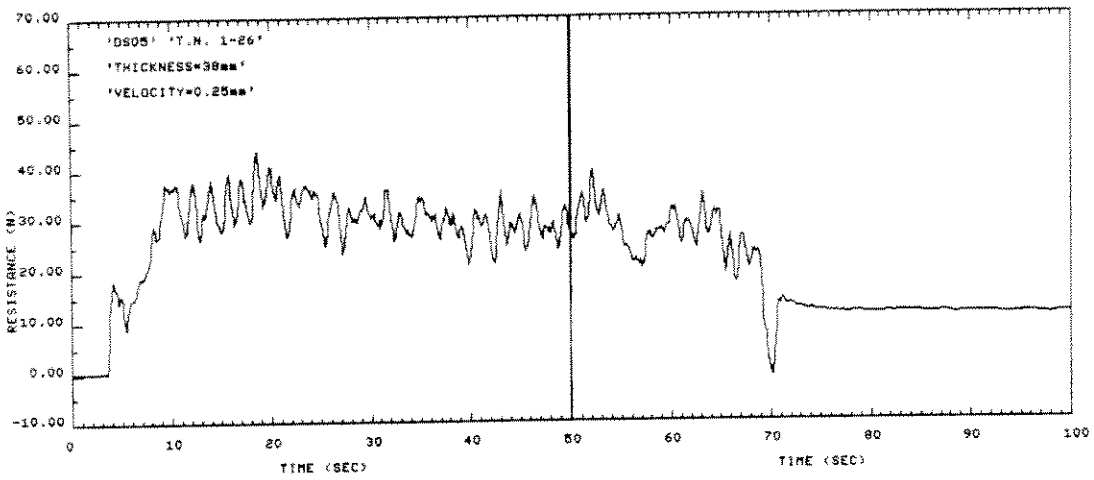
'DS05' 'T.N. 1-26'
'THICKNESS=38mm'
'VELOCITY=0.25mm'
RESISTANCE (N)
TIME (SEC)

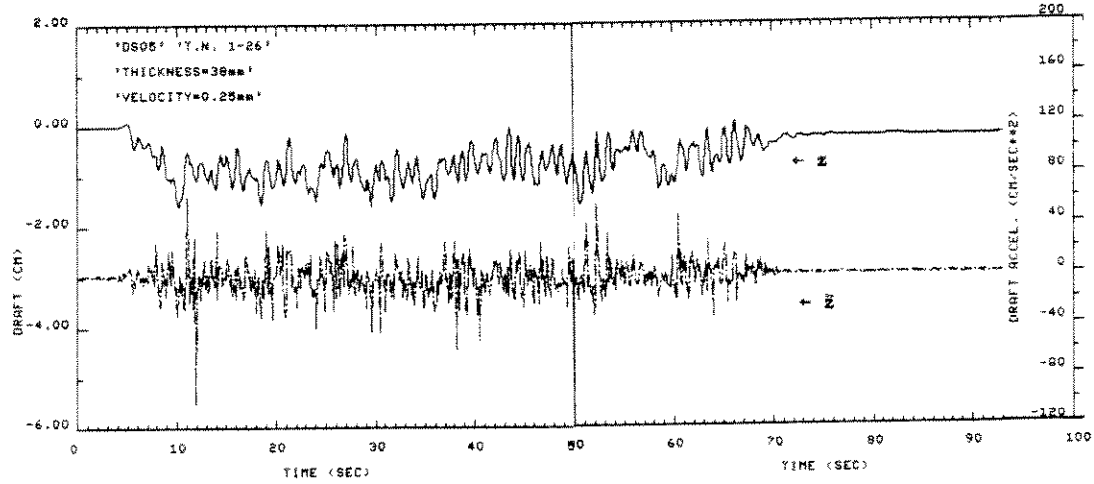
'DS05' 'T.N. 1-26'
'THICKNESS=38mm'
'VELOCITY=0.25mm'
DRAFT (CM)
DRAFT ACCEL. (CM/SEC**2)
TIME (SEC)

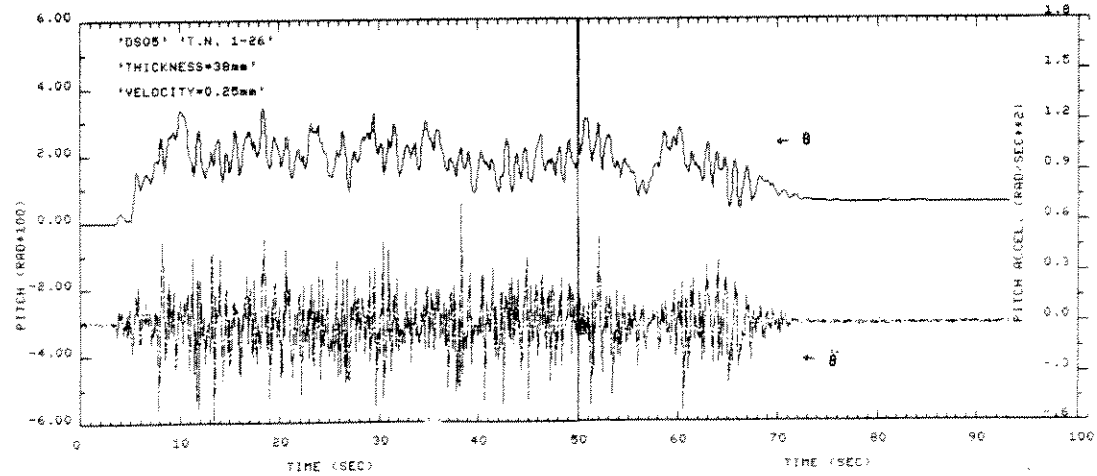
'DS05' 'T.N. 1-26'
'THICKNESS=38mm'
'VELOCITY=0.25mm'
PITCH (RAD*100)
PITCH ACCEL. (RAD/SEC**2)
TIME (SEC)

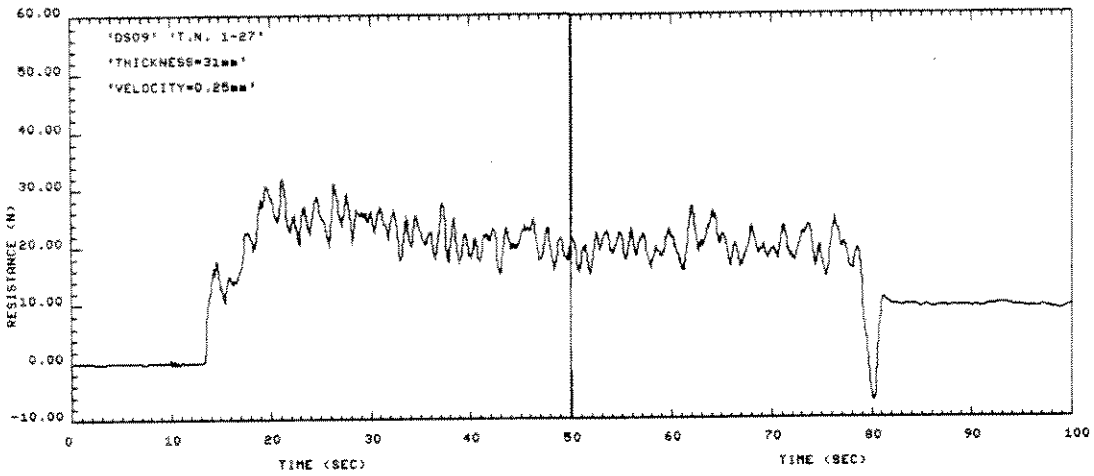
'DS09' 'T.N. 1-27'
'THICKNESS=31mm'
'VELOCITY=0.25mm'
RESISTANCE (N)
TIME (SEC)

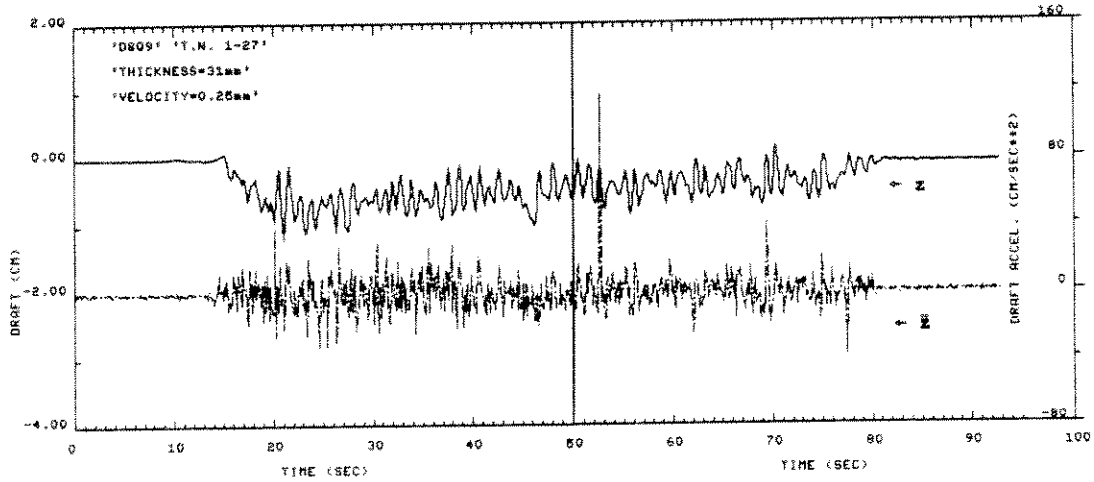
'DS09' 'T.N. 1-27'
'THICKNESS=31mm'
'VELOCITY=0.25mm'
DRAFT (CM)
DRAFT ACCEL. (CM/SEC**2)
← Z
← Z̈
TIME (SEC)

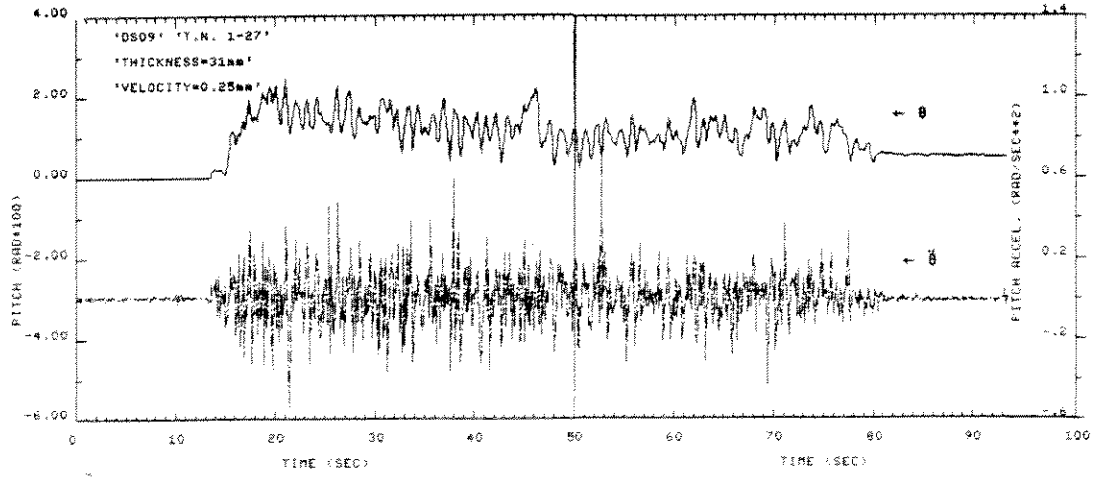
'DS09' 'T.N. 1-27'
'THICKNESS=31mm'
'VELOCITY=0.25mm'
PITCH (RAD*100)
PITCH ACCEL. (RAD/SEC**2)
← θ
← θ̈
TIME (SEC)

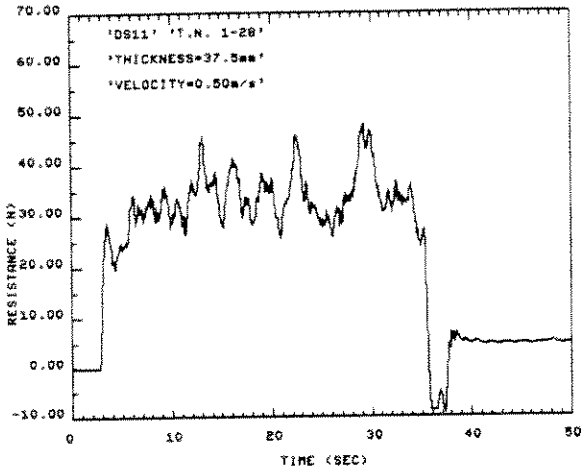
'DS11' 'T.N. 1-28'
'THICKNESS=37.5mm'
'VELOCITY=0.50m/s'
RESISTANCE (N)
TIME (SEC)

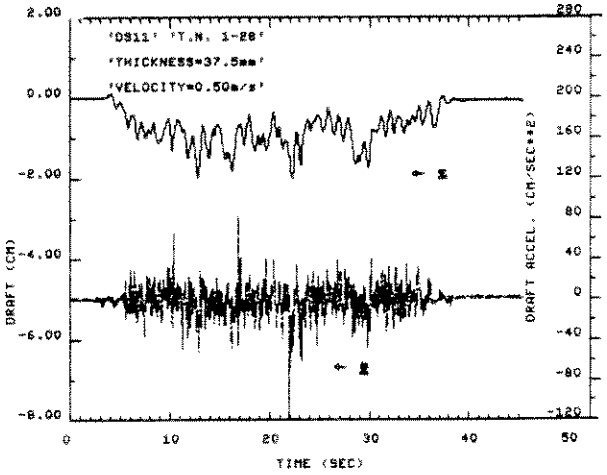
'DS11' 'T.N. 1-28'
'THICKNESS=37.5mm'
'VELOCITY=0.50m/s'
DRAFT (CM)
DRAFT ACCEL. (CM/SEC**2)
TIME (SEC)

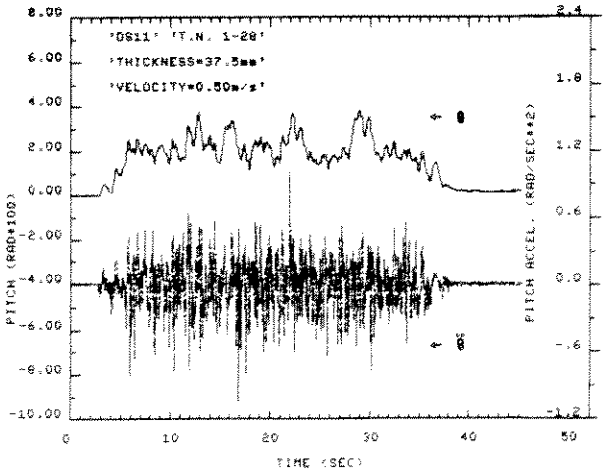
'DS11' 'T.N. 1-28'
'THICKNESS=37.5mm'
'VELOCITY=0.50m/s'
PITCH (RAD*10)
PITCH ACCEL. (RAD/SEC**2)
TIME (SEC)

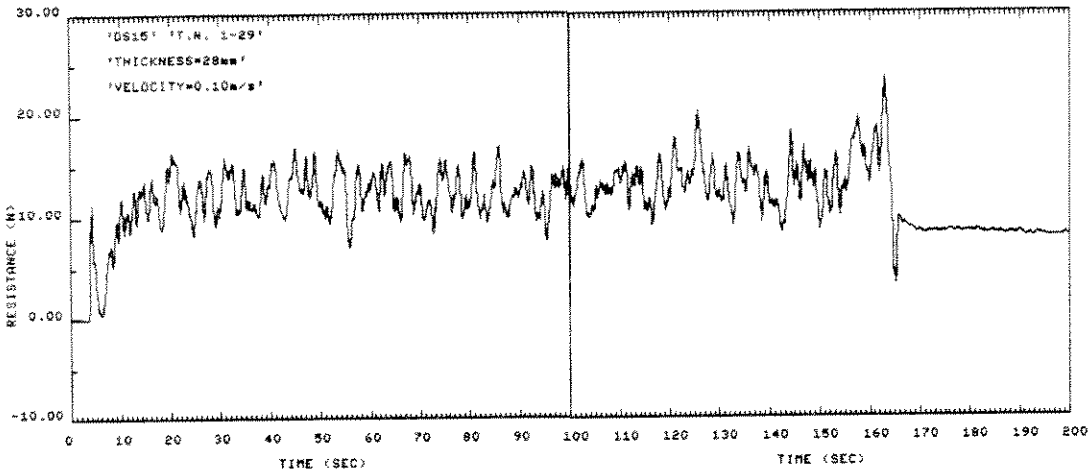
'DS15' 'T.N. 1-29'
'THICKNESS=28mm'
'VELOCITY=0.10m/s'
RESISTANCE (N)
30.00
20.00
10.00
0.00
-10.00
0 10 20 30 40 50 60 70 80 90 100 110 120 130 140 150 160 170 180 190 200
TIME (SEC)
TIME (SEC)

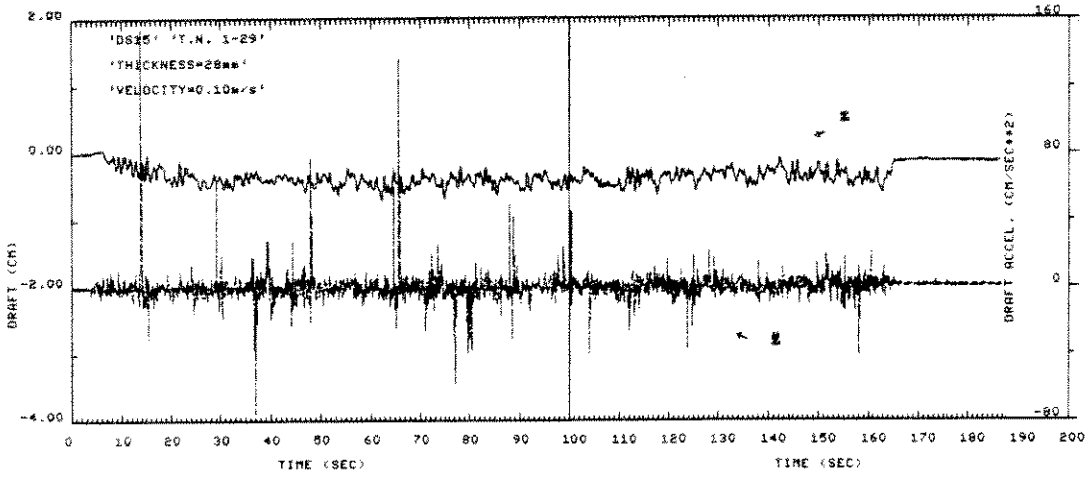
'DS15' 'T.N. 1-29'
'THICKNESS=28mm'
'VELOCITY=0.10m/s'
DRAFT (CM)
2.00
0.00
-2.00
-4.00
DRAFT ACCEL. (CM/SEC**2)
160
80
0
-80
0 10 20 30 40 50 60 70 80 90 100 110 120 130 140 150 160 170 180 190 200
TIME (SEC)
TIME (SEC)

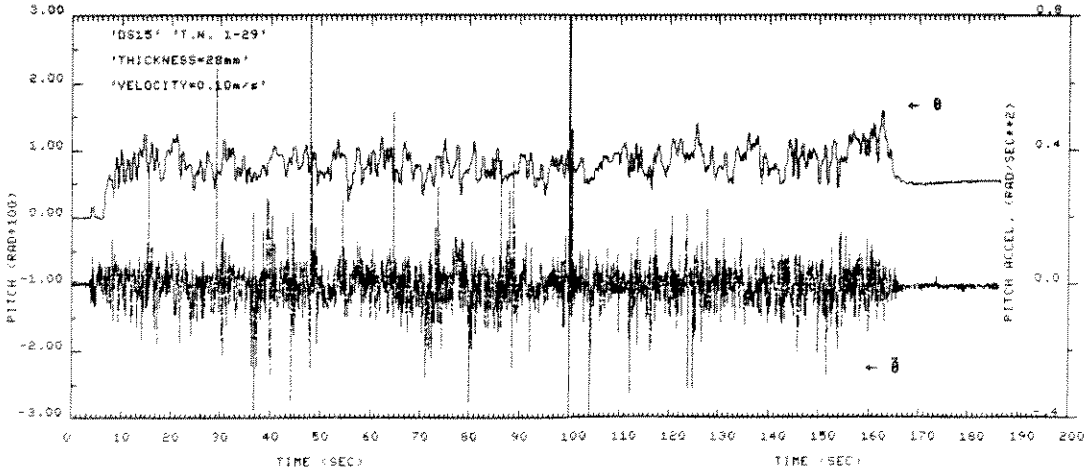
'DS15' 'T.N. 1-29'
'THICKNESS=28mm'
'VELOCITY=0.10m/s'
PITCH (RAD*100)
3.00
2.00
1.00
0.00
-1.00
-2.00
-3.00
PITCH ACCEL. (RAD/SEC**2)
0.8
0.4
0.0
-.4
0 10 20 30 40 50 60 70 80 90 100 110 120 130 140 150 160 170 180 190 200
TIME (SEC)
TIME (SEC)

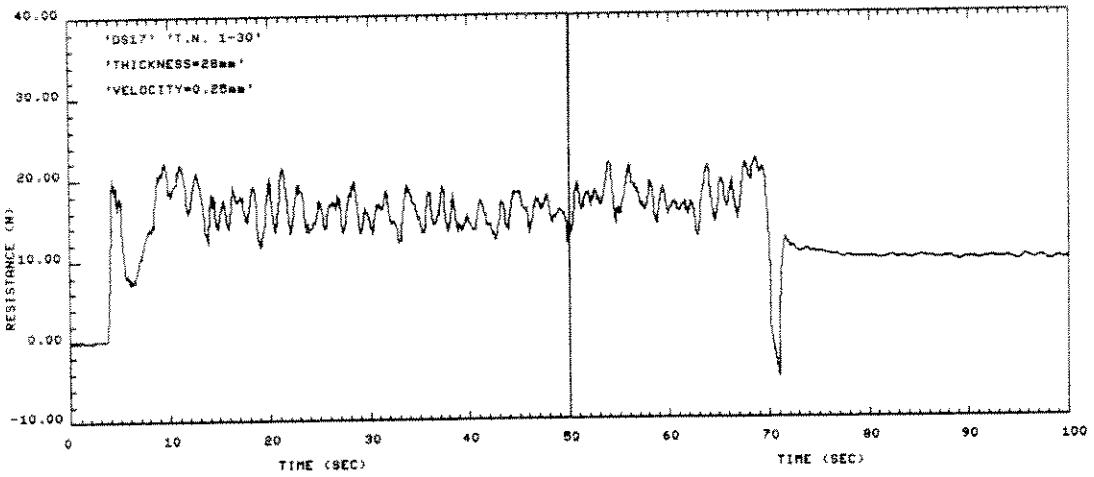
'DS17' 'T.N. 1-30'
'THICKNESS=28mm'
'VELOCITY=0.25mm'
RESISTANCE (N)
40.00
30.00
20.00
10.00
0.00
-10.00
0
10
20
30
40
50
60
70
80
90
100
TIME (SEC)
TIME (SEC)

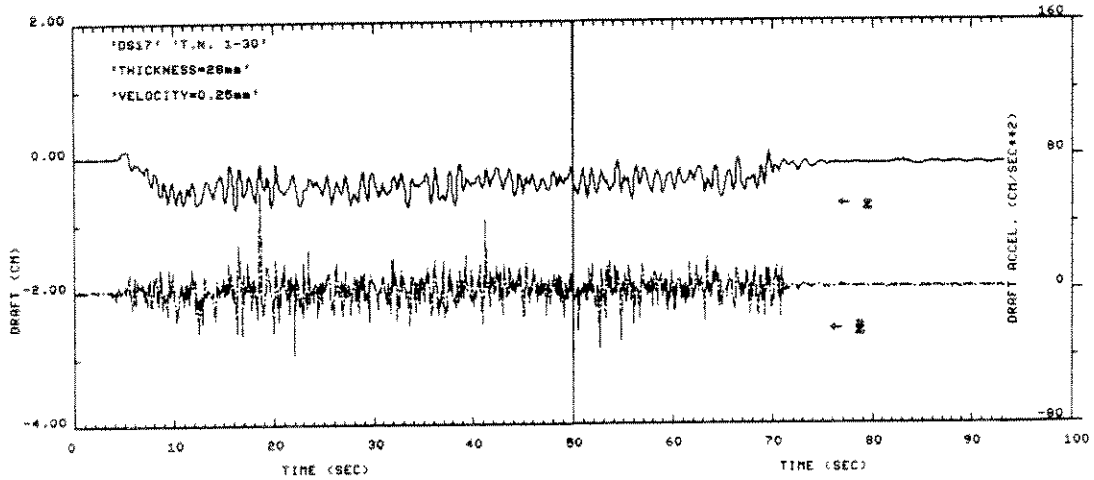
'DS17' 'T.N. 1-30'
'THICKNESS=28mm'
'VELOCITY=0.25mm'
DRAFT (CM)
2.00
0.00
-2.00
-4.00
DRAFT ACCEL. (CM/SEC**2)
160
80
0
-80
← Z
← Z̈
0
10
20
30
40
50
60
70
80
90
100
TIME (SEC)
TIME (SEC)

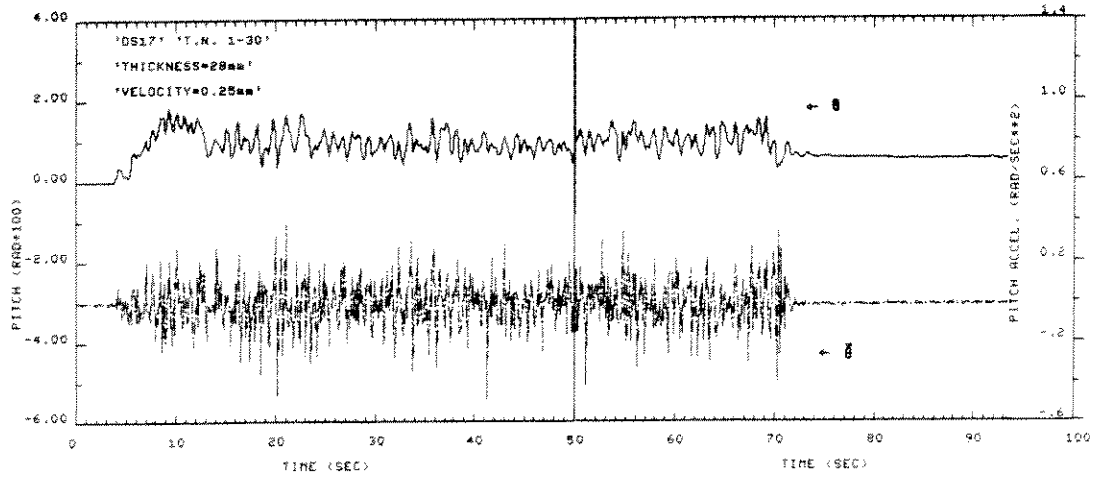
'DS17' 'T.N. 1-30'
'THICKNESS=28mm'
'VELOCITY=0.25mm'
PITCH (RAD*100)
4.00
2.00
0.00
-2.00
-4.00
-6.00
PITCH ACCEL. (RAD/SEC**2)
1.4
1.0
0.6
0.2
-.2
-.6
← θ
← θ̈
0
10
20
30
40
50
60
70
80
90
100
TIME (SEC)
TIME (SEC)

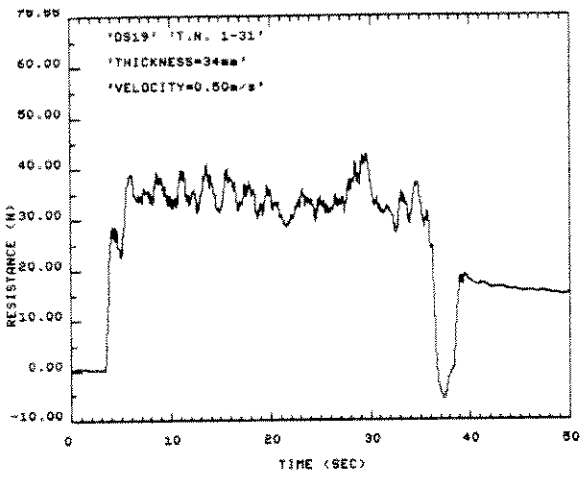
'DS19' 'T.N. 1-31'
'THICKNESS=34mm'
'VELOCITY=0.50m/s'
RESISTANCE (N)
TIME (SEC)

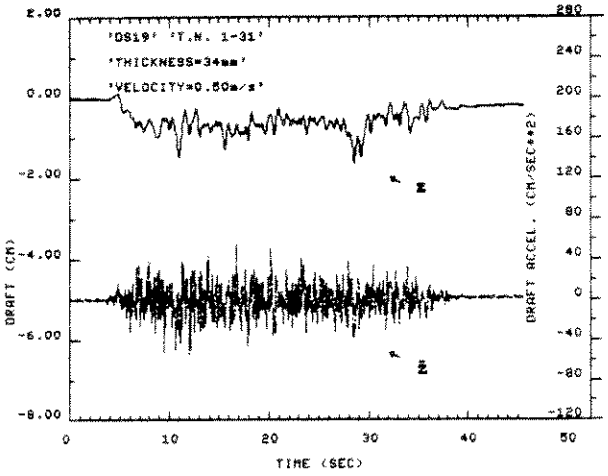
'DS19' 'T.N. 1-31'
'THICKNESS=34mm'
'VELOCITY=0.50m/s'
DRAFT (CM)
DRAFT ACCEL. (CM/SEC**2)
TIME (SEC)

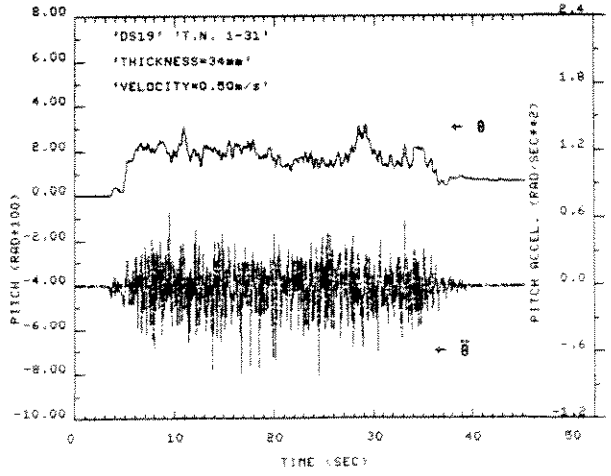
'DS19' 'T.N. 1-31'
'THICKNESS=34mm'
'VELOCITY=0.50m/s'
PITCH (RAD*100)
PITCH ACCEL. (RAD/SEC**2)
TIME (SEC)

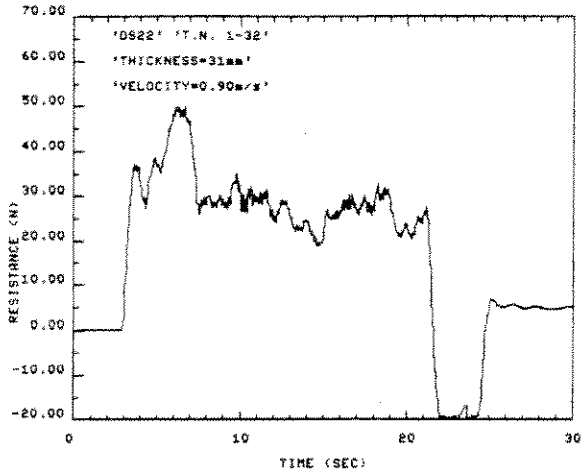
'DS22' 'T.N. 1-32'
'THICKNESS=31mm'
'VELOCITY=0.90m/s'
RESISTANCE (N)
70.00
60.00
50.00
40.00
30.00
20.00
10.00
0.00
-10.00
-20.00
0
10
20
30
TIME (SEC)

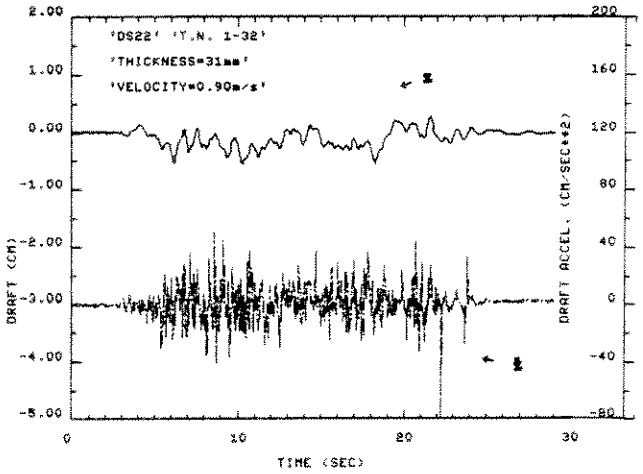
'DS22' 'T.N. 1-32'
'THICKNESS=31mm'
'VELOCITY=0.90m/s'
Z
Z
DRAFT (CM)
DRAFT ACCEL. (CM/SEC**2)
2.00
1.00
0.00
-1.00
-2.00
-3.00
-4.00
-5.00
200
160
120
80
40
0
-40
-80
0
10
20
30
TIME (SEC)

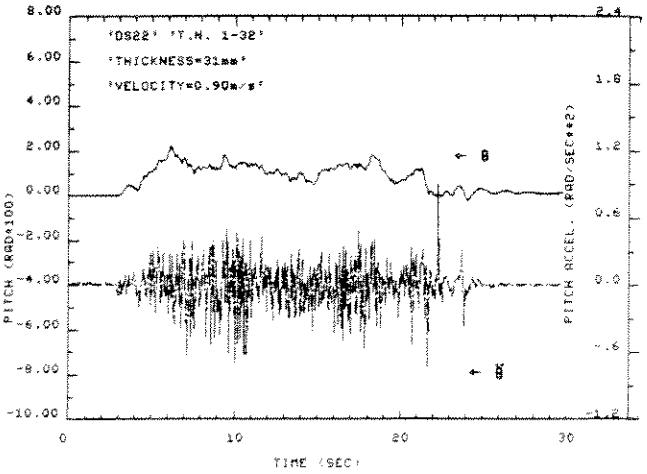
'DS22' 'T.N. 1-32'
'THICKNESS=31mm'
'VELOCITY=0.90m/s'
θ
θ
PITCH (RAD*100)
PITCH ACCEL. (RAD/SEC**2)
8.00
6.00
4.00
2.00
0.00
-2.00
-4.00
-6.00
-8.00
-10.00
2.4
1.8
1.2
0.6
0.0
-.6
-1.2
0
10
20
30
TIME (SEC)

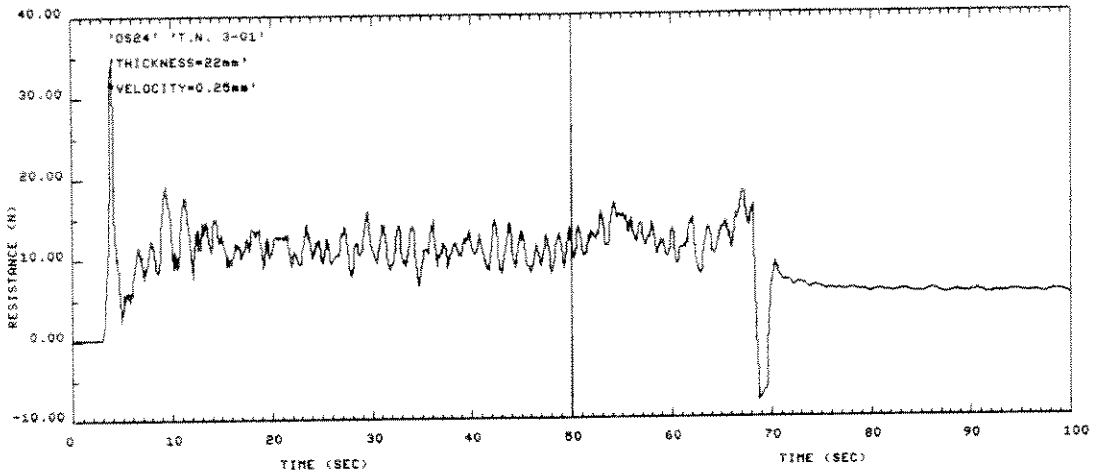
'OS24' 'T.N. 3-01'
'THICKNESS=22mm'
'VELOCITY=0.25mm'
RESISTANCE (N)
TIME (SEC)

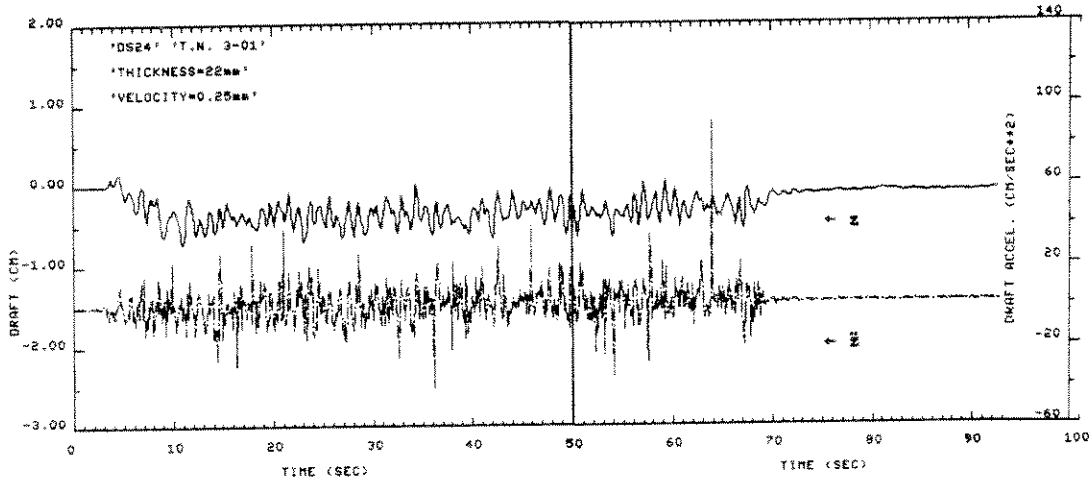
'OS24' 'T.N. 3-01'
'THICKNESS=22mm'
'VELOCITY=0.25mm'
DRAFT (CM)
DRAFT ACCEL. (CM/SEC**2)
← z
← z̈
TIME (SEC)

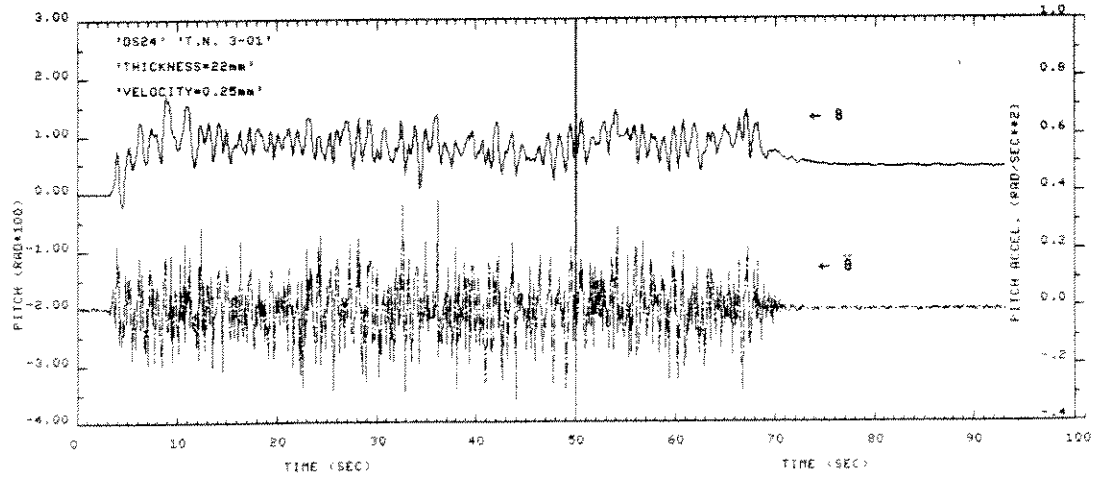
'OS24' 'T.N. 3-01'
'THICKNESS=22mm'
'VELOCITY=0.25mm'
PITCH (RAD*100)
PITCH ACCEL. (RAD/SEC**2)
← θ
← θ̈
TIME (SEC)

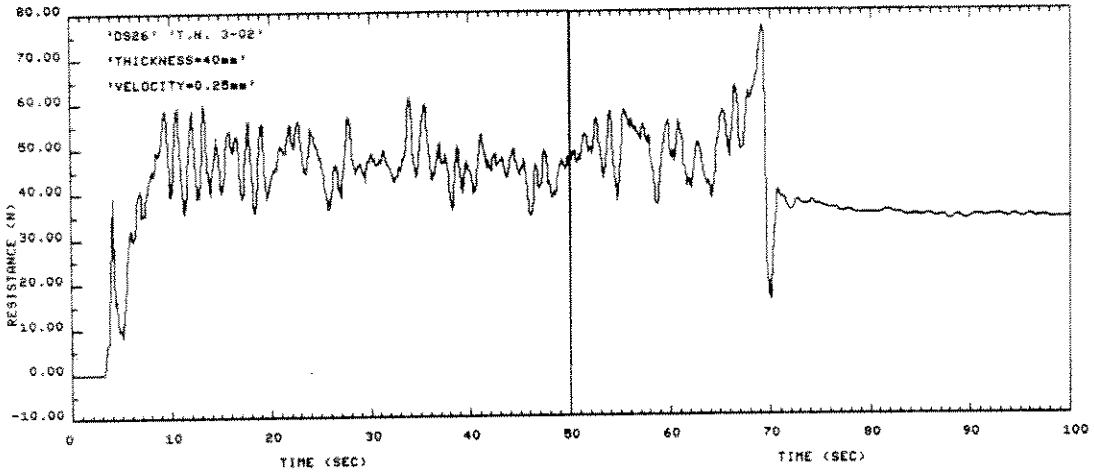
'DS26' 'T.N. 3-02'
'THICKNESS=40mm'
'VELOCITY=0.25mm'
RESISTANCE (N)
TIME (SEC)

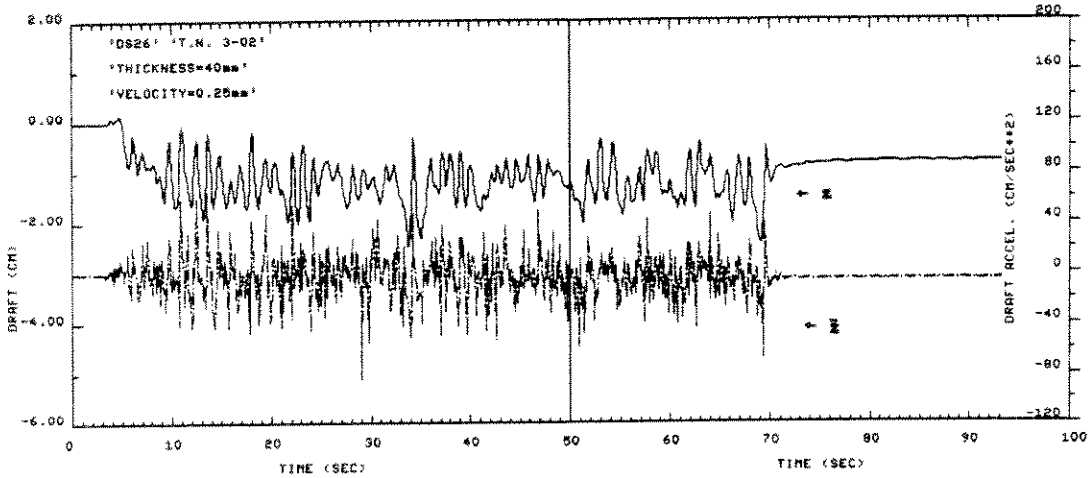
'DS26' 'T.N. 3-02'
'THICKNESS=40mm'
'VELOCITY=0.25mm'
DRAFT (CM)
DRAFT ACCEL. (CM/SEC**2)
TIME (SEC)

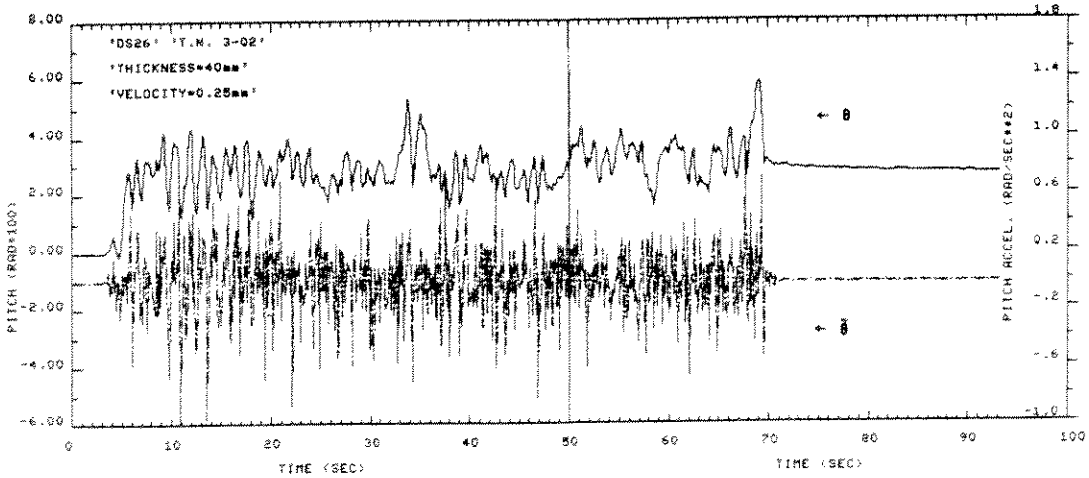
'DS26' 'T.N. 3-02'
'THICKNESS=40mm'
'VELOCITY=0.25mm'
PITCH (RAD*100)
PITCH ACCEL. (RAD/SEC**2)
TIME (SEC)

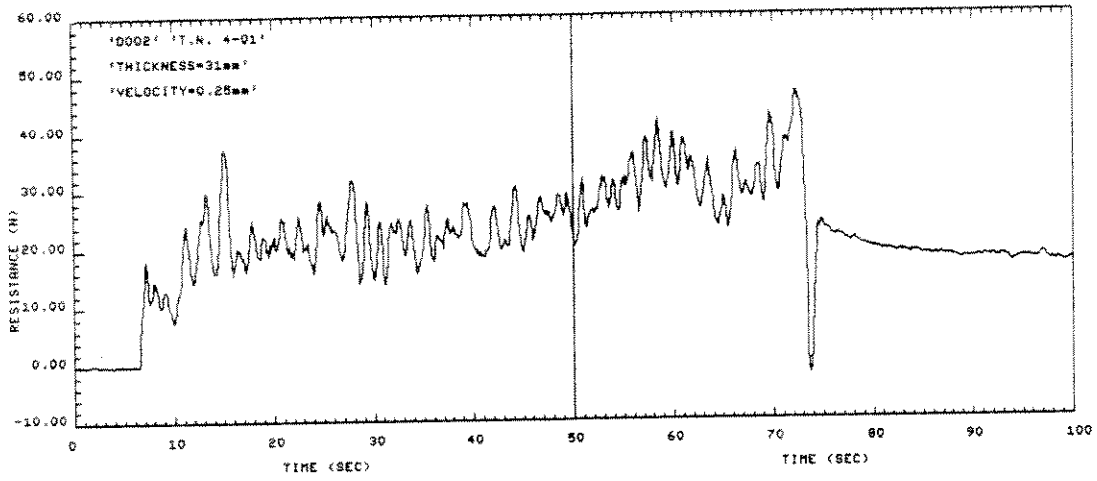
'D002' 'T.N. 4-01'
'THICKNESS=31mm'
'VELOCITY=0.25mm'
RESISTANCE (N)
TIME (SEC)

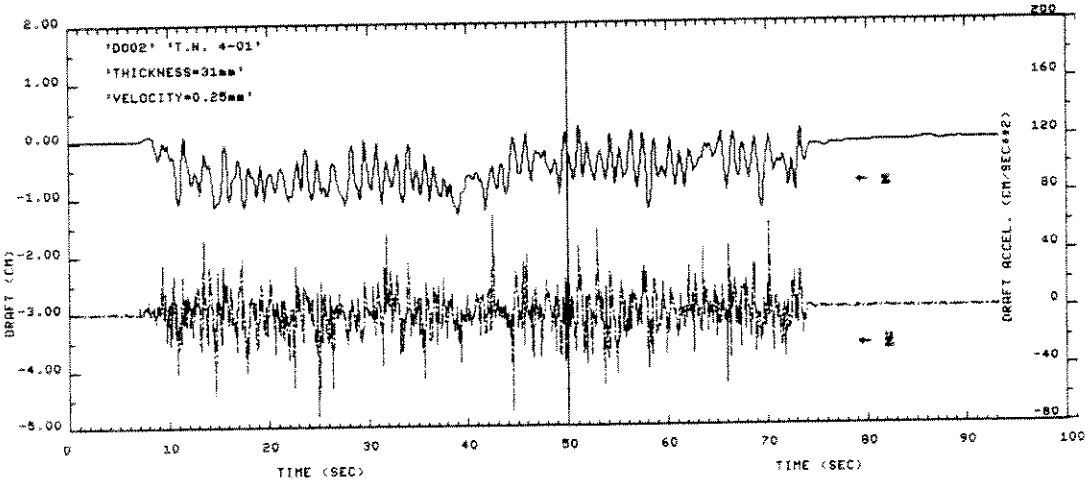
'D002' 'T.N. 4-01'
'THICKNESS=31mm'
'VELOCITY=0.25mm'
DRAFT (CM)
DRAFT ACCEL. (CM/SEC**2)
TIME (SEC)

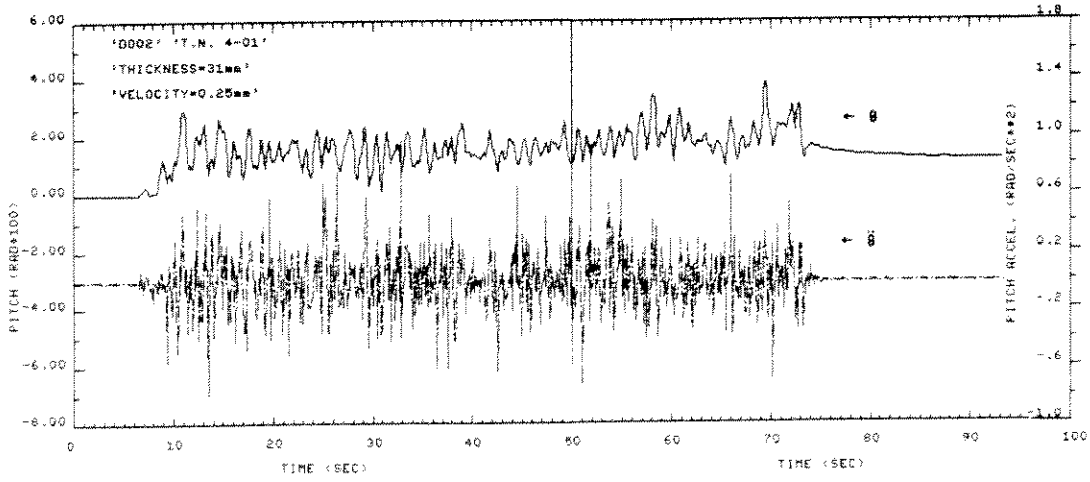
'D002' 'T.N. 4-01'
'THICKNESS=31mm'
'VELOCITY=0.25mm'
PITCH (RAD*100)
PITCH ACCEL. (RAD/SEC**2)
TIME (SEC)

APPENDIX B

TIME SERIES: FIXED HULL

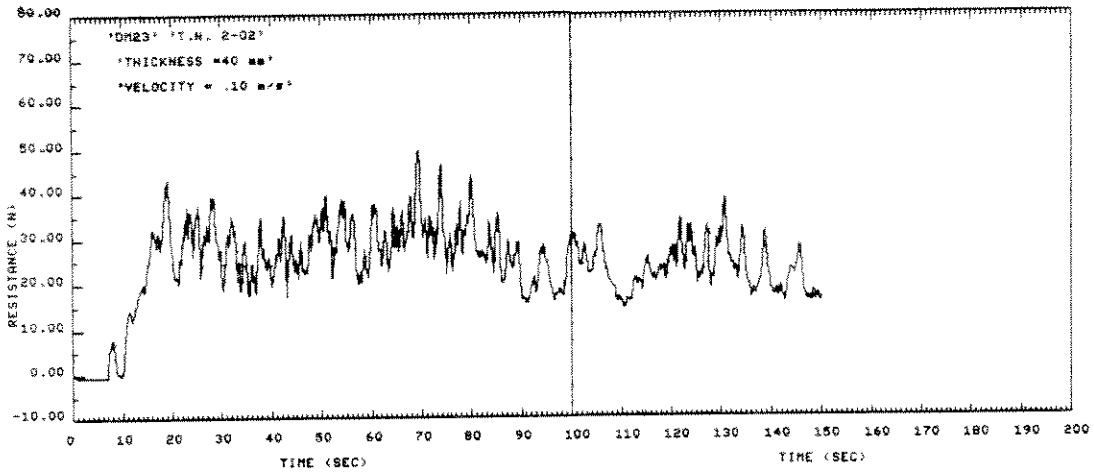
'DM23' 'T.N. 2-02'
'THICKNESS =40 mm'
'VELOCITY = .10 m/s'
RESISTANCE (N)
TIME (SEC)

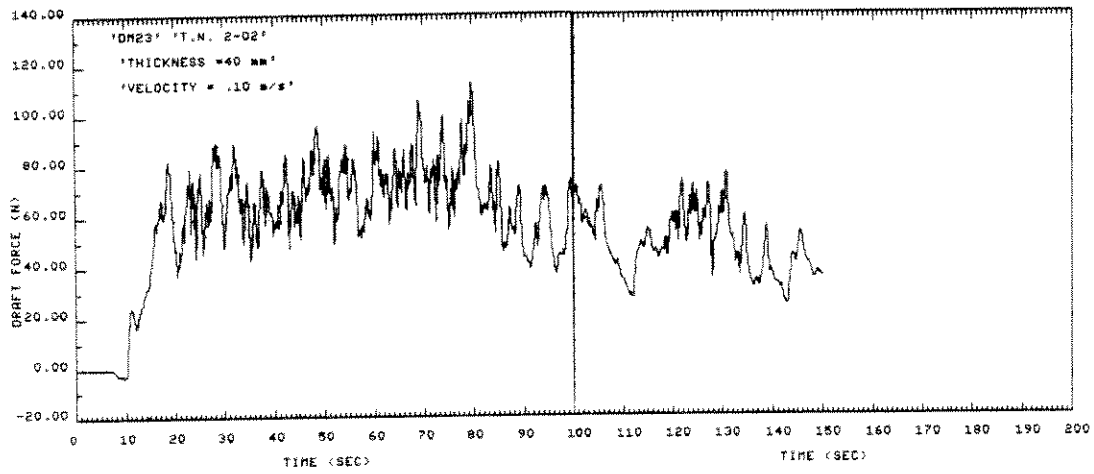
'DM23' 'T.N. 2-02'
'THICKNESS =40 mm'
'VELOCITY = .10 m/s'
DRAFT FORCE (N)
TIME (SEC)

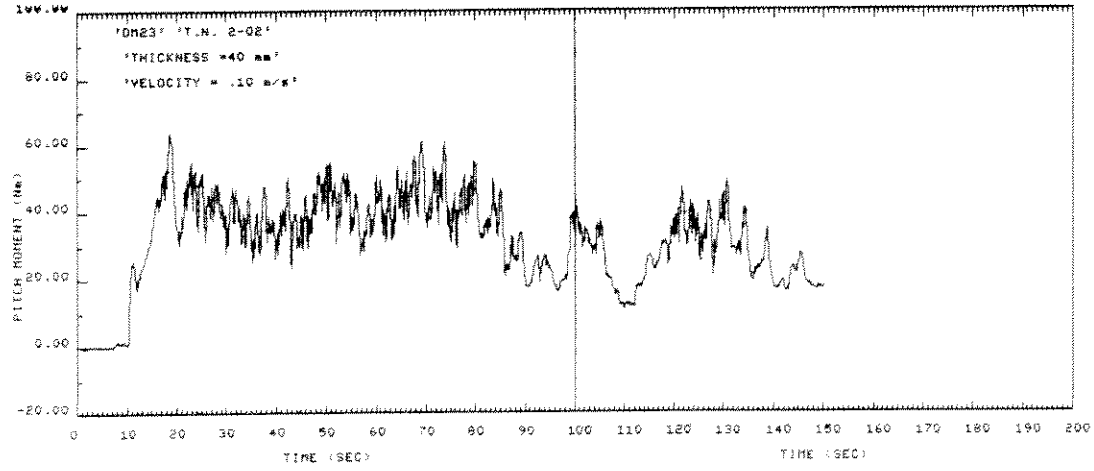
'DM23' 'T.N. 2-02'
'THICKNESS =40 mm'
'VELOCITY = .10 m/s'
PITCH MOMENT (Nm)
TIME (SEC)

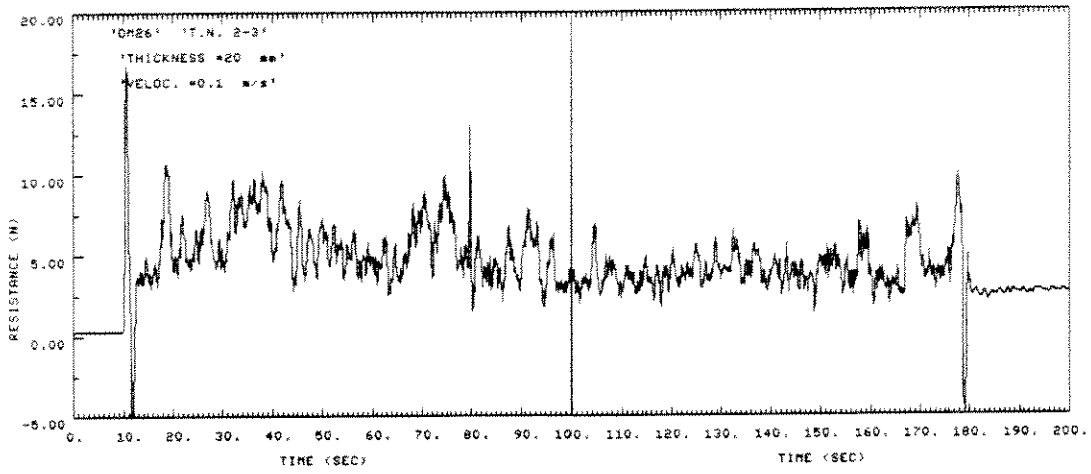
'DM26' 'T.N. 2-3'
'THICKNESS =20 mm'
'VELOC. =0.1 m/s'
RESISTANCE (N)
20.00
15.00
10.00
5.00
0.00
-5.00
0. 10. 20. 30. 40. 50. 60. 70. 80. 90. 100. 110. 120. 130. 140. 150. 160. 170. 180. 190. 200.
TIME (SEC)
TIME (SEC)

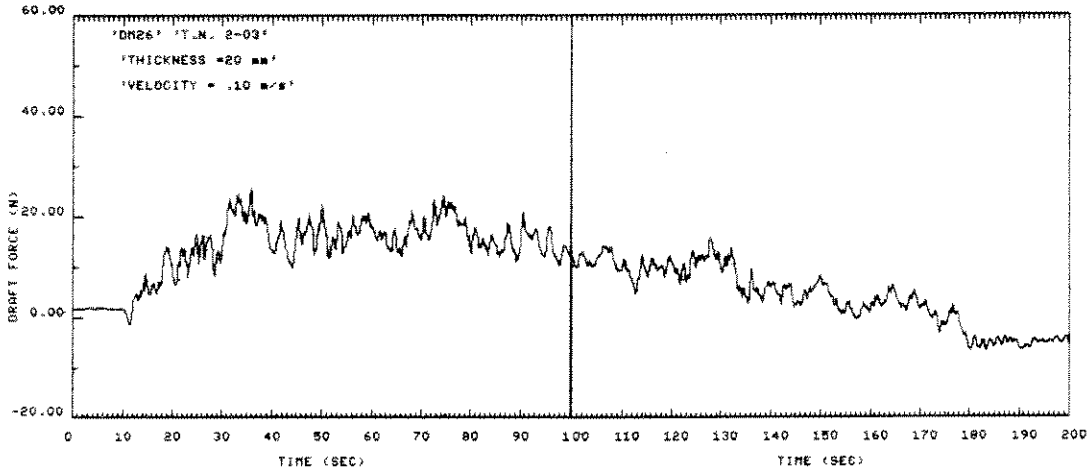
'DM26' 'T.N. 2-03'
'THICKNESS =20 mm'
'VELOCITY = .10 m/s'
DRAFT FORCE (N)
60.00
40.00
20.00
0.00
-20.00
0 10 20 30 40 50 60 70 80 90 100 110 120 130 140 150 160 170 180 190 200
TIME (SEC)
TIME (SEC)

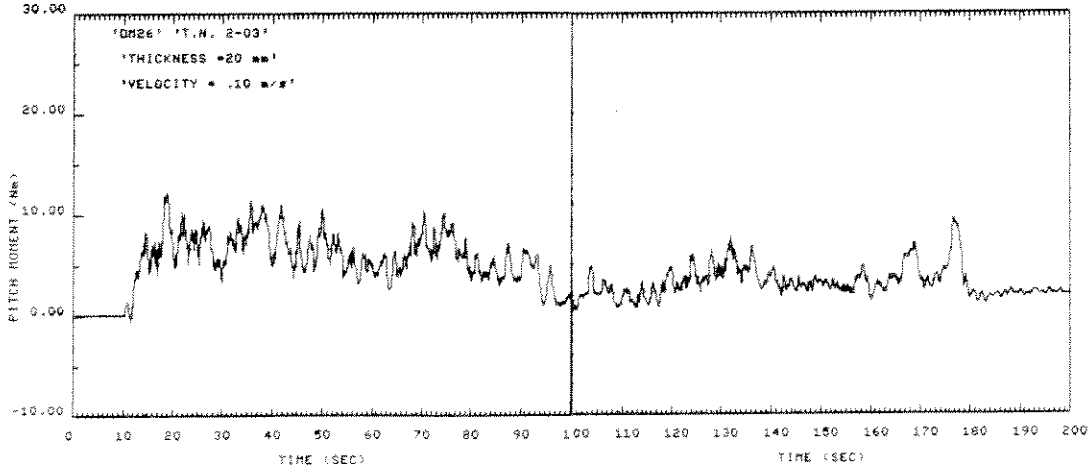
'DM26' 'T.N. 2-03'
'THICKNESS =20 mm'
'VELOCITY = .10 m/s'
PITCH MOMENT (Nm)
30.00
20.00
10.00
0.00
-10.00
0 10 20 30 40 50 60 70 80 90 100 110 120 130 140 150 160 170 180 190 200
TIME (SEC)
TIME (SEC)

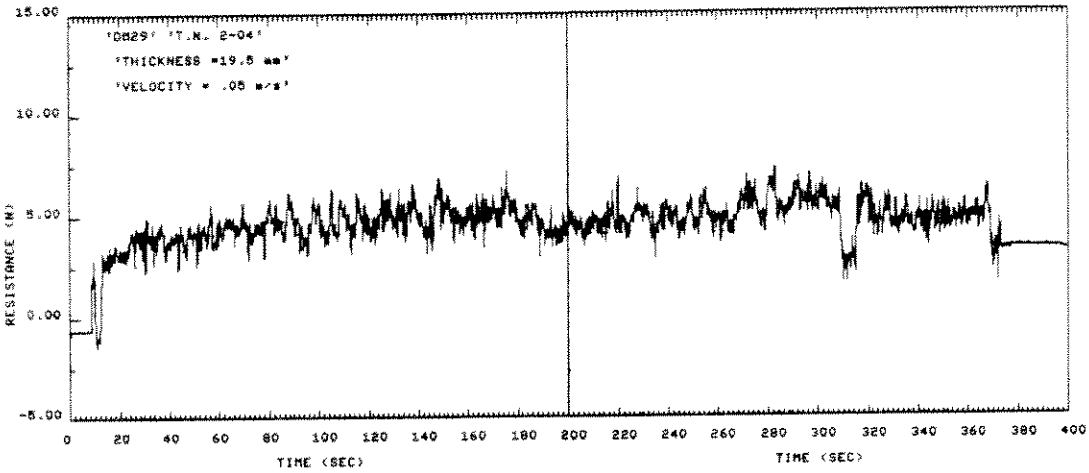
'0829' 'T.N. 2-04'
'THICKNESS =19.5 mm'
'VELOCITY = .05 m/s'
RESISTANCE (N)
15.00
10.00
5.00
0.00
-5.00
0 20 40 60 80 100 120 140 160 180 200 220 240 260 280 300 320 340 360 380 400
TIME (SEC)
TIME (SEC)

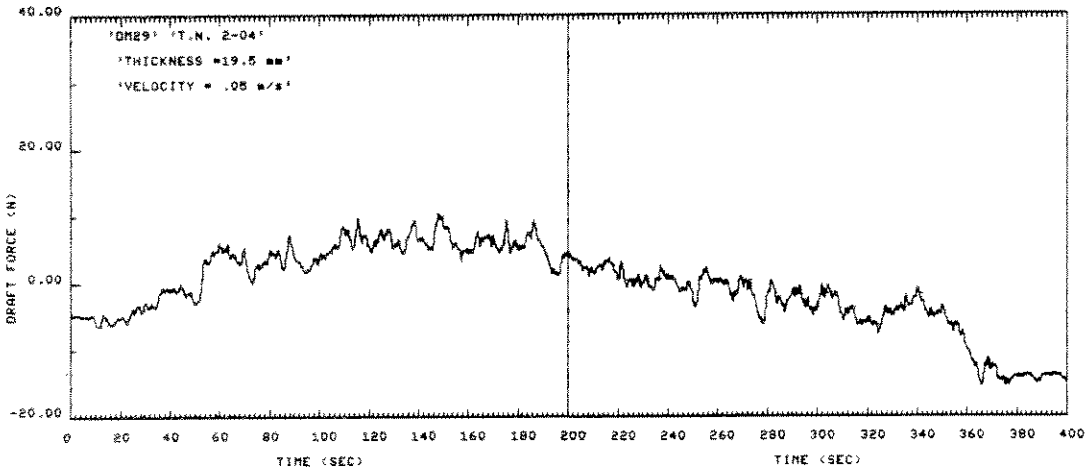
'0829' 'T.N. 2-04'
'THICKNESS =19.5 mm'
'VELOCITY = .05 m/s'
DRAFT FORCE (N)
40.00
20.00
0.00
-20.00
0 20 40 60 80 100 120 140 160 180 200 220 240 260 280 300 320 340 360 380 400
TIME (SEC)
TIME (SEC)

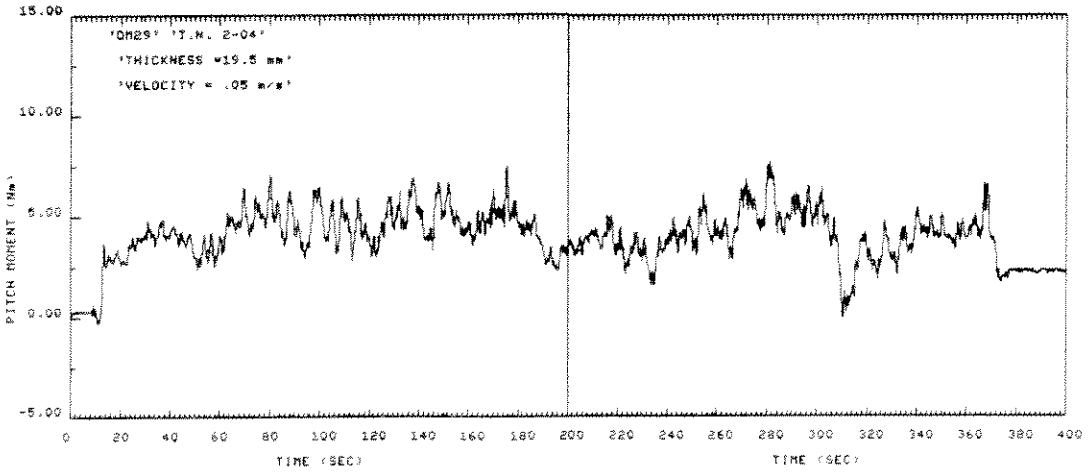
'0829' 'T.N. 2-04'
'THICKNESS =19.5 mm'
'VELOCITY = .05 m/s'
PITCH MOMENT (Nm)
15.00
10.00
5.00
0.00
-5.00
0 20 40 60 80 100 120 140 160 180 200 220 240 260 280 300 320 340 360 380 400
TIME (SEC)
TIME (SEC)

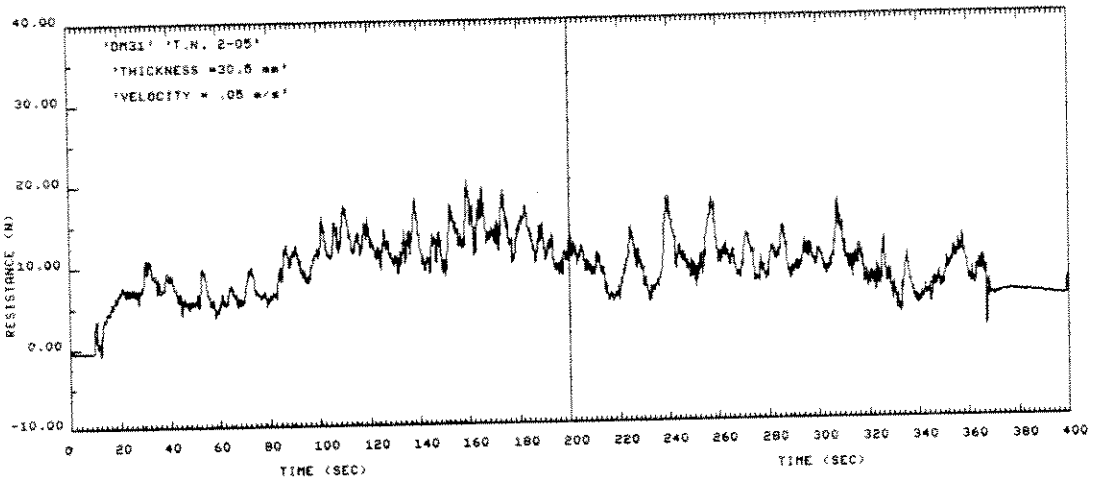
'DM31' 'T.N. 2-05'
'THICKNESS =30.5 mm'
'VELOCITY = .05 m/s'
RESISTANCE (N)
40.00
30.00
20.00
10.00
0.00
-10.00
0 20 40 60 80 100 120 140 160 180 200 220 240 260 280 300 320 340 360 380 400
TIME (SEC)
TIME (SEC)

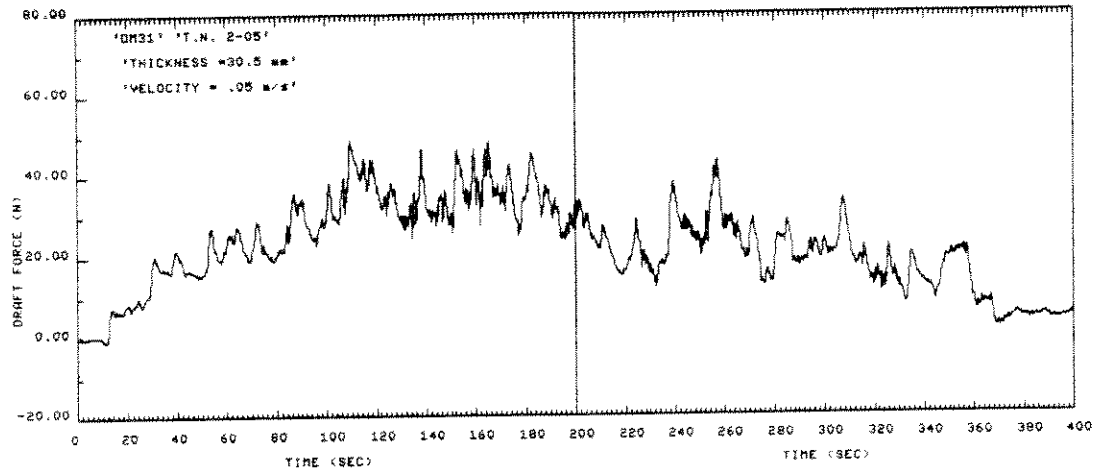
'DM31' 'T.N. 2-05'
'THICKNESS =30.5 mm'
'VELOCITY = .05 m/s'
DRAFT FORCE (N)
60.00
40.00
20.00
0.00
-20.00
0 20 40 60 80 100 120 140 160 180 200 220 240 260 280 300 320 340 360 380 400
TIME (SEC)
TIME (SEC)

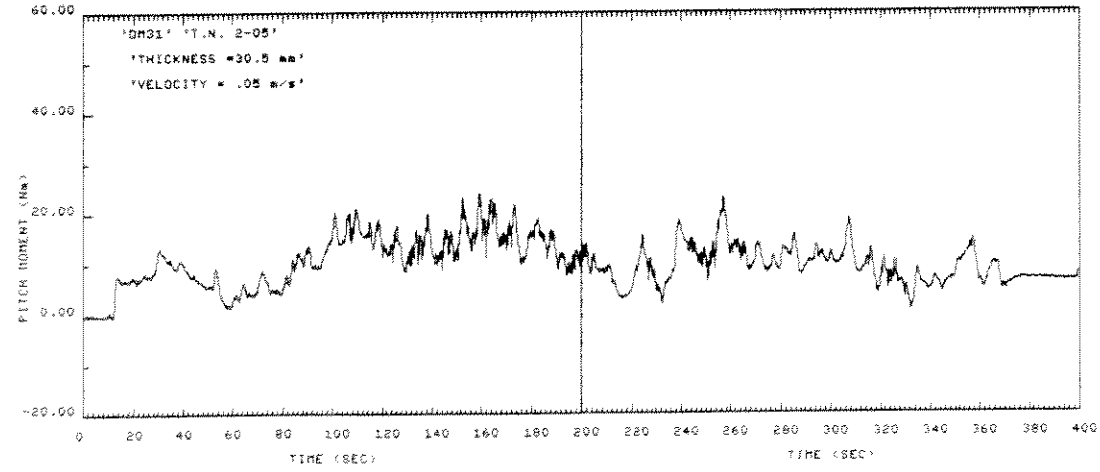
'DM31' 'T.N. 2-05'
'THICKNESS =30.5 mm'
'VELOCITY = .05 m/s'
PITCH MOMENT (Nm)
40.00
20.00
0.00
-20.00
0 20 40 60 80 100 120 140 160 180 200 220 240 260 280 300 320 340 360 380 400
TIME (SEC)
TIME (SEC)

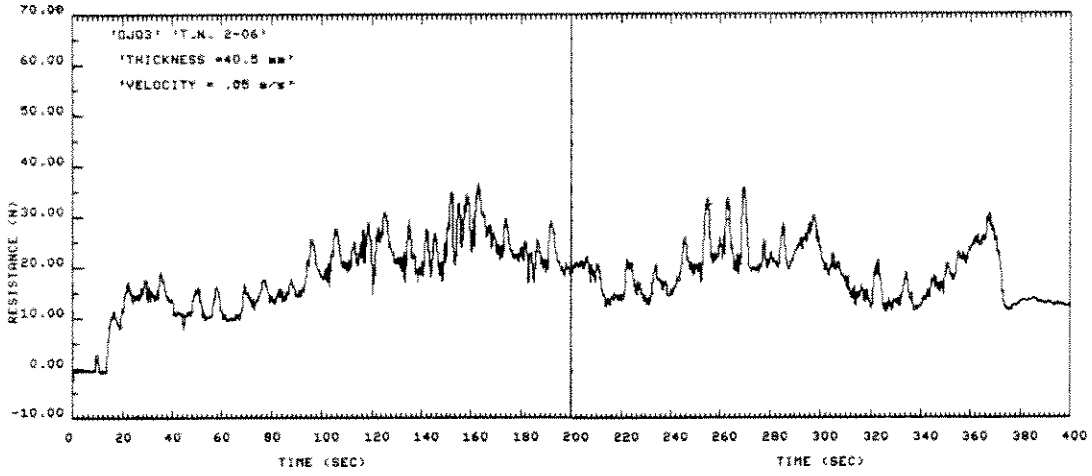
'DJ03' 'T.N. 2-06'
'THICKNESS =40.5 mm'
'VELOCITY = .05 m/s'
RESISTANCE (N)
70.00
60.00
50.00
40.00
30.00
20.00
10.00
0.00
-10.00
0 20 40 60 80 100 120 140 160 180 200 220 240 260 280 300 320 340 360 380 400
TIME (SEC)
TIME (SEC)

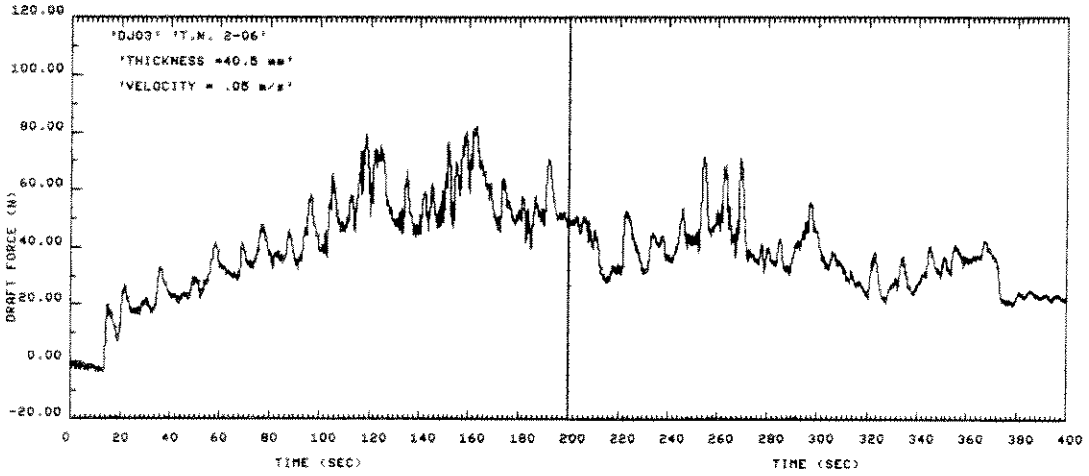
'DJ03' 'T.N. 2-06'
'THICKNESS =40.5 mm'
'VELOCITY = .05 m/s'
DRAFT FORCE (N)
120.00
100.00
80.00
60.00
40.00
20.00
0.00
-20.00
0 20 40 60 80 100 120 140 160 180 200 220 240 260 280 300 320 340 360 380 400
TIME (SEC)
TIME (SEC)

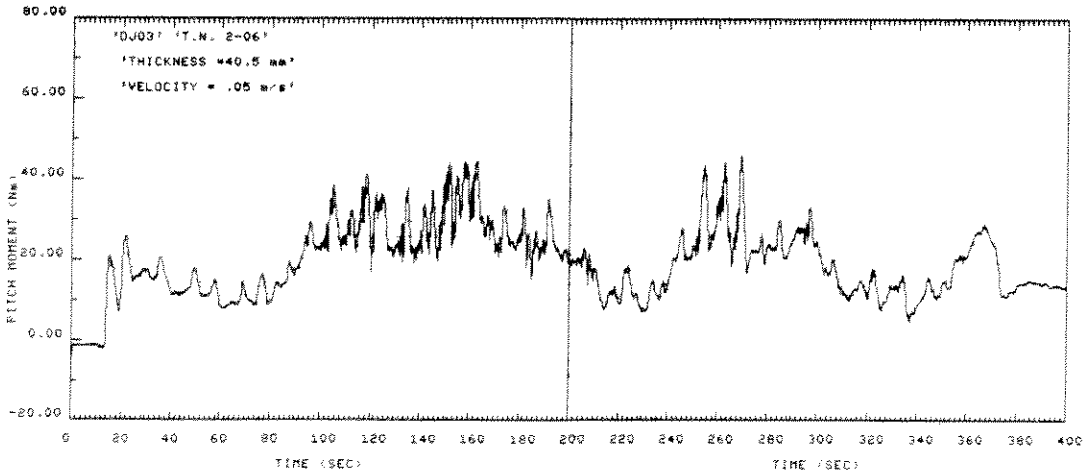
'DJ03' 'T.N. 2-06'
'THICKNESS =40.5 mm'
'VELOCITY = .05 m/s'
PITCH MOMENT (Nm)
80.00
60.00
40.00
20.00
0.00
-20.00
0 20 40 60 80 100 120 140 160 180 200 220 240 260 280 300 320 340 360 380 400
TIME (SEC)
TIME (SEC)

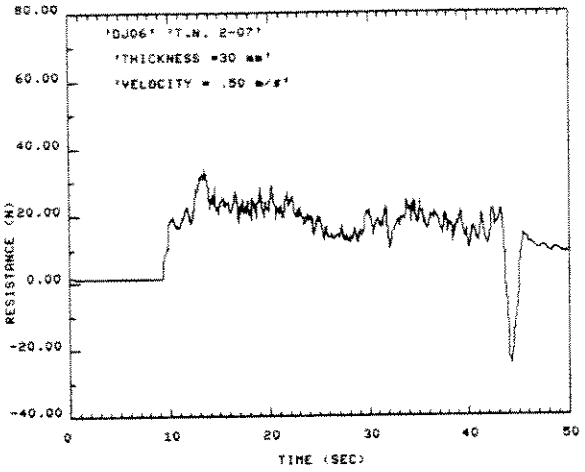
'DJ06' 'T.N. 2-07'
'THICKNESS =30 mm'
'VELOCITY = .50 m/s'
RESISTANCE (N)
80.00
60.00
40.00
20.00
0.00
-20.00
-40.00
0
10
20
30
40
50
TIME (SEC)

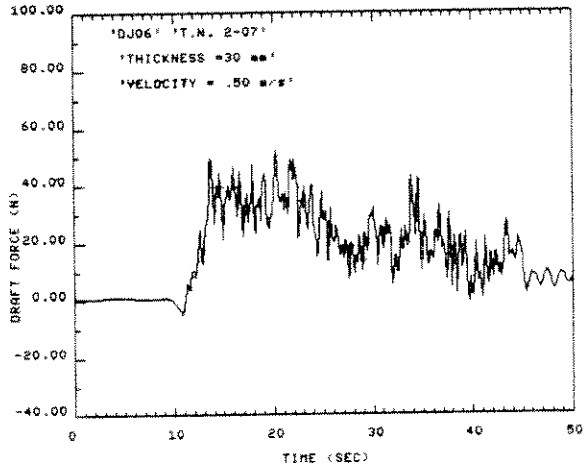
'DJ06' 'T.N. 2-07'
'THICKNESS =30 mm'
'VELOCITY = .50 m/s'
DRAFT FORCE (N)
100.00
80.00
60.00
40.00
20.00
0.00
-20.00
-40.00
0
10
20
30
40
50
TIME (SEC)

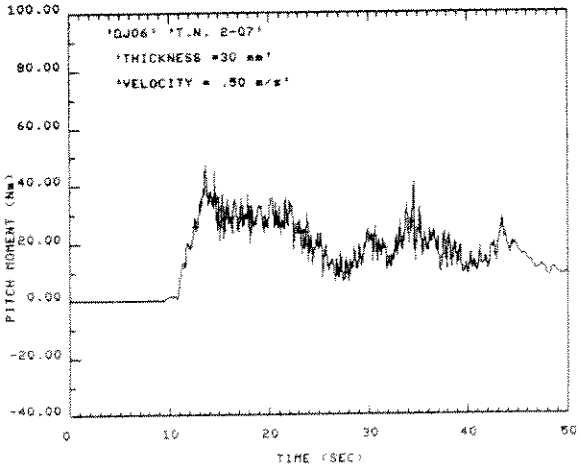
'DJ06' 'T.N. 2-07'
'THICKNESS =30 mm'
'VELOCITY = .50 m/s'
PITCH MOMENT (Nm)
100.00
80.00
60.00
40.00
20.00
0.00
-20.00
-40.00
0
10
20
30
40
50
TIME (SEC)

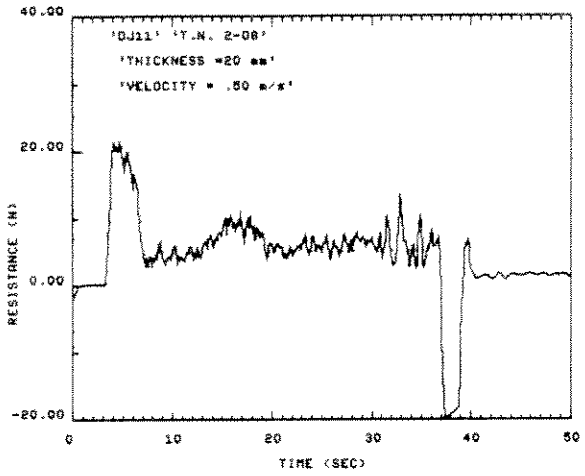
'DJ11' 'T.N. 2-08'
'THICKNESS =20 mm'
'VELOCITY = .50 m/s'
RESISTANCE (N)
40.00
20.00
0.00
-20.00
0
10
20
30
40
50
TIME (SEC)

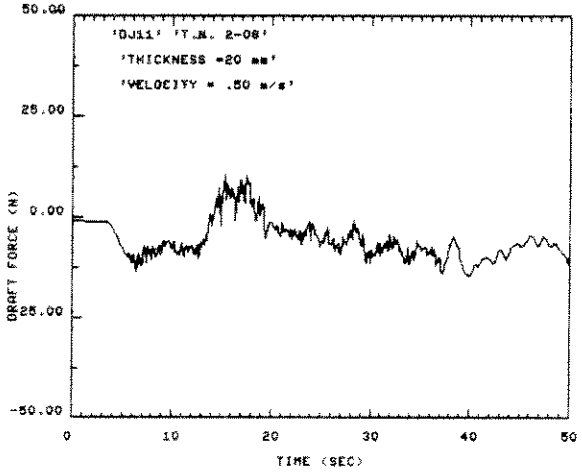
'DJ11' 'T.N. 2-08'
'THICKNESS =20 mm'
'VELOCITY = .50 m/s'
DRAFT FORCE (N)
50.00
25.00
0.00
-25.00
-50.00
0
10
20
30
40
50
TIME (SEC)

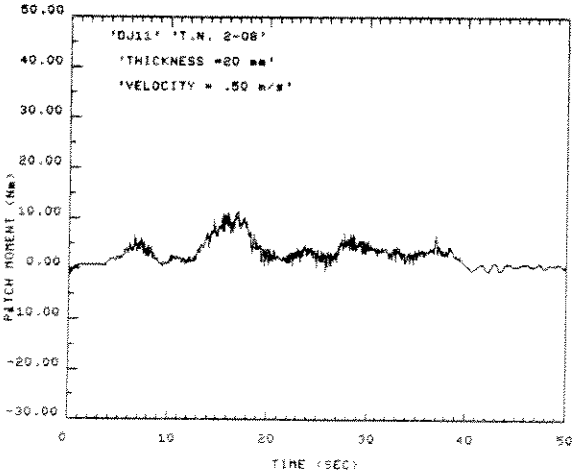
'DJ11' 'T.N. 2-08'
'THICKNESS =20 mm'
'VELOCITY = .50 m/s'
PITCH MOMENT (Nm)
50.00
40.00
30.00
20.00
10.00
0.00
-10.00
-20.00
-30.00
0
10
20
30
40
50
TIME (SEC)

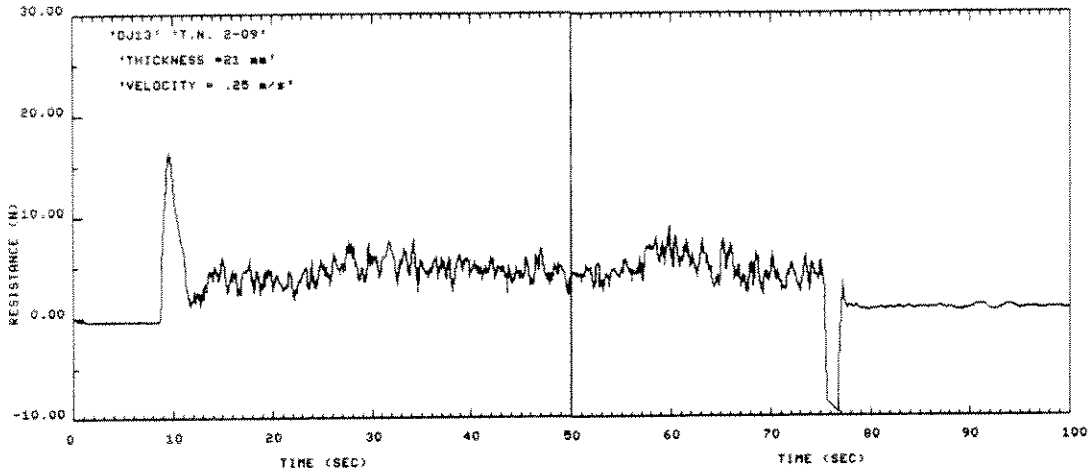
'DJ13' 'T.N. 2-09'
'THICKNESS =21 mm'
'VELOCITY = .25 m/s'
RESISTANCE (N)
30.00
20.00
10.00
0.00
-10.00
0
10
20
30
40
50
60
70
80
90
100
TIME (SEC)
TIME (SEC)

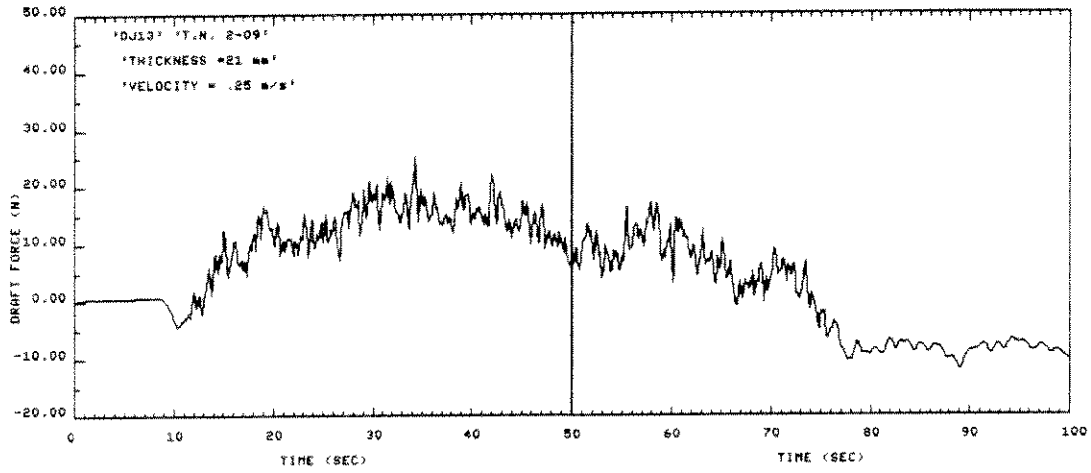
'DJ13' 'T.N. 2-09'
'THICKNESS =21 mm'
'VELOCITY = .25 m/s'
DRAFT FORCE (N)
50.00
40.00
30.00
20.00
10.00
0.00
-10.00
-20.00
0
10
20
30
40
50
60
70
80
90
100
TIME (SEC)
TIME (SEC)

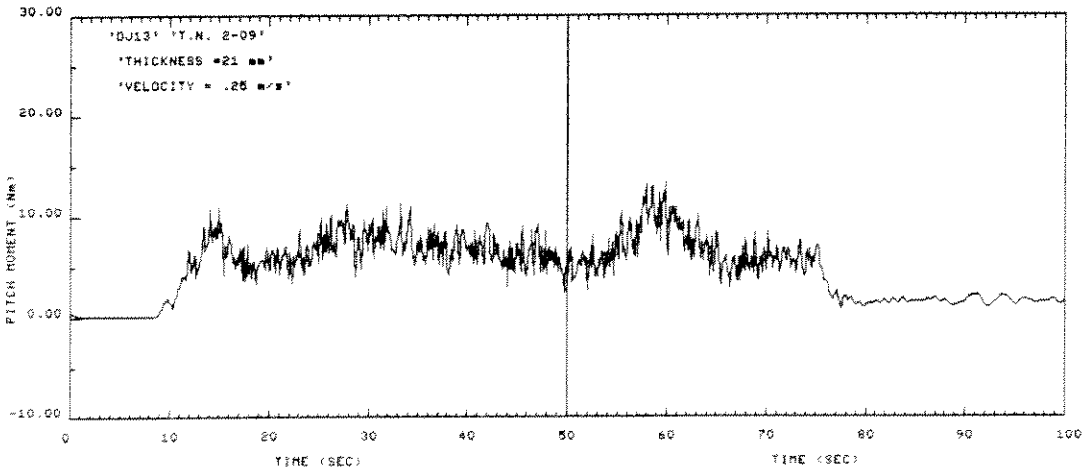
'DJ13' 'T.N. 2-09'
'THICKNESS =21 mm'
'VELOCITY = .25 m/s'
PITCH MOMENT (Nm)
30.00
20.00
10.00
0.00
-10.00
0
10
20
30
40
50
60
70
80
90
100
TIME (SEC)
TIME (SEC)

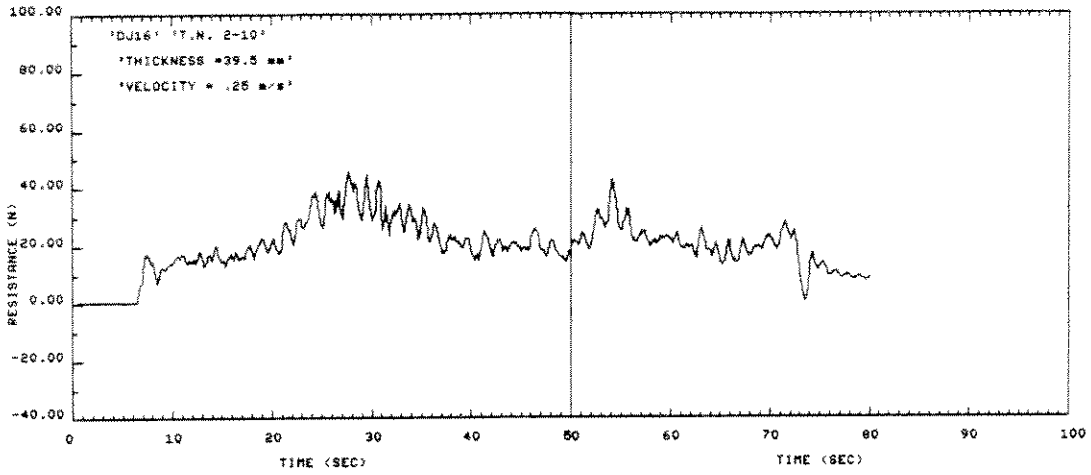
'DJ16' 'T.N. 2-10'
'THICKNESS =39.5 mm'
'VELOCITY = .25 m/s'
RESISTANCE (N)
100.00
80.00
60.00
40.00
20.00
0.00
-20.00
-40.00
0
10
20
30
40
50
60
70
80
90
100
TIME (SEC)
TIME (SEC)

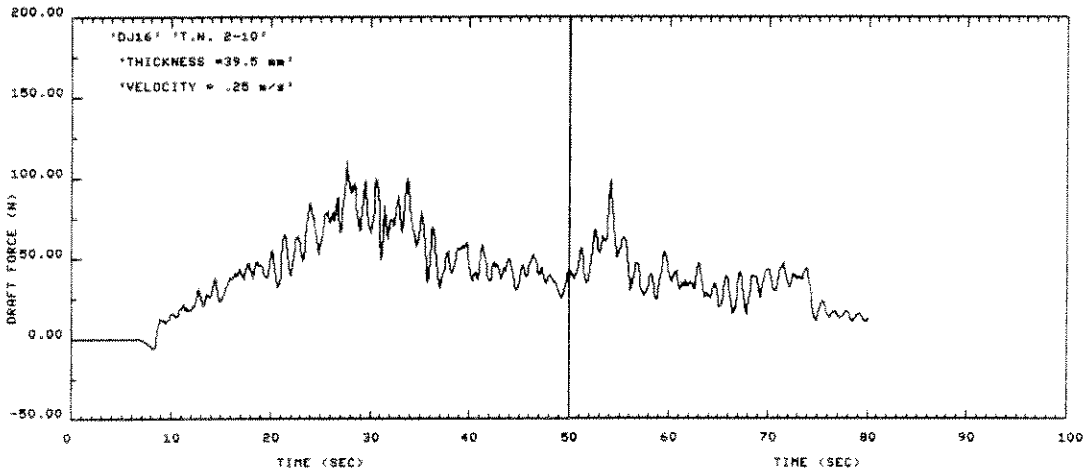
'DJ16' 'T.N. 2-10'
'THICKNESS =39.5 mm'
'VELOCITY = .25 m/s'
DRAFT FORCE (N)
200.00
150.00
100.00
50.00
0.00
-50.00
0
10
20
30
40
50
60
70
80
90
100
TIME (SEC)
TIME (SEC)

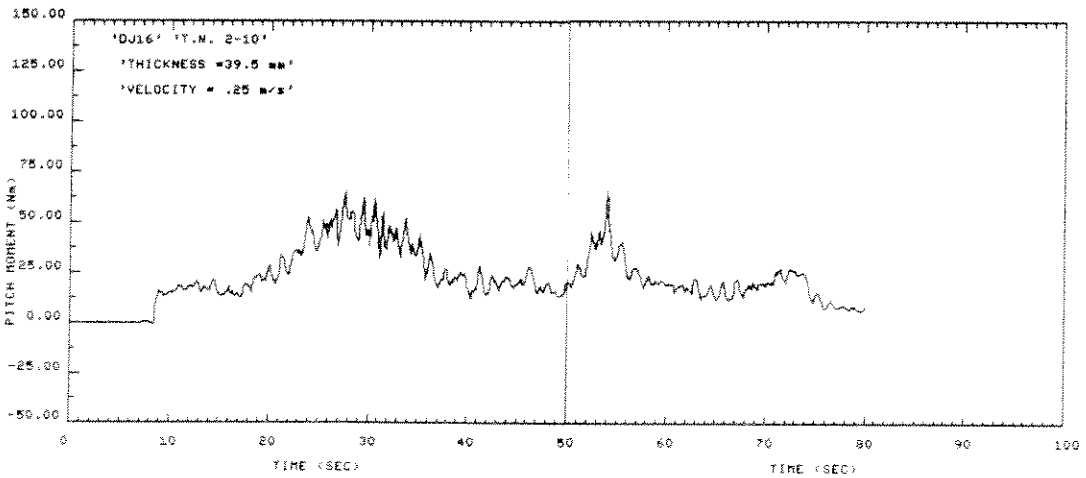
'DJ16' 'T.N. 2-10'
'THICKNESS =39.5 mm'
'VELOCITY = .25 m/s'
PITCH MOMENT (Nm)
150.00
125.00
100.00
75.00
50.00
25.00
0.00
-25.00
-50.00
0
10
20
30
40
50
60
70
80
90
100
TIME (SEC)
TIME (SEC)

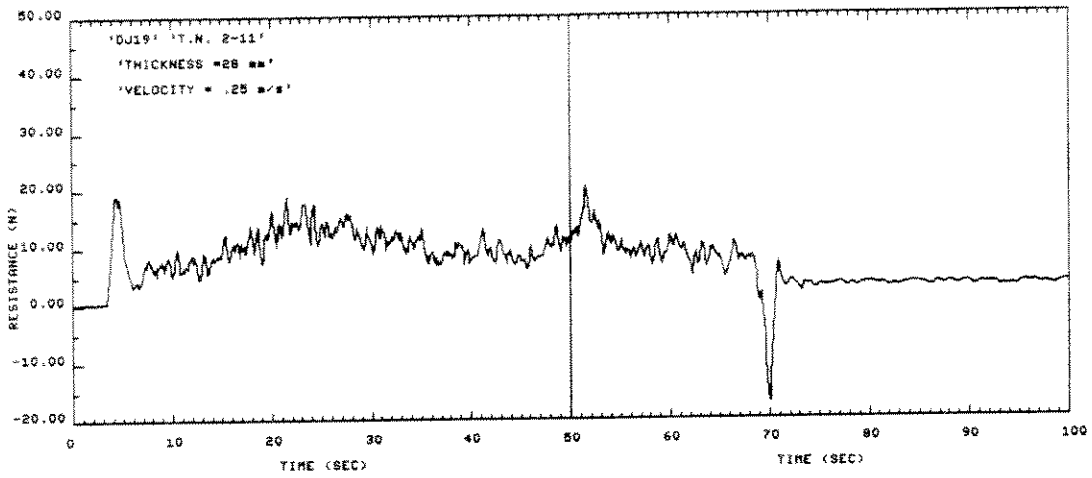
'DJ19' 'T.N. 2-11'
'THICKNESS =28 mm'
'VELOCITY = .25 m/s'
RESISTANCE (N)
50.00
40.00
30.00
20.00
10.00
0.00
-10.00
-20.00
0
10
20
30
40
50
60
70
80
90
100
TIME (SEC)
TIME (SEC)

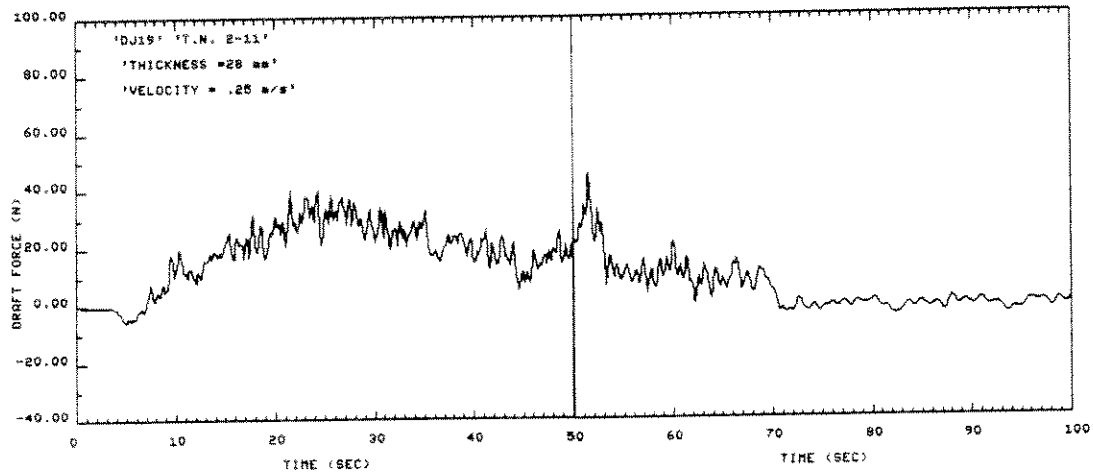
'DJ19' 'T.N. 2-11'
'THICKNESS =28 mm'
'VELOCITY = .25 m/s'
DRAFT FORCE (N)
100.00
80.00
60.00
40.00
20.00
0.00
-20.00
-40.00
0
10
20
30
40
50
60
70
80
90
100
TIME (SEC)
TIME (SEC)

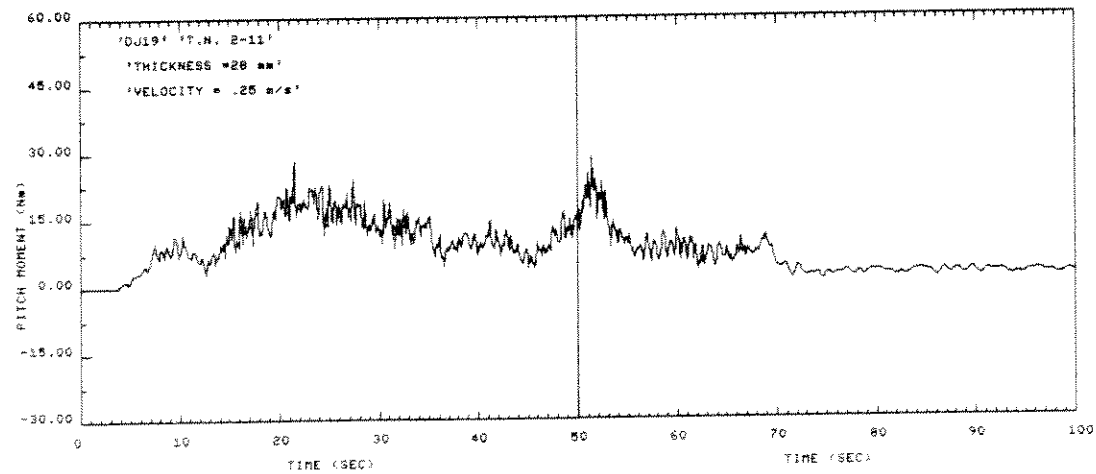
'DJ19' 'T.N. 2-11'
'THICKNESS =28 mm'
'VELOCITY = .25 m/s'
PITCH MOMENT (Nm)
60.00
45.00
30.00
15.00
0.00
-15.00
-30.00
0
10
20
30
40
50
60
70
80
90
100
TIME (SEC)
TIME (SEC)

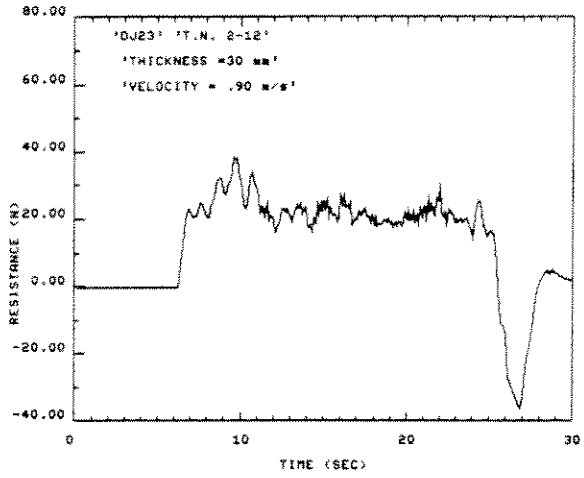
'DJ23' 'T.N. 2-12'
'THICKNESS =30 mm'
'VELOCITY = .90 m/s'
RESISTANCE (N)
80.00
60.00
40.00
20.00
0.00
-20.00
-40.00
0
10
20
30
TIME (SEC)

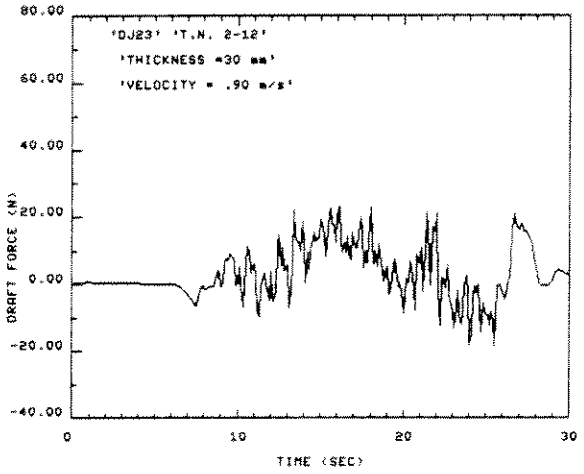
'DJ23' 'T.N. 2-12'
'THICKNESS =30 mm'
'VELOCITY = .90 m/s'
DRAFT FORCE (N)
80.00
60.00
40.00
20.00
0.00
-20.00
-40.00
0
10
20
30
TIME (SEC)

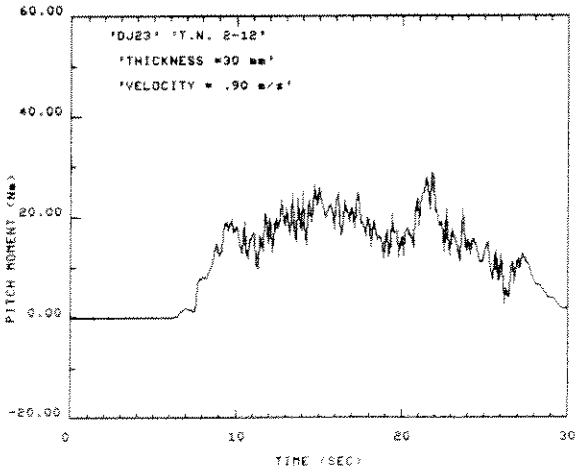
'DJ23' 'T.N. 2-12'
'THICKNESS =30 mm'
'VELOCITY = .90 m/s'
PITCH MOMENT (Nm)
60.00
40.00
20.00
0.00
-20.00
0
10
20
30
TIME (SEC)

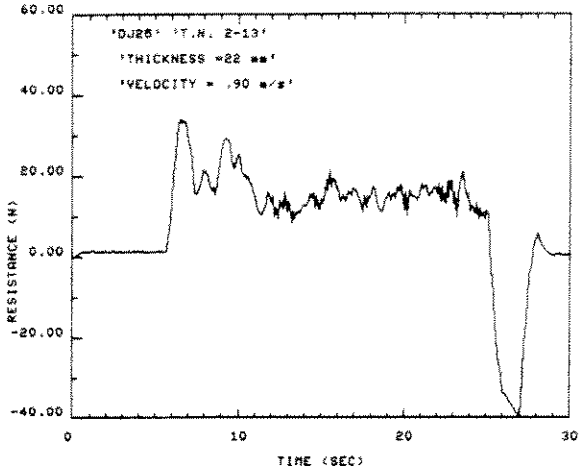
'DJ26' 'T.N. 2-13'
'THICKNESS =22 mm'
'VELOCITY = .90 m/s'
RESISTANCE (N)
60.00
40.00
20.00
0.00
-20.00
-40.00
0
10
20
30
TIME (SEC)

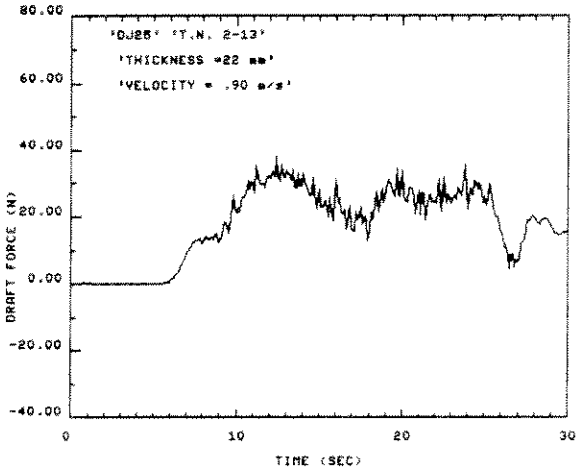
'DJ26' 'T.N. 2-13'
'THICKNESS =22 mm'
'VELOCITY = .90 m/s'
DRAFT FORCE (N)
80.00
60.00
40.00
20.00
0.00
-20.00
-40.00
0
10
20
30
TIME (SEC)

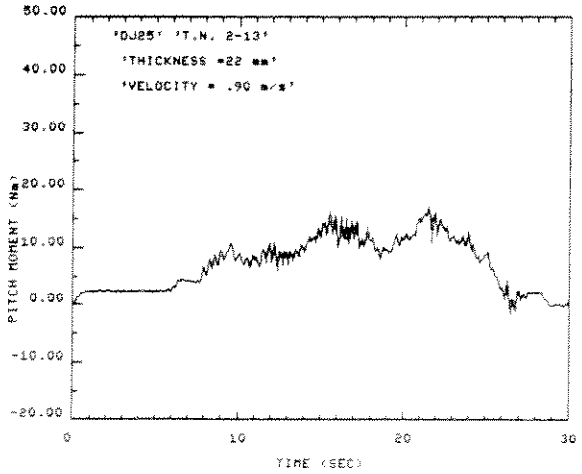
'DJ26' 'T.N. 2-13'
'THICKNESS =22 mm'
'VELOCITY = .90 m/s'
PITCH MOMENT (Nm)
50.00
40.00
30.00
20.00
10.00
0.00
-10.00
-20.00
0
10
20
30
TIME (SEC)

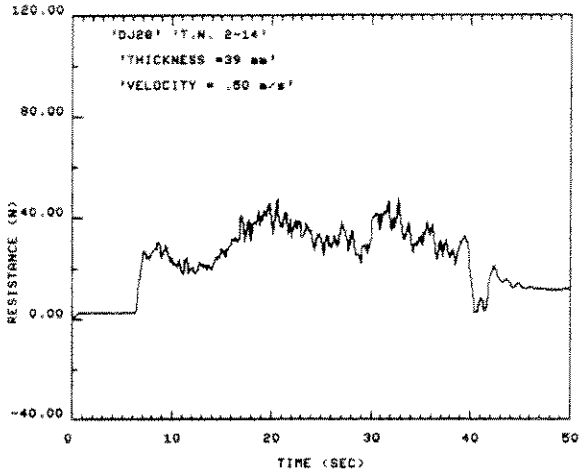
'DJ28' 'T.N. 2-14'
'THICKNESS =39 mm'
'VELOCITY = .50 m/s'
RESISTANCE (N)
120.00
80.00
40.00
0.00
-40.00
0
10
20
30
40
50
TIME (SEC)

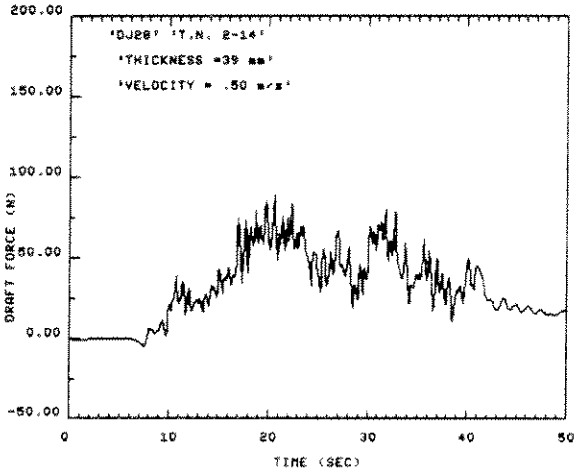
'DJ28' 'T.N. 2-14'
'THICKNESS =39 mm'
'VELOCITY = .50 m/s'
DRAFT FORCE (N)
200.00
150.00
100.00
50.00
0.00
-50.00
0
10
20
30
40
50
TIME (SEC)

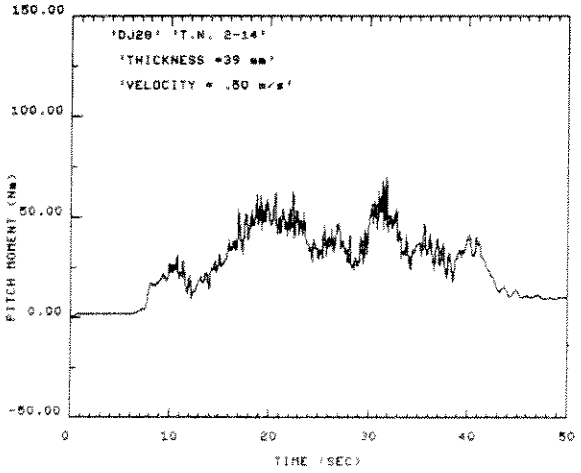
'DJ28' 'T.N. 2-14'
'THICKNESS =39 mm'
'VELOCITY = .50 m/s'
PITCH MOMENT (Nm)
150.00
100.00
50.00
0.00
-50.00
0
10
20
30
40
50
TIME (SEC)

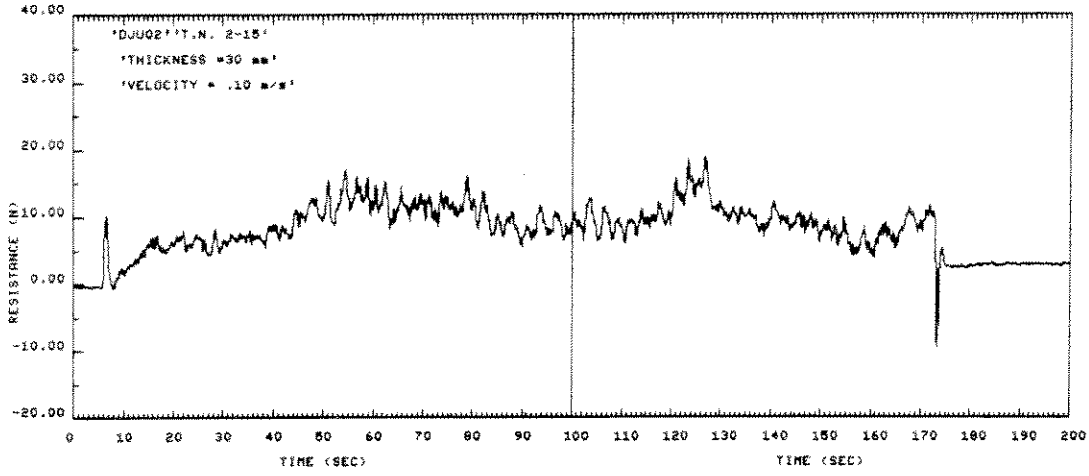
'DJU02''T.N. 2-15'
'THICKNESS =30 mm'
'VELOCITY = .10 m/s'
RESISTANCE (N)
40.00
30.00
20.00
10.00
0.00
-10.00
-20.00
0 10 20 30 40 50 60 70 80 90 100 110 120 130 140 150 160 170 180 190 200
TIME (SEC)
TIME (SEC)

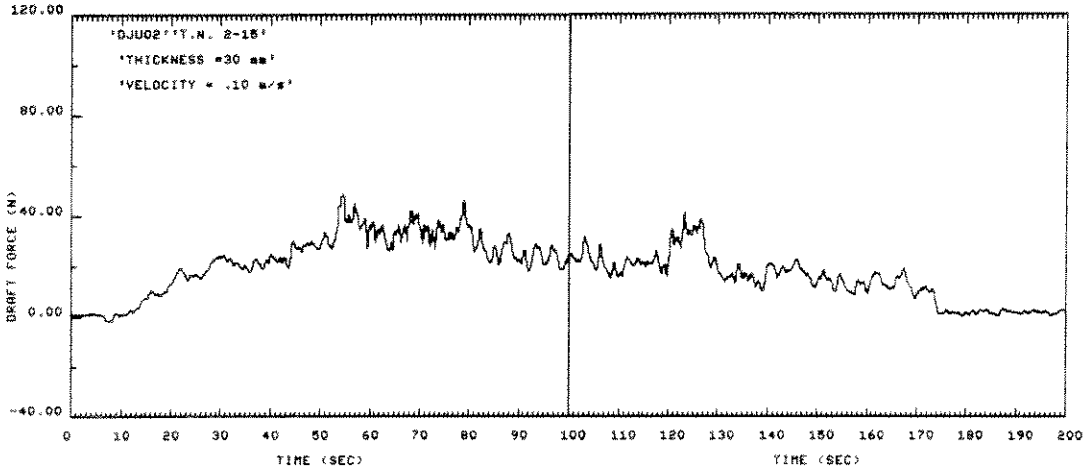
'DJU02''T.N. 2-15'
'THICKNESS =30 mm'
'VELOCITY = .10 m/s'
DRAFT FORCE (N)
120.00
80.00
40.00
0.00
-40.00
0 10 20 30 40 50 60 70 80 90 100 110 120 130 140 150 160 170 180 190 200
TIME (SEC)
TIME (SEC)

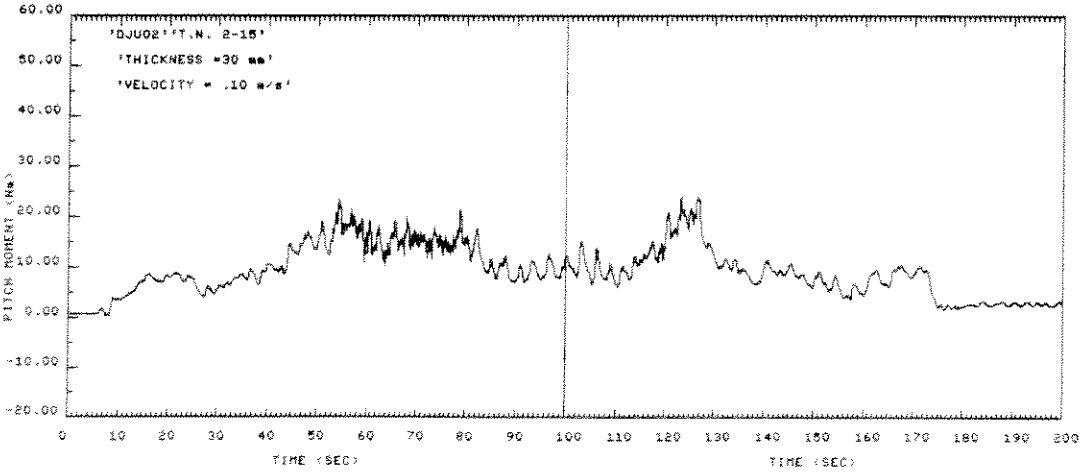
'DJU02''T.N. 2-15'
'THICKNESS =30 mm'
'VELOCITY = .10 m/s'
PITCH MOMENT (Ns)
60.00
50.00
40.00
30.00
20.00
10.00
0.00
-10.00
-20.00
0 10 20 30 40 50 60 70 80 90 100 110 120 130 140 150 160 170 180 190 200
TIME (SEC)
TIME (SEC)

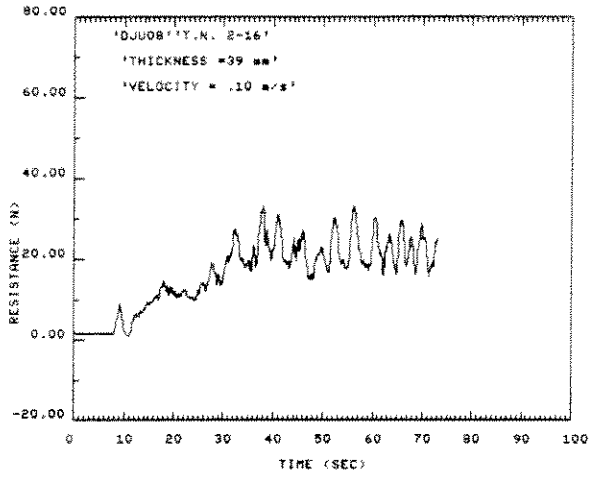
'DJU08''Y.N. 2-16'
'THICKNESS =39 mm'
'VELOCITY = .10 m/s'
RESISTANCE (N)
80.00
60.00
40.00
20.00
0.00
-20.00
0
10
20
30
40
50
60
70
80
90
100
TIME (SEC)

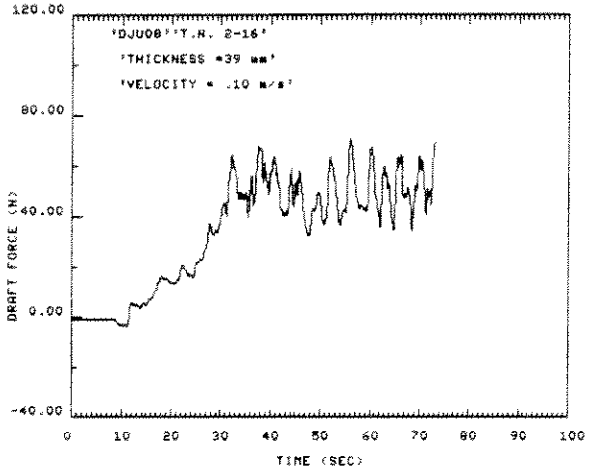
'DJU08''Y.N. 2-16'
'THICKNESS =39 mm'
'VELOCITY = .10 m/s'
DRAFT FORCE (N)
120.00
80.00
40.00
0.00
-40.00
0
10
20
30
40
50
60
70
80
90
100
TIME (SEC)

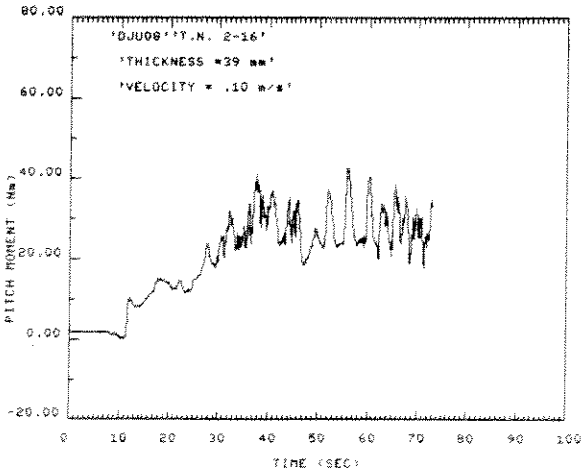
'DJU08''Y.N. 2-16'
'THICKNESS =39 mm'
'VELOCITY = .10 m/s'
PITCH MOMENT (Nm)
80.00
60.00
40.00
20.00
0.00
-20.00
0
10
20
30
40
50
60
70
80
90
100
TIME (SEC)

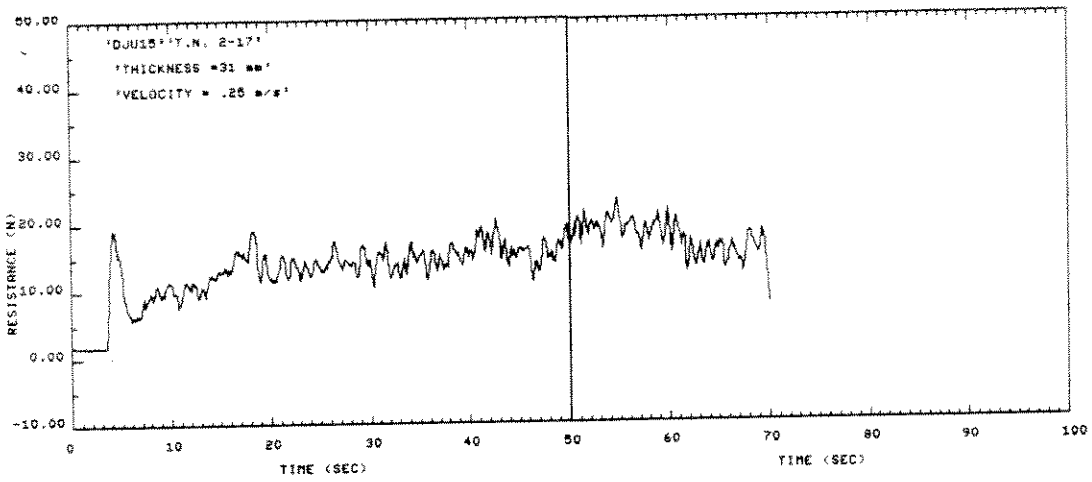
'DJU15''T.N. 2-17'
'THICKNESS =31 mm'
'VELOCITY = .25 m/s'
RESISTANCE (N)
50.00
40.00
30.00
20.00
10.00
0.00
-10.00
0
10
20
30
40
50
60
70
80
90
100
TIME (SEC)
TIME (SEC)

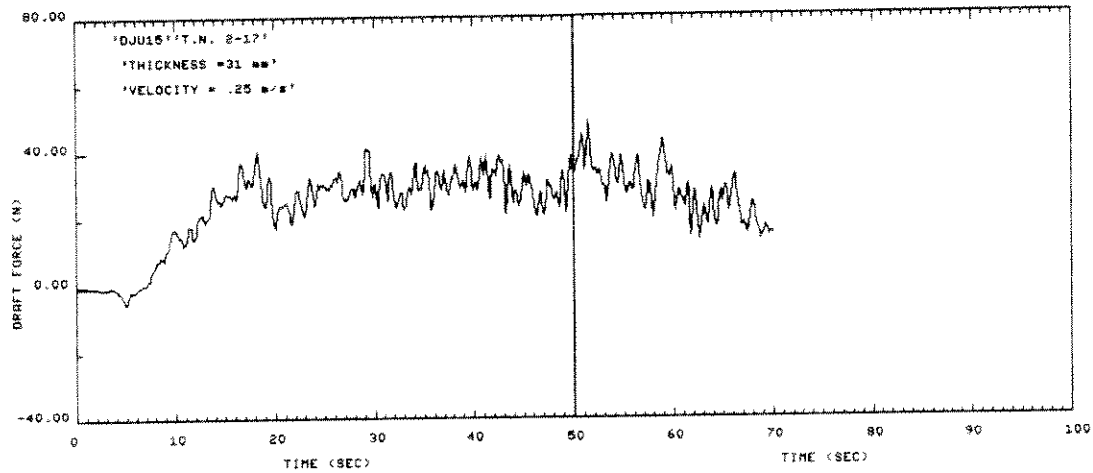
'DJU15''T.N. 2-17'
'THICKNESS =31 mm'
'VELOCITY = .25 m/s'
DRAFT FORCE (N)
80.00
40.00
0.00
-40.00
0
10
20
30
40
50
60
70
80
90
100
TIME (SEC)
TIME (SEC)

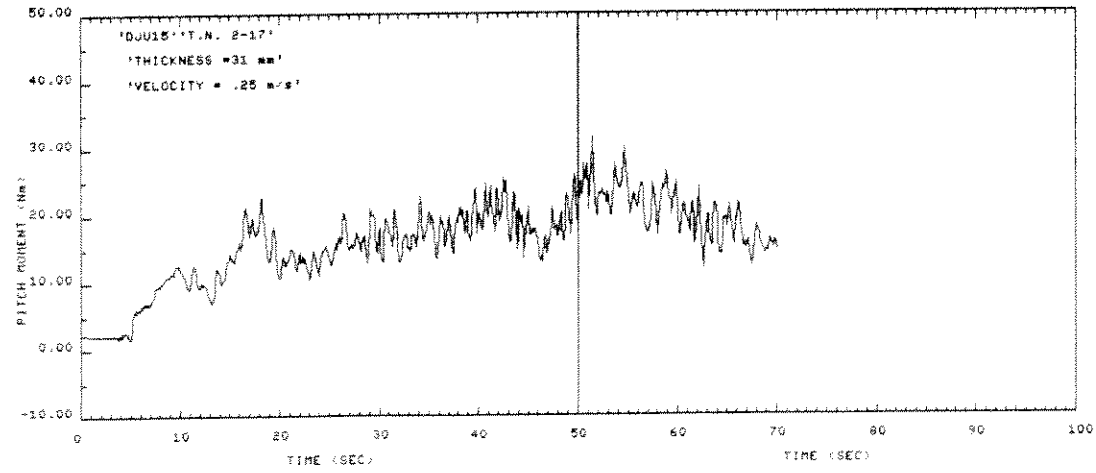
'DJU15''T.N. 2-17'
'THICKNESS =31 mm'
'VELOCITY = .25 m/s'
PITCH MOMENT (Nm)
50.00
40.00
30.00
20.00
10.00
0.00
-10.00
0
10
20
30
40
50
60
70
80
90
100
TIME (SEC)
TIME (SEC)

APPENDIX C

TIME SERIES: ROLL ANGLE AND YAW-RESTRAINING MOMENT

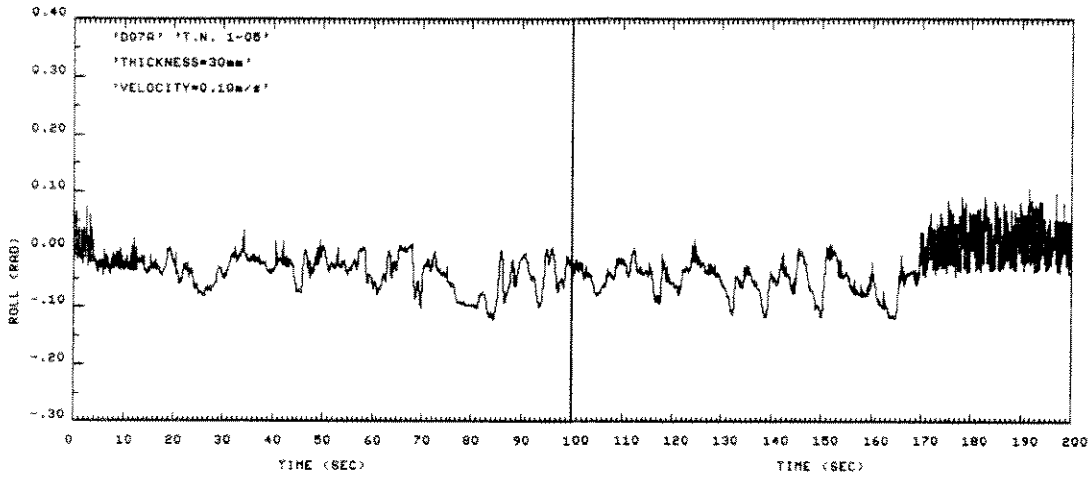
'D07R' 'T.N. 1-05'
'THICKNESS=30mm'
'VELOCITY=0.10m/s'
ROLL (RAD)
0.40
0.30
0.20
0.10
0.00
-.10
-.20
-.30
0 10 20 30 40 50 60 70 80 90 100 110 120 130 140 150 160 170 180 190 200
TIME (SEC)
TIME (SEC)

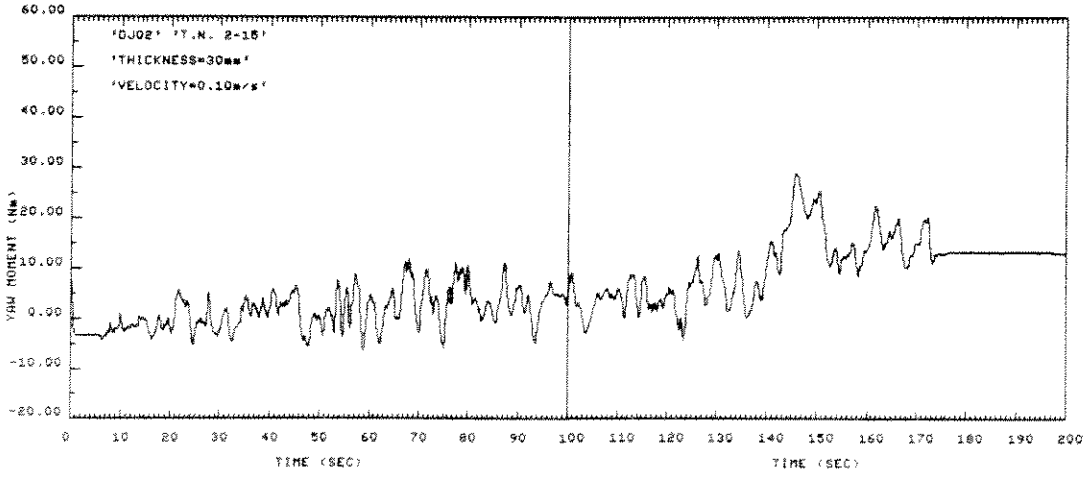
'DJ02' 'T.N. 2-15'
'THICKNESS=30mm'
'VELOCITY=0.10m/s'
YAW MOMENT (Nm)
60.00
50.00
40.00
30.00
20.00
10.00
0.00
-10.00
-20.00
0 10 20 30 40 50 60 70 80 90 100 110 120 130 140 150 160 170 180 190 200
TIME (SEC)
TIME (SEC)

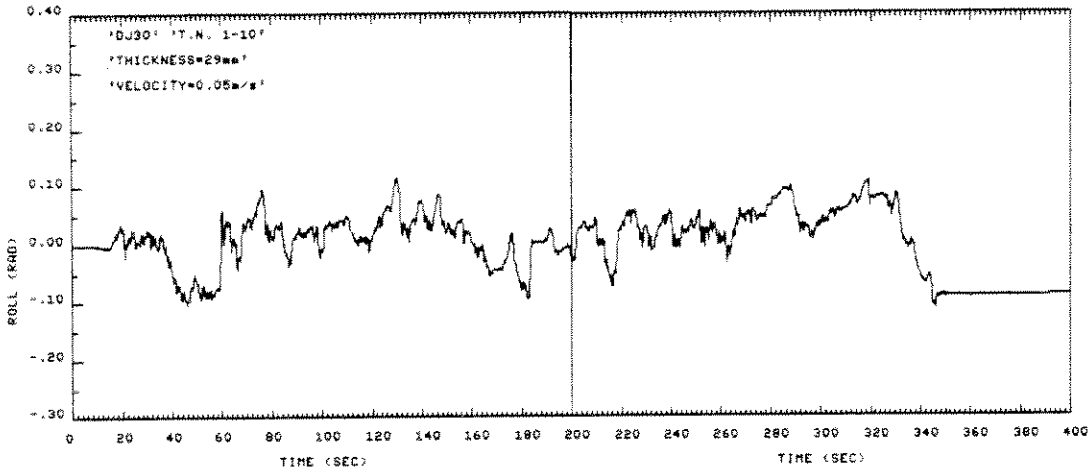
'DJ30' 'T.N. 1-10'
'THICKNESS=29mm'
'VELOCITY=0.05m/s'
ROLL (RAD)
0.40
0.30
0.20
0.10
0.00
-.10
-.20
-.30
0 20 40 60 80 100 120 140 160 180 200 220 240 260 280 300 320 340 360 380 400
TIME (SEC)
TIME (SEC)

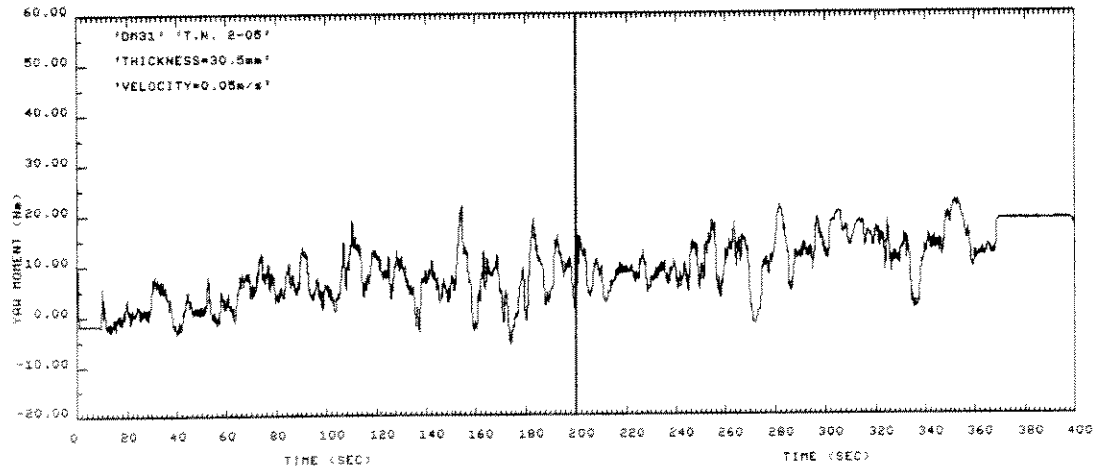
'DM31' 'T.N. 2-05'
'THICKNESS=30.5mm'
'VELOCITY=0.05m/s'
YAW MOMENT (Nm)
60.00
50.00
40.00
30.00
20.00
10.00
0.00
-10.00
-20.00
0 20 40 60 80 100 120 140 160 180 200 220 240 260 280 300 320 340 360 380 400
TIME (SEC)
TIME (SEC)

APPENDIX D

LOG-LOG PLOT OF RESISTANCE VERSUS THICKNESS

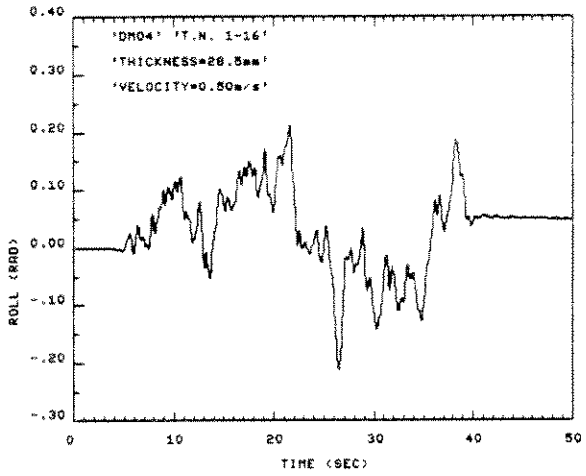
'DH04' 'T.N. 1-16'
'THICKNESS=28.5mm'
'VELOCITY=0.50m/s'
ROLL (RAD)
0.40
0.30
0.20
0.10
0.00
-.10
-.20
-.30
0
10
20
30
40
50
TIME (SEC)

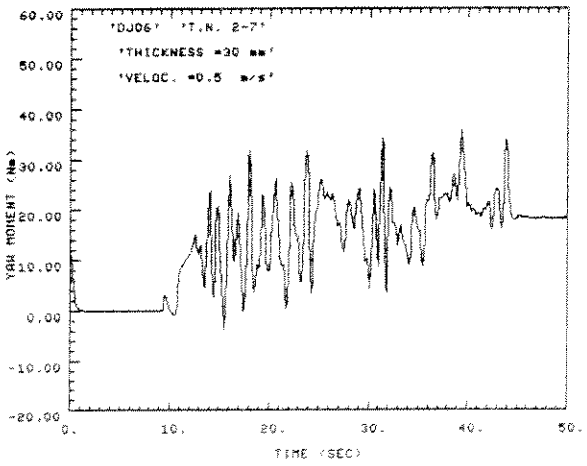
'DJ06' 'T.N. 2-7'
'THICKNESS =30 mm'
'VELOC. =0.5 m/s'
YAW MOMENT (Nm)
60.00
50.00
40.00
30.00
20.00
10.00
0.00
-10.00
-20.00
0.
10.
20.
30.
40.
50.
TIME (SEC)